Design and analysis of peptide based nanoparticles

INAUGURALDISSERTATION

ZUR
ERLAGUNG DER WÜRDE EINES DOKTORS DER PHILOSOPHIE
VORGELEGT DER
PHILOSOPHISCH-NATURWISSENSCHAFTLICHEN FAKULTÄT
DER UNIVERSITÄT BASEL

VON
SENTHILKUMAR RAMAN
AUS
INDIEN

Basel, May 2008

Genehmigt von der Philosophich-Naturwissenschaftlichen Fakültät

Auf Antrag von

Professor. Dr. Ueli Aebi *(University of Basel)*

Und

Associate Professor. Dr. Peter Burkhard *(University of Connecticut, USA)*

Und

Professor. Dr. Harald Herrmann *(University of Heidelberg, Germany)*

Basel, den 24.04.2007

Professor. Dr. Hans-Peter Hauri

Dekan

Declaration

I declare that I wrote this thesis, **Design and analysis of peptide based nanoparticles**, with the help indicated and only handed it into the Faculty of Science of the University of Basel and to no other faculty and no other university.

(Senthilkumar Raman)

Acknowledgements

I would like to thank my thesis supervisor Associate Professor. Dr. Peter Burkhard, first of all for giving me the opportunity to work in his group. I also thank him for his scientific guidance and encouragement, which he provided throughout my PhD studies. My sincere thanks to Professor. Dr. Ueli Aebi for accepting to act as "Doctor Father" during my PhD. I am grateful to Professor. Dr. Harald Herrmann for accepting to act as co-referee and to Professor. Dr. Tilman Schirmer for moderating the viva-voce.

I would like to thank my lab colleague Dr. Alexandra Graff for her constant support and encouragement and especially for her inputs and corrections during my thesis writing. I would like to thank also our former group members Dr. David Tropel and Dr. Markus Meier for their healthy discussions and ideas. I also thank Dr. Larisa Kapinos for her encouragement and scientific discussions. I am also thankful to Arundhati my lab colleague for her company and discussions during our working hours in the lab.

My affectionate thanks to Dr. Joseph for his valuable support and suggestions especially with the experimental techniques. I am really thankful to Dr.Gia Machiadze, Vesna Olivieri for providing wonderful Electron Microscopy (EM) pictures of our peptide nanoparticles. In addition, I am thankful to Vesna Olivieri for teaching me how to handle EM machine and in preparation of samples for EM. I am also very thankful to Ariel Lustig for his AUC studies with our nanoparticles and for his scientific discussions regarding the results. My earnest thanks to Kitaru Suda for helping me with Blue Native PAGE experiment. My sincere thanks to Dr. Annet Bachmann for helping me in handling the Circular Dichroism (CD) machine in Professor. Thomas Kiefhaber group. My hearty thanks to Therese Schulthess for her valuable technical help during my PhD.

I would like to thank Elizabeth Tucker, Dr. Shiva Prasad and his wife for their invaluable thesis corrections. Thanks to Liselotte Walti, Marisa Muller and Andrea Thoma for their great help with the administration work. Thanks to Roland Buerki and Margrit Jenny for their computer installation.

My special thanks to Dr. Dinesh, Kavitha and my beloved Charan for making my life in Basel very homely and for their lovely relationship which I hope to continue forever. In addition, I thank Dr. Dinesh for his support and scientific discussions that he provided during my PhD in particular during my thesis writing.

I am really thankful to Dr. Sivaraman (Juni) for his friendship, support and scientific discussions that he provided during my PhD. My hearty thanks to Dr. Mathimaran for his help during my thesis writing. Thanks to my friends Balasubramanian, Rathi, Dr. Rajeshwaran, Dr. Satheesh anna and his family, Dr. Balamurugan, Dr. Murali, Dr. Uday, Chandrasekaran and Balaji for their support during my PhD studies.

I am really thankful to Pastor. Siva annan and his family and to all the church members, for their constant support and prayers during my PhD studies. Even though Siva annan passed away, he always remains in my thoughts and he is a big inspiration to me. I am also thankful to Rajendran annan, Selvakumar annan and Balan annan family for their support and encouragement.

My special thanks to my parents and to my beloved sister and brother. They are my constant support and encouragement both in my personal life and in my academic career and hats off to them. Hearty thanks to my adorable wife Ida Mercy who made my life very happy and beautiful. In addition, thanks to my lovable father-in-law, mother-in-law and to thambu (brother-in-law) for their love and encouragement.

Dedicated to the Almighty who is the beginning and the end and to my parents

Abbreviations

AUC	**Analytical Ultracentrifugation**
BN-PAGE	**Blue Native Polyacrylamide Gel Electrophoresis**
BNPs	**Bionanoparticles**
COMP	**Cartilage Oiligomeric Matrix Protein**
CD	**Circular Dichroism**
DTT	**Dithiothreitol**
Da	**Dalton**
EDTA	**Ethylenediaminetetraacetic acid**
EM	**Electron Microscopy**
His-tag	**Hexahistidine-tag**
kDa	**Kilo Dalton**
RT	**Room temperature**
rpm	**Rotation per minute**
SDS-PAGE	**Sodium dodecylsulphate polyacrylamide gel electrophoresis**
VLPs	**Virus like particles**

Summary

Viruses are naturally formed bionanoparticles (BNPs), ranging in size from 22-150 nm. Remarkably, small viruses are composed of one single protein chain folding into a capsid structure with icosahedral symmetry. The icosahedron is built up from 60 asymmetric units and is the largest closed shell in which every subunit is in an identical environment. It is characterized by 2-fold, 3-fold and 5-fold rotational symmetry axes. By superposition of different protein oligomerization domains onto the symmetry axes of the icosahedron, a nanoparticle with icosahedral symmetry can be designed.

To test our concept, we have designed a peptide comprising a slightly modified form of a pentameric coiled-coil domain of cartilage oligomeric matrix protein (COMP) linked to a *de novo* designed trimeric coiled-coil domain as a single chain. These two different oligomeric domains were linked by two glycine residues to provide flexibility between them and were fixed in their relative orientation with an intramolecular disulfide bridge. Computer modeling predicted that such a design would result in an icosahedral peptide based nanoparticle with a diameter of 17 nm. We chemically synthesized the above designed peptide and performed refolding studies and biophysical characterization using analytical ultra centrifugation (AUC) and electron microscopy (EM), thereby showing the formation of icosahedral nanoparticles with a diameter of ~ 17 nm.

Subsequently, we switched to recombinant expression of the designed peptide. Again, we performed refolding studies with the expressed peptide and biophysical characterization (AUC and EM), thereby showing the formation of icosahedral nanoparticles with a diameter of ~ 17 nm. In addition, we showed that during refolding, parameters such as ionic strength, pH of the refolding buffer and presence of glycerol influence the formation of icosahedral nanoparticles. Moreover, we observed icosahedral nanoparticles in conditions in which the formation of intramolecular disulfide bridges is not possible. This showed that even in the absence of intramolecular disulfide bridge the helices of the two different oligomeric domains like to be arranged close to each other, as this will favor the formation of icosahedral nanoparticles.

In parallel, we also modified the designed peptide to include charged residues at the interface between the two oligomeric domains. The idea was to fix the relative orientation between the two oligomeric domains through ionic interactions. The subsequent expression, refolding studies and biophysical characterization showed the formation of nanoparticles, but they were lacking icosahedral symmetry. This result showed that the design has to be optimized further to obtain icosahedral nanoparticles.

Moreover, we wanted to study whether in our design principles oligomerization motifs other than coiled-coils can be used to form icosahedral nanoparticles. Accordingly, we used globular foldon domain as the trimerization domain and the COMP as the pentamerization domain. The results showed the formation of nanoparticles, but they were lacking icosahedral symmetry. In addition, in the above design we studied the effect of linker region by increasing the liker region to four and six residues, but it did not help in the formation of icosahedral nanoparticles. However, when the foldon domain extended with the trimeric coiled-coil domain as a single trimerization domain and with COMP as the penatmerization domain, we observed icosahedral nanoparticles.

Viruses are known for their induction of strong antibody (B-cell) mediated immune response in the host even against the self-antigens. This property is conferred by the repetitive arrangement of the antigens on their surface. Peptide based nanoparticles have similar properties to viruses, such as self-assembly and most importantly the repetitive arrangement of subunits (peptide based nanoparticles are composed of 60 identical monomeric chains). Therefore, we wanted to use our system as a ‘repetitive antigen display carrier’ in vaccination, as an alternative to viral and viral based platforms such as virus like particles (VLPs). To this end, and in order to understand the effect of our nanoparticle size on immune response, we built different constructs displaying the pilin epitope of *Pseudomonas* pathogen at their C-terminus. Computer modeling indicated that these constructs would form icosahedral nanoparticles of three sizes: small (18 nm), medium (23 nm) and large (29 nm). From the refolding studies, we observed mostly aggregation and precipitation of the nanoparticles.

This effect presumably due to interparticle cross-linking, by the cysteine residues of pilin epitope which are present at the periphery of nanoparticles, as we observed aggregation of small size icosahedral nanoparticles upon changing from reducing to oxidizing condition. Immunization results, because of the aggregation and precipitation behavior of nanoparticles, showed poor immune response. However, the immunization results showed that our nanoparticles present the attached epitope in their native form, as we observed binding against native pilin protein. Moreover, immunization results from our laboratory using medium size nanoparticles displaying Salmonella epitope D2 showed promising results, as we got antibody titer values which were well comparable to the values obtained with VLPs. This places our system alongside with VLPs, which are in clinical trials as a carrier in vaccination.

Table of contents

General Introduction

Nanotechnology

"The growing field of nanotechnology finds its full expression in the words of that abstract of the artist-scientist Leonardo da vinci: '*Where Nature finishes producing its own species, man begins, using natural things and with the help of this nature, to create infinity of species*.'" Nobel laureate Jean-Marie Lehn used these words to give an outlook on the future and perspectives of supramolecular chemistry [1].

The definition of nanotechnology according to National Nanotechnology Initiative (NNI) is as follows: *research and technology development at the atomic, molecular, or macromolecular scale, leading to the controlled creation and use of structures, devices, and systems with a length scale of 1-100 nanometers (nm)*. The advantage of operating at the nanoscale realm is that the objects at this scale, take on novel properties and functions that differ markedly from those seen in the macro scale. For example, carbon nanotubes [2] and gold nanoshells [3], two different types of nanomaterials, have physical properties different from carbon or gold on the macro scale. Other examples of nanotechnology include dendrimers [4], liposomes [5], and semi-conducting quantum dots [6].

Ron Hardman [7] nicely describes the impact of nanotechnology with the following words "In 1959 Richard Feynman's seminal talk on nanotechnology, 'There's Plenty of Room at the Bottom' [8] presented what was theoretically possible by manipulating matter at the atomic and molecular scales. Today, nanotechnology is an applied science, a rapidly growing industry generating a diverse array of nanoscale materials (e.g., carbon nanotubes, fullerene derivatives and quantum dots). Manipulation of materials on a nanometer scale is opening a world of creative possibilities, and the benefits afforded by nanoscale technologies are expected to have substantial impacts on almost all industries and areas of society (e.g., medicine, plastics, energy, electronics and aerospace)".

Especially, nanotechnology manifests itself in a wide range of nanoparticles that can be useful to biologist as Scott E. McNeil [9] describes the application of nanotechnology for the biologist with the following words "nanotechnology manifests itself in a wide range of nanoparticles that can be useful to biologist.

For example, dendrimers [10, 11] and magnetic nanoparticles [12, 13] are used in targeting of cancer cells and in tissue imaging and gold nanoshells [14] in cancer therapy and liposomes [15, 16] in gene therapy and drug delivery. Virtually, all of these nanoparticles have been designed with chemically modifiable surfaces to attach a variety of ligands that can turn these nanoparticles into biosensors, molecular-scale fluorescent tags, imaging agents, targeted molecular delivery vehicles, and other useful biological tools (Figure 1). An obvious advantage of nanotechnology as it relates to biological systems is the ability to control the size of the resulting nanoparticles. Nanoparticles are of the same basic size as biological entities (1-100 nm)" (Figure 2).

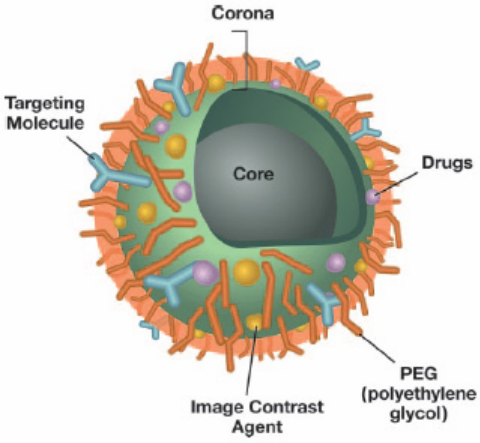

Figure 1. Schematic diagram of multifunctional nanoparticle. The nanoparticle's "corona" (outer surface) can be functionalized with hydrophilic polymers, targeting molecules, therapeutic molecules, therapeutic drugs, and image contrast agents. The interior surface can be solid (e.g., quantum dots) or liquid (e.g., liposomes). Reprinted from [9], with permission from Society for Leukocyte Biology.

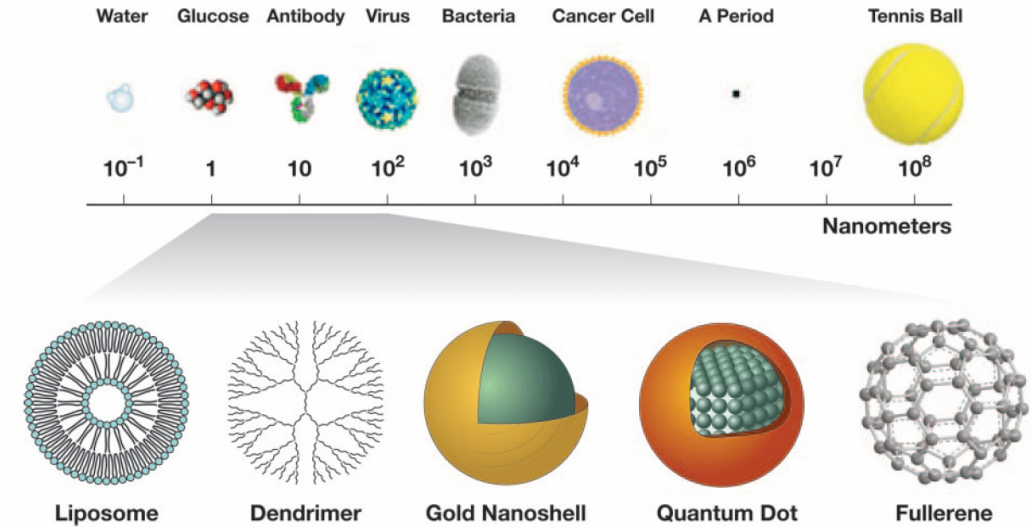

Figure 2. Relative size of nanoparticles compared with familiar items. Reprinted from [9], with permission from Society for Leukocyte Biology.

As the applications of inorganic, metallic, semiconductor and polymer based nanoparticles in biology is increasing, there is also increasing concern about its toxicological properties. For example, carbon nanoparticles have been shown to induce lipid per-oxidation in the brain cells of fish and pulmonary inflammation in rats [17, 18]. Therefore, as an alternative people started using peptides and proteins as building blocks to build nanoparticles. This opened up a new filed called '**bionanotechnology**'.

Protein and peptides as building blocks - Bionanotechnology

Bionanotechnology, a subdivision of nanotechnology focuses on research and development of novel nanoscale materials from biological building blocks for medical applications such as gene delivery, bio-imaging, drug delivery and vaccine development.

Self-assembly is one of the processes used in nanotechnology to make ensembles of nanostructures [19]. Mainly, self-assembly process is exploited in the field of bionanotechnology to create novel nanoscale biomaterials. Therefore, in the following paragraphs, the self-assembly process is described.

Self-assembly

The term "self-assembly" does not have a precise definition, and indeed has often been overused. Processes ranging from the non-covalent association of organic molecules in solution to the growth of semiconductor quantum dots on solid substrates have been called self assembly.

Whitesides and Grazybowski [19] limit the term "self-assembly" to the following definition: "*processes that involve pre-existing components which exhibit reversible and co-operative assembly of predefined components into an ordered superstructure*". In addition, Whitesides and Grazybowski classified the self-assembly process into two main kinds: (i) static and; (ii) dynamic self-assembly. **Static** self-assembly involves systems at global or local equilibrium that do not dissipate energy. For example, molecular crystals and most of the folded globular proteins are formed by static self-assembly. In static self-assembly, formation of the ordered structure may require energy (for example in the form of stirring), but once it is formed, it is stable.

On the other hand, in **dynamic** self-assembly the formation of structures or patterns occurs when the system dissipates energy. Examples are patterns formed during reaction and diffusion processes in oscillating chemical reactions.

Shuguang Zhang [20] describes the characteristics of self-assembly with the following words "Self-assembly is mediated by weak, non-covalent bonds notably hydrogen bonds, ionic bonds (electrostatic interactions), hydrophobic interactions, van der Waals interactions, and water mediated hydrogen bonds. Although these bonds are relatively insignificant in isolation, when combined together as a whole, they govern the structural conformation of all biological macromolecules and influence their interactions with other molecules. Moreover, it is a powerful approach for fabricating novel supramolecular architectures. It is ubiquitous in the natural world. For example, lipid molecules form oil drops in water; four hemoglobin polypeptides form a functional tetrameric hemoglobin protein; ribosomal proteins and RNA coalesce into functional ribosomes".

Self-assembled nanoscale bioassemblies derived from nature's design

Nature has provided us with rich source of self-assembled nanoscale bioassemblies such as viruses. By combining molecular biology and recombinant protein expression, several self-assembled nanoscale bioassemblies derived from nature's design have been prepared for bionanotechnological applications. It includes:

- Virus capsid or virus-like particles (VLPs) [21, 22];
- Ferritin protein cages [23-25];
- Heat shock protein cages [26-28];
- Other self-assembled protein cages, such as enzyme complexes [29], chaperones [30], and carboxysomes [31].

The above mentioned bionanoparticles (BNPs) self-assemble primarily based on multiple noncovalent interactions to highly organized nanosystems with a diverse array of shapes and sizes (Figure 3).

Distinctive features of Bionanoparticles:

Lee and Wang [32] describes the following points which make BNPs more attractive when compared to the synthetic nanoparticles.

- Well organized architectures with a broad selection of sizes in the nanometer scale (Figure 3).
- Monodispersed particles with uniform size and shape.
- Three dimensional (3D) structures resolved at atomic or near-atomic levels.
- Economic large scale production in gram or even kilogram quantities.
- Availability of genomic sequence, through which the composition and surface properties can be controlled through recombinant technology.
- In particular, both genetic and chemical modification techniques can be used to model the scaffolds. Thereby, allowing theoretically unlimited alterations of the nanomaterials with submolecular precision.

Bionanoparticles (BNPs) and their characteristic features

Virus capsid or virus like particles (VLPs)

Recently, several investigations have recognized virus capsids as versatile building blocks that can serve as scaffolds for producing nanomaterials [33-35]. In addition, Singh and co-workers [36] describes the usefulness of viral capsids with the following words “Viral particles are robust protein cages in the nanometer range exhibiting well-defined geometry and remarkable uniformity ideal for nanoscale fabrication. The atomic structures of many viruses have been resolved allowing researchers to identify or modify amino acids in the viral capsid for bioconjugation. With the ease of genetic manipulation for producing mutants displaying lysines or cysteines in the accessible virus capsid regions, it is feasible to chemically conjugate molecules to those amino acids both on the interior and exterior.

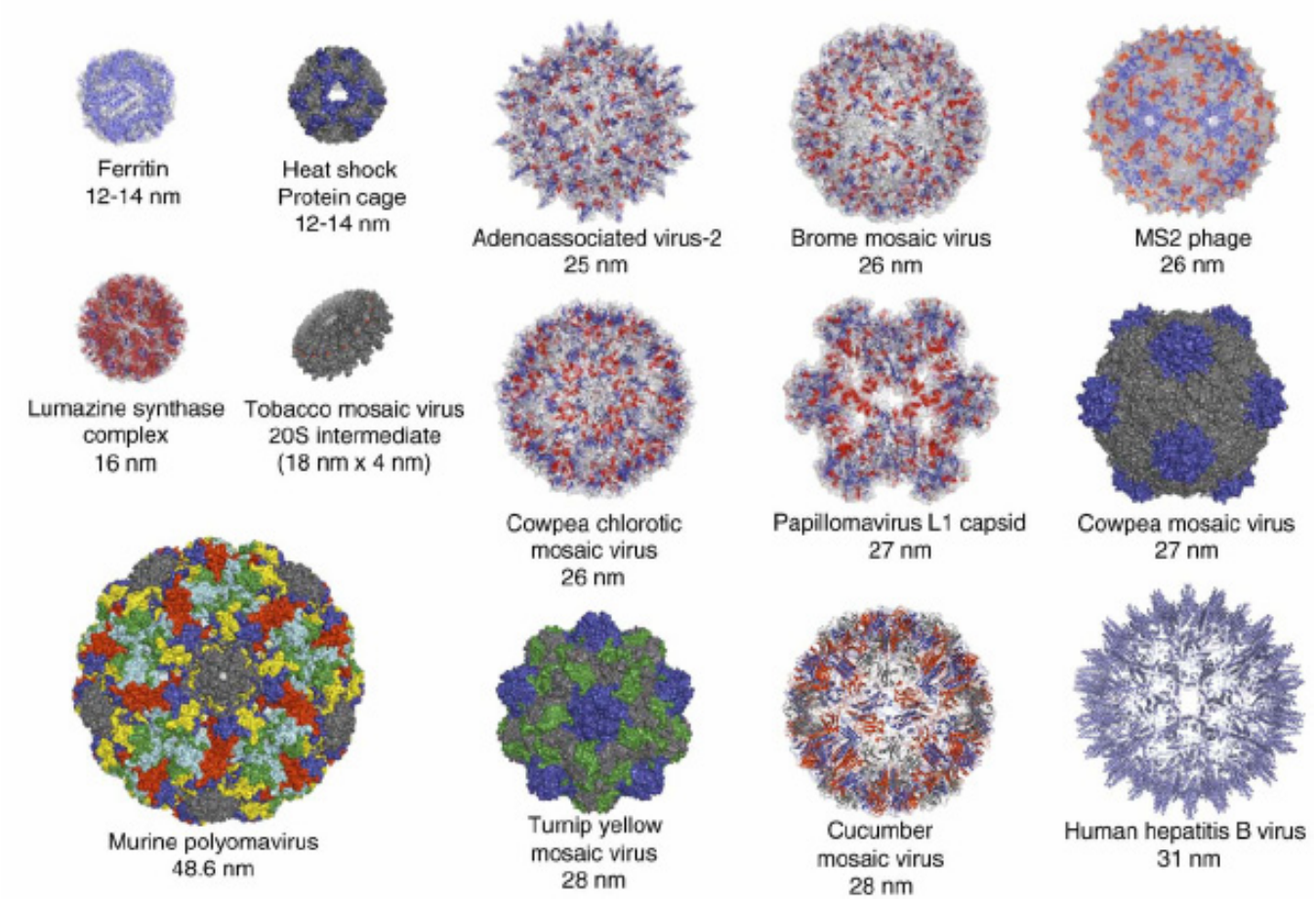

Figure 3. Structural illustration of protein cages that have been used in bionanotechnology or biomedical applications. Reprinted from [32], with permission from Elsevier.

Bioconjugation to virus-based nanoparticles has been performed using commercially available homo- or hetero-bifunctional linkers using the lysines and/or cysteines of the viral capsid [37-40]. Molecules derivatized with NHS-esters can conjugate to the lysines, while maleimide-derivatized molecules that are thiol selective can react and link with the cysteines". A schematic representation of commonly used basic bioconjugation methods is shown in Figure 4. For example using bioconjugation, cowpea mosaic virus (CPMV) has been demonstrated to be a robust platform for conjugation with variety of molecules, including **fluorescent dyes** [41], **polyethylene glycol (PEG) chains** [42], **DNA** [43], **peptides** [44], **antibodies** [35], and **carbohydrates** [45].

As virus capsids are relatively rigid, it has also become feasible to display molecules in a precise spatial distribution at a nanoscale level. The above point was demonstrated using VLPs to display antigens in a repetitive and highly ordered manner for the purpose of designing modular system for novel vaccines [46].

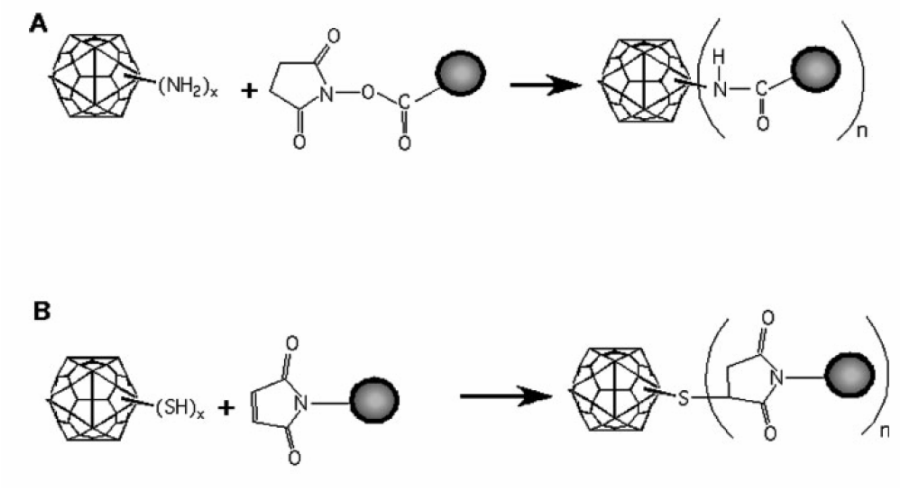

Figure 4. Chemical bioconjugation of viral nanoparticles. Bioconjugation methods for (**A**) lysines in virus capsid reacting with NHS-ester derivatized molecules or (**B**) thiols of cysteines in virus capsid reacting with maleamide-derivatized molecules. Molecule to be conjugated is shown as a filled circle. Adapted from reference [36].

Ferritin protein cages

Ferritins are a class of iron storage and mineralization proteins found throughout the animal, plant and microbial kingdoms.

In higher eukaryotes, ferritins are composed of 24 nearly identical subunits and are self-assembled into a spherical cage with an octahedral symmetry (4-fold, 3-fold and 2-fold) [47] (Figure 5). Ferritin has an outer diameter of 12 nm and an inner cavity diameter of 8 nm that stores the mineralized iron core [48].

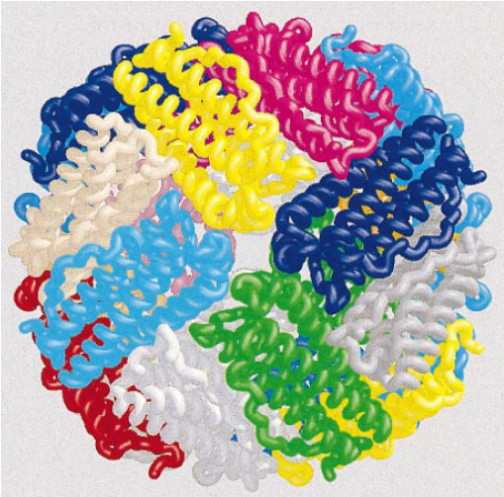

Figure 5. Human heavy (H) subunit ferritin structure (HuHF). 24 subunits in 432 symmetry viewed down the four-fold symmetry axis. Reprinted from [47], with permission from Elsevier.

Ferritin because of its natural mineralization property has been used as a reaction vessel for the synthesis of inorganic nanomaterials with controlled dimensions. For example, apoferritin (lacking the iron oxide core) has been used in the mineralization of metals such as cobalt, nickel and palladium [49-51]. In addition, Kramer and co-workers showed that the ferritin protein cages can be functionalized through genetic engineering to impart specific functionalities for the constrained synthesis of silver nanoparticles [23].

Other protein cages

Other protein cages such as heat shock proteins [26-28], enzyme complexes (luzamine synthase capsid) [29], chaperones [30], and carboxysomes [31] which are similar to virus capsid and ferritin protein cages, have also been used as alternative scaffolds. Each individual system is a precisely assembled platform based on symmetry based arrangement (octahedral or icosahedral symmetry). Similar to virus like cages, these platforms also offer high degree of spatial organization with well characterized self- assembly motifs, a major advantage in BNPs for controlling functional group density and orientation.

Many of these protein cages have been demonstrated with medically relevant functionalizations with genetic insertions of heterologous peptides or through bioconjugations will be described in the following applications section.

Biomedical applications of BNPs

In recent years the **polyvalent display nature** of BNPs has been exploited to a greater degree in biomedical applications such as cell specific drug and gene delivery. This is because of the emerging paradigm that the collective binding between multiple ligands and receptors often leads to increased affinity, and such multiplex bindings elicit fundamentally different biological events when compared with an individual ligand binding. For example, Finn and coworkers [45] showed that the polyvalent display of carbohydrates (mannose units) on cowpea mosaic virus (CPMV) capsid, enhanced their binding affinity for their complementary lectin concanavalin-A (con-A). This caused them to exhibit nearly a thousand-fold greater efficiency than monomeric mannose units in inhibiting erythrocyte agglutination with concanavalin-A.

In the following paragraphs, we will see the applications of BNPs in the field of cell targeting, drug delivery, bio-imaging and vaccine design.

Cell targeting

The principle of targeting specific diseased cell type is to localize the therapeutic agent, thereby reducing the potential side effects and increasing the therapeutic efficiency.

The natural affinity of BNPs especially viral capsids to target host cells is exploited for cell targeting purposes. For example, polyomavirus VP1 based VLPs naturally targets a cell surface glycoprotein with a terminal α 2,3-linked N-acetylneuraminic acid [52], and is internalized by the cells via $\alpha_4\beta_1$-integrin receptors [53]. Also, Hepatitis B virus large (L)-surface antigen based VLPs naturally targets human hepatocytes and the information is specified by the sequence located at the N-terminus of large subunit. These VLPs have been demonstrated as safe vehicles for delivery of genes with high *ex vivo* and *in vivo* transfection efficiencies and high targeting specificity to human hepatocyte-derived cells [54, 55].

The natural affinity of viral capsids towards host cells is altered by inserting peptide ligands through recombinant cloning technique. Using this technique people have produced VLPs with altered affinities. Folk and co-workers [56], genetically inserted the urokinase plasminogen activator (uPA) sequences to the VP1 proteins of polyomaviruses and showed that the resulting VLPs were directed towards the upA receptor expressing cells. In HBV L-surface antigen based VLPs, its native bio-recognition motif was replaced with epidermal growth factor (EGF) moiety to direct the particles to EGF receptor-overexpressing cells [54]. The recombinant cloning in BNPs opens vast possibilities of incorporating different cell-specific targeting moieties, but the chimeric sequence insertions can vary immensely upon each BNP (location of insert) and the composition of peptide insert (number and sequence of amino acids).

Drug delivery

The interior hollow cavities of BNPs are exploited to encapsulate small molecules for drug delivery by genetic and chemical modifications. Recent studies with polyoma VLPs and heat shock protein (Hsp) cages demonstrated the feasibility of packaging proteins and chemical compounds within the protein cage.

Abbing and co-workers [57] used polyoma VP1 based VLPs to encapsulate methotrexate drug (MTX) and green fluorescent protein (GFP). In polyoma virus, VP1 forms the major capsid protein enclosing the inner coat proteins VP2 and VP3. The encapsulation of molecules was achieved by the development of an anchoring technique based upon the specific interaction of the inner core protein VP2 with VP1 pentamers. A stretch of 49 amino acids of VP2 served as an anchor molecule, either expressed as a fusion protein with green fluorescent protein (GFP) or covalently linked to methotrexate (MTX). The 49 amino acids of VP2 specifically anchored GFP or MTX to VP1 pentamers and the further assembly of VP1 pentamers in to capsid structure resulted in VP1 VLPs enclosing GFP or MTX. The encapsulated MTX retained cytotoxicity in the cells, and destroyed MTX-resistant cells, which suggests that the system circumvents the MTX transport.

In another study by Douglas and co-workers [27] used small heat shock protein (Hsp) cages from *Methanococcus jannaschii* to encapsulate the anti-tumor drug doxorubicin by chemical coupling and showed subsequent release of drug from the cage in a pH dependent manner. Hsp assembles into a 24-subunit spherical structure with octahedral symmetry, which is 12 nm in diameter and has a porous protein shell that allows the free small-molecular exchange between the interior and bulk solution [26]. In this study, the Hsp cage was genetically modified to include cysteine residues at the interior surface and the (6-maleimidocaprol) hydrazone derivative of doxorubicin was linked to the interior surface of this Hsp via coupling of maleimide to cysteine. The quantitative analysis by absorbance spectroscopy indicated that 24 doxorubicin moieties were encapsulated, and under acidic conditions doxorubicin was selectively released through the hydrolysis of hydrazone linkage. This study can be a crucial step in future drug delivery designs.

Bio-imaging

Based on two main points, BNPs are considered as valuable tools in *in vivo* or *in vitro* imaging applications. The fist one is the **biocompatibility**. For example, Manchester and co-workers [58] tested the biocompatibility nature of cowpea mosaic virus (CPMV) particles by dosing through oral and intravenous route in mice. They found out that after several days of dosing, the CPMV particles were detectable in a wide variety of tissues including liver, kidney, lung, spleen, and lymph nodes. Thus, confirming the biocompatibility nature of CPMV particles.

The second point is the **large surface area** presented by the BNPs for coupling fluorescent probes. For example, Finn and co-workers showed using cowpea mosaic virus (CPMV) particles (made up of 60 subunits) that at least 60 copies of fluorescent molecules can be attached to the virus capsid using the highly reactive lysine which is present in each subunit [39]. In addition, the rigid and highly ordered surface feature of BNPs was exploited to attach imaging agents at designed positions on the surface. This resulted in no mobility of attached fluorescent molecules to interact or aggregate with each other, which often quenches the fluorescence. Soto and co-workers [59] demonstrated that the spatial distribution of carbocyanine dye Cy5 on the virus capsid overcomes the problem of fluorescence quenching observed in Cy5 molecules and showed increased fluorescence signal.

One of the applications of BNPs in bio-imaging is that they are used to sensitively image the vasculature during development and disease states such as tumorigenesis and atherosclerosis. For example, Manchester and co-workers [60] used fluorescent labeled CPMV particles to visualize the vasculature blood flow in living mouse and chick embryos to a depth of about 500 μm. In addition, they also showed the intravital visualization of human fibrosarcoma-mediated tumor angiogenesis.

Vaccine development

Repetitive antigen display concept:

Repetitive antigen display concept started with the work of Dintzis and co-workers [61, 62]. To understand the minimum requirements of antigen for triggering the primary B-cell mediated immune response, the group used haptenated polymers as antigens and showed that arrays of 20-30 haptens (small organic molecules of defined structure), spaced optimally by 5-10 nm, can activate B-cells. Still, these responses depend on some T-cell help for activation of B-cells.

Later, Zinkernagal and co-workers [63] studied the influence of antigen density and order on B-cell induction using the antigen glycoprotein of vesicular stomatis virus serotype Indiana (VSV-G (IND)). Naturally, VSV-G (IND) exists in a highly repetitive form in the envelope of vesicular stomatis virus (VSV-IND) and in a poorly organized form on the surface of infected cells. By generating transgenic mice expressing VSV-G (IND), the authors showed that the B-cells were unresponsive to the poorly organized form of VSV-G (IND) present as self antigen but responded to the same antigen when presented in the highly ordered, repetitive manner. Subsequently, Zinkernagal and co-workers showed that the induction of B-cells is completely independent of the T-cell help and concluded that the B-cells respond best against the rigid and highly repetitive surface antigens [64].

Repetitive antigen display was also the key in producing high-titer, high affinity monospecific antibodies that were used some time ago to localize the different protein subunits within the capsid of bacteriophage T4 [65-67]. Also recently, Aebi and co-workers [68] used the repetitive antigen display concept to directly visualize the dependence of antibody affinity and specificity on antigen presentation.

Based on the above studies on repetitive antigen display concept, BNPs such as virus-like particles (VLPs) and ferritin protein cages are used to present bacterial or viral antigens for the production of novel vaccines *because of their rigid and repetitive surface.*

Virus like particles (VLPs)

VLPs are a highly effective type of subunit vaccines that mimic the overall structure of virus particles without the requirement of containing infectious genetic material [69]. VLPs are produced by utilizing the intrinsic property of viral capsid proteins to self-assemble spontaneously. For example, VLPs of papillomavirus are produced using the self-assembly of major capsid protein L1.

VLPs are considered as strong immunogens because of the following properties: (i) they have the authentic conformation of viral capsid proteins seen with inactivated and attenuated virus vaccines; and (ii) their ability to induce both B-cell [70] and T-cell mediated immune responses in the absence of adjuvants [71, 72]. These properties made VLPs as immunogens. For example, the immunization of young healthy woman with human papillomavirus (HPV16) VLPs composed of the major structural protein L1 induced high titer neutralizing antibodies and protected the patient from HPV infection and associated cervical dysplasia [73].

In addition to vaccine candidates, VLPs are used as '**repetitive antigen display system or carrier**' to present foreign antigens on their surface to create novel vaccine candidates [46, 74]. The best studied example is the Hepatitis B-virus core (HBc) particles [70, 75-77]. The HBc particles are formed by the self assembly process during which the monomers associate to form dimers (stable intermediate form) (Figure 6, A) and the dimers further associate to form HBc particles. The assembled particles are shown to form two different sized particles of 34 and 30 nm in diameter and correspond to a triangulation number T=4 and T=3 packings, containing 120 dimers (240 monomers) and 90 dimers (180 monomers), respectively. The T=4 capsid structure of HBc particle is shown in Figure 6, B. The major immunodominant loop region (ILR) in each monomer, which is the preferred region for inserting antigenic sequences, is highlighted in Figure 6. The insertion of antigenic sequences is done using chemical coupling to the ILR [78] or recombinantly fused to replace the ILR.

The examples of HBc particle based novel vaccines include *malaria vaccine* which is in the phase I clinical trial [79, 80] and the *universal vaccine for Influenza A virus* [81, 82].

Ferritin protein cage based antigen display system

Recently, Carter and co-workers showed that ferritin protein cages can be used as an alternative '*repetitive antigen display system*' to HBc particles [83]. They fused the HIV-tat peptide to the N-terminus of the monomer and expressed as a fusion protein in *E.coli*. After expression, purification and assembly the resultant chimeric particles are shown to elicit a potent antibody mediated immune (humoral) response.

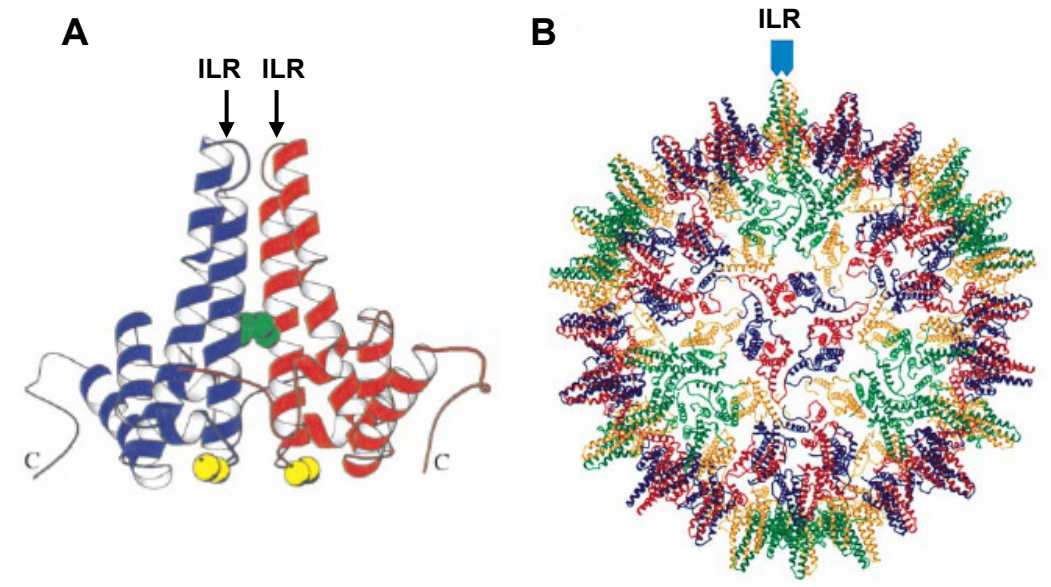

Figure 6. (**A**) Dimer unit of Hepatitis B-virus core (HBc) particles. Two monomers are depicted in blue and red color, respectively. Cys-61, which forms a disulfide bridge between the two monomers, is shown in green, and Cys-48, which does not form disulfides, in yellow. The C-terminal regions provide most of the interdimer interactions that build the particles. Major immunodominant loop region (ILR) in each monomer is highlighted. (**B**) T=4 HBc particle viewed along the icosahedral three-fold axis. Four independent monomers A, B, C and D in the particles are shown in green, yellow, red and blue, respectively. In the particle, the immunodominant loop region (ILR) from two monomers is highlighted. Reproduced from [77, 84], with permission from Elsevier.

De novo designed nanoscale bioassemblies through self-assembly of peptides and proteins

Rajagopal and Schneider [85] review the molecular self-assembly using peptide and proteins as monomeric building blocks with the following words "As early as 1981, Eric Drexler [86] proposed that protein design could be used to fabricate devices through a 'bottom-up' approach, in which proteins are used as monomeric building blocks for the fabrication of higher order structures via self-assembly. Peptides and proteins are particularly attractive as building blocks because a great deal is known about their folding and stability, and rules governing protein–protein interactions are actively being established.

Based on this knowledge, the field of *de novo* design emerged and tests our expertise in answering the simple question: can one build structural and functional proteins from first principles? To date, most *de novo* design efforts have centered on self-assembled proteinaceous structures of finite size. However, the design principles established from these endeavors are now being extended to the fabrication of larger nanoscale devices and materials. The challenge is twofold: first, to rationally design building blocks amenable to self-assembly that form nanostructured materials and, next, to impart desired functionality. Functionality can arise from either the extremely small feature sizes inherent to the material, such as those needed for photonics applications, or the incorporation of specific functional molecules into the self-assembled scaffold. In the following section, we will see examples of designed nanoscale bioassemblies through self-assembly of peptides and their applications".

Peptide nanotubes (cyclic peptide)

Martin and Kohli [87] review the field of peptide based nanotubes with the following words "In 1993, Ghadiri and co-workers described a fascinating class of nanotubes that are based on cyclic peptide molecules that consist of an even number of alternating D- and L-amino acids. They showed that these molecules self-assemble through 'hydrogen-bonding' interactions into nanotubes, which in turn self-assemble into ordered parallel arrays of nanotubes [88] (Figure 7).

The number of amino acid residues in the ring determines the inside diameter of the nanotubes obtained; as an example, a 12-aminoacid ring produces nanotubes with an inside diameter of 1.3 nm. The chemical functional groups on the outside of the walls of these nanotubes can be varied by varying the amino-acid composition of the ring.

Ghadiri and colleagues have shown a number of biomedical/biotechnological applications for these nanotubes. Perhaps the most interesting is as a new class of antibiotics against bacterial pathogens. Fernadanez-Lopez et al. [89] showed that cyclic peptides comprising six and eight amino acid residues act preferentially on both Gram-positive and Gram-negative bacteria relative to mammalian cells. These data indicate that nanotubes formed from these peptides insert into the cell wall of the bacterium, which results in rapid cell death. Ghadiri and colleagues have also shown that these nanotubes can function as artificial ion channels in lipid bilayer membranes by self-assembling across the membrane [90], and ion-transport rates comparable to those of naturally occurring ion channels were observed".

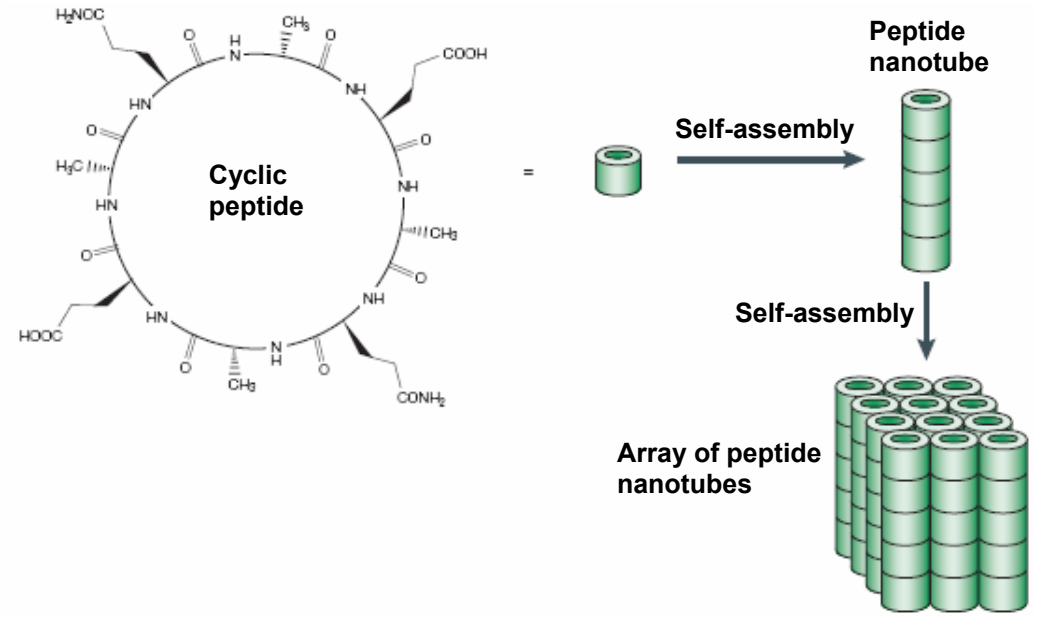

Figure 7. A typical chemical structure of cyclic peptide and schematic representation of the self-assembly of such peptides into nanotubes and nanotube arrays. Reproduced from [87], with permission from Nature publishing Group.

Peptide nanofibers (ionic self complementary peptide)

Zhang and co-workers fabricated nanofibers that are based on linear peptide molecules that consist of an even number of alternating hydrophobic and hydrophilic amino acids (natural L-amino acids) [91-93]. They showed that these molecules form β-sheet structures in solution with two distinct surfaces-one hydrophilic, the other hydrophobic and self-assemble through 'complementary ionic interactions' between the charged residues to form nanofibers (Figure 8). The nanofibers was shown to form interwoven matrices that further form hydrogel with very high water content, >99.5% (Figure 8).

The hydrogel matrix formed by the peptide nanofibers was shown to be a good biological material for cell cultures in 3D environment [94]. Thus, providing the first *de-novo* designed scaffolds for three-dimensional cell culture, with potential implications for basic studies of cell growth, applied studies in tissue engineering and, ultimately, regenerative medicine.

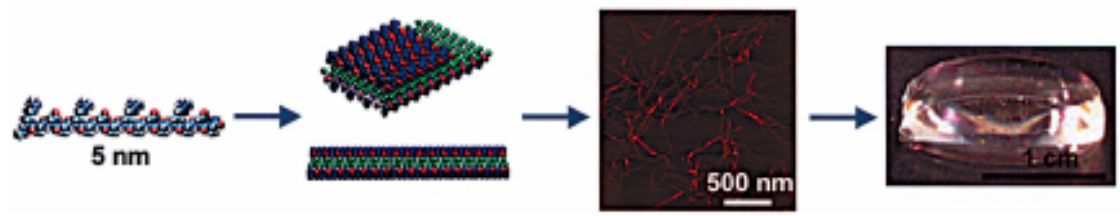

Figure 8. The self-assembly process of ionic self-complementary peptide which is <5 nm in size, with an alternating polar and nonpolar pattern. The peptides form stable β-strand and β-sheet structures; thus, the side chains partition into two sides, one polar and the other nonpolar. They undergo self-assembly to form nanofibers with the nonpolar residues inside (green), and + (blue) and – (red) charged residues form complementary ionic interactions, like a checkerboard. These nanofibers form interwoven matrices that further form a scaffold hydrogel with very high water content, >99.5%. Reproduced from [20], with permission from Nature Publishing Group.

For detailed examples of *de novo* designed nanoscale bioassemblies based on self assembly of peptides and proteins, we will refer the readers to the review by Zhang and co-workers [20].

Power of symmetry in design of nanoscale bioassemblies

Yeates and co-workers work

The use of symmetry as a powerful tool for building large regular objects was considered in detail by Yeates and co-workers [95]. Yeates and co-workers described a general strategy for designing proteins that self-assemble into large symmetrical nanomaterials, including protein cages, filaments, layers and porous materials. In this strategy one molecule of protein A, which naturally forms a self-assembling oligomer (m), is fused rigidly to one molecule of protein B, which forms another self-assembling oligomer (n). The result is a fusion protein, A-B, which self assembles with other identical copies of itself into a designed nanohedral particle or material (Figure 9, A). What kind of assembly will result depends on the geometric relationship between the oligomeric components once they are fused.

To join the two oligomeric proteins in a relatively rigid fashion, Yates and co-workers introduced the following method. They first of all choose the oligomeric domains whose three-dimensional structures are known and which begin or end in α-helices. Then the two oligomeric domains were fused by genetically engineering a connecting segment that strongly prefers the α-helical conformation. By doing so, they ensured that the continuous α-helix extending from one oligomerization domain into another provides the rigidity and directionality and also the required geometric relationship between the two oligomeric domains (Figure 9, B). They also presented 'construction rules' for creating symmetric nanomaterials from dimeric and trimeric oligomerization domains (for details refer to [95]).

However, Yeates and co-workers design was largely restricted to protein oligomers with highly specific geometrical requirements, i.e. one helix of one oligomer has to be extended into the other oligomer in a unique angle. Only a few such combinations of given protein oligomers are suitable for proper nanoparticle formation using their design principles.

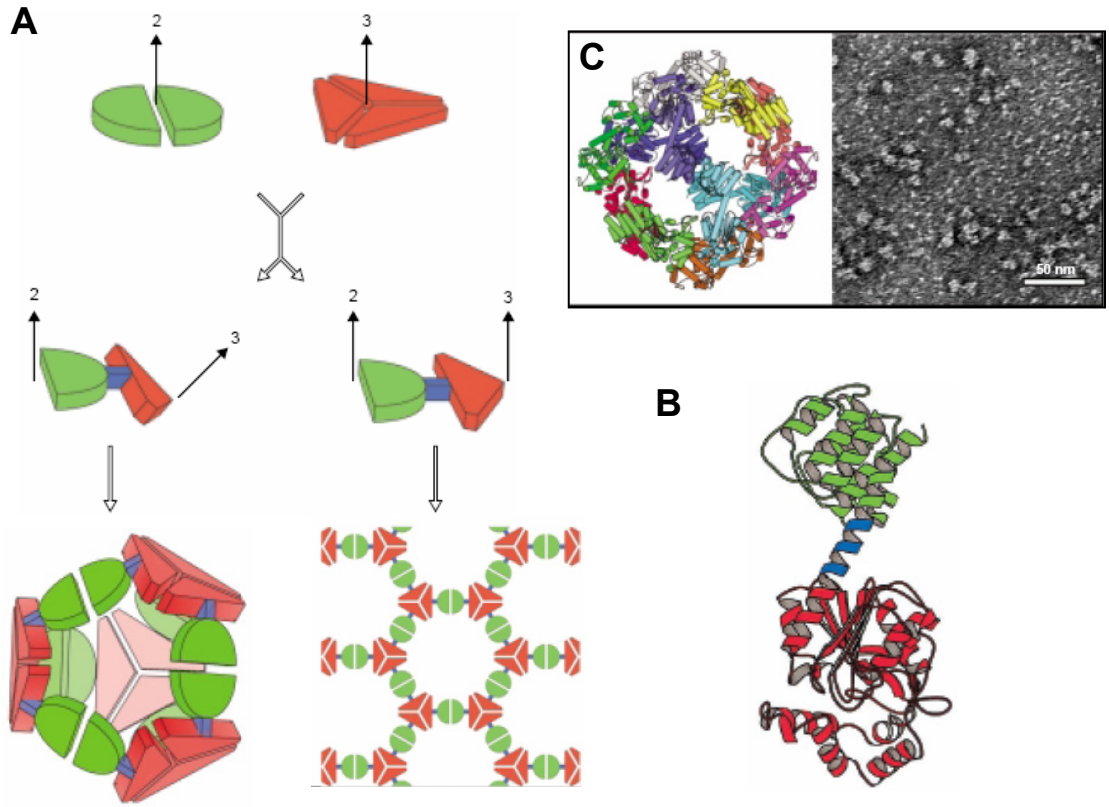

Figure 9. A general strategy for creating various regular protein assemblies by genetically fusing two naturally oligomeric proteins. (**A**) a dimeric protein (green) is fused to a trimeric protein (red) in an arrangement controlled by an α-helical linker (blue). 2 and 3 represent the 2-fold and 3-fold rotation axis. Different choices of dimeric and trimeric proteins, combined with varied helical linker lengths, lead to different geometries of the symmetry axes (arrows) carried by the component oligomerization domains. Depending on the geometry of the symmetry axes, different fusion proteins self-assemble into different regular complexes. A tetrahedral shaped protein cage and a two-dimensional hexagonal layer are illustrated. (**B**) A ribbon diagram of a fusion protein showing one method for joining two oligomerization domains (red and green) in a relatively rigid fashion. α-helical linker region which extend from one oligomeric domain to another is highlighted in blue. (**C**) A molecular model and experimentally observed EM picture of tetrahedral shaped protein cage are shown. Reproduced from [95, 96], with permission from Elsevier and Copyright (2001) National Academy of Sciences, U.S.A.

Our Design

Virus capsid and capsid like protein cages are finding variety of applications in the field of nanomedicine as we have seen before in the introduction. Here, we describe that it is possible to imitate virus capsid to design *de novo* protein or peptide that is able to self-assemble into icosahedral (or dodecahedral) shell structures. Our design strategy is more novel and flexible when compared to the work of Yeates and co-workers [95].

Design principle

Remarkably, many small viruses are composed of a single polypeptide chain assembling into a capsid structure with icosahedral symmetry. A T=1 icosahedron is built of 60 identical protein subunits (asymmetric units) and is the largest closed shell in which every subunit is in an equivalent environment. It is characterized by 2-fold, 3-fold and 5-fold rotational symmetry axes (Figure 10, A). By superposition of different protein oligomerization domains onto the corresponding symmetry axes of the icosahedron and by applying the symmetry elements, a nanoparticle with icosahedral symmetry can be designed (Figure 10, B and C).

Design strategy

Peter Burkhard [97] describes our design strategy with the following words "Monomer of peptidic oligomerization domain D1, which is a synthetic or natural peptide having a tendency to form oligomers of m subunits D1, $(D1)_m$, is linked by a linker (L) to the monomer of peptidic oligomerization domain D2, which is a another synthetic or natural peptide having a tendency to form oligomers of n subunits D2, $(D2)_n$. The result is a continuous peptide chain (D1-L-D2). The linker (L) is usually two glycine residues (GG) to provide the flexibility between the two domains.

The continuous peptide chain based on the oligomeric state of D1 and D2, is superpositioned onto the corresponding symmetry axes of the icosahedron (Figure 10, B). By applying the symmetry elements along the 5-fold, 3-fold and 2-fold rotational axes of the icosahedron, the peptide chain (D1-L-D2) self assembles with other identical copies of itself into a designed icosahedral shaped nanoparticle (Figure 10, C)".

Preferred oligomerization domains in our design

In our designs, we used the well studied protein oligomerization motif '*α-helical coiled-coils*' [98], as the peptidic oligomerization domains (for details on design and results refer to chapter 1 of this thesis). Also, by using molecular modeling and simulation programs, we designed coiled-coil oligomerization domains in combination with other well studied oligomerization domains such as foldon domain of T4 phage fibritin protein [99] (for details on design and results refer to chapter 3 of this thesis).

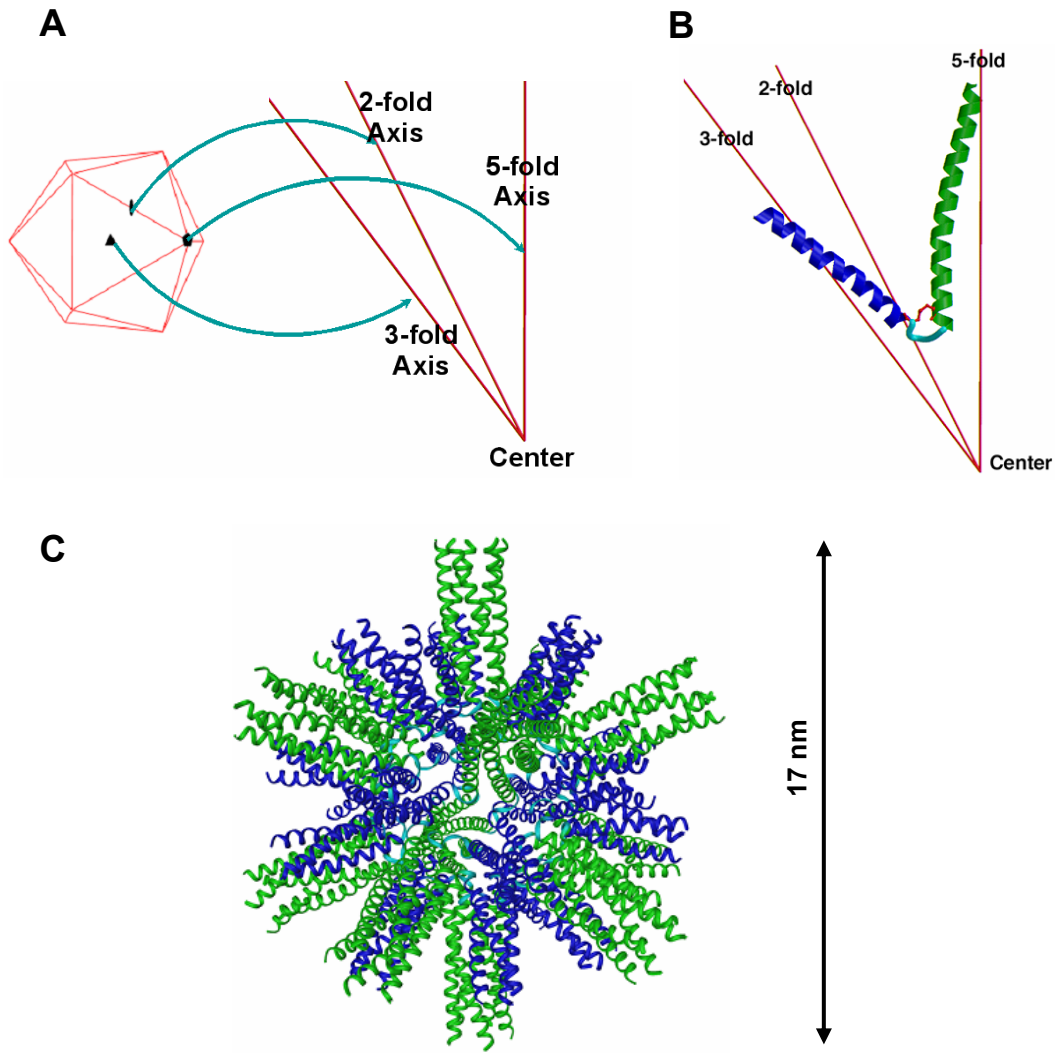

Figure 10. Design of peptide based icosahedral nanoparticles. (**A**) A simple T=1 icosahedron of virus capsid with highlighted rotational symmetry elements 5-fold, 3-fold and 2-fold. On the right side, the three symmetry axes (5-fold, 3-fold and 2-fold) are drawn by extending from the centre of the icosahedron. (**B**) A pentameric oligomerization domain (green) and trimeric oligomerization domain (blue) joined by a linker (turquoise) is superpositioned onto the corresponding symmetry axes of the icosahedron. (**C**) Applying the symmetry elements of the icosahedron to the peptide chain of figure **B** generates an artificial nanoparticle with icosahedral symmetry. The diameter of the designed particle is calculated to be 17 nm.

Coiled-coils an introduction:

The α-helical coiled-coil structural motif mediates subunit oligomerization of a large number of proteins [100]. Predictions based on primary sequence analyses suggest that roughly 2-3% of all protein residues form coiled-coils [101].

Yu, YB [102] describes the characteristic features of coiled-coils as follows: “Coiled-coils consist of two to five amphipathic right-handed α-helices that twist around one another to form a left-handed supercoil. Sequences of parallel left-handed coiled-coils are characterized by a 7-residue periodicity ("heptad" repeat) and it is conventionally denoted as *a-b-c-d-e-f-g*. Positions *a* and *d* are often occupied by hydrophobic residues and positions *e* and *g* are often occupied by charged residues. Such distribution of amino acid residues makes the helices amphipathic with residues *a* and *d* forming the inter-helical hydrophobic core and the residues at *e* and *g* forming inter-helical ionic interactions”. For example, the arrangement of residues in parallel left-handed dimeric coiled-coil is illustrated by the helical-wheel diagram, as shown in Figure 11.

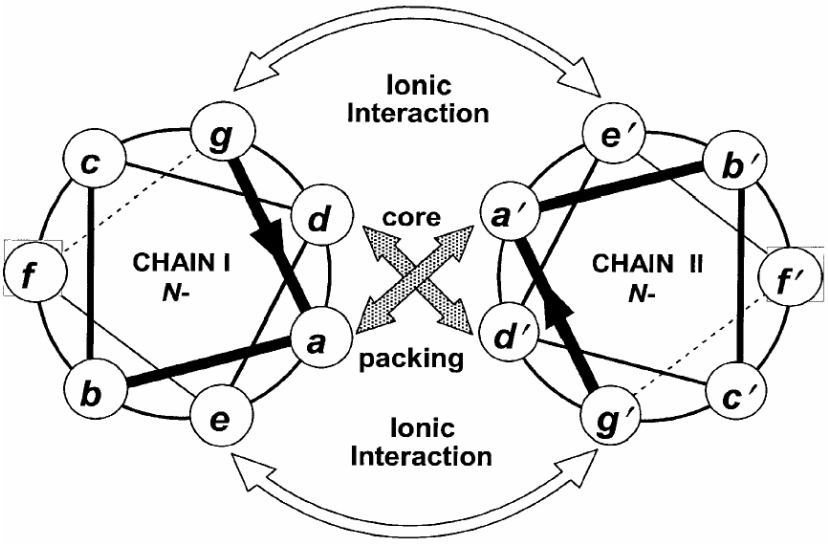

Figure 11. Helical-wheel diagram of a parallel left-handed dimeric coiled-coil, showing the helical cross section. The seven positions in each heptad are labeled a-b-c-d-e-f-g. The core hydrophobic interactions and the ionic interactions between the two helices are highlighted. Reproduced from [102], with permission from Elsevier.

Stability of coiled-coils is mainly achieved by a distinctive ‘knobs-into-holes’ packing of the hydrophobic side chains into a hydrophobic core, which was first postulated by Crick [103]. However, sometimes even relatively long polypeptides derived from stable coiled-coil domains fail to associate into coiled-coils. In this context, it has been shown that distinct coiled-coil ‘trigger sites’ within heptad repeat containing amino acid sequences might be necessary to mediate coiled-coil formation [104, 105].

As a hallmark, the coiled-coil trigger site of the actin-bundling protein cortexillin I contains a distinct inter- and intra-helical salt bridge pattern, which includes charged residues even at core positions [106].Other results also suggest that the ionic interactions contribute considerably to stability of coiled coils [107-109], thereby modulating assembly of coiled coils in a pH-dependent manner [110, 111].

Why coiled-coils in our design:

- The symmetry elements of virus capsid (5-fold, 3-fold and 2-fold) can be found in coiled-coils as it exists as a dimer, trimer, tetramer and pentamer. Some of the best studied examples are the GCN4 leucine zipper [112], fibritin [99], tetrabrachion [113] and Cartilage Oligomeric Matrix Protein (COMP) [114], representing dimeric, trimeric, tetrameric and penatmeric coiled-coils, respectively.
- Design principles of coiled-coils are well studied and understood [115].
- Moreover, based on the work done in our laboratory regarding coiled-coils design and analysis. Peter Burkhard summarizes the work done in our lab regarding coiled-coils with the following words "in our lab starting from the structure determination of the coiled-coil trigger site of cortexillin [106] and of intermediate filaments [116], and other coiled-coil proteins [117, 118] including the analysis of coiled-coil geometries and interactions [119], we have gradually improved our protein *de novo* design of coiled-coils. Minimal protein oligomerization domains based on coiled-coils as building blocks have been optimized using a combination of structural biology, biophysics and computational approaches [108, 120]. Based on the knowledge obtained from these studies we have progressed into the design of peptide nanoparticles of smaller in sizes [109]".

Possible applications of our design in the field of nanomedicine

Peptide based nanoparticles as multifunctional bionanoparticles (BNPs)

Peter Burkhard describes the promising applications of our peptide based nanoparticles as follows: "Peptide nanoparticles can be functionalized in several ways (Figure 12): (1) At either end (N- or C-terminus) the peptide chain can be extended with peptide sequences of a particular function like targeting peptides, cell penetrating peptides, nuclear localization sequences or epitopes from a pathogen. Furthermore, specific dyes, chelators (for binding of radionuclides), or drugs can covalently be attached to the peptide. The high density of ligands or dyes will significantly increase the avidity for the specific receptor or the signal-to-noise ratio in imaging applications. (2) The central cavity of the nanoparticle with a calculated diameter of about 6 nm is ideally suited for the encapsulation of quantum dots. For example, SeCd nanocrystals can be used as highly efficient fluorescence probes, gold nanoparticles as contrasting agents for electron microscopy and iron nanoparticles as probes for NMR imaging. (3) The cavity of the pentameric coiled-coil domain allows to incorporate small hydrophobic molecules like Vitamin D or Vitamin B12 [121].

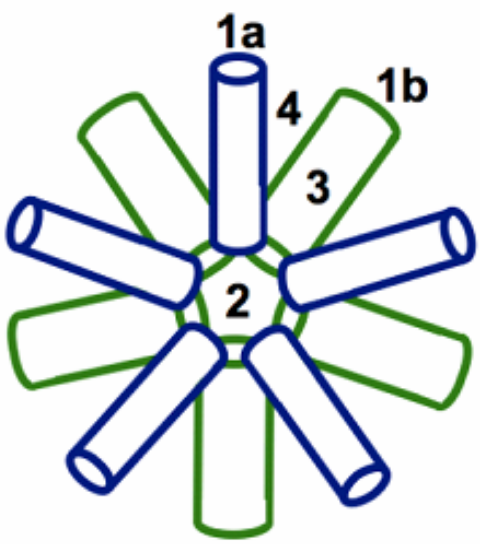

Figure 12. Schematic diagram of the peptide nanoparticles with possible modification sites. The blue and green represents the trimeric and pentameric coiled-coil domain, respectively. Explanations for the specified numbers refer to text.

(4) Finally, the trimeric coiled-coil can be modified to allow binding of nucleic acids (like the trimeric coiled-coil of the macrophage scavenger receptor) and ultimately a gene delivery system can be engineered. By co-assembly of peptide chains with different modifications multifunctional nanoparticles can be engineered for a wide variety of medical applications".

In particular, peptide nanoparticles can be used as repetitive antigen display platform for synthetic vaccine design. The geometry of the nanoparticles and their resemblance to small virus capsids will trigger a strong immune response - a concept that is now increasingly exploited for producing novel vaccines that yield high titers of specific antibodies [46].

Our peptide nanoparticles eliminate the need for virus-based designs, and allow for high flexibility in vaccine design. Epitopes of any pathogen can readily be engineered onto the surface of the nanoparticle, thus allowing for the easy generation of a whole variety of different vaccines. Especially, enveloped viruses (e.g. HIV, influenza, Ebola, SARS, etc.) represent an ideal target as their surface proteins are characterized by trimeric coiled-coil proteins, which are also building blocks of our nanoparticles. Therefore, by simply extending the trimeric coiled-coil domain of peptide nanoparticles with the virus specific trimeric coiled-coil, an ideal repetitive antigen display system against enveloped viruses can be developed.

In essence the characteristic features of our system can be summarized as follows:

- **Ease of handling** in terms of protein expression (*E.coli*), protein purification and storage, hence leading to low production costs (for details on recombinant production of peptide nanoparticles refer to chapter 2A of this thesis).
- **Biocompatible and biodegradable**, as our system is made up of peptide as the building blocks.
- Our system because of its repetitive nature can be used as a '**repetitive antigen display system**' alternative to virus like particles (VLPs). Specifically, a **non-viral based carrier system** (for details on design and results refer to chapter 2B of this thesis).
- As a carrier for presenting epitopes, our system represents an **ideal candidate for the presentation of trimeric coiled-coil B-cell epitopes**, which might prove to be an efficient vaccination strategy against enveloped viruses.

References

1. Lehn, J.M. (1993). Supramolecular chemistry. Science *260*, 1762-1763.

2. Leroy, B.J., Lemay, S.G., Kong, J., and Dekker, C. (2004). Electrical generation and absorption of phonons in carbon nanotubes. Nature *432*, 371-374.

3. West, J.L., and Halas, N.J. (2003). Engineered nanomaterials for biophotonics applications: improving sensing, imaging, and therapeutics. Annu Rev Biomed Eng *5*, 285-292.

4. Yang, H., and Kao, W.J. (2006). Dendrimers for pharmaceutical and biomedical applications. J Biomater Sci Polym Ed *17*, 3-19.

5. Miller, A.D. (2004). Nonviral liposomes. Methods Mol Med *90*, 107-137.

6. Weng, J., and Ren, J. (2006). Luminescent quantum dots: a very attractive and promising tool in biomedicine. Curr Med Chem *13*, 897-909.

7. Hardman, R. (2006). A toxicologic review of quantum dots: toxicity depends on physicochemical and environmental factors. Environ Health Perspect *114*, 165-172.

8. Feynman, R. (1960). There's plenty of room at the bottom. Engineering and Science, 22-36.

9. McNeil, S.E. (2005). Nanotechnology for the biologist. J Leukoc Biol *78*, 585-594.

10. Quintana, A., Raczka, E., Piehler, L., Lee, I., Myc, A., Majoros, I., Patri, A.K., Thomas, T., Mule, J., and Baker, J.R., Jr. (2002). Design and function of a dendrimer-based therapeutic nanodevice targeted to tumor cells through the folate receptor. Pharm Res *19*, 1310-1316.

11. Wang, S.J., Brechbiel, M., and Wiener, E.C. (2003). Characteristics of a new MRI contrast agent prepared from polypropyleneimine dendrimers, generation 2. Invest Radiol *38*, 662-668.

12. Bergey, E.J., Levy, L., Wang, X.P., Krebs, L.J., Lal, M., Kim, K.S., Pakatchi, S., Liebow, C., and Prasad, P.N. (2002). DC magnetic field induced magnetocytolysis of cancer cells targeted by LH-RH magnetic nanoparticles in vitro. Biomed Microdevices *4*, 293-299.

13. Jirak, D., Kriz, J., Herynek, V., Andersson, B., Girman, P., Burian, M., Saudek, F., and Hajek, M. (2004). MRI of transplanted pancreatic islets. Magn Reson Med *52*, 1228-1233.

14. Hirsch, L.R., Stafford, R.J., Bankson, J.A., Sershen, S.R., Rivera, B., Price, R.E., Hazle, J.D., Halas, N.J., and West, J.L. (2003). Nanoshell-mediated near-infrared thermal therapy of tumors under magnetic resonance guidance. Proc Natl Acad Sci U S A *100*, 13549-13554.

15. Reszka, R.C., Jacobs, A., and Voges, J. (2005). Liposome-mediated suicide gene therapy in humans. Methods Enzymol *391*, 200-208.

16. ten Hagen, T.L. (2005). Liposomal cytokines in the treatment of infectious diseases and cancer. Methods Enzymol *391*, 125-145.

17. Zhu, S., Oberdorster, E., and Haasch, M.L. (2006). Toxicity of an engineered nanoparticle (fullerene, C60) in two aquatic species, Daphnia and fathead minnow. Mar Environ Res *62 Suppl*, S5-9.

18. Warheit, D.B., Laurence, B.R., Reed, K.L., Roach, D.H., Reynolds, G.A., and Webb, T.R. (2004). Comparative pulmonary toxicity assessment of single-wall carbon nanotubes in rats. Toxicol Sci *77*, 117-125.

19. Whitesides, G.M., and Grzybowski, B. (2002). Self-assembly at all scales. Science *295*, 2418-2421.

20. Zhang, S. (2003). Fabrication of novel biomaterials through molecular self-assembly. Nat Biotechnol *21*, 1171-1178.

21. Georgens, C., Weyermann, J., and Zimmer, A. (2005). Recombinant virus like particles as drug delivery system. Curr Pharm Biotechnol *6*, 49-55.

22. May, T., Gleiter, S., and Lilie, H. (2002). Assessment of cell type specific gene transfer of polyoma virus like particles presenting a tumor specific antibody Fv fragment. J Virol Methods *105*, 147-157.

23. Kramer, R.M., Li, C., Carter, D.C., Stone, M.O., and Naik, R.R. (2004). Engineered protein cages for nanomaterial synthesis. J Am Chem Soc *126*, 13282-13286.

24. Ensign, D., Young, M., and Douglas, T. (2004). Photocatalytic synthesis of copper colloids from CuII by the ferrihydrite core of ferritin. Inorg Chem *43*, 3441-3446.

25. Hosein, H.A., Strongin, D.R., Allen, M., and Douglas, T. (2004). Iron and cobalt oxide and metallic nanoparticles prepared from ferritin. Langmuir *20*, 10283-10287.

26. Flenniken, M.L., Willits, D.A., Brumfield, S., Young, M.J., and Douglas, T. (2003). The Small Heat Shock Protein Cage from *Methanococcus jannaschii* Is a Versatile Nanoscale Platform for Genetic and Chemical Modification. Nano Lett *3*, 1573-1576.

27. Flenniken, M.L., Liepold, L.O., Crowley, B.E., Willits, D.A., Young, M.J., and Douglas, T. (2005). Selective attachment and release of a chemotherapeutic agent from the interior of a protein cage architecture. Chem Commun (Camb), 447-449.

28. Flenniken, M.L., Willits, D.A., Harmsen, A.L., Liepold, L.O., Harmsen, A.G., Young, M.J., and Douglas, T. (2006). Melanoma and lymphocyte cell-specific targeting incorporated into a heat shock protein cage architecture. Chem Biol *13*, 161-170.

29. Seebeck, F.P., Woycechowsky, K.J., Zhuang, W., Rabe, J.P., and Hilvert, D. (2006). A simple tagging system for protein encapsulation. J Am Chem Soc *128*, 4516-4517.

30. Paavola, C.D., Chan, S.L., Li, Y., Mazzarella, K.M., McMillan, R.A., and Trent, J.D. (2006). A versatile paltform for nanotechnology based on circular permutation of a chaperonin protein. Nanotechnology *17*, 1171-1176.

31. Kerfeld, C.A., Sawaya, M.R., Tanaka, S., Nguyen, C.V., Phillips, M., Beeby, M., and Yeates, T.O. (2005). Protein structures forming the shell of primitive bacterial organelles. Science *309*, 936-938.

32. Lee, L.A., and Wang, Q. (2006). Adaptations of nanoscale viruses and other protein cages for medical applications. Nanomedicine *2*, 137-149.

33. Brumfield, S., Willits, D., Tang, L., Johnson, J.E., Douglas, T., and Young, M. (2004). Heterologous expression of the modified coat protein of Cowpea chlorotic mottle bromovirus results in the assembly of protein cages with altered architectures and function. J Gen Virol *85*, 1049-1053.

34. Klem, M.T., Willits, D., Young, M., and Douglas, T. (2003). 2-D array formation of genetically engineered viral cages on au surfaces and imaging by atomic force microscopy. J Am Chem Soc *125*, 10806-10807.

35. Wang, Q., Raja, K.S., Janda, K.D., Lin, T., and Finn, M.G. (2003). Blue fluorescent antibodies as reporters of steric accessibility in virus conjugates. Bioconjug Chem *14*, 38-43.

36. Singh, P., Gonzalez, M.J., and Manchester, M. (2006). Viruses and Their Uses in Nanotechnology. Drug Dev Res *67*, 23-41.

37. Brown, W.L., Mastico, R.A., Wu, M., Heal, K.G., Adams, C.J., Murray, J.B., Simpson, J.C., Lord, J.M., Taylor-Robinson, A.W., and Stockley, P.G. (2002). RNA bacteriophage capsid-mediated drug delivery and epitope presentation. Intervirology *45*, 371-380.

38. Chatterji, A., Ochoa, W., Shamieh, L., Salakian, S.P., Wong, S.M., Clinton, G., Ghosh, P., Lin, T., and Johnson, J.E. (2004). Chemical conjugation of heterologous proteins on the surface of Cowpea mosaic virus. Bioconjug Chem *15*, 807-813.

39. Wang, Q., Kaltgrad, E., Lin, T., Johnson, J.E., and Finn, M.G. (2002). Natural supramolecular building blocks. Wild-type cowpea mosaic virus. Chem Biol *9*, 805-811.

40. Wang, Q., Lin, T., Johnson, J.E., and Finn, M.G. (2002). Natural supramolecular building blocks. Cysteine-added mutants of cowpea mosaic virus. Chem Biol *9*, 813-819.

41. Wang, Q., Lin, T., Tang, L., Johnson, J.E., and Finn, M.G. (2002). Icosahedral virus particles as addressable nanoscale building blocks. Angew Chem Int Ed Engl *41*, 459-462.

42. Raja, K.S., Wang, Q., Gonzalez, M.J., Manchester, M., Johnson, J.E., and Finn, M.G. (2003). Hybrid virus-polymer materials. 1. Synthesis and properties of PEG-decorated cowpea mosaic virus. Biomacromolecules *4*, 472-476.

43. Strable, E., Johnson, J.E., and Finn, M.G. (2004). Natural Nanochemical Building Blocks:Icosahedral Virus Particles Organized by Attached Oligonucleotides. Nano Lett *4*, 1385-1389.

44. Chatterji, A., Burns, L.L., Taylor, S.S., Lomonossoff, G.P., Johnson, J.E., Lin, T., and Porta, C. (2002). Cowpea mosaic virus: from the presentation of antigenic peptides to the display of active biomaterials. Intervirology *45*, 362-370.

45. Raja, K.S., Wang, Q., and Finn, M.G. (2003). Icosahedral virus particles as polyvalent carbohydrate display platforms. Chembiochem *4*, 1348-1351.

46. Lechner, F., Jegerlehner, A., Tissot, A.C., Maurer, P., Sebbel, P., Renner, W.A., Jennings, G.T., and Bachmann, M.F. (2002). Virus-like particles as a modular system for novel vaccines. Intervirology *45*, 212-217.

47. Chasteen, N.D., and Harrison, P.M. (1999). Mineralization in ferritin: an efficient means of iron storage. J Struct Biol *126*, 182-194.

48. Lawson, D.M., Artymiuk, P.J., Yewdall, S.J., Smith, J.M., Livingstone, J.C., Treffry, A., Luzzago, A., Levi, S., Arosio, P., Cesareni, G., and et al. (1991). Solving the structure of human H ferritin by genetically engineering intermolecular crystal contacts. Nature *349*, 541-544.

49. Douglas, T., and Stark, V.T. (2000). Nanophase cobalt oxyhydroxide mineral synthesized within the protein cage of ferritin. Inorg Chem *39*, 1828-1830.

50. Okuda, M., Iwahori, K., Yamashita, I., and Yoshimura, H. (2003). Fabrication of nickel and chromium nanoparticles using the protein cage of apoferritin. Biotechnol Bioeng *84*, 187-194.

51. Ueno, T., Suzuki, M., Goto, T., Matsumoto, T., Nagayama, K., and Watanabe, Y. (2004). Size-selective olefin hydrogenation by a Pd nanocluster provided in an apo-ferritin cage. Angew Chem Int Ed Engl *43*, 2527-2530.

52. Smith, A.E., Lilie, H., and Helenius, A. (2003). Ganglioside-dependent cell attachment and endocytosis of murine polyomavirus-like particles. FEBS Lett *555*, 199-203.

53. Caruso, M., Belloni, L., Sthandier, O., Amati, P., and Garcia, M.I. (2003). Alpha4beta1 integrin acts as a cell receptor for murine polyomavirus at the postattachment level. J Virol *77*, 3913-3921.

54. Yamada, T., Ueda, M., Seno, M., Kondo, A., Tanizawa, K., and Kuroda, S. (2004). Novel tissue and cell type-specific gene/drug delivery system using surface engineered hepatitis B virus nano-particles. Curr Drug Targets Infect Disord *4*, 163-167.

55. Yu, D., Amano, C., Fukuda, T., Yamada, T., Kuroda, S., Tanizawa, K., Kondo, A., Ueda, M., Yamada, H., Tada, H., and Seno, M. (2005). The specific delivery of proteins to human liver cells by engineered bio-nanocapsules. Febs J *272*, 3651-3660.

56. Shin, Y.C., and Folk, W.R. (2003). Formation of polyomavirus-like particles with different VP1 molecules that bind the urokinase plasminogen activator receptor. J Virol *77*, 11491-11498.

57. Abbing, A., Blaschke, U.K., Grein, S., Kretschmar, M., Stark, C.M., Thies, M.J., Walter, J., Weigand, M., Woith, D.C., Hess, J., and Reiser, C.O. (2004). Efficient intracellular delivery of a protein and a low molecular weight substance via recombinant polyomavirus-like particles. J Biol Chem *279*, 27410-27421.

58. Rae, C.S., Khor, I.W., Wang, Q., Destito, G., Gonzalez, M.J., Singh, P., Thomas, D.M., Estrada, M.N., Powell, E., Finn, M.G., and Manchester, M. (2005). Systemic trafficking of plant virus nanoparticles in mice via the oral route. Virology *343*, 224-235.

59. Soto, C.M., Blum, A.S., Vora, G.J., Lebedev, N., Meador, C.E., Won, A.P., Chatterji, A., Johnson, J.E., and Ratna, B.R. (2006). Fluorescent signal amplification of carbocyanine dyes using engineered viral nanoparticles. J Am Chem Soc *128*, 5184-5189.

60. Lewis, J.D., Destito, G., Zijlstra, A., Gonzalez, M.J., Quigley, J.P., Manchester, M., and Stuhlmann, H. (2006). Viral nanoparticles as tools for intravital vascular imaging. Nat Med *12*, 354-360.

61. Dintzis, H.M., Dintzis, R.Z., and Vogelstein, B. (1976). Molecular determinants of immunogenicity: the immunon model of immune response. Proc Natl Acad Sci U S A *73*, 3671-3675.

62. Dintzis, R.Z., Middleton, M.H., and Dintzis, H.M. (1983). Studies on the immunogenicity and tolerogenicity of T-independent antigens. J Immunol *131*, 2196-2203.

63. Bachmann, M.F., Rohrer, U.H., Kundig, T.M., Burki, K., Hengartner, H., and Zinkernagel, R.M. (1993). The influence of antigen organization on B cell responsiveness. Science *262*, 1448-1451.

64. Bachmann, M.F., Hengartner, H., and Zinkernagel, R.M. (1995). T helper cell-independent neutralizing B cell response against vesicular stomatitis virus: role of antigen patterns in B cell induction? Eur J Immunol *25*, 3445-3451.

65. Aebi, U., ten Heggeler, B., Onorato, L., Kistler, J., and Showe, M.K. (1977). New method for localizing proteins in periodic structures: Fab fragment labeling combined with image processing of electron micrographs. Proc Natl Acad Sci U S A *74*, 5514-5518.

66. Buhle, E.L., Jr., and Aebi, U. (1984). Specific labeling of protein domains with antibody fragments. J Ultrastruct Res *89*, 165-178.

67. Kistler, J., Aebi, U., Onorato, L., ten Heggeler, B., and Showe, M.K. (1978). Structural changes during the transformation of bacteriophage T4 polyheads: characterization of the initial and final states by freeze-drying and shadowing Fab-fragment-labelled preparations. J Mol Biol *126*, 571-589.

68. Baschong, W., Hasler, L., Haner, M., Kistler, J., and Aebi, U. (2003). Repetitive versus monomeric antigen presentation: direct visualization of antibody affinity and specificity. J Struct Biol *143*, 258-262.

69. Noad, R., and Roy, P. (2003). Virus-like particles as immunogens. Trends Microbiol *11*, 438-444.

70. Pumpens, P., Borisova, G.P., Crowther, R.A., and Grens, E. (1995). Hepatitis B virus core particles as epitope carriers. Intervirology *38*, 63-74.

71. Schirmbeck, R., Bohm, W., and Reimann, J. (1996). Virus-like particles induce MHC class I-restricted T-cell responses. Lessons learned from the hepatitis B small surface antigen. Intervirology *39*, 111-119.

72. Paliard, X., Liu, Y., Wagner, R., Wolf, H., Baenziger, J., and Walker, C.M. (2000). Priming of strong, broad, and long-lived HIV type 1 p55gag-specific CD8+ cytotoxic T cells after administration of a virus-like particle vaccine in rhesus macaques. AIDS Res Hum Retroviruses *16*, 273-282.

73. Koutsky, L.A., Ault, K.A., Wheeler, C.M., Brown, D.R., Barr, E., Alvarez, F.B., Chiacchierini, L.M., and Jansen, K.U. (2002). A controlled trial of a human papillomavirus type 16 vaccine. N Engl J Med *347*, 1645-1651.

74. Fehr, T., Skrastina, D., Pumpens, P., and Zinkernagel, R.M. (1998). T cell-independent type I antibody response against B cell epitopes expressed repetitively on recombinant virus particles. Proc Natl Acad Sci U S A *95*, 9477-9481.

75. Ulrich, R., Nassal, M., Meisel, H., and Kruger, D.H. (1998). Core particles of hepatitis B virus as carrier for foreign epitopes. Adv Virus Res *50*, 141-182.

76. Pumpens, P., and Grens, E. (1999). Hepatitis B core particles as a universal display model: a structure-function basis for development. FEBS Lett *442*, 1-6.

77. Pumpens, P., and Grens, E. (2001). HBV core particles as a carrier for B cell/T cell epitopes. Intervirology *44*, 98-114.

78. Jegerlehner, A., Tissot, A., Lechner, F., Sebbel, P., Erdmann, I., Kundig, T., Bachi, T., Storni, T., Jennings, G., Pumpens, P., Renner, W.A., and Bachmann, M.F. (2002). A molecular assembly system that renders antigens of choice highly repetitive for induction of protective B cell responses. Vaccine *20*, 3104-3112.

79. Birkett, A., Lyons, K., Schmidt, A., Boyd, D., Oliveira, G.A., Siddique, A., Nussenzweig, R., Calvo-Calle, J.M., and Nardin, E. (2002). A modified hepatitis B virus core particle containing multiple epitopes of the Plasmodium falciparum circumsporozoite protein provides a highly immunogenic malaria vaccine in preclinical analyses in rodent and primate hosts. Infect Immun *70*, 6860-6870.

80. Nardin, E.H., Oliveira, G.A., Calvo-Calle, J.M., Wetzel, K., Maier, C., Birkett, A.J., Sarpotdar, P., Corado, M.L., Thornton, G.B., and Schmidt, A. (2004). Phase I testing of a malaria vaccine composed of hepatitis B virus core particles expressing Plasmodium falciparum circumsporozoite epitopes. Infect Immun *72*, 6519-6527.

81. Fiers, W., De Filette, M., Birkett, A., Neirynck, S., and Min Jou, W. (2004). A "universal" human influenza A vaccine. Virus Res *103*, 173-176.

82. De Filette, M., Fiers, W., Martens, W., Birkett, A., Ramne, A., Lowenadler, B., Lycke, N., Jou, W.M., and Saelens, X. (2006). Improved design and intranasal delivery of an M2e-based human influenza A vaccine. Vaccine *24*, 6597-6601.

83. Li, C.Q., Soistman, E., and Carter, D.C. (2006). Ferritin nanoparticle technology A new platform for antigen presentation and vaccine development. Industrial Biotechnology *2*, 143-147.

84. Wynne, S.A., Crowther, R.A., and Leslie, A.G. (1999). The crystal structure of the human hepatitis B virus capsid. Mol Cell *3*, 771-780.

85. Rajagopal, K., and Schneider, J.P. (2004). Self-assembling peptides and proteins for nanotechnological applications. Curr Opin Struct Biol *14*, 480-486.

86. Drexler, K.E. (1981). Molecular engineering: An approach to the development of general capabilities for molecular manipulation. Proc Natl Acad Sci U S A *78*, 5275-5278.

87. Martin, C.R., and Kohli, P. (2003). The emerging field of nanotube biotechnology. Nat Rev Drug Discov *2*, 29-37.

88. Ghadiri, M.R., Granja, J.R., Milligan, R.A., McRee, D.E., and Khazanovich, N. (1993). Self-assembling organic nanotubes based on a cyclic peptide architecture. Nature *366*, 324-327.

89. Fernandez-Lopez, S., Kim, H.S., Choi, E.C., Delgado, M., Granja, J.R., Khasanov, A., Kraehenbuehl, K., Long, G., Weinberger, D.A., Wilcoxen, K.M., and Ghadiri, M.R. (2001). Antibacterial agents based on the cyclic D,L-alpha-peptide architecture. Nature *412*, 452-455.

90. Ghadiri, M.R., Granja, J.R., and Buehler, L.K. (1994). Artificial transmembrane ion channels from self-assembling peptide nanotubes. Nature *369*, 301-304.

91. Zhang, S., Holmes, T., Lockshin, C., and Rich, A. (1993). Spontaneous assembly of a self-complementary oligopeptide to form a stable macroscopic membrane. Proc Natl Acad Sci U S A *90*, 3334-3338.

92. Zhang, S., Holmes, T.C., DiPersio, C.M., Hynes, R.O., Su, X., and Rich, A. (1995). Self-complementary oligopeptide matrices support mammalian cell attachment. Biomaterials *16*, 1385-1393.

93. Holmes, T.C., de Lacalle, S., Su, X., Liu, G., Rich, A., and Zhang, S. (2000). Extensive neurite outgrowth and active synapse formation on self-assembling peptide scaffolds. Proc Natl Acad Sci U S A *97*, 6728-6733.

94. Zhang, S., Gelain, F., and Zhao, X. (2005). Designer self-assembling peptide nanofiber scaffolds for 3D tissue cell cultures. Semin Cancer Biol *15*, 413-420.

95. Padilla, J.E., Colovos, C., and Yeates, T.O. (2001). Nanohedra: using symmetry to design self assembling protein cages, layers, crystals, and filaments. Proc Natl Acad Sci U S A *98*, 2217-2221.

96. Yeates, T.O., and Padilla, J.E. (2002). Designing supramolecular protein assemblies. Curr Opin Struct Biol *12*, 464-470.

97. Burkhard, P. (2004). PCT patent application. *WO 2004/071493*.

98. Burkhard, P., Stetefeld, J., and Strelkov, S.V. (2001). Coiled coils: a highly versatile protein folding motif. Trends Cell Biol *11*, 82-88.

99. Tao, Y., Strelkov, S.V., Mesyanzhinov, V.V., and Rossmann, M.G. (1997). Structure of bacteriophage T4 fibritin: a segmented coiled coil and the role of the C-terminal domain. Structure *5*, 789-798.

100. Lupas, A.N., and Gruber, M. (2005). The structure of alpha-helical coiled coils. Adv Protein Chem *70*, 37-78.

101. Wolf, E., Kim, P.S., and Berger, B. (1997). MultiCoil: a program for predicting two- and three-stranded coiled coils. Protein Sci *6*, 1179-1189.

102. Yu, Y.B. (2002). Coiled-coils: stability, specificity, and drug delivery potential. Adv Drug Deliv Rev *54*, 1113-1129.

103. Crick, F.H.C. (1953). The packing of alpha-helices: simple coiled-coils. Acta Crystallogr *6*, 689-698.

104. Steinmetz, M.O., Stock, A., Schulthess, T., Landwehr, R., Lustig, A., Faix, J., Gerisch, G., Aebi, U., and Kammerer, R.A. (1998). A distinct 14 residue site triggers coiled-coil formation in cortexillin I. Embo J *17*, 1883-1891.

105. Frank, S., Lustig, A., Schulthess, T., Engel, J., and Kammerer, R.A. (2000). A distinct seven-residue trigger sequence is indispensable for proper coiled-coil formation of the human macrophage scavenger receptor oligomerization domain. J Biol Chem *275*, 11672-11677.

106. Burkhard, P., Kammerer, R.A., Steinmetz, M.O., Bourenkov, G.P., and Aebi, U. (2000). The coiled-coil trigger site of the rod domain of cortexillin I unveils a distinct network of interhelical and intrahelical salt bridges. Structure *8*, 223-230.

107. Spek, E.J., Bui, A.H., Lu, M., and Kallenbach, N.R. (1998). Surface salt bridges stabilize the GCN4 leucine zipper. Protein Sci *7*, 2431-2437.

108. Burkhard, P., Ivaninskii, S., and Lustig, A. (2002). Improving coiled-coil stability by optimizing ionic interactions. J Mol Biol *318*, 901-910.

109. Meier, M., Lustig, A., Aebi, U., and Burkhard, P. (2002). Removing an interhelical salt bridge abolishes coiled-coil formation in a de novo designed peptide. J Struct Biol *137*, 65-72.

110. Bullough, P.A., Hughson, F.M., Skehel, J.J., and Wiley, D.C. (1994). Structure of influenza haemagglutinin at the pH of membrane fusion. Nature *371*, 37-43.

111. Suzuki, K., Doi, T., Imanishi, T., Kodama, T., and Tanaka, T. (1997). The conformation of the alpha-helical coiled coil domain of macrophage scavenger receptor is pH dependent. Biochemistry *36*, 15140-15146.

112. O'Shea, E.K., Klemm, J.D., Kim, P.S., and Alber, T. (1991). X-ray structure of the GCN4 leucine zipper, a two-stranded, parallel coiled coil. Science *254*, 539-544.

113. Stetefeld, J., Jenny, M., Schulthess, T., Landwehr, R., Engel, J., and Kammerer, R.A. (2000). Crystal structure of a naturally occurring parallel right-handed coiled coil tetramer. Nat Struct Biol *7*, 772-776.

114. Malashkevich, V.N., Kammerer, R.A., Efimov, V.P., Schulthess, T., and Engel, J. (1996). The crystal structure of a five-stranded coiled coil in COMP: a prototype ion channel? Science *274*, 761-765.

115. Woolfson, D.N. (2005). The design of coiled-coil structures and assemblies. Adv Protein Chem *70*, 79-112.

116. Strelkov, S.V., Herrmann, H., Geisler, N., Wedig, T., Zimbelmann, R., Aebi, U., and Burkhard, P. (2002). Conserved segments 1A and 2B of the intermediate filament dimer: their atomic structures and role in filament assembly. Embo J *21*, 1255-1266.

117. De Marco, V., Burkhard, P., Le Bot, N., Vernos, I., and Hoenger, A. (2001). Analysis of heterodimer formation by Xklp3A/B, a newly cloned kinesin-II from Xenopus laevis. Embo J *20*, 3370-3379.

118. Lee, D.L., Ivaninskii, S., Burkhard, P., and Hodges, R.S. (2003). Unique stabilizing interactions identified in the two-stranded alpha-helical coiled-coil: crystal structure of a cortexillin I/GCN4 hybrid coiled-coil peptide. Protein Sci *12*, 1395-1405.

119. Strelkov, S.V., and Burkhard, P. (2002). Analysis of alpha-helical coiled coils with the program TWISTER reveals a structural mechanism for stutter compensation. J Struct Biol *137*, 54-64.

120. Burkhard, P., Meier, M., and Lustig, A. (2000). Design of a minimal protein oligomerization domain by a structural approach. Protein Sci *9*, 2294-2301.

121. Guo, Y., Bozic, D., Malashkevich, V.N., Kammerer, R.A., Schulthess, T., and Engel, J. (1998). All-trans retinol, vitamin D and other hydrophobic compounds bind in the axial pore of the five-stranded coiled-coil domain of cartilage oligomeric matrix protein. Embo J *17*, 5265-5272.

Chapter 1

Structure-based design of peptides that self-assembles into regular polyhedral nanoparticles

Available online at www.sciencedirect.com

SCIENCE DIRECT®

Nanomedicine: Nanotechnology, Biology, and Medicine 2 (2006) 95–102

nanomedicine

www.nanomedjournal.com

Materials Science

Structure-based design of peptides that self-assemble into regular polyhedral nanoparticles

Senthilkumar Raman, MS, Gia Machaidze, PhD, Ariel Lustig, PhD, Ueli Aebi, PhD, Peter Burkhard, PhD*

M.E. Müller Institute for Structural Biology, Biozentrum, University of Basel, Basel, Switzerland

Received 22 February 2006; accepted 7 April 2006

Abstract Artificial particulate systems such as polymeric beads and liposomes are being applied in drug delivery, drug targeting, antigen display, vaccination, and other technologies. Here we used computer modeling to design a novel type of nanoparticles composed of peptides as building blocks. We verified the computer models via solid-phase peptide synthesis and biophysical analyses. We describe the structure-based design of a novel type of nanoparticles with regular polyhedral symmetry and a diameter of about 16 nm, which self-assembles from single polypeptide chains. Each peptide chain is composed of two coiled coil oligomerization domains with different oligomerization states joined by a short linker segment. In aqueous solution the peptides form nanoparticles of about 16 nm diameter. Such peptide nanoparticles are ideally suited for medical applications such as drug targeting and drug delivery systems, such as imaging devices, or they may be used for repetitive antigen display.

Key words: Peptide nanoparticles; Antigen display; Drug targeting; Drug delivery; Protein design

Researchers are finding a variety of biomedical applications for nanoparticles such as liposomes or polymeric beads in drug delivery, drug targeting, vaccination, protein separation, enzyme immobilization, and blood cell substitution [1-6]. Liposomes have a flexible, cell-like lipid bilayer surface that acts as a permeability barrier to trap compounds in their aqueous interior. However, liposomes can be mechanically unstable and their loading capacity limited by the water solubility of the material to be loaded.

Other approaches for the preparation of spherical polymer shells in the size range of nanometers to microns can involve, for example, the layer-by-layer deposition of polyelectrolytes on the surface of a charged nanoparticle and subsequent dissolution of the templating particle, or the self-assembly of amphiphilic diblock or triblock copolymers into micelles, selective cross-linking of their hydrophilic shell, and subsequent degradation of the hydrophobic core [7]. Preparation of such nanocapsules is complex and may be ineffective. Also, polymeric beads, though mechanically more stable with a larger loading capacity than liposomes, lack many of the useful surface properties of a lipid bilayer shell. Furthermore, they do not biodegrade easily and hence may be toxic.

Here we present the structure-based design of mechanically and chemically stable nanoparticles, using the ability of peptides and proteins to self-assemble into particles of well-defined size and shape. Once assembled these peptide nanoparticles can serve as vehicles for drug targeting. Currently used drug targeting systems include, for example, antibodies that deliver radioactive isotopes to proliferating blood vessels [8] and peptides that target tumor blood vessels [9].

Alternatively, peptide nanoparticles can be used as repetitive antigen display systems for the development of vaccines. During the past decade several immunogenic vaccination strategies have been identified [10-14]. However, at this point vaccines for many pathogens worldwide, including malaria (*Plasmodium falciparum*) [15], *Mycobacterium tuberculosis* [16], group A streptococci [17], hepatitis viruses [11], herpesviruses [18], human immunodeficiency virus (HIV) [10,12], and influenza [19], are still ineffective or simply unavailable.

No financial conflict of interest was reported by the authors of this paper.

This research was supported by the M.E. Müller Foundation and the NCCR Nanoscale Science (SNF). The authors would like to thank J. Engel and W. Meier for critical reading of the manuscript.

* Corresponding author. The Institute of Materials Science, University of Connecticut, Storrs, CT 06269-3136, United States.

E-mail address: peter.burkhard@uconn.edu (P. Burkhard).

1549-9634/$ – see front matter © 2006 Elsevier Inc. All rights reserved.
doi:10.1016/j.nano.2006.04.007

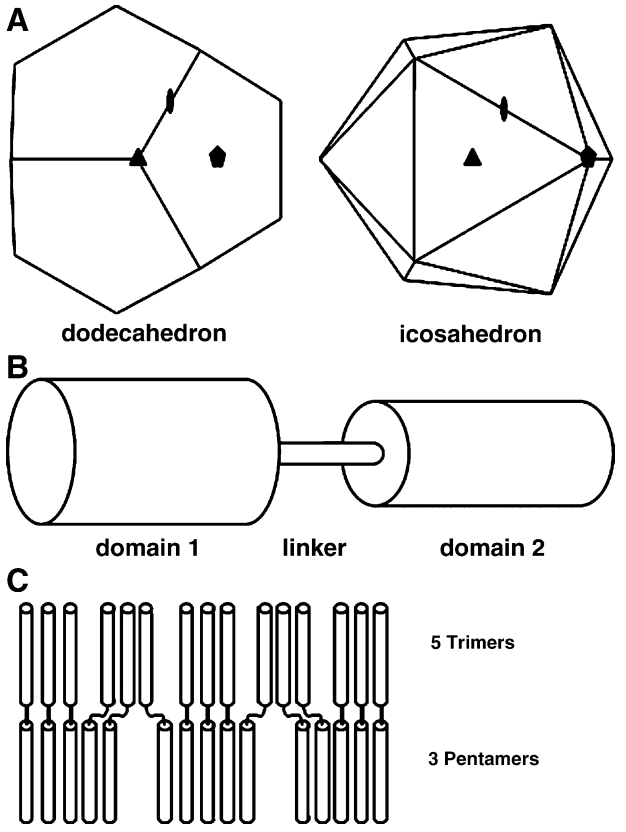

Fig 1. Basic concepts of the design. **A,** Possible regular polyhedra built from two-, three-, and five-fold symmetry elements. The symmetry elements are denoted as black symbols. The dodecahedron and the icosahedron have the same internal symmetry elements and are built from 60 identical 3-dimensional building blocks (asymmetric units). **B,** Architecture of the monomeric building block for self-assembly into regular polyhedra. The building block is composed of an oligomerization domain 1, a linker domain, and a second oligomerization domain. **C,** Even units consisting of trimers and pentamers. The number of monomers (building blocks) is defined by the least common multiple (LCM) of the oligomerization states of the two domains 1 and 2 of the building blocks.

Because of the broad range of humoral and cellular immune responses they elicit as well as the memory responses they induce, live attenuated vaccines are still the vaccines of choice [10-14]. From a practical point of view, however, live attenuated vaccines raise issues related to manufacturing and safety that may preclude their widespread use [10-14]. As an alternative, peptide-based vaccines have been developed and used for vaccination. However, synthetic peptides alone are often not immunogenic enough, and a strong immunoadjuvant is usually included to enhance their immunogenicity. There remain concerns, however, about toxic adjuvants, which are critical to the immunogenicity of synthetic peptides [20-22].

Because their architecture is similar to that of virus capsids, the peptide nanoparticles described here combine the strong immunogenic effect of live attenuated vaccines with the purity and high specificity in eliciting immune responses of peptide-based vaccines, while avoiding both the safety risks of live attenuated vaccines and the need for toxic adjuvants of peptide-based vaccines.

Table 1
Possible combinations of oligomerization states

ID	Domain 1	Domain 2	Polyhedron type	LCM	No. of even units	No of asymmetric units
1	5	2	Dodecahedron/ icosahedron	10	6	60
2	5	3	Dodecahedron/ icosahedron	15	4	60
3	4	3	Cube/ octahedron	12	2	24
4	3	4	Cube/ octahedron	12	2	24
5	3	5	Dodecahedron/ icosahedron	15	4	60
6	2	5	Dodecahedron/ icosahedron	10	6	60
7a*	5	4	Irregular	20	1	20
7b*	4	5	Irregular	20	1	20

* The entries 7a and 7b do not correspond to regular polyhedra but represent the largest even units that may be formed with oligomerization states ranging from 2 to 5.

Methods

Peptide synthesis

The peptide was synthesized by Peptide Specialities (Heidelberg, Germany). Its purity (>95%) was verified by high-performance liquid chromatography and mass spectrometric analyses.

Refolding of the peptide

The peptide folding procedure was carried out under four different regimes.

Preparation 1 (oxidizing conditions)

1 mg/mL peptide was dissolved directly in 150 mM NaCl, 20 mM Tris pH 7.5.

Preparation 2 (reducing conditions)

1 mg/mL peptide was dissolved directly in 150 mM NaCl, 20 mM Tris pH 7.5, 2 mM dithiothreitol (DTT).

Preparation 3 (denaturation, renaturation under oxidizing conditions)

0.07 mg/mL peptide was dissolved in 150 mM NaCl, 20 mM Tris pH 7.5, 2 mM DTT, 8 M urea. The solution was then dialyzed in steps from 150 mM NaCl, 20 mM Tris, pH 7.5; 8 M urea/4 M urea/2 M urea/no urea. Finally, the solution was concentrated to 1 mg/mL in 150 mM NaCl, 20 mM Tris pH 7.5.

Preparation 4 (denaturation, renaturation under reducing conditions)

0.07 mg/mL peptide was dissolved in 150 mM NaCl, 20 mM Tris pH 7.5, 8 M urea, 2 mM DTT. The solution was then dialyzed in steps from 150 mM NaCl, 20 mM Tris pH 7.5, 8 M urea and 2 mM DTT/4 M urea and 2 mM DTT/ 2 M urea and 2 mM DTT/no urea and 2 mM DTT/no urea

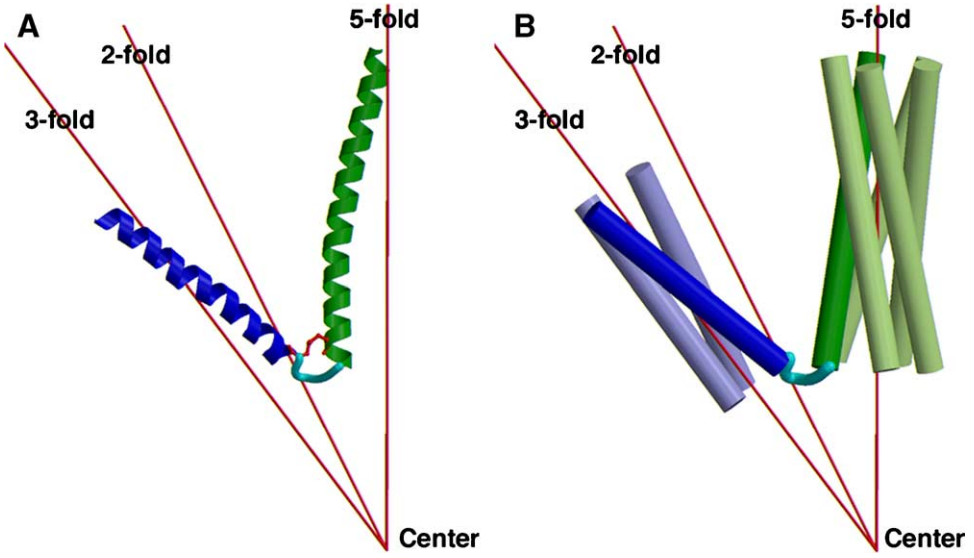

Fig 2. Internal symmetry elements of the dodecahedron. **A,** A 3D building block composed of domain 1 (blue; coiled coil domain with three-fold symmetry), a linker segment (cyan), and domain 2 (green; coiled coil domain with five-fold symmetry) is displayed such that the internal symmetry elements of the domains 1 and 2 are superimposed onto the symmetry axes of the polyhedron. The intrahelical disulfide bridge between the helices is displayed in red. **B,** The complete coiled coil domains are displayed as cylinders. The additional symmetry objects generated by the three-fold and the five-fold rotational symmetry elements of the polyhedron are displayed in light colors, whereas the original molecule is displayed in dark colors. The rotational symmetry axes (two-fold, three-fold, and five-fold) are displayed as red lines in **A** and **B**.

and no DTT. Finally the solution was concentrated to 1 mg/mL in 150 mM NaCl, 20 mM Tris pH 7.5.

Analytical ultracentrifugation

Analytical ultracentrifugation (AUC) was carried out on an Optima XL-A analytical ultracentrifuge (Beckman Instruments, Palo Alto, CA) equipped with a 12-mm Epon double-sector cell in an An-60 Ti rotor. Sedimentation equilibrium runs were performed at 20°C at rotor speeds between 5200 and 15,000 rpm and peptide concentrations of 0.15 to 1.0 mg/mL. Average molecular masses were evaluated by using a floating baseline computer program that adjusts the baseline absorbance to obtain the best linear fit of ln(absorbance) versus the square of the radial distance. A partial specific volume of 0.73 mL/g was used.

Electron microscopy

Specimens were prepared for electron microscopy (EM) by negative staining with 2% uranyl acetate and at a peptide concentration of 0.01 mg/mL. They were analyzed and photographed on a Zeiss EM910 transmission electron microscope (Carl Zeiss, Oberkochen, Germany).

Results

Design principles

There exist only five regular polyhedra: the tetrahedron, the cube, the octahedron, the dodecahedron, and the icosahedron. These polyhedra show different internal rotational symmetry elements; for example the dodecahedron and the icosahedron have two-fold, three-fold, and five-fold rotational symmetry axes (Figure 1, *A*). The cube and the octahedron are built up from 24 asymmetric units, whereas the dodecahedron and icosahedron are built up from 60 asymmetric units, thus generating the largest closed shell in which every subunit is in an identical environment [23] (Table 1). These asymmetric units are tri-pyramids, and each of the pyramid edges corresponds to one of the rotational symmetry axes; hence the edges of these asymmetric units represent two-fold, three-fold, four-fold, or five-fold symmetry axes depending on the type of polyhedron. If the symmetry axes of peptidic oligomerization domains are superpositioned onto the edges of these tri-pyramids, such 3-dimensional building blocks can be built up from peptidic oligomerization domains (Figure 2, *A* and *B*). As a consequence, it may be possible to design a peptide nanoparticle with regular polyhedral symmetry by connecting peptidic oligomerization domains with different oligomerization states. Hence, to construct a nanoparticle as a regular dodecahedron, a continuous peptide chain comprising a trimerization domain, a short linker sequence, and a pentamerization domain is needed (Figures 1, *B* and 2, *A*). Such a continuous peptide chain will be the basic building block of the nanoparticle, the content of one asymmetric unit. A similar approach using dimeric and trimeric proteins joined in a specific angle by means of a rigid α-helical linker between the two building blocks has been presented by Padilla et al. [24].

Protein oligomerization domains are well known; the most simple and most abundant oligomerization domain is probably the coiled coil folding motif [25,26]. This oligomerization motif has been shown to exist as a dimer, trimer, tetramer, and pentamer. Some of the best-known

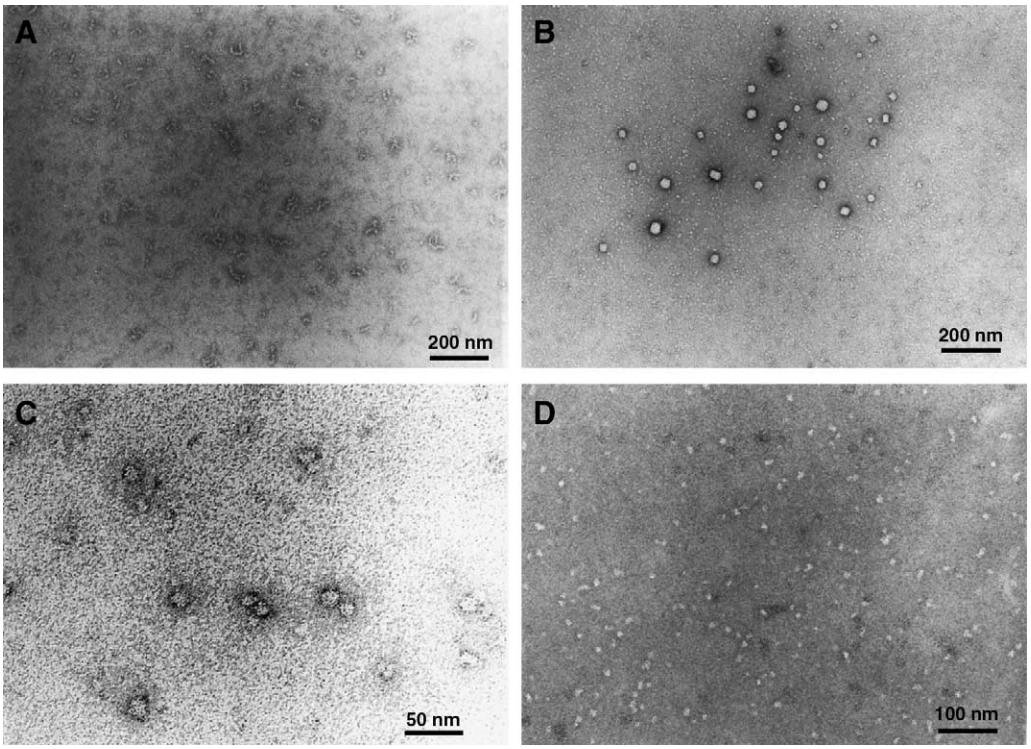

Fig 3. Electron micrographs of the peptide nanoparticles. **A,** The peptide nanoparticles formed under oxidizing conditions (preparation 1). **B,** The peptide nanoparticles formed under reducing conditions (preparation 2). **C,** The peptide nanoparticles formed under oxidizing conditions after denaturation (preparation 3). **D,** The peptide nanoparticles formed under reducing conditions after denaturation (preparation 4). The pictures were prepared by negative staining with 2% uranyl acetate; the concentration of the peptide was 0.01 mg/mL. In **B** the average diameter of the particles is roughly 25 nm. In **C** and **D** the average diameter of the particles is roughly 16 nm.

examples are the GCN4 leucine zipper [27], fibritin [28], tetrabrachion [29], and cartilage oligomerization matrix protein (COMP) [30], representing dimeric, trimeric, tetrameric, and pentameric coiled coils, respectively. Other simple oligomerization motifs are also known, such as the trimerization domain (the so-called foldon) of fibritin [28].

If these monomeric building blocks consisting of a continuous peptide chain composed of two linked oligomerization domains with different oligomerization states assemble, they will first form "even units" (Figure 1, *C*). The number of monomers that will assemble into such an even unit is defined by the least common multiple (LCM) of their oligomerization states. Hence if the oligomerization domains of the monomeric building block consist of a trimer and a pentamer, 15 monomers will form an even unit. The geometry of these even units, however, may not be regular. Several of these even units may then further assemble into larger nanoparticles (cf. Table 1). For example, to form a dodecahedron four even units composed of 15 monomeric building blocks each are needed; that is, the nanoparticle with regular geometry will be composed of 60 monomeric building blocks (see Figure 4, *A*). The possible combinations of oligomerization states of the two domains to form any of the regular polyhedra are shown in Table 1.

Whether the even units will assemble additionally to form a regular polyhedron depends on (1) the interactions at the interface between neighboring oligomerization domains within a nanoparticle, (2) the length of the linker segment, and (3) the shape of the individual oligomerization domains. Optimizing the interactions at the interface between neighboring domains can significantly improve the packing and stability of the regular polyhedron. Such improvements can be achieved by optimizing the hydrophobic and the ionic interactions between the interacting oligomerization domains or by their chemical cross-linking, for example by introducing cysteine residues so that a disulfide bridge is formed between two interacting oligomerization domains (cf. Figure 2, *A*). The linker domain should be long enough to avoid disruption of the protein fold of the oligomerization domains but short enough to maintain close contact between the two oligomerization domains.

Self-assembly of nanoparticles

According to the principles outlined above [31] we have rationally designed a peptide nanoparticle composed of a monomeric building block with the following sequence:

```
1         10        20        30        40        50        60
Ac-DEMLRELQETNAALQDVRELLRQQVKQITFLKCLLMGGRLLCRLEELERRLEELERRLEELERR-NH2
```

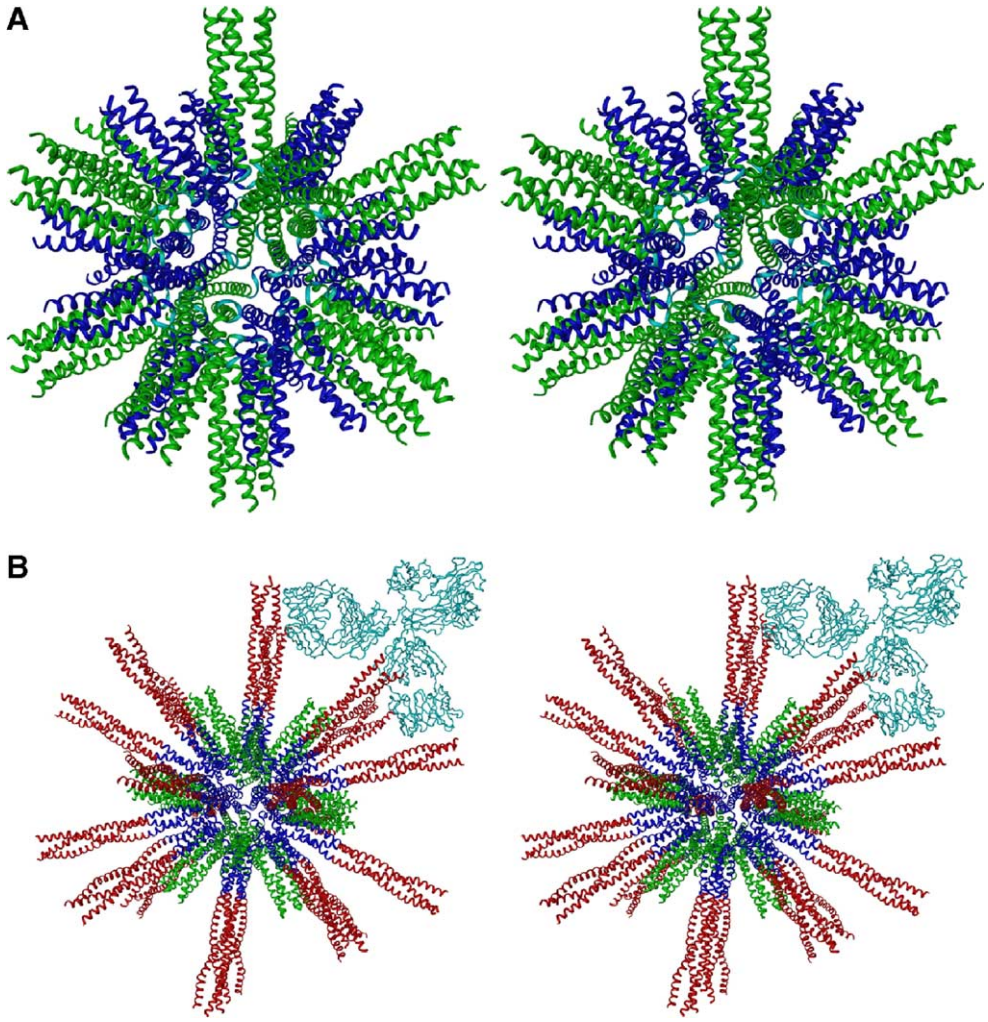

Fig 4. Stereo picture of a computer model of the complete peptide nanoparticle with dodecahedral symmetry. **A,** The particles are composed from the pentameric coiled coil domain of COMP (green) and a trimeric de novo designed coiled coil domain (blue). The calculated diameter of this particle is about 16 nm. **B,** The same nanoparticle as in **A** but wherein the trimeric coiled coils are further extended by the coiled coil sequence of the HIV surface protein gp41 (red). This portion of the gp41 protein is ideally displayed in many copies on the surface of the nanoparticle to be recognized by an antibody (cyan), thus eliciting a strong immune response.

The 36 N-terminal amino acids (green) of this peptide correspond to the slightly modified pentameric coiled coil domain of COMP [30]. The 26 C-terminal amino acids (blue) correspond to a de novo-designed minimal trimeric coiled coil domain according to the principles as outlined by Burkhard et al. [32-34]. These two oligomerization domains with different oligomerization states are joined by a linker segment consisting of two glycine residues (black). According to model building three of the four C-terminal residues of COMP have been modified to optimize interhelical contacts between the two oligomerization domains including an intramolecular disulfide bridge. The cysteine residues in position 33 and 42 are optimally placed for such an intramolecular disulfide bridge between the helices. They are at **f** positions in the heptad repeats of the respective coiled coils and one turn away from the respective helix ends (cf. Figure 2, *A*) and may form a disulfide bridge without disturbing the coiled coil geometry of the two oligomerization domains. Finally, the positively charged N-terminal amino group is replaced by an acetyl moiety and the negatively charged C-terminal carboxyl group is replaced by an amide group to avoid destabilization of the helices due to their helix-macrodipole [33].

Because of the complexities of folding of a protein containing intramolecular disulfide bridges, four different refolding conditions were tested for their assembly into polyhedral nanoparticles (for details see Methods). In a first regime (preparation 1) the assembly process of the peptide at a relatively high concentration was performed under oxidizing conditions, allowing for disulfide bridge formation. To test whether the intramolecular disulfide bridge is needed for proper self-assembly of the peptide into particles with regular dodecahedral symmetry, the peptide, again at relatively high concentration, was assembled under reducing conditions (preparation 2).

Because high peptide concentrations can lead to intermolecular disulfide bridge formation and consequently to aggregation, we tested two other refolding regimes. The peptide concentration was reduced to minimize intermolecular contacts, and then the peptide was completely denatured in 8 M urea. Then the refolding process was started by a stepwise dialysis of the urea under either oxidizing (preparation 3) or reducing (preparation 4) conditions. In a final step of preparation 4 the disulfide bridges were allowed to form by changing to oxidizing conditions.

The assembly behavior of the nanoparticles under these four regimes was analyzed by AUC to determine the molecular weight of the aggregates. Furthermore, the morphology of the aggregates was investigated by EM.

In preparation 1 (1 mg/mL) AUC revealed a mixture of components with molecular weights ranging from about 380 to 2200 kDa corresponding to aggregates of 48 to 280 monomers. Accordingly, electron micrographs showed that the peptides do not form spherical nanoparticles but instead form elongated irregular aggregates (Figure 3, *A*).

AUC of preparation 2 (1 mg/mL) revealed again a mixture of components with molecular masses ranging from about 130 to 330 kDa. This corresponds to nanoparticles composed of about 16 to 42 monomers. The lowest molecular mass components roughly correspond to even units (cf. Figure 1, *C*), which are composed of 15 peptide chains. In contrast to preparation 1, under reducing conditions the peptides do form nanoparticles as shown by EM (Figure 3, *B*). The size of these nanoparticles is variable, however, with diameters ranging from about 15 to 45 nm, but they are not always completely spherical.

The refolding processes starting at lower peptide concentrations and complete denaturation of the peptide gave much more homogeneous results. The measured molecular mass of the particles from preparation 3 was only slightly concentration dependent (Table 2). At lower final peptide concentrations the nanoparticles are composed of three even units, whereas at higher final peptide concentrations they are composed of four even units. The latter is in agreement with nanoparticles with regular dodecahedral symmetry being composed of four even units or 60 monomeric peptide chains, respectively (Table 1). As judged by EM the peptide forms nanoparticles of roughly homogeneous size and spherical appearance (Figure 3, *C*). The diameter of these nanoparticles is about 16 nm, in good agreement with the value predicted for a modeled regular dodecahedron.

By AUC the measured molecular mass of the particles from preparation 4 is again concentration dependent (Table 2). Their sizes range from particles composed of 80 to as many as about 121 peptide chains. Again, the peptides form nanoparticles of nearly identical size with mostly spherical appearance (Figure 3, *D*). The diameter of the peptide nanoparticles is very similar to that of the particles from preparation 3. These micrographs were taken for samples assembled at low peptide concentrations, conditions under which their molecular mass was shown to be close to that of particles with regular dodecahedral symmetry (Table 2).

Table 2
Molecular masses of nanoparticles

	Concentration (mg/mL)	MW (kDa)	No. of monomers	No. of even units
Preparation 3	0.15	347	43.9	2.9
	0.3	356	45.1	3.0
	0.4	461	58.4	3.9
	0.6	437	55.3	3.7
	0.8	489	61.9	4.1
Preparation 4	0.15	633	80.1	5.3
	0.25	718	90.9	6.1
	0.8	960	121.5	8.1

Discussion

The peptide sequence outlined above was rationally designed so as to form nanoparticles showing regular polyhedral symmetry, that is, consisting of 60 monomeric building blocks (see Figure 4, *A*). Computer modeling predicted that such a particle would have a diameter of about 16 nm and a molecular mass of 473 kDa, corresponding to a particle composed of 60 monomeric peptide chains (see Table 2). The appropriate folding regime was crucial to obtain a homogeneous population of nanoparticles with regular polyhedral symmetry. This can be rationalized by the different possibilities of disulfide formation during the refolding process. In high peptide concentrations the peptide chains may easily form intermolecular disulfide bridges leading to irregular aggregates (cf. Figure 3, *A*). Such a behavior was observed in the refolding procedure of preparation 1: EM revealed elongated aggregates devoid of any regular structure. The oligomerization properties of the peptide made of two distinct oligomerization domains joined by a linker segment, when combined with the formation of intermolecular disulfide bridges between different peptide chains, leads to a network of peptides, which are cross-linked either by oligomerization of the coiled coil domains or by intermolecular disulfide bridges.

Therefore, it is crucial to avoid intermolecular disulfide bridge formation during refolding. Keeping the system under reducing conditions in the refolding process (preparation 2) leads to the formation of spherical nanoparticles. However, by EM the nanoparticles are not of unique appearance, either in shape or in size (Figure 3, *B*). This result is in agreement with those obtained by AUC, showing that under these conditions the peptide can form particles of different sizes. The measured molecular mass represents a distribution of particles of various sizes. The smaller particles in Figure 3, *B* presumably correspond to even units composed of 15 monomers (roughly corresponding to the smallest measured molecular mass; cf. Table 2), whereas the larger particles are multiples thereof. When the intramolecular disulfide bridge is missing, the peptide does form spherical nanoparticles but not with regular dodecahedral symmetry. This documents the

importance of the intramolecular disulfide bridge for proper formation of nanoparticles with regular symmetry.

The aim was to avoid intermolecular disulfide bridge formation while allowing for intramolecular disulfide bridge formation. The coiled coil domains of COMP and of the de novo-designed trimer are known to form very stable oligomers [34,35]. During refolding out of 8 M urea these coiled coil domains will already form in urea concentrations that are moderately high. Formation of the helices within the two coiled coil domains will bring the two cysteines of the same peptide chain into close contact (cf. Figure 2, *A*). Furthermore, they will be located close to the center of the even units and/or the regular dodecahedral particles; hence they are shielded from the solvent and no longer accessible for intermolecular contacts. Under oxidizing conditions (preparation 3) intramolecular disulfide bridge formation will then immediately and predominantly occur while avoiding intermolecular cross-linking. However, also under reducing conditions (preparation 4) the cysteine residues cannot form intermolecular disulfide bridges and the intramolecular disulfide bridge will be formed only when changing to oxidizing conditions in a final step, that is, when the cysteine residues are already shielded from the solvent.

The intramolecular disulfide bridge between the two helices of adjacent oligomers fixes the spatial orientation of the two helices relative to each other. In agreement with our design, this disulfide bridge proves to be a prerequisite for the effective formation of nanoparticles with regular dodecahedral symmetry.

Conclusions

Such nanoparticles with regular polyhedral symmetry represent an ideal repetitive antigen display system. Surface proteins of pathogens or fragments of such proteins can easily be engineered into the peptide sequence of the nanoparticle. Notably, many surface proteins of pathogens contain coiled coil sequences. For example, by simply extending the trimeric coiled coil of the nanoparticle by the coiled coil sequence of the HIV surface protein gp41, a HIV vaccine candidates can be designed (Figure 4, *B*). The predicted strong immune response against such a vaccine can be rationalized by the optimal binding geometry of an IgG molecule to the nanoparticle (cf. Figure 4, *B*). Whereas in the past, different kinds of adjuvants were tested to improve the immunogenicity of an antigen or a specific epitope, such a repetitive antigen display can strongly augment the immunogenicity of a certain epitope [36], thus avoiding the need for sometimes highly toxic adjuvants [37]. We have designed peptide nanoparticles aimed at eliciting a strong immune response, and our preliminary immunization results confirm the correctness of this hypothesis.

References

[1] Langer R. Drug delivery and targeting. Nature 1998;392:5-10.

[2] Kiser PF, Wilson G, Needham D. A synthetic mimic of the secretory granule for drug delivery. Nature 1998;394:459-62.

[3] Ong S, Liu H, Qiu X, Bhat G, Pidgeon C. Membrane partition coefficients chromatographically measured using immobilized artificial membrane surfaces. Anal Chem 1995;67:755-62.

[4] Rogers JA, Choi YW. The liposome partitioning system for correlating biological activities of imidazolidine derivatives. Pharm Res 1993;10:913-7.

[5] Savic R, Luo L, Eisenberg A, Maysinger D. Micellar nanocontainers distribute to defined cytoplasmic organelles. Science 2003;300:615-8.

[6] Allen TM, Cullis PR. Drug delivery systems: entering the mainstream. Science 2004;303:1818-22.

[7] Meier W. Polymer nanocapsules. Chem Soc Rev 2000;29:295-303.

[8] Tabata M, Kondo M, Haruta Y, Seon BK. Antiangiogenic radioimmunotherapy of human solid tumors in SCID mice using 125I-labeled anti-endoglin monoclonal antibodies. Int J Cancer 1999;82:737-42.

[9] Arap W, Pasqualini R, Ruoslahti E. Cancer treatment by targeted drug delivery to tumor vasculature in a mouse model. Science 1998;279:377-80.

[10] Berzofsky JA, Ahlers JD, Derby MA, Pendleton CD, Arichi T, Belyakov IM. Approaches to improve engineered vaccines for human immunodeficiency virus and other viruses that cause chronic infections. Immunol Rev 1999;170:151-72.

[11] Lechmann M, Liang TJ. Vaccine development for hepatitis C. Semin Liver Dis 2000;20:211-26.

[12] Paul WE. Can the immune response control HIV infection? Cell 1995;82:177-82.

[13] Gahery-Segard H, Pialoux G, Charmeteau B, Sermet S, Poncelet H, et al. Multiepitopic B- and T-cell responses induced in humans by a human immunodeficiency virus type 1 lipopeptide vaccine. J Virol 2000;74:1694-703.

[14] Gras-Masse H. Single-chain lipopeptide vaccines for the induction of virus-specific cytotoxic T cell responses in randomly selected populations. Mol Immunol 2001;38:423-31.

[15] Hoffman SL, Subramanian GM, Collins FH, Venter JC. *Plasmodium*, human and *Anopheles* genomics and malaria. Nature 2002;415:702-9.

[16] Wang J, Zganiacz A, Xing Z. Enhanced immunogenicity of BCG vaccine by using a viral-based GM-CSF transgene adjuvant formulation. Vaccine 2002;20:2887-98.

[17] Hayman WA, Toth I, Flinn N, Scanlon M, Good MF. Enhancing the immunogenicity and modulating the fine epitope recognition of antisera to a helical group A streptococcal peptide vaccine candidate from the M protein using lipid-core peptide technology. Immunol Cell Biol 2002;80:178-87.

[18] Nesburn AB, Burke RL, Ghiasi H, Slanina SM, Wechsler SL. Therapeutic periocular vaccination with a subunit vaccine induces higher levels of herpes simplex virus-specific tear secretory immunoglobulin A than systemic vaccination and provides protection against recurrent spontaneous ocular shedding of virus in latently infected rabbits. Virology 1998;252:200-9.

[19] Wareing MD, Tannock GA. Influenza update: vaccine development and clinical trials. Curr Opin Pulm Med 2002;8:209-13.

[20] Parmiani G, Castelli C, Dalerba P, Mortarini R, Rivoltini L, et al. Cancer immunotherapy with peptide-based vaccines: what have we achieved? Where are we going? J Natl Cancer Inst 2002;94:805-18.

[21] Van Regenmortel MH. Antigenicity and immunogenicity of synthetic peptides. Biologicals 2001;29:209-13.

[22] BenMohamed L, Wechsler SL, Nesburn AB. Lipopeptide vaccines—yesterday, today, and tomorrow. Lancet Infect Dis 2002;2:425-31.

[23] Johnson JE, Reddy VS. Biggest virus molecular structure yet! Nat Struct Biol 1998;5:849-54.

[24] Padilla JE, Colovos C, Yeates TO. Nanohedra: using symmetry to design self assembling protein cages, layers, crystals, and filaments. Proc Natl Acad Sci USA 2001;98:2217-21.

[25] Burkhard P, Strelkov SV, Stetefeld J. Coiled coils: a highly versatile protein folding motif. Trends Cell Biol 2001;11:82-8.

[26] Lupas A. Coiled coils: new structures and new functions. Trends Biochem Sci 1996;21:375-82.
[27] O'Shea EK, Klemm JD, Kim PS, Alber T. X-ray structure of the GCN4 leucine zipper, a two-stranded, parallel coiled coil. Science 1991;254:539-44.
[28] Tao Y, Strelkov SV, Mesyanzhinov VV, Rossmann MG. Structure of bacteriophage T4 fibritin: a segmented coiled coil and the role of the C-terminal domain. Structure 1997;5:789-98.
[29] Stetefeld J, Jenny M, Schulthess T, Landwehr R, Engel J, Kammerer RA. Crystal structure of a naturally occurring parallel right-handed coiled coil tetramer. Nat Struct Biol 2000;7:772-6.
[30] Malashkevich VN, Kammerer RA, Efimov VP, Schulthess T, Engel J. The crystal structure of a five-stranded coiled coil in COMP: a prototype ion channel? [see comments] Science 1996; 274:761-5.
[31] Sanner MF, Stolz M, Burkhard P, Kong XP, Min G, et al. Visualizing nature at work from the nano to the macro scale. Nanobiotechnology 2005;1:7-22.
[32] Burkhard P, Meier M, Lustig A. Design of a minimal protein oligomerization domain by a structural approach. Protein Sci 2000;9: 2294-301.
[33] Burkhard P, Kammerer RA, Steinmetz MO, Bourenkov GP, Aebi U. The coiled-coil trigger site of the rod domain of cortexillin I unveils a distinct network of interhelical and intrahelical salt bridges. Structure Fold Des 2000;8:223-30.
[34] Burkhard P, Ivaninskii S, Lustig A. Improving coiled-coil stability by optimizing ionic interactions. J Mol Biol 2002;318:901-10.
[35] Guo Y, Kammerer RA, Engel J. The unusually stable coiled-coil domain of COMP exhibits cold and heat denaturation in 4-6 M guanidinium chloride [in process citation]. Biophys Chem 2000;85:179-86.
[36] Fehr T, Skrastina D, Pumpens P, Zinkernagel RM. T cell-independent type I antibody response against B cell epitopes expressed repetitively on recombinant virus particles. Proc Natl Acad Sci USA 1998;95: 9477-81.
[37] Hunter RL. Overview of vaccine adjuvants: present and future. Vaccine 2002;20(Suppl 3):S7-12.

Chapter 2

- *Chapter 2 is divided in to Chapter 2A and 2B.* ***Chapter 2A*** *deals with "Recombinant production of peptide based nanoparticles and their biophysical characterization"*

- ***Chapter 2B*** *deals with the application part of recombinantly produced peptide based nanoparticles as a "Vaccine carrier".*

- *Chapter 2 is written in the following order: first comes the 'design principle and results section of chapter 2A and 2B' followed by the 'Discussion section of chapter 2A and 2B' and finally the 'Materials and Methods section' for both the chapters.*

Chapter 2A

Recombinant production of peptide based nanoparticles and their Biophysical characterization

Design principles

In Chapter 1, we showed that we can prepare nanoparticles by using peptides as building blocks. The monomeric chain of the peptide sequence which formed the basic building blocks is depicted in Figure 1, A, as synthetic peptide **(sp)**. The purpose behind our preparation of peptide based nanoparticles is to use them as carriers in vaccination and drug targeting. To prepare the nanoparticles for their application studies, the monomeric chains of **sp** sequence have to be produced in reasonable quantities.

Chemical synthesis of peptide sequence is a costly and troublesome process. Therefore, we decided to use the recombinant expression method for the production of sp sequence. We choose *E.coli* as the expression system, because of its ease of handling, modular nature, high expression levels and low production costs [1]. In a first step towards production, the sp sequence is inserted into the modified prokaryotic expression plasmid pPEP-T vector (mpPEP-T), resulting in **np1 construct** (for details regarding mpPEP-T vector refer to Materials & Methods section). In **np1** sequence, amino acids 23 to 86 correspond to the peptide sequence **sp**. The extra 22 N-terminal amino acids, of vector origin, includes His-tag (brown), residues important for UV-spectrometer based protein estimation (red), residue for chemical coupling (yellow) and thrombin recognition sequence (pink) (for sequence details of np1 construct, refer to Figure 1, A). A schematic model of monomeric chain of **np1** construct is depicted in Figure 1, B. In this model, the intended intramolceular disulfide bridge at the interface between the two domains is indicated as a red line.

In sp sequence, the formation of an intramolecular disulfide bridge between the two oligomerization domains is found to be crucial for the formation of nanoparticles with regular polyhedral symmetry (refer to Discussion section of Chapter 1). This stresses the importance of interactions at the interface between the two domains. We wanted to optimize the interactions between the two domains through intramolecular ionic interactions. For this reason, the np1 sequence is modified to include charged residues at the interface between two domains.

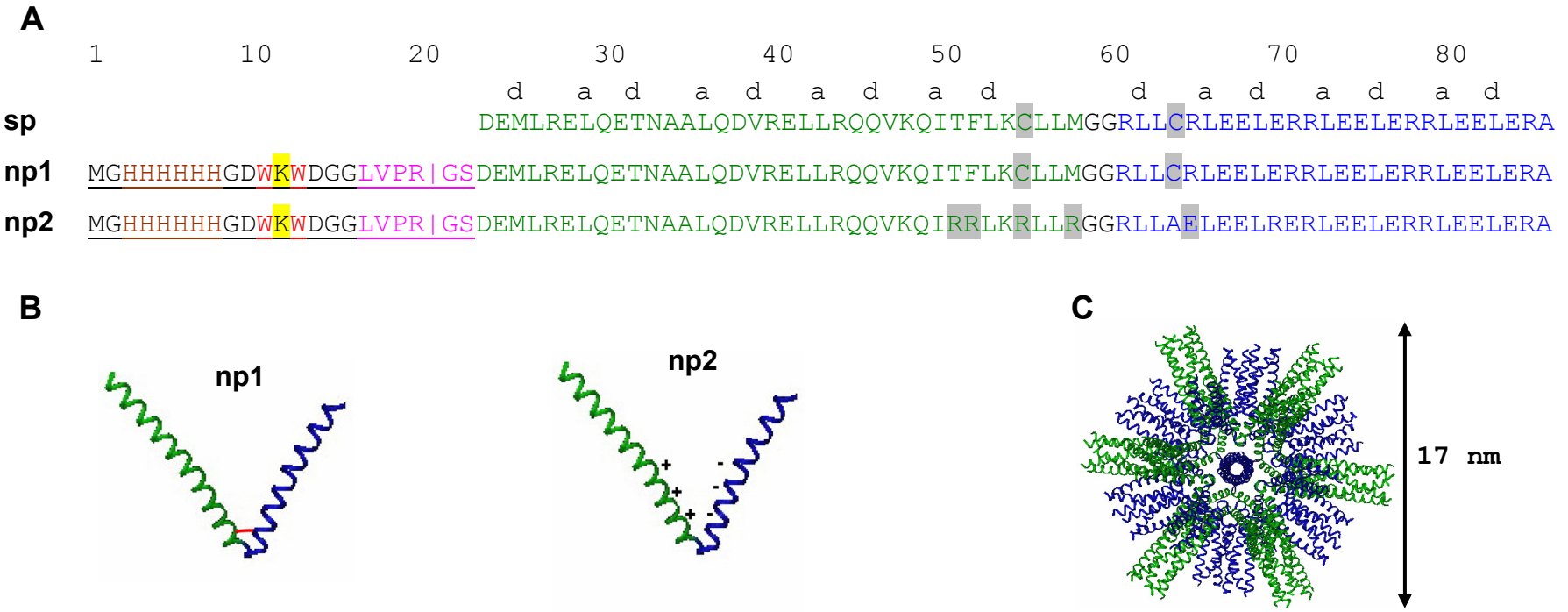

Figure 1. **A**, amino acid sequences of sp, np1 and np2 constructs. In sp, np1 and np2 constructs, the green colored residues represent the pentameric coiled-coil domain of COMP and the blue colored residues represent the *de novo* designed trimeric coiled-coil domain. In sp and np1 constructs, the cysteine residues intended for an intramolecular disulfide bridge at the interface between the two domains are highlighted in grey. In np2 construct, the modified residues for intramolecular ionic interactions at the interface between two domains are highlighted in grey. In np1 and np2 constructs, the underlined residues represent the 22 N-terminal residues of vector origin, which include 6X His-tag (brown), residues important for UV-spectrometer based estimation of protein (red), residue for chemical coupling (yellow) and thrombin recognition sequence (pink). The thrombin cleavage site is represented as a vertical line. The **a** and **d** positions of the heptad repeats of the pentameric and trimeric coiled coil domains are indicated. **B**, Schematic representation of monomeric chains of np1 and np2 constructs. In the np1 model, the red line depicts the intramolecular disulfide bridge; in the np2 model the + and - sign depicts the positive and negatively charged amino acids, respectively. **C**, Computer generated nanoparticle model of np1 and np2 constructs (17 nm in diameter).

The modified np1 sequence is called **np2 construct** (Figure 1, A; the modified residues are highlighted in grey). Similar to np1 construct, the first 22 N-terminal amino acids of np2 construct are of vector origin (for np2 sequence details refer to Figure 1, A).

In np2 construct, the modification of charged residues was done at **b**, **c**, **e**, **f** and **g** positions of heptad repeats of the coiled-coil domains of COMP and trimer. Thus not affecting the hydrophobic interactions at **a** and **d** positions of the heptad repeat, which comprise one of the key factors for coiled-coil stability [2, 3]. A schematic model of the monomeric chain of np2 construct is depicted in Figure 1, B. In this model, the charged residues at the interface between the two domains is indicated as + and -, representing the positively and negatively charged amino acids. In Figure 2, computer designed 3D model of np2 nanoparticle is depicted, highlighting the charged residues at the interface between the pentameric coiled-coil domain of COMP (green helix) and the *de novo* designed trimeric coiled-coil domain (blue helix).

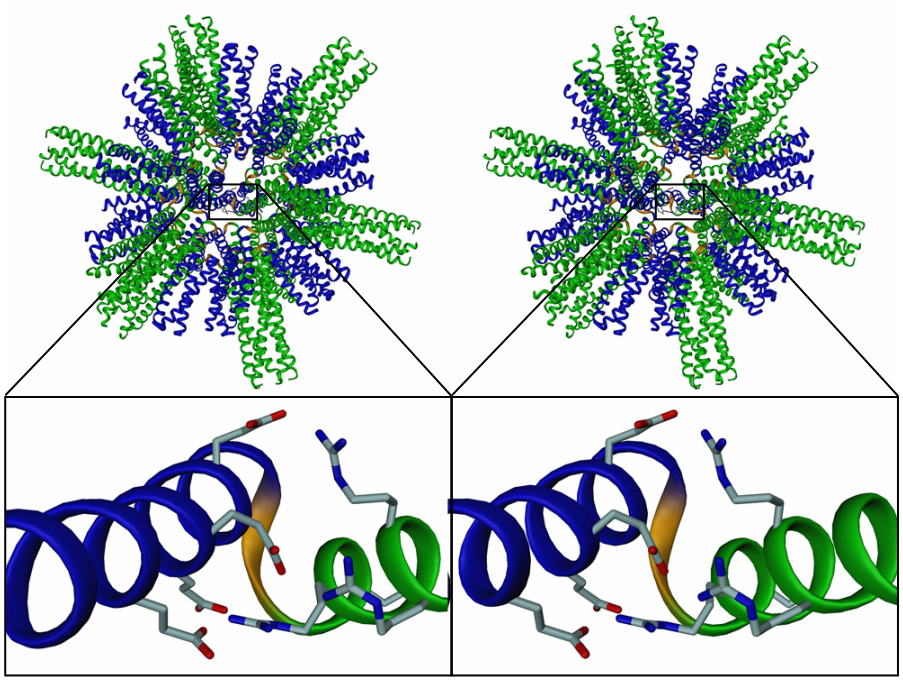

Figure 2. Computer model of np2 nanoparticle (stereo). The monomeric unit of np2 nanoparticle is highlighted with an emphasis on the charged residues at the interface between the pentameric coiled-coil domain of COMP (green helix) and the trimeric coiled-coil domain (blue helix). The positively charged arginine (R) residues on COMP domain (green helix) and the negatively charged glutamic acid (E) residues on trimeric coiled-coil domain (blue helix) is indicated as stick models.

Results

Purification results of np1 and np2 proteins

The np1 and np2 constructs are expressed and purified along with their N-terminal amino acids of vector origin (underlined residues in Figure 1, A). Ni^{2+}-affinity column chromatography is used as the method of purification. The purification is carried out under denaturing conditions using 8 M urea. (for expression and purification details refer to Materials and Methods section). The purification results of np1 and np2 proteins are summarized in Figure 3.

np1 protein

The imidazole eluted fractions of np1 protein is observed to run as a lower and upper band which corresponds to a theoretically calculated monomer (10289.7 Daltons) and trimer (30869.1 Daltons) (Figure 3, A). Western blot analysis using anti His-tag antibody confirmed the presence of monomer and trimer species in the eluted fractions of np1 protein (Figure 4). The observed trimeric band in denaturing conditions of SDS-PAGE suggests about the stability of the trimeric coiled-coil domain.

np2 protein

The np2 protein is observed to elute in small amounts during the pH 5.0 elution step (lane 4; Figure 3, B). But the majority of the eluted protein is observed in 250 mM imidazole elution fractions (lanes 5 to 8; Figure 3, B).

The eluted fractions are observed to run as a single band which corresponds to a theoretically calculated monomer (10372.7 Daltons). However, the observed trimeric band in np1 purified samples (Figure 3, A) was absent in np2 purified samples (Figure 3, B). This suggests about the less stable trimeric coiled-coil domain of np2 protein when compared to the trimeric coiled-coil domain of np1 protein.

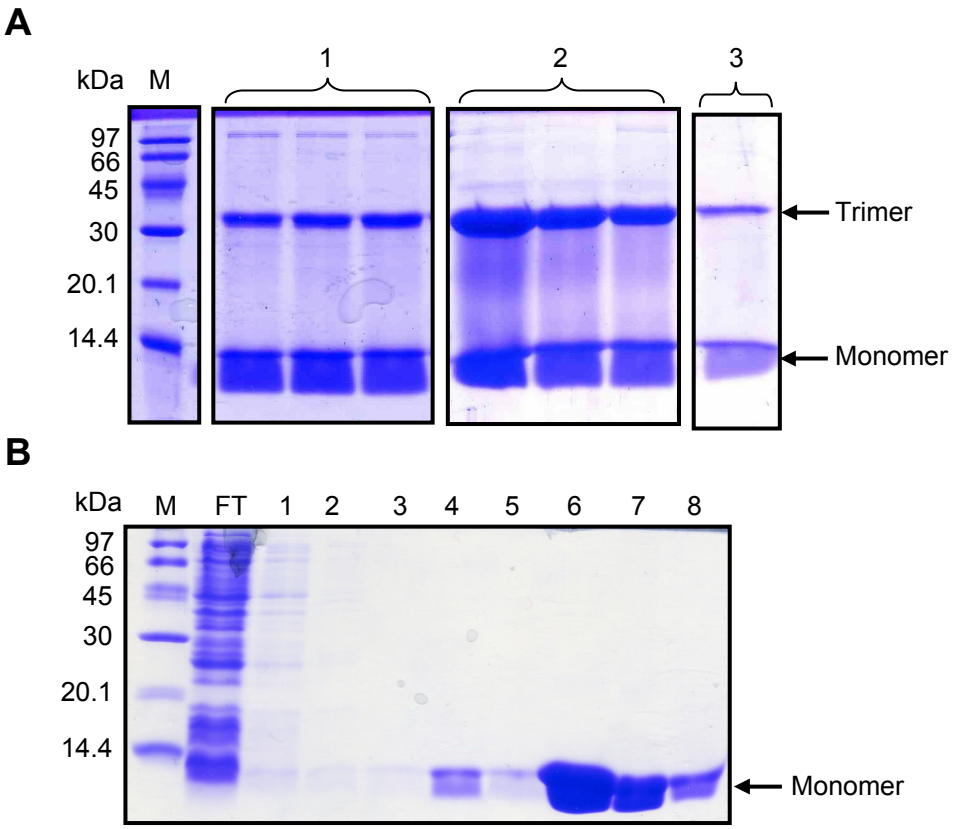

Figure 3. 17% SDS-PAGE of np1 and np2 purified proteins. **A**, purification results of np1 protein. 1, 2 and 3 represent 150 mM, 250 mM and 500 mM imidazole elution fractions, respectively. **B**, purification results of np2 protein. FT - Flow through; lane 1 - pH 8.0 wash fraction; lane 2 - pH 6.3 wash fraction; lane 3 - pH 5.9 elution fraction; lane 4 - pH 5.0 elution fraction; lanes 5 to 8 - 250 mM imidazole elution fractions. In both the gels, M - correspond to molecular weight marker, marked in kilo Daltons (kDa).

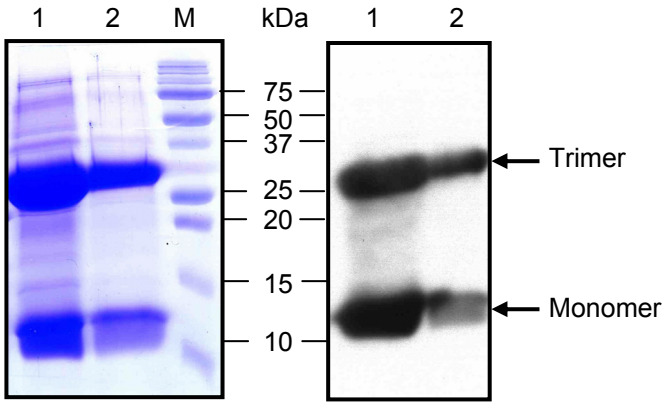

Figure 4. 15% Tricine SDS-PAGE and the corresponding western blot of np1 elution fractions. Lanes 1 and 2 - 250 mM imidazole elution fractions of np1 samples. M - Bio-Rad prestained marker; kDa - kilo Daltons.

Self-assembly properties of np1 protein

From our design principles, we know that np1 construct is the replica of sp peptide except for the first 22 N-terminal amino acids of vector origin (Figure 1, A). In chapter 1, we showed that the sp peptide formed nanoparticles of regular icosahedral shape under two different refolding conditions. The first condition is **preparation 3 refolding**, in which the peptide was refolded by step wise dialysis of the urea under oxidizing condition. The second condition is **preparation 4 refolding**, in which the peptide was refolded by step wise dialysis of the urea under reducing condition up to 0 M urea and then to oxidizing condition. These refolding conditions favored the formation of intramolecular disulfide bridge in sp peptide, as we showed that in sp peptide the formation of intramolecular disulfide bridge is crucial for the formation of regular icosahedral shaped nanoparticles. Therefore, for refolding studies of np1 protein, we decided to refold the protein under preparation 3 and preparation 4 refolding conditions.

The np1 protein refolded under the two different refolding conditions was characterized by the following techniques: 1. Electron Microscopy (EM) to characterize the morphology; 2. Analytical Ultra Centrifugation (AUC) to determine the molecular mass; 3. Circular Dichroism (CD) spectroscopy to study the secondary structural content and the stability of the nanoparticles.

Biophysical Characterization

Electron Microscopy (EM) results

The preparation 3 refolded protein is observed to form mixed population of aggregates of not regular in shape and expected size nanoparticles of ~ 17 nm in diameter (Figure 5, A). A single nanoparticle and an irregular aggregate are highlighted as inset in Figure 5, A.

The preparation 4 refolded protein (refolded in 1mM DTT) is observed under two different conditions in order to understand the influence of intramolecular disulfide bridge on np1 nanoparticle formation.

In the first condition, the sample is observed in the refolding buffer (20 mM Tris pH 7.5, 150 mM NaCl and 10% glycerol) containing 0 M urea and 1 mM DTT (reducing condition; not favoring intramolecular disulfide bridge formation).

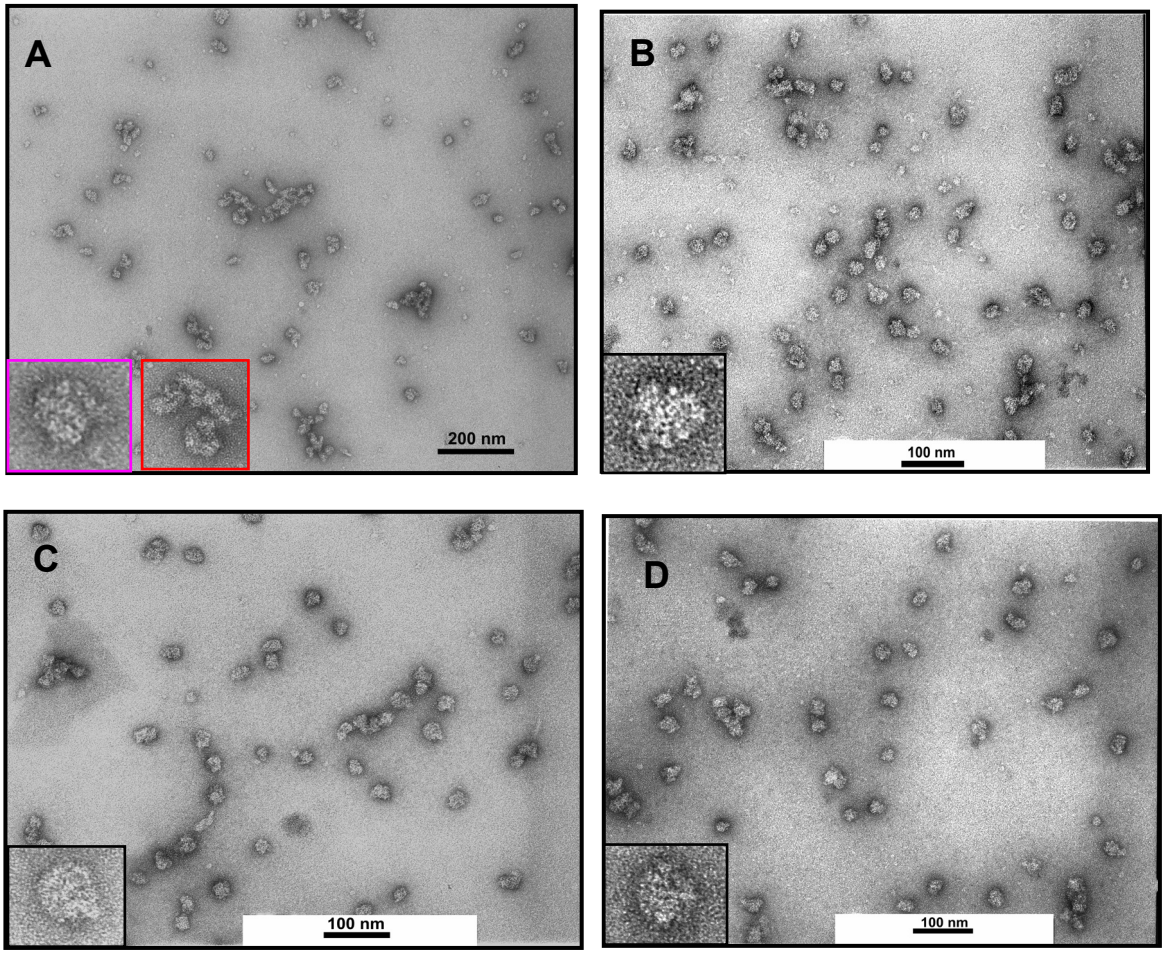

Figure 5. Electron micrographs of refolded np1 protein under different refolding conditions. **A**, preparation 3 refolded np1 protein (oxidizing condition). Inset: highlighting one single nanoparticle (pink) and an irregular aggregate (red) **B**, preparation 4 refolded np1 protein (reducing condition). Refolded up to 0 M urea and analyzed in the buffer 20 mM Tris pH 7.5, 150 mM NaCl, 1 mM DTT and 10% glycerol. Inset: one single nanoparticle. **C**, same refolding condition as **B**, but the protein was dialyzed to remove DTT (oxidizing condition). Analyzed in the buffer 20 mM Tris pH 7.5, 150 mM NaCl and 10% glycerol. Inset: one single nanoparticle. **D**, Same condition as **C**, but the Tris buffer was exchanged with Hepes buffer (20 mM Hepes pH 7.5, 150 mM NaCl and 10% glycerol). Inset: one single nanoparticle. The pictures were prepared by negative staining with 2% uranyl acetate; the concentration of the protein was 50 µg/ml.

In the second condition, the sample is observed in the refolding buffer containing 0 M urea and no DTT (oxidizing condition; favoring intramolecular disulfide bridge formation).

From the EM pictures, we observed nanoparticles of roughly homogenous size (~ 17 nm in diameter) and spherical shape already in reducing condition (Figure 5, B). In addition, we observed that the nature of the nanoparticles (referring to its homogenous size and shape) in reducing condition is not altered after the removal of DTT (oxidizing condition) (Figure 5, C) followed by buffer exchange (Figure 5, D). In both, preparation 3 and 4 refolding conditions the diameter of the observed nanoparticles is about 17 nm, in good agreement with the value predicted for a computer modeled regular icosahedron (Figure 1, C).

Analytical Ultra Centrifugation (AUC) results

The nanoparticles observed under preparation 4 refolding (Figure 5, D) are studied with AUC to determine their molecular weight and distribution.

Sedimentation equilibrium (SE) runs of preparation 4 sample gave us a molecular mass corresponding to icosahedral shaped nanoparticles (4 even units) + higher order aggregates at lower speed (5600 rpm) (Table 1, B). At higher speed sedimentation equilibrium runs (12000 rpm), the calculated molar mass is roughly corresponded to even units (Table 1, B). The observation of two different species during SE runs is well corroborated by the sedimentation velocity runs forming two different boundaries (bimodal boundary) over time (Figure 6), with the calculated sedimentation coefficient (*s*) values of 5.7 S and 19.4 S (Table 1, A).

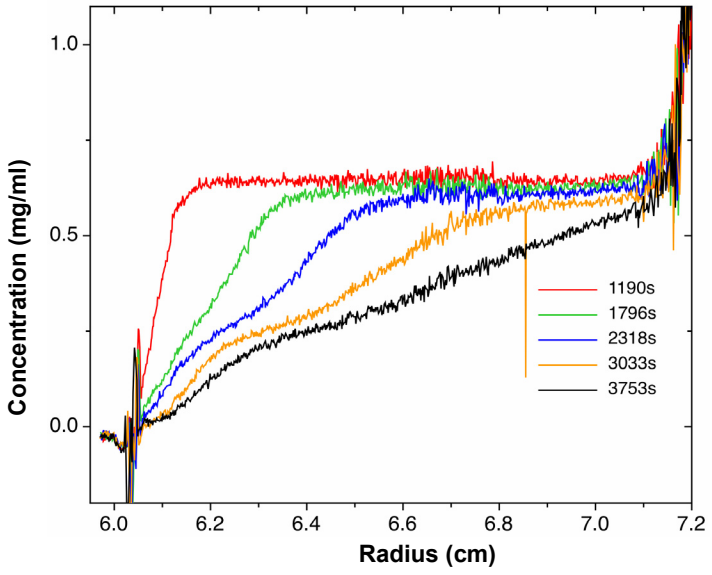

Figure 6. Sedimentation velocity (SV) data for a preparation 4 refolded np1 sample (oxidizing condition). The concentration is shown versus radius distributions at different times (in seconds), after the start of the sedimentation at 44,000 rpm. The protein concentration was 0.56 mg/ml.

The calculated 5.7 S value represent approximate mass of an even unit (129 kDa) and the 19.4 S represent the polydisperse species containing icosahedral nanoparticles (~700 kDa) and higher order aggregates (~ 2 million Daltons).

Table 1: AUC results for np1 protein - Monomer molecular weight 10289.7 Daltons.

A. Sedimentation velocity results

Refolding condition#	Rotor speed (rpm)	Concentration (mg/ml)	Calculated Sedimentation velocity coefficient value ($s_{20,w}$)
preparation 4	44000	0.1	5.7 S + 19.4 S
		0.56	4.5 S + 17 S

B. Sedimentation equilibrium results

Refolding condition#	Rotor speed (rpm)	Concentration (mg/ml)	Calculated MW (kDa)	No. of monomers	No. of even units
preparation 4	5600	0.1	766 + 2228	74.4 + 216.5	4.9 + 14.4
		0.56	710 + 2376	69 + 230.9	4.6 + 15.3
	12000	0.1	129	12.5	~ 1 even unit
		0.56	121	11.8	

- Analyzed in buffer 20 mM Hepes pH 7.5, 150 mM NaCl and 10% glycerol.

Parameters studied to understand its influence on nanoparticle assembly property of np1 protein under preparation 4 refolding condition

We wanted to understand the effect of ionic strength, pH of the refolding buffer, DTT concentration and glycerol on nanoparticle assembly property of np1 protein under preparation 4 refolding condition. The observed effect of these parameters on nanoparticle assembly is presented in the following sections.

Ionic strength

To understand the effect of ionic strength on nanoparticle assembly, the np1 protein is refolded in two different salt concentrations: (i) 0 M NaCl and (ii) in 500 mM NaCl. Refolding was done according to preparation 4 refolding and in refolding buffer 20 mM Tris pH 7.5, 10% glycerol containing 1 mM DTT. After refolding, samples were analyzed in buffer 20 mM Tris pH 7.5, 10% glycerol containing either 0 M or 500 mM NaCl (oxidizing condition).

From the EM picture, the np1 protein refolded in 0 M NaCl is observed to form flat looking nanoparticles (indicated by blue arrow) along with structures of not regular in shape (Figure 7, A). The AUC result for the above sample gave a molar mass corresponding approximately to a trimer and an even unit (Table 2).

The np1 protein refolded in 500 mM NaCl is observed to form nanoparticles of expected size, 17 nm in diameter. However, the formed nanoparticles are observed to be mostly clumped together, with a few individual particles around them (Figure 7, B).

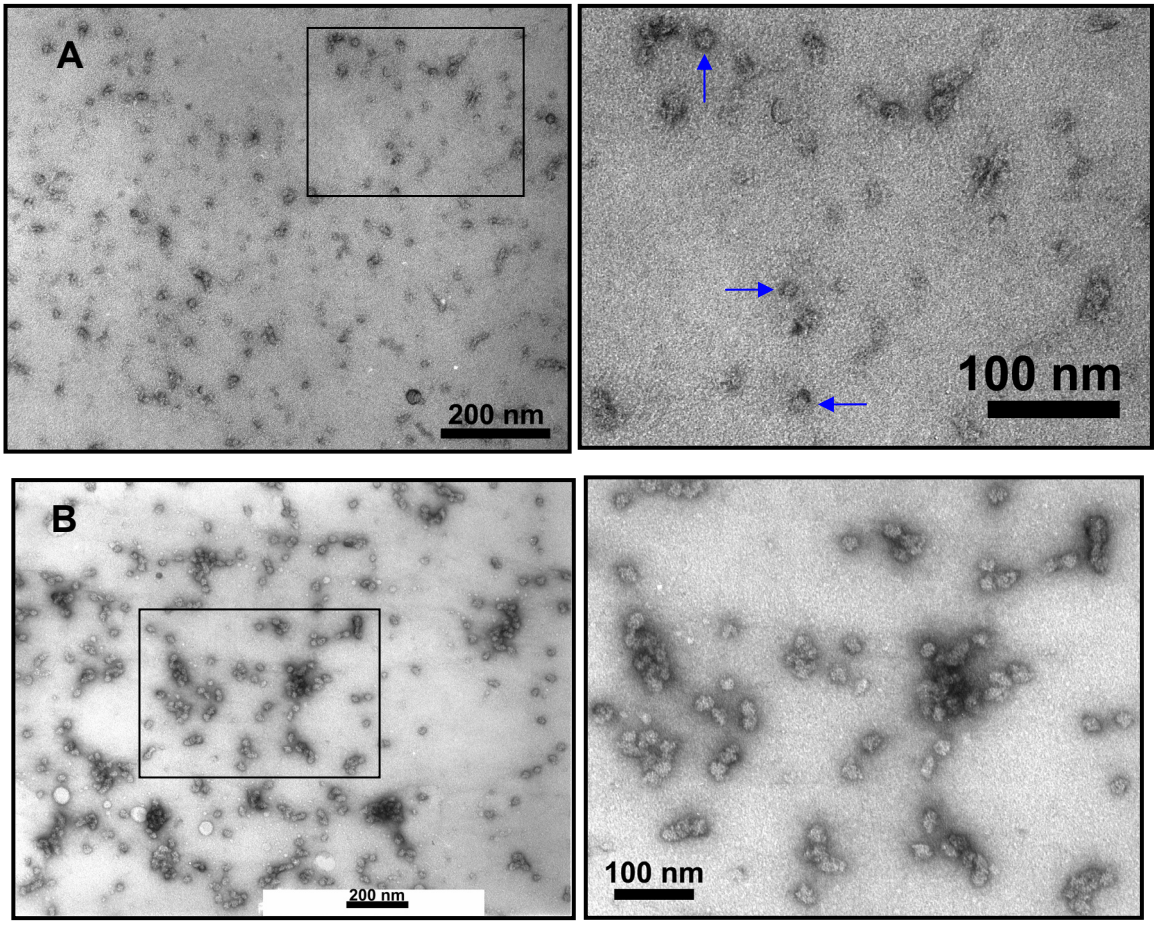

Figure 7. EM pictures of preparation 4 refolded np1 protein in 0 M and 500 mM NaCl. **A**, refolded np1 protein in 0 M NaCl. Observed flat looking nanoparticles are highlighted in blue arrows. **B**, refolded np1 protein in 500 mM NaCl. For better viewing, in **A** and **B** a portion of the EM picture (area denoted in rectangle box) is enlarged and presented on the right side. In both the conditions, samples were analyzed in the buffer containing 20 mM Tris pH 7.5 and 10% glycerol. The pictures were prepared by negative staining with 2% uranyl acetate; the concentration of the protein was 50 µg/ml.

Table 2: AUC result for preparation 4 refolded np1 protein in 0 M NaCl.

Refolding condition#	Rotor speed (rpm)	Concentration (mg/ml)	Calculated MW (kDa)	No. of monomers
preparation 4	14000	0.1	25 + 119	2.4 + 11.6
		0.7	119	11.6

- np1 protein refolded in buffer 20 mM Tris pH 7.5, 10% glycerol, 1 mM DTT and no salt

pH of the refolding buffer

The effect of pH on nanoparticle assembly is studied by refolding the np1 protein in buffers of varying pH, as summarized in Table 3. The other parameters of the refolding buffer such as NaCl concentration (150 mM), DTT concentration (1 mM DTT) and glycerol (10%) are kept constant. The refolded samples are analyzed in the buffer containing 150 mM NaCl and 10% glycerol (oxidizing condition).

The np1 protein refolded at pH 5.6 and 6.5 resulted in protein precipitation at 6 M and 2 M urea concentration, respectively (Table 3). In pH 5.6 refolding, changing the buffer from sodium acetate to MES did not help as the protein precipitated at 6 M urea in both buffers. The np1 protein refolded in 20 mM Hepes buffer pH 7.5 is observed to form expected size nanoparticles of ~ 17 nm in diameter (Figure 8, A). Also, np1 protein refolded at pH 8.5 is observed to form expected size nanoparticles (~ 17 nm in diameter) but with high amount of background (Figure 8, B). The background could possibly the mixture of trimers, pentamers, even units and multiples thereof.

Table 3: Summary of np1 protein refolded under varying pH conditions

Buffer#	pH	Observation
20 mM sodium acetate	5.6	precipitates in 6 M urea
20 mM MES	5.6	precipitates in 6 M urea
20 mM HEPES	6.5	precipitates in 2 M urea
20 mM HEPES	7.5	forms nanoparticles of expected size (~ 17 nm)
20 mM TRIS	8.5	aggregated structures

- preparation 4 refolding condition was followed for refolding in varying pH conditions.

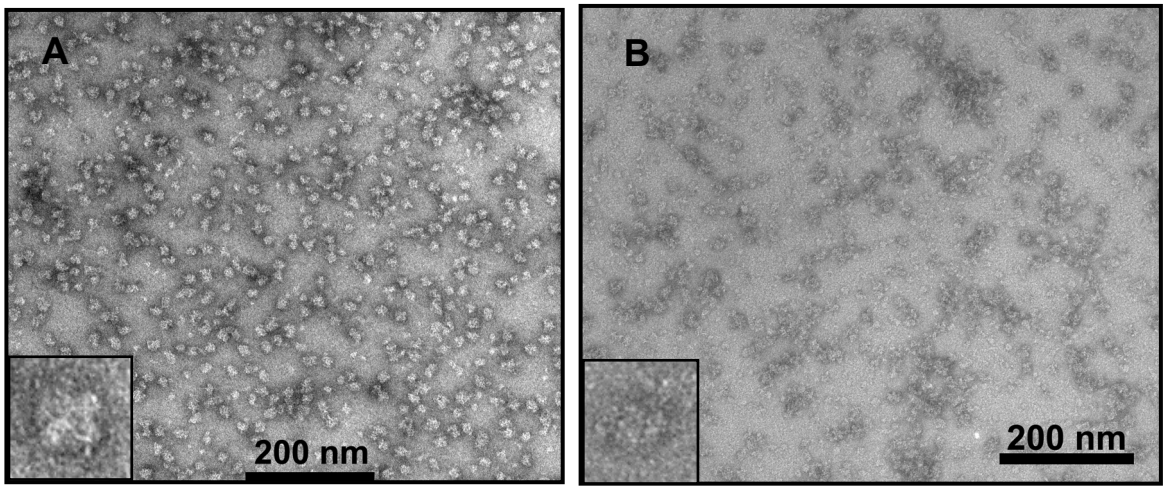

Figure 8. EM pictures of preparation 4 refolded np1 protein in varying pH. **A**, refolded np1 protein in 20 mM Hepes buffer pH 7.5. Inset: highlighting one single nanoparticle. **B**, refolded np1 protein in 20 mM Tris buffer pH 8.5. Inset: highlighting one single nanoparticle. The pictures were prepared by negative staining with 2% uranyl acetate; the concentration of the protein was 50 µg/ml.

DTT concentration

To understand the effect of DTT concentration on nanoparticle assembly, the np1 protein is folded in refolding buffer containing higher concentrations of DTT (2 mM DTT).

We followed preparation 4 refolding and after refolding, the refolded np1 protein is studied in the buffer containing 20 mM Tris pH 7.5, 150 mM NaCl, 10% glycerol and 2 mM DTT (reducing condition). From EM picture, we observed expected size nanoparticles of ~ 17 nm in diameter (Figure 9) similar to the observation of np1 protein refolded in 1 mM DTT concentration (Figure 5, B).

Glycerol

The icosahedral nanoparticles observed in preparation 4 refolded sample are found to be stabilized by the presence of 10% glycerol, because in 10% glycerol the nanoparticles are mostly individual in nature (Figure 5, C) but upon removal of glycerol the nanoparticles are observed to be mostly clumped (Figure 10; highlighted in red arrows).

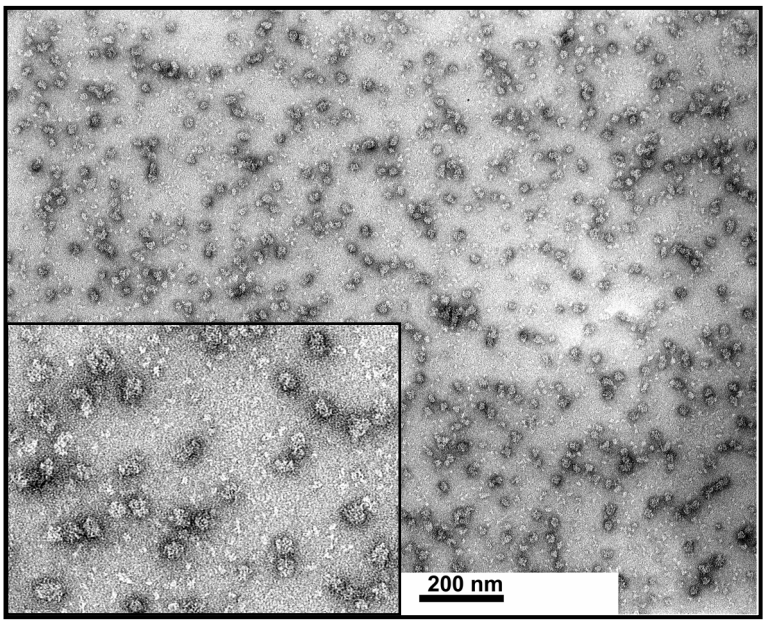

Figure 9. EM picture of preparation 4 refolded np1 protein in refolding buffer (20 mM Tris pH 7.5, 150 mM NaCl and 10% glycerol) with 2 mM DTT (reducing condition). Inset: highlighting the expected size nanoparticles of 17 nm in diameter. The picture was prepared by negative staining with 2% uranyl acetate; the concentration of the protein was 50 µg/ml.

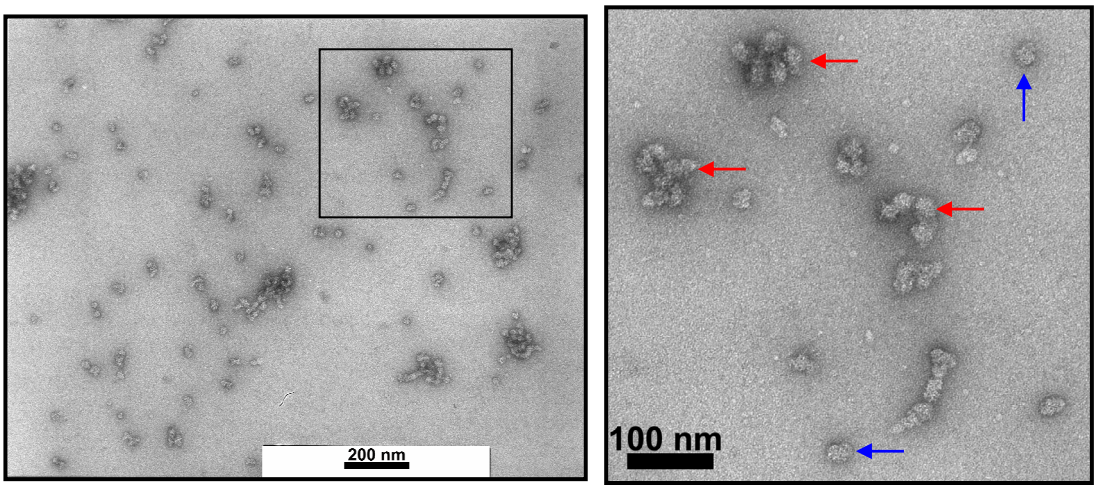

Figure 10. EM picture of np1 nanoparticles in buffer containing no glycerol (20 mM Tris pH 7.5, 150 mM NaCl). For better viewing, a portion of the EM picture (area denoted in rectangle box) is enlarged and presented on the right side. Clumped (red) and single nanoparticles (blue) are highlighted. The picture was prepared by negative staining with 2% uranyl acetate; the concentration of the protein was 50 µg/ml.

Self-assembly properties of np2 protein

As we know from our design principles, the np2 protein is designed to have charged residues at the interface between the two different coiled-coil oligomerization domains (Figure 2). The purpose of charged residues is to keep the helices of the two different oligomerization domains in close proximity to favor the formation of nanoparticles with regular icosahedral symmetry. To test our design principles, the purified np2 samples were refolded under preparation 3 refolding condition (oxidizing condition refolding from 8 M to 0 M urea). We did not refold the samples under preparation 4 refolding condition (reducing condition refolding from 8 M to 0 M urea), because, of the absence of cysteine residues in np2 protein sequence (for sequence details see Figure 1, A).

Initially, the np2 samples are refolded in physiological salt concentration (150 mM NaCl), to understand the role of intramolecular ionic interactions in the assembly process.

Biophysical characterization

EM results

The np2 protein refolded in 150 mM NaCl concentration and in buffer 20 mM Tris pH 7.5 containing 10% glycerol is observed to form mostly flat, spherical shaped nanoparticles (indicated in black arrows). In addition, we observed aggregated nanoparticles forming big aggregates (indicated in red arrows) (Figure 11).

AUC results

Initial runs of sedimentation equilibrium (SE) (8000 rpm speed) gave concentration dependent molecular mass values of 262 kDa (0.5 mg/ml) and 164 + 46 kDa (0.1 mg/ml) (Table 4, A). The monomeric mass of np2 protein is 10372.2 Daltons. Therefore, the above molecular mass values suggest that it could be the mixture of species and can be roughly correlated to trimers and even units (15-mers). In the subsequent runs (11000 and 18000 rpm), over the time we observed only molecular weight species corresponding to pentamers and trimers (Table 4, A).

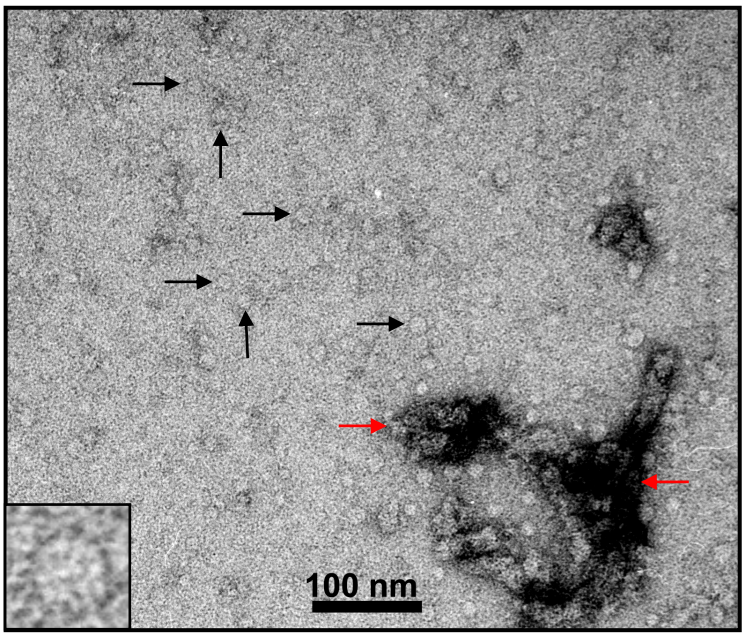

Figure 11. EM picture of np2 protein refolded in 150 mM NaCl concentration and in buffer 20 mM Tris pH 7.5, 10% glycerol. The observed flat, spherical shaped nanoparticles are indicated in black arrows and the big aggregates in red arrows. Inset: highlighting one single flat nanoparticle.

In addition, after the SE runs we performed sedimentation velocity (SV) runs. The result gave us a sedimentation velocity coefficient value of 2.3 S (Table 4, B). This again suggested us the presence of low molecular weight species possibly the pentamers sand trimers. Based on the result of SE and SV runs, it seems that the refolded np2 sample precipitates over the time. This was further supported by the observed precipitation behavior in the stored samples of refolded np2 protein.

Table 4. Preliminary AUC results for refolded np2 protein

A. Sedimentation equilibrium results. Monomer molecular weight - 10372.2 Daltons

Refolding condition	Rotor speed (rpm)	Concentration (mg/ml)	Calculated MW (kDa)	No. of monomers
preparation 3	8000	0.5	262	25.3
		0.16	46 + 164	4.4 + 15.8
	11000	0.5	70	6.7
		0.25	52	5.0
		0.16	62	5.9
	18000	0.5	40	3.9
		0.25	30	2.9
		0.16	33	3.2

B. Sedimentation velocity results.

Refolding condition	Rotor speed (rpm)	Concentration (mg/ml)	Calculated Sedimentation velocity coefficient value ($s_{20,w}$)
preparation 3	50000	0.24	2.3

The purified np2 samples were also refolded in buffer (20 mM Tris pH 7.5, 10% glycerol) containing no NaCl to understand the screening effect of salt on ionic interactions. From the refolding results, we observed strong precipitation in the refolded np2 samples, compared to the precipitation behavior of np2 protein refolded in 150 mM NaCl concentration.

Circular Dichroism (CD) spectral analysis of np1 and np2 nanoparticles

The np1 (Figure 5, C) and np2 (Figure 10) nanoparticles are studied for secondary structural contents and stability properties using CD spectroscopy. The CD spectra of np1 and np2 nanoparticles showed a typical and similar α-helical spectrum with characteristic minima at 222 and 208 nm (Figure 12, A). The α-helical values calculated from the CD spectra of np1 and np2 nanoparticles are in very good agreement with the theoretically calculated α-helical values (Table 5).

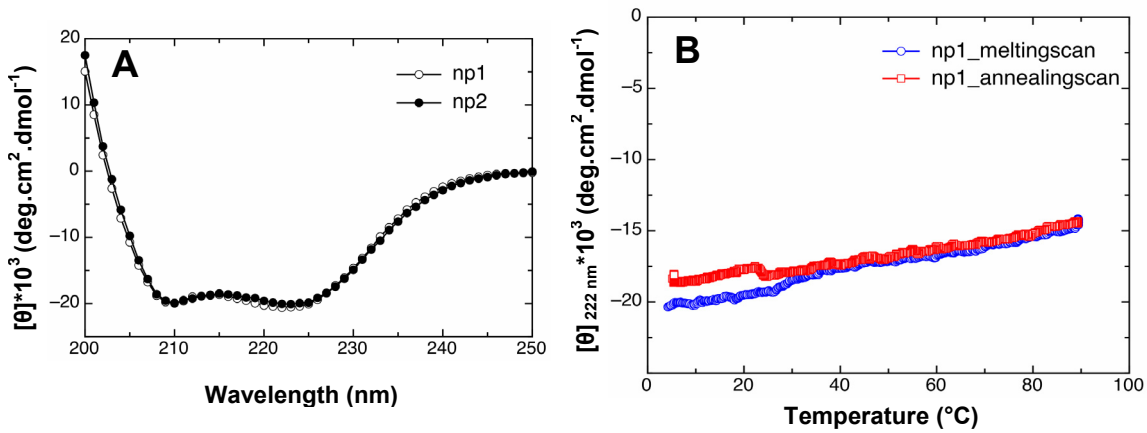

Figure 12. **A**, far UV-CD spectra of np1 nanoparticles (○) (preparation 4 refolded) compared with np2 nanoparticles (●) (preparation 3 refolded). The protein concentration was 0.1 mg/ml. **B**, Thermal denaturation profile of np1 nanoparticles. The melting scan (blue open circles) and the corresponding annealing scan (red open squares) are shown. The protein concentration was 0.28 mg/ml. In both **A** and **B**, the nanoparticles were analyzed in the buffer 20 mM Tris pH 7.5, 150 mM NaCl and 10% glycerol.

Table 5. Calculated α-helical contents (%) from the CD spectra of np1 & np2 nanoparticles using CDPro program [4]. (http://lamar.colostate.edu/~sreeram/CDPro)

CDPro analysis programs	Calculated α-helical content (%) from the CD spectra		Theoretically calculated α-helical content (%) from the sequence# (for both np1 and np2 proteins)
	np1	np2	
SELCON3	65.4	70.2	72.1
CONTINLL	65.8	67.1	
CDSSTR	71.3	75.7	

- Calculated using the formula: (total number of aa (86)) / (number of aa from COMP domain (36)) + (number of aa from *de novo* designed trimer (26)).

It is observed that the transition point of thermal denaturation curve exceeds 90°C (Figure 12, B; blue circles). This indicates the stability of the formed nanoparticles. The observed renaturation curve is very similar to the denaturation curve and more than 90% of the initial signal is recovered up on cooling (Figure 12, B; red circles).

Thrombin cleavage results for np1 and np2 nanoparticles

The purpose of this experiment is to understand whether it is possible to remove the first 22 N-terminal amino acids which are of vector origin from np1 and np2 nanoparticles, using thrombin cleavage site (see Figure 1, A). To achieve the above purpose, the np1 (preparation 4 refolded) and np2 (preparation 3 refolded) nanoparticles are digested with varying ratios of thrombin to nanoparticles. The np2 nanoparticles showed a precipitation behavior during the incubation period with thrombin enzyme. Therefore, we are presenting only the thrombin cleavage result of np1 nanoparticles.

The thrombin cleavage result of np1 nanoparticles are summarized in Figure 13. The thrombin digested np1 nanoparticles even in the presence of a 50 times greater concentration of thrombin to protein (lane 7; Figure 13) is observed to be similar to the undigested np1 nanoparticles (lane 2; Figure 13). This possibly suggest about the unavailability of the thrombin cleavage site in np1 nanoparticles.

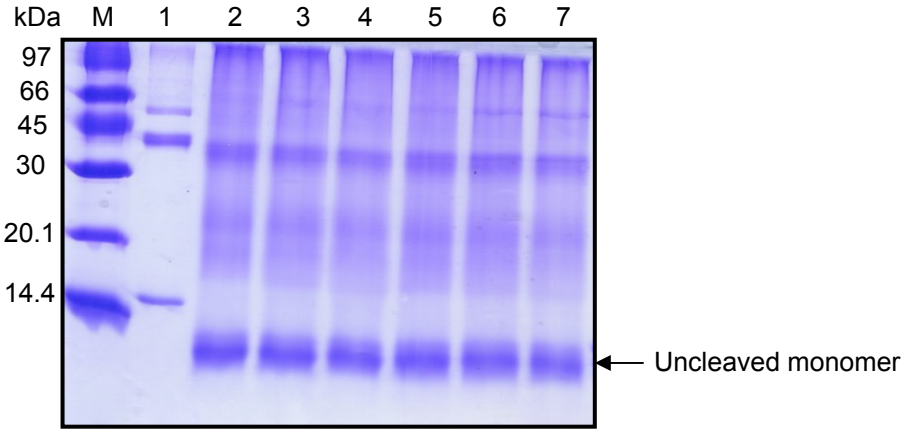

Figure 13. 17% SDS-PAGE results of thrombin digested np1 nanoparticles. For cleavage reactions, the amount of np1 nanoparticles used was 10 µg. Lane 1 - positive control protein (4 µg) in the presence of 0.04 U of thrombin; lane 2 - undigested np1 nanoparticles; lane 3 - np1 nanoparticles in the presence of 0.02 U of thrombin (2X); lane 4 - np1 nanoparticles in the presence of 0.05 U of thrombin (5X); lane 5 - np1 nanoparticles in the presence of 0.1 U of thrombin (10X); lane 6 - np1 nanoparticles in the presence of 0.2 U of thrombin (20X); lane 7 - np1 sample in the presence of 0.5 U of thrombin (50X). In the gel, the uncleaved positive control protein corresponds to a size of 48 kDa and its cleaved fragments to 32 and 16 kDa, respectively.

Chapter 2B

Peptide based nanoparticles as an antigen display carrier in vaccination

Design principles

The arrangement of antigens in a highly ordered and repetitive manner on the surface of virus particles was shown to be a critical factor for directly activating B-cells to produce antigen specific antibodies [5, 6]. Also, many viruses examined for induction of B-cell responses were shown to exhibit repetitive, identical neutralizing epitopes that were of highly organized [7]. The antibodies produced against the repetitively arranged antigens were of high titer and were shown to have high affinity and specificity, as opposed to the antibodies produced against monomeric antigens [8]. Using this concept, systems such as **virus like particles (VLPs)** have been employed for producing novel vaccines which yield high titers of specific antibodies [9, 10].

Because of its resemblance to VLPs in the property of repetitive arrangement of identical protein subunits, we wanted to use our nanoparticle system as a **repetitive antigen display system**. For comparison, in the hepatitis B virus core protein based VLPs, known as the '**universal display model**', the particles were made up of 180 or 240 identical protein subunits [11, 12] and in our peptide based nanoparticle system the particles were made up of 60 identical protein subunits (Chapter 1). So, by fusing the epitope of choice to **np1** or **np2** protein (for sequence details refer to Chapter 2A; Figure 1, A) at either the N- or C-terminus and assembling the proteins into nanoparticles, such a repetitive antigen display system could be built (Figure 14).

Pseudomonas aeruginosa pilin protein as an epitope of choice

In collaboration with Dr. Robert S. Hodges from University of Colorado Health Sciences Center, we wanted to develop an effective anti-adhesin vaccine against *Pseudomonas* pathogen using our peptide based nanoparticle as a repetitive antigen display system. In his review, Hodges et al. [13] describes the importance of a vaccine against pseudomonas as follows: '*Pseudomonas aeruginosa* and *Pseudomonas maltophilia* account for 80% of opportunistic infections by *Pseudomonas*. *Pseudomonas aeruginosa* is an opportunistic pathogen that causes urinary tract infections, respiratory system infections, dermatitis, soft tissue infections, bacteremia, and a variety of systemic infections, particularly in patients with severe burns, and in cancer and AIDS patients who are immunosuppressed.

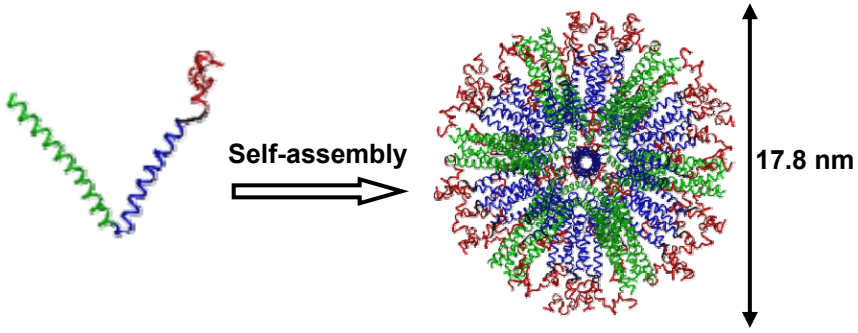

Figure 14. Concept of the peptide based nanoparticles as a repetitive antigen display system. The monomeric chains of np1 or np2 protein attached with epitope sequence (red) forms the basic building blocks. The pentameric coiled-coil domain and the *de novo* designed trimeric coiled-coil domain in np1 or np2 protein is depicted in green and blue, respectively. The computer assembled nanoparticle model with the epitopes displayed repetitively on the surface is depicted on the right side. It was calculated to be a size of 17.8 nm.

Pseudomonas aeruginosa is notable for its resistance to antibiotics, and is therefore a particularly dangerous pathogen. Only a few antibiotics are effective against *Pseudomonas*, including fluoroquinolones, gentamicin, and imipenem, and even these antibiotics are not effective against all strains. The difficulty in treating *Pseudomonas* infections with antibiotics is most dramatically illustrated in cystic fibrosis patients, virtually all of whom eventually become infected with a strain that is so resistant that it cannot be treated. Since antibiotic therapy has proved so ineffective as a treatment, we embarked on a research program to investigate the development of a synthetic peptide consensus sequence vaccine for this pathogen'.

Dr. Hodges group provided us with the sequence of *Pseudomonas aeruginosa* strain O (PAO) pilin protein (pilA; C-terminal residues 124 to 149) as an epitope sequence to be attached to our nanoparticle system. We chose pilin protein as an epitope because it forms the basic building blocks of pilus, which is a key adhesin that *P.aeruginosa* employs to attach to epithelial cell surfaces [14-16] and mucous proteins [17].

Also, Hodges and co-workers showed that the native *P. aeruginosa* strain K (PAK) monomeric protein subunit, PAK pilin, contains the epithelial cell-surface binding domain in the C-terminal region of the pilin protein sequence [18].

Moreover, Hodges and co-workers showed that the antipeptide antibodies generated against the C-terminal region residues 128-144 of PAK strain, which is a disulfide bonded loop region, were able to block adhesion [19]. In PAO strain, this region corresponds to C-terminal region residues 133-149 and was also shown to form a loop structure through the formation of a disulfide bridge between residues 134 and 147 [20]. The disulfide bonded loop region of PAO strain along with its sequence is depicted in Figure 15.

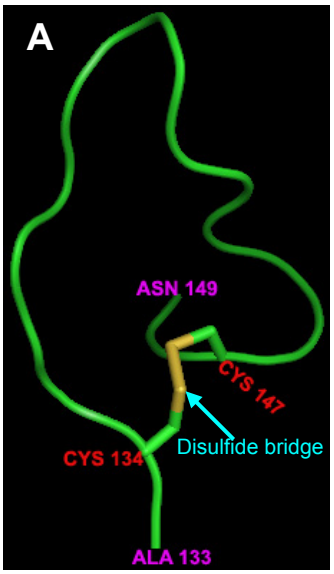

B

```
124    130         140        149
LNRTADG VWACKSTQDP MFTPKGCDN
```

Figure 15. (**A**) Cartoon depicting the C-terminal disulfide bonded loop region of *Pseudomonas aeruginosa* PAO strain pilin protein (residues 133 to 149). The start and end amino acids of the loop region are indicated in pink. Cysteine residues involved in disulfide bond are indicated in red. (**B**) C-terminal amino acid sequences of *Pseudomonas* (PAO) pilin protein involved in this study (residues 124 to 149). Amino acids that form the loop region are highlighted in green. The picture was prepared using PyMol program (http://www.pymol.org) (PDB file 1PAN).

Nanoparticle constructs for repetitive antigen display

To test our nanoparticle system as a repetitive antigen display system, we recombinantly fused the *Pseudomonas* pilin epitope at the C-terminus of np1 and np2 constructs, resulting in **np1e** and **np2e** constructs (for sequence details refer to Figure 16, A and B). We also wanted to generate **different sized nanoparticles** in order to determine the effect of size on the immunogenicity of the nanoparticles.

A

```
          1         10         20         30         40         50         60         70         80         90
np1       MGHHHHHHGDWKWDGGLVPRGSDEMLRELQETNAALQDVRELLRQQVKQITFLKCLLMGGRLLCRLEELERRLEELERRLEELERA
np1e      np1(1-86)-RGLNRTADGVWACKSTQDPMFTPKGCDN
                    a  d  a  d  a  d
np1ev1    np1(1-86)-INTVDLELAALRRRLEELARGLNRTADGVWACKSTQDPMFTPKGCDN
                    a  d  a  d  a  d  a  d  a  d  a  d
np1ev2    np1(1-86)-ISAIKADLSALKANLASLQADINTVDLELAALRRRLEELARGLNRTADGVWACKSTQDPMFTPKGCDN
```

B

```
          1         10         20         30         40         50         60         70         80         90
np2       MGHHHHHHGDWKWDGGLVPRGSDEMLRELQETNAALQDVRELLRQQVKQIRRLKRLLRGGRLLAELEELRERLEELERRLEELERA
np2e      np2(1-86)-RGLNRTADGVWACKSTQDPMFTPKGCDN
                    a  d  a  d  a  d
np2ev1    np2(1-86)-INTVDLELAALRRRLEELARGLNRTADGVWACKSTQDPMFTPKGCDN
                    a  d  a  d  a  d  a  d  a  d  a  d
np2ev2    np2(1-86)-ISAIKADLSALKANLASLQADINTVDLELAALRRRLEELARGLNRTADGVWACKSTQDPMFTPKGCDN
```

Figure 16. Sequence details our nanoparticle constructs for repetitive antigen display. In **A**, np1 construct formed the template for design and in **B**, the template is np2 construct. In both np1 and np2, the residues corresponding to the pentameric coiled-coil domain of COMP and the *de novo* designed trimeric coiled-coil domain are colored green and blue, respectively. In addition, for convenience the first 86 amino acids of np1 and np2 based constructs are denoted as $np1_{1-86}$ and $np2_{1-86}$, respectively. The pilin antigen residues from *Pseudomonas* pathogen (strain PAO) are colored red. The extended trimeric coiled-coil domain I in np1ev1 and np2ev1 constructs is highlighted in turquoise. Similarly, in np1ev2 and np2ev2 constructs the extended trimeric coiled-coil domain II is highlighted in pink. The **a** and **d** positions of the heptad repeats in the extended trimeric coiled-coil domains are indicated. The first 22 amino acids of np1 and np2 constructs, which correspond to the vector sequence, are underlined.

As a first step, we extended the C-terminus of the trimeric coiled-coil domain of np1e and np2e constructs by adding an additional three heptad repeats, resulting in **np1ev1** and **np2ev1** constructs, respectively (for sequence details refer to Figure 16, A and B).

Again, by using np1ev1 and np2ev1 as templates, we further extended the trimeric coiled-coil domain by adding an additional three heptad repeats resulting in **np1ev2** and **np2ev2** constructs, respectively (for sequence details refer to Figure 16, A and B). According to computer modeling, these will lead to nanoparticles ranging in size from about 17 nm to 29 nm (Figure 17, B).

Results

Modular nature of our nanoparticle constructs designed for repetitive antigen display

Our nanoparticle constructs were designed so that they can be **easily modulable**, as depicted in the Figure 17, A. First of all, the core peptide of the designed constructs, comprising the pentameric coiled-coil domain (COMP) and the trimeric coiled-coil domain can easily be exchanged by cutting with BamHI and XhoI restriction enzymes. Similarly, the epitope attached to the core peptide or to the extended core peptide can be readily exchanged with other epitopes by cutting with XmaI and EcoRI restriction enzymes. Also, the first part of the extended trimeric coiled-coil domain (extended trimer I) can easily be exchanged by cutting with SalI + XmaI, and the second part of the extended trimeric coiled-coil domain (extended trimer II) by cutting with XhoI + SalI restriction enzymes.

Purification results of our nanoparticle constructs designed for repetitive antigen display

All the nanoparticle constructs were expressed along with the 22 amino acids of vector sequence at the N-terminus (underlined residues in Figure 16). All the constructs were purified using Ni^{2+}-affinity column chromatography. The purification was carried out under denaturing conditions using 8 M urea (for expression and purification details refer to Materials and Methods section).

Purification results of np1e and np2e proteins

The np1e protein is observed to elute during pH 5.0 (lane 2) and pH 4.5 (lanes 3 and 4) elution fractions, in minute amounts (Figure 18, A). The eluted fractions correspond to a theoretically calculated monomer of molecular weight 13341.2 Daltons. A majority of the monomeric form of np1e samples are observed in 500 mM imidazole elution fractions (lanes 4 to 9; Figure 18, A). In the first two fractions of 500 mM imidazole elution, in addition to a monomeric band, bands corresponding to theoretically calculated dimeric (26682.4 Daltons), trimeric (40023.6 Daltons) and tetrameric (53364.8 Daltons) forms are observed.

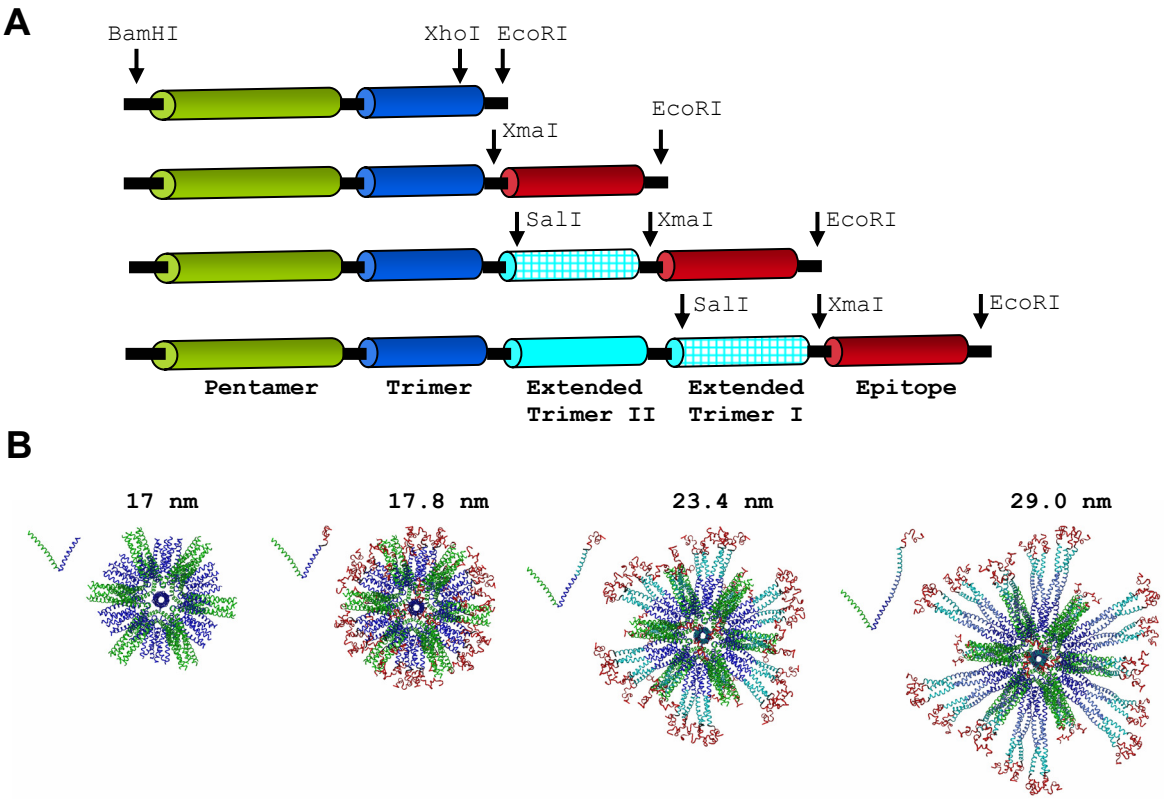

Figure 17. **A**, Modular nature of our nanoparticle constructs designed for repetitive antigen display. The pentameric coiled-coil domain of COMP (green) and the *de novo* designed trimeric coiled-coil domain (blue) form the core peptide in the designed constructs. Either np1 or np2 construct forms the core peptide region. The epitope sequence is depicted in red. The extended trimer I domain is depicted in rectangular meshed turquoise. The extended trimer II domain is depicted in completely filled turquoise. The restriction enzyme sites are marked with bold arrows. **B**, From left to right, the computer designed models of core peptide (np1 or np2), core peptide with epitope (np1e or np2e), core peptide with the one time extended trimer domain + epitope (np1ev1 or np2ev1) and core peptide with two times extended trimer domain + epitope (np1ev2 or np2ev2). Each model is depicted beneath its calculated size.

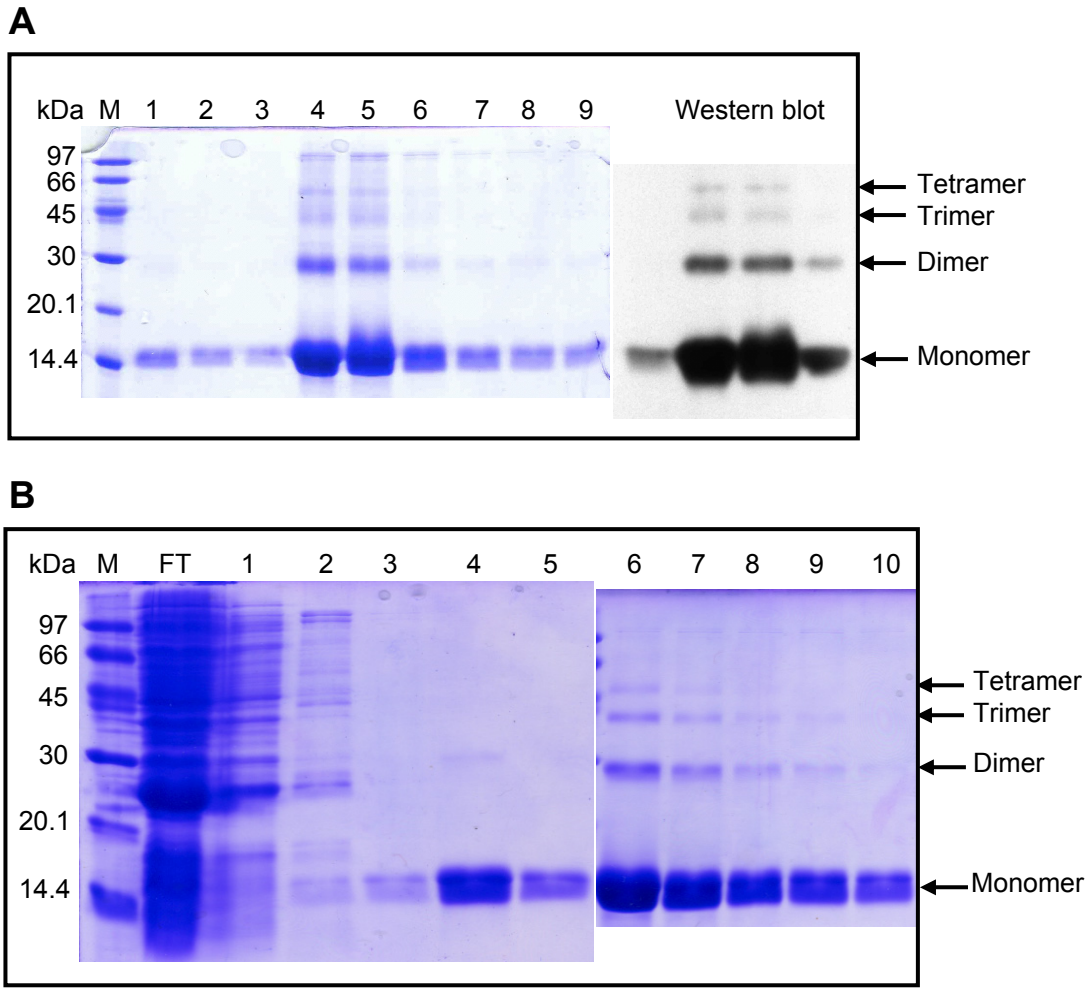

Figure 18. 15% SDS-PAGE of np1e and np2e purified fractions. **A**, np1e protein. Lane 1 - pH 5.0 elution fraction; lanes 2 & 3 - pH 4.5 elution fractions; lanes 4 to 9 - 500 mM imidazole elution fractions. Western blot results correspond to the samples in lanes 3 to 6. **B**, np2e protein. FT - Flow through; lane 1 - pH 8.0 wash fraction; lane 2 - pH 6.3 wash fraction; lane 3 - pH 5.9 elution fraction; lanes 4 to 5 - pH 5.0 elution fractions; lanes 6 to 10 - 250 mM imidazole elution fractions. In both **A** and **B**, M correspond to molecular weight marker, marked in kilo Daltons (kDa).

The result of western blot confirmed the presence of oligomeric forms along with the monomeric form in 500 mM imidazole elution fractions (Figure 18, A). The np2e protein is observed to start eluting in pH 5.0 elution fractions (lanes 4 and 5) and to continue eluting in 250 mM imidazole elution fractions (lanes 6 to 10) (Figure 18, B). The pH 5.0 eluted fractions correspond to a theoretically calculated monomer of molecular weight 13424.2 Daltons. In the 250 mM imidazole elution fractions, in addition to monomeric band, bands corresponding to theoretically calculated dimeric (26848.4 Daltons), trimeric (40272.6 Daltons) and tetrameric (53698.8 Daltons) forms are observed, as in the case of np1e 500 mM imidazole elution fractions.

Purification results of np1ev1 and np2ev1 proteins

The np1ev1 protein is observed to start eluting in a pH 5.0 elution fraction (lane 4) and to continue eluting in 500 mM (lanes 5 to 12) and 1 M (lanes 13 and 14) imidazole elution fractions (Figure 19, A). The pH 5.0 eluted fraction corresponds to a theoretically calculated monomer of molecular weight 15518.7 Daltons. In both 500 mM and 1 M imidazole elution fractions, in addition to a monomeric band a strong band corresponding to theoretically calculated trimer (46556.1 Daltons) is observed.

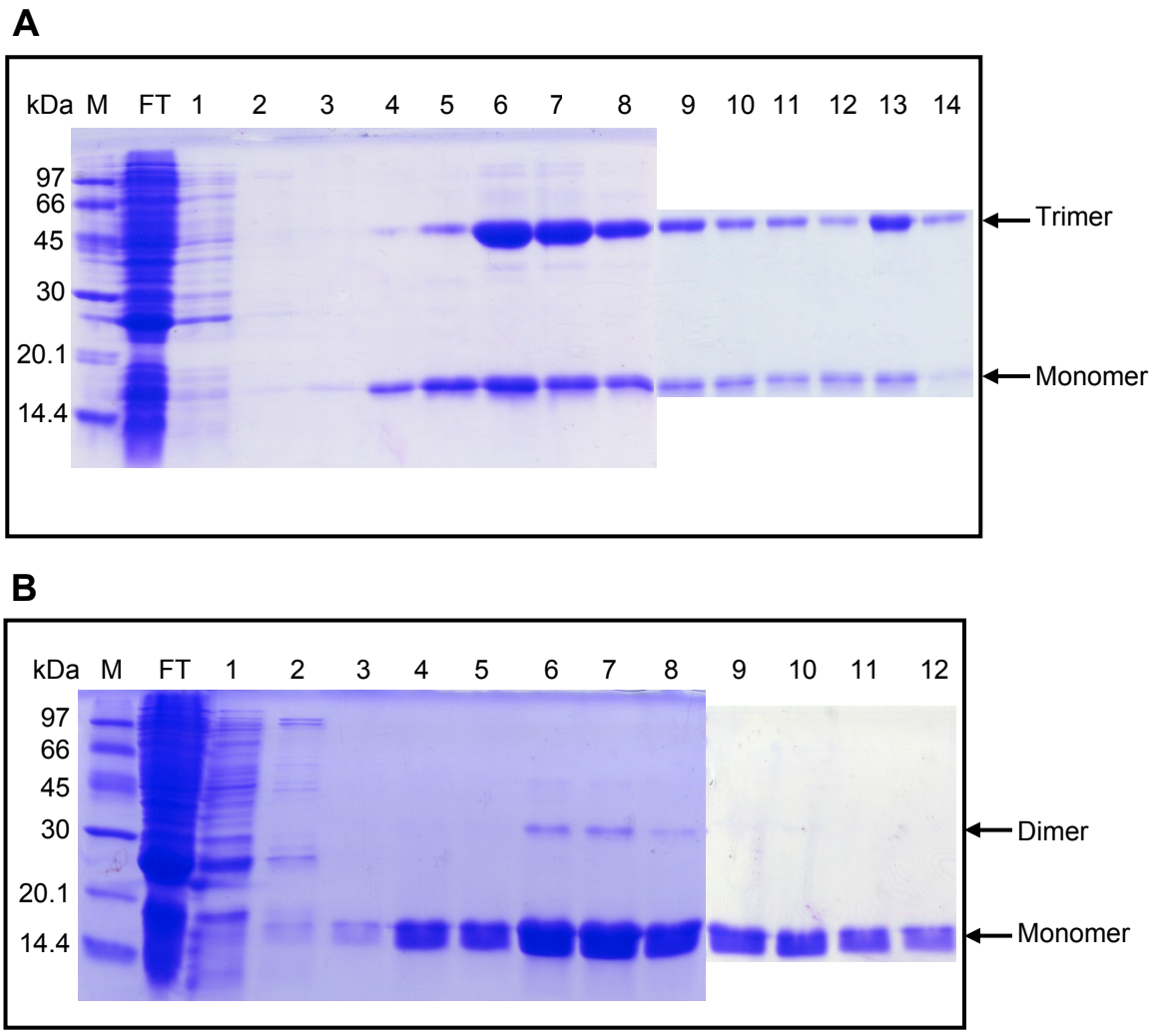

Figure 19. 15% SDS-PAGE of np1ev1 and np2ev1 purified fractions. **A**, np1ev1 protein. Lanes 5 to 12 - 500 mM imidazole elution fractions; lanes 13 and 14 - 1 M imidazole elution fractions. **B**, np2ev1 protein. Lanes 5 to 12 - 250 mM imidazole elution fractions. In both **A** and **B**, FT denotes flow through; lane 1 - pH 8.0 wash fraction; lane 2 - pH 6.3 wash fraction; lane 3 - pH 5.9 elution fraction; lane 4 - pH 5.0 elution fraction; M - molecular weight marker, marked in kilo Daltons (kDa).

Similar to np1ev1 protein elution, the np2ev1 protein is also observed to start eluting in a pH 5.0 elution fraction (lane 4; Figure 19, B). The eluted fractions correspond to a theoretically calculated monomer of molecular weight 15601.7 Daltons. In 250 mM imidazole elution fractions (lanes 5 to 12; Figure 19, B), in the 6th and 7th lane in addition to a monomeric band a faint band corresponding to a theoretically calculated dimer (31203.4 Daltons) is observed.

Purification results of np1ev2 and np2ev2 proteins

The np1ev2 protein is observed to start eluting in minute amounts during the pH 5.0 elution step (lane 4; Figure 20, A). The eluted fraction corresponds to a theoretically calculated monomer with a molecular weight of 17614.1 Daltons.

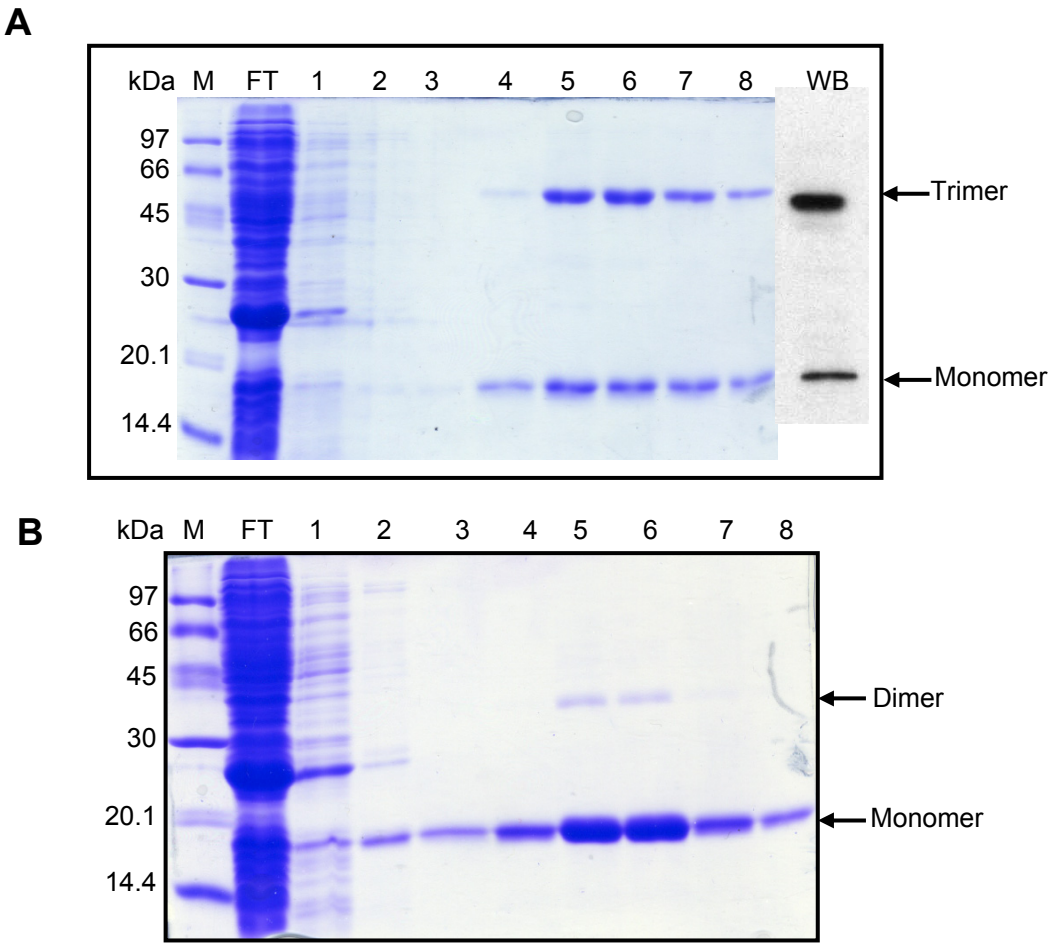

Figure 20. 15% SDS-PAGE of np1ev2 and np2ev2 purified fractions. **A**, np1ev2 protein. Lanes 5 to 8 - 500 mM imidazole elution fractions. WB - western blot result of 500 mM imidazole fraction. **B**, np1ev2 protein. Lanes 5 to 8 - 250 mM imidazole elution fractions. In both **A** and **B**, FT denotes flow through; lane 1 - pH 8.0 wash fraction; lane 2 - pH 6.3 wash fraction; lane 3 - pH 5.9 elution fraction; lane 4 - pH 5.0 elution fraction; M - molecular weight marker, marked in kilo Daltons (kDa).

Most of the eluted samples are observed in 500 mM imidazole fractions (lanes 5 to 8; Figure 20, A). In 500 mM imidazole eluted fractions, in addition to a monomeric band an extra band is observed, corresponding to a theoretically calculated trimer (35394.2 Daltons). The result of the western blot confirmed the presence of monomer and trimer species in 500 mM imidazole elution fractions (lane denoted as WB; Figure 20, A).

For np2ev2 protein, it is observed that the protein starts to elute in pH 5.9 and 5.0 elution fractions (lane 3 and 4; Figure 20, B). The eluted samples in pH 5.9 and 5.0 fractions correspond to a theoretically calculated monomer (17697.1 Daltons). But the majority of the samples are eluted in 250 mM imidazole eluted fractions (lanes 5 to 8; Figure 20, B). In 250 mM imidazole elution fractions, in the first two fractions in addition to a monomer band a faint band is observed, corresponding to a theoretically calculated dimer (35394.2 Daltons).

Summary of purification results

- In np1e (np1 protein with epitope) purified samples, we observed a dimer band in addition to monomeric band. Moreover, we observed faint bands corresponding to trimer and tetramer species of np1e protein (Figure 18, A).
- Contrary to np1e protein, for np1ev1 (np1e protein with the extended trimeric coiled-coil domain by three heptad repeats) and np1ev2 (np1e protein with the extended trimeric coiled-coil domain by six heptad repeats) purified proteins, we observed a strong trimer band in addition to monomeric band (Figure 19, A and 20, A). No dimer and tetramer bands were observed, as in np1e protein.
- For np2e purified samples (np2 protein with epitope), we observed a dimer band in addition to monomer band and faint bands corresponding to trimer and tetramer species (Figure 18, B). This observation was similar to np1e purified samples. Contrary to np1ev1 and np1ev2 purified samples, for np2ev1 and np2ev2 purified samples, we observed mainly monomeric band and in addition a less intense dimer band (Figure 19, B and 20, B).

Self-assembly properties of our nanoparticle constructs designed for repetitive antigen display

The aim of this section is to understand the nanoparticle forming ability of each designed construct. Because of the complexities of folding a protein containing intramolecular disulfide bridges, the purified proteins are refolded under two different refolding conditions (for details see Chapter 1 under heading Self-assembly of nanoparticles). In the first refolding condition, the samples are refolded completely under oxidizing condition by step wise dialysis of the urea from 8 M to 0 M urea (**preparation 3**). In the second refolding condition, the samples are refolded in reducing condition (2 mM DTT) by step wise dialysis from 8 M to 0 M urea and then exchanged to oxidizing condition (**preparation 4**). The refolded samples are characterized by using Electron Microscopy (EM). The result of the constructs will be grouped according to their calculated size from the computer model (for size details refer to Figure 17, B).

Self-assembly properties of np1e & np2e proteins

EM results for np1e protein

The preparation 4 refolded np1e protein is initially analyzed in buffer containing 0 M urea and 2 mM DTT (reducing condition). From the EM picture, the protein is observed to form nanoparticles of roughly spherical in shape (Figure 21, A). The size of the observed nanoparticles was calculated to be 17 to 18 nm in diameter, which is in good correlation with the size of computer modeled icosahedron with epitope (17.8 nm) (refer to Figure 17, B). But, upon removal of DTT (0 M urea and no DTT; oxidizing condition), the observed nanoparticles are found to be mostly aggregate with a few individual particles (Figure 21, B).

EM results for np2e protein

The preparation 4 refolded np2e protein is analyzed in a buffer containing 0 M urea and 2 mM DTT. During refolding, the pH of the buffer is kept at pH 8.0 instead of pH 7.5. This is because the calculated pI of the protein was around 7.03.

From the EM picture, the refolded protein is observed to form small, irregular shaped structures (Figure 22). No nanoparticle formation is observed.

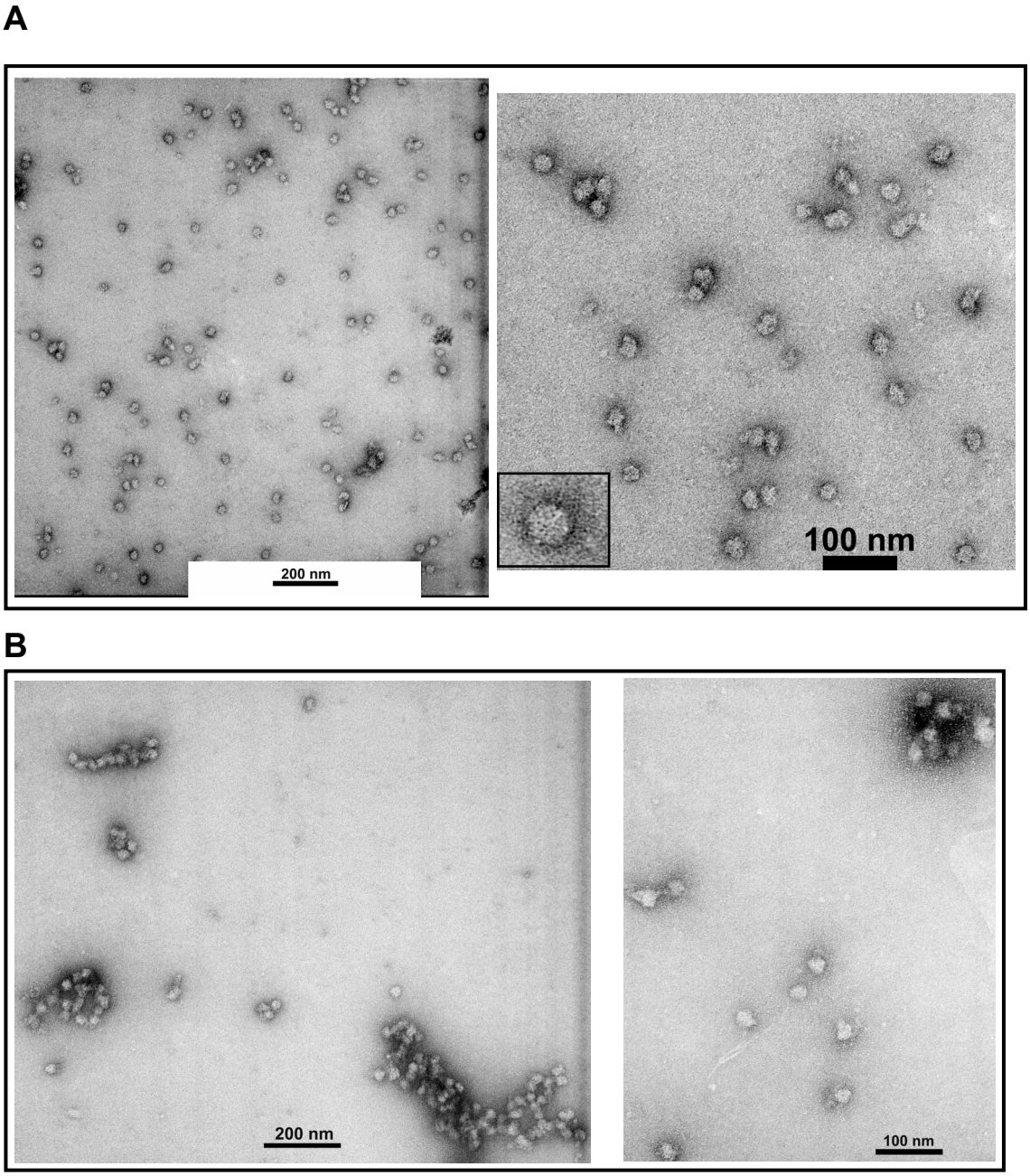

Figure 21. EM pictures of preparation 4 refolded np1e protein. **A**, np1e protein in 0 M urea and 2 mM DTT. The overall view of the sample is presented on the left and an enlarged version is presented on the right. Inset: highlighting one single nanoparticle. **B**, np1e protein in 0 M urea and no DTT. 50X magnification of the sample is presented on the left and the 100X magnification on the right.

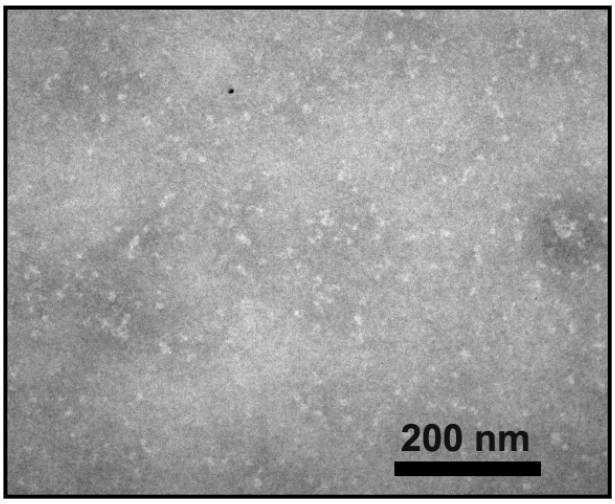

Figure 22. EM picture of preparation 4 refolded np2e protein. np2e protein in 0 M urea and 2 mM DTT (20 mM Tris pH 8.0, 150 mM NaCl and 10% glycerol).

Self-assembly properties of np1ev1 & np2ev1 proteins

EM results for np1ev1 protein

The preparation 3 refolded np1ev1 protein is observed to precipitate at 4 M urea. From the EM picture, the precipitated material is observed to form large irregular aggregates (Figure 23, A).

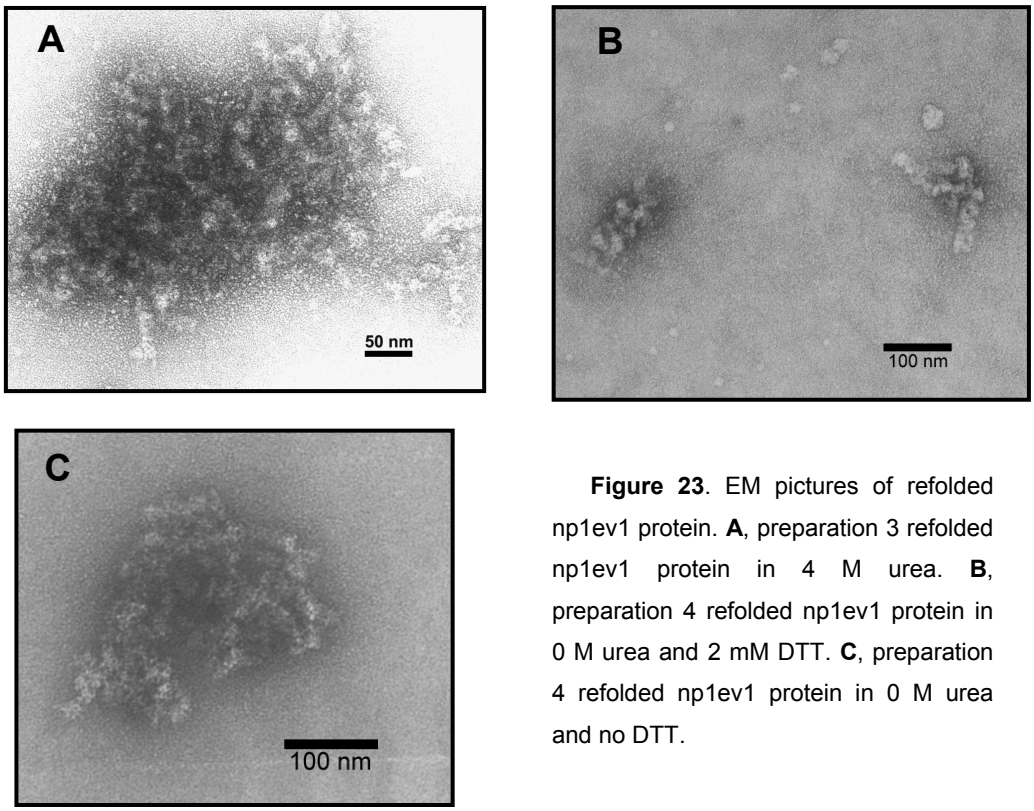

Figure 23. EM pictures of refolded np1ev1 protein. **A**, preparation 3 refolded np1ev1 protein in 4 M urea. **B**, preparation 4 refolded np1ev1 protein in 0 M urea and 2 mM DTT. **C**, preparation 4 refolded np1ev1 protein in 0 M urea and no DTT.

The preparation 4 refolded np1ev1 protein is observed to precipitate upon reaching 0 M urea and in 2 mM DTT. From EM picture, the refolded np1ev1 in 0 M urea and in 2 mM DTT is observed to form irregular aggregates (Figure 23, B). Also in 0 M urea and no DTT, we observed big aggregates (Figure 23, C).

EM results for np2ev1 protein

The preparation 4 refolded np2ev1 protein is analyzed in a buffer containing 0 M urea and 2 mM DTT (reducing condition). From the EM picture (Figure 24), the refolded protein is observed to form a large population of mostly flat, spherical shaped nanoparticles (indicated in red arrow). However, we also observed nanoparticles which are not of flat in shape (indicated in pink arrow) but appeared to lack the icosahedral symmetry.

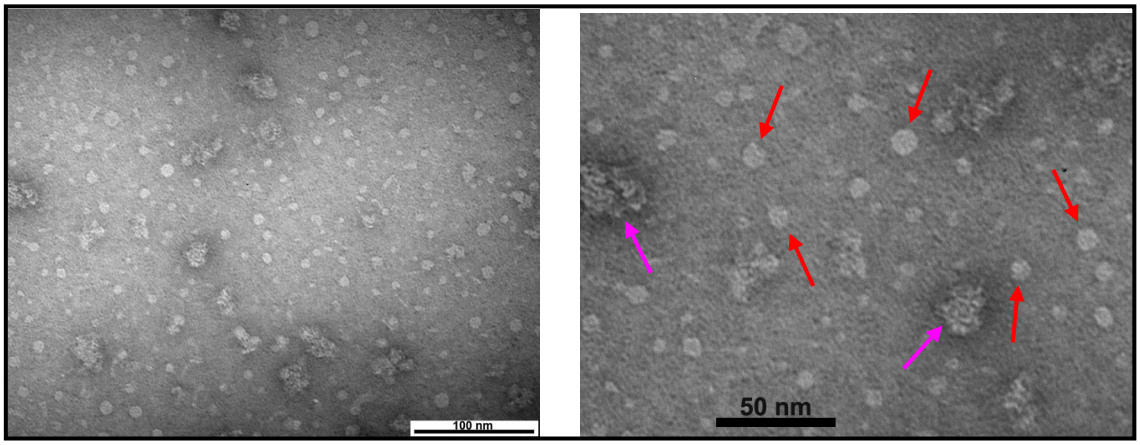

Figure 24. Preparation 4 refolded np2ev1 protein in 0 M urea and 2 mM DTT. The overall view of the sample is presented on the left and the enlarged view on the right. The observed nanoparticles of flat and not flat are highlighted in red and pink colored arrows, respectively.

Fluorescence Correlation Spectroscopy (FCS) results for np2ev1 nanoparticles

Fluorescence correlation spectroscopy (FCS) is used to study the size distribution of preparation 4 refolded np2ev1 nanoparticles. The refolded protein was labeled with fluorophore Alexa Fluor 488 (for details see FCS section in Materials and Methods). The labeled protein was studied in Tris buffered saline (TBS) (pH 7.5, 10% glycerol, no DTT).

FCS is a singe molecule spectroscopy technique. It is based on the emitted fluorescence by molecules diffusing through a very small detection volume (1 femtoliter) which is given by a confocal microscope. These intensity fluctuations, detected by a highly sensitive avalanche photo diode (APD), are reflected in the obtained intensity profile (Figure 25, A). The fluorescent intensity profile shows an average peak intensity of approximately 5 kHz (expressed as the difference from the base line intensity).

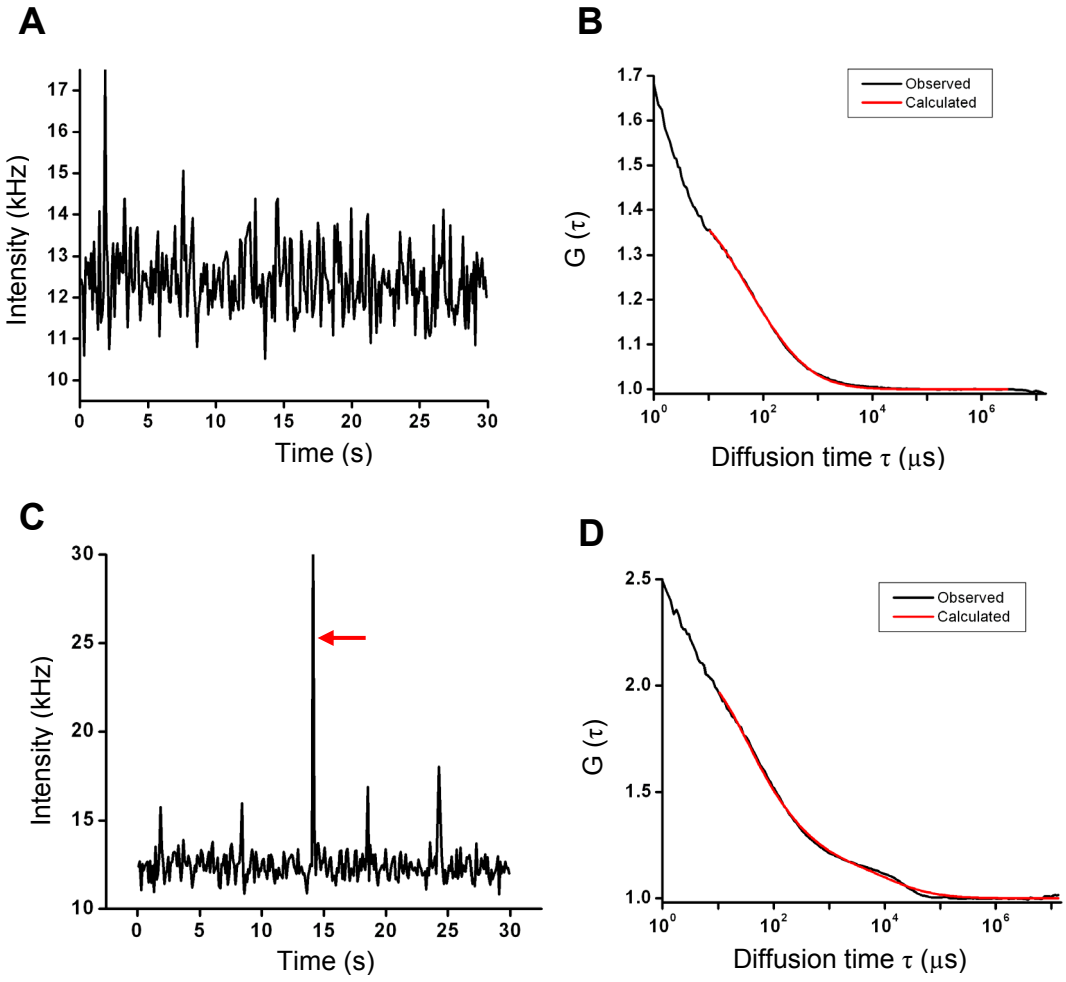

Figure 25. Fluorescence correlation spectroscopy results for np2ev1 nanoparticles (preparation 4 refolded). **A**, graph representing the fluorescent intensity fluctuations and **B**, the corresponding calculated autocorrelation curve of np2ev1 nanoparticles. **C**, fluorescence intensity fluctuations graph representing the rarely observed peaks with higher peak intensity (indicated by red arrow) and **D**, the corresponding calculated autocorrelation curve.

The intensity autocorrelation function G (τ) (refer to equation 1 in methodology section of FCS in Materials and Methods), calculated from the fluorescent intensity peaks, shows an autocorrelation curve indicating that the measured sample consists of particles with a monomodal distribution (Figure 25, B). The autocorrelation curve can be fitted with a model resulting in the determination of the number of particles/molecules and their specific diffusion time through the detection volume. The diffusion time, τ_D, obtained from fitting the autocorrelation curve is 345 ± 192 µs. By using the Stoke-Einstein relation (refer to equation 3 in methodology section of FCS in Materials and Methods), the corresponding hydrodynamic radius is calculated to be 6.4 ± 3.6 nm.

When including the whole data set obtained by FCS, an occurrence of rarely appearing peaks, with intensities up to five times higher than the values obtained from the restricted data set, can be observed (Figure 25, C; indicated by red arrow). The corresponding autocorrelation curve showed a bimodal distribution (Figure 25, D). From the fluorescent intensity fluctuations, in addition to the 345 ± 192 µs diffusion time, the diffusion time of the rarely observed peaks is calculated to be approximately 13 ms. This finding suggest that the sample also contains aggregates with a significantly larger size.

Self-assembly properties of np1ev2 & np2ev2 proteins

EM results for np1ev2 protein

The preparation 3 refolded np1ev2 protein is observed to start precipitating at 8 M urea and more precipitation is observed at 6 M urea. From the EM picture, the precipitated material at 8 M urea resemble short filament-like structures (Figure 26, A; indicated by black arrow).

The preparation 4 refolded np1ev2 protein is observed to start precipitating during 2 M to 0 M urea transition. From the EM picture, the sample at 2 M urea resemble short filament like structures (Figure 26, B; indicated by black arrow).

EM results for np2ev2 protein

The preparation 4 refolded np2ev2 protein is analyzed in a buffer containing 0 M urea and 2 mM DTT. From the EM picture (Figure 27), the refolded protein is observed to form flat, spherical shaped nanoparticles (indicated in black arrow).

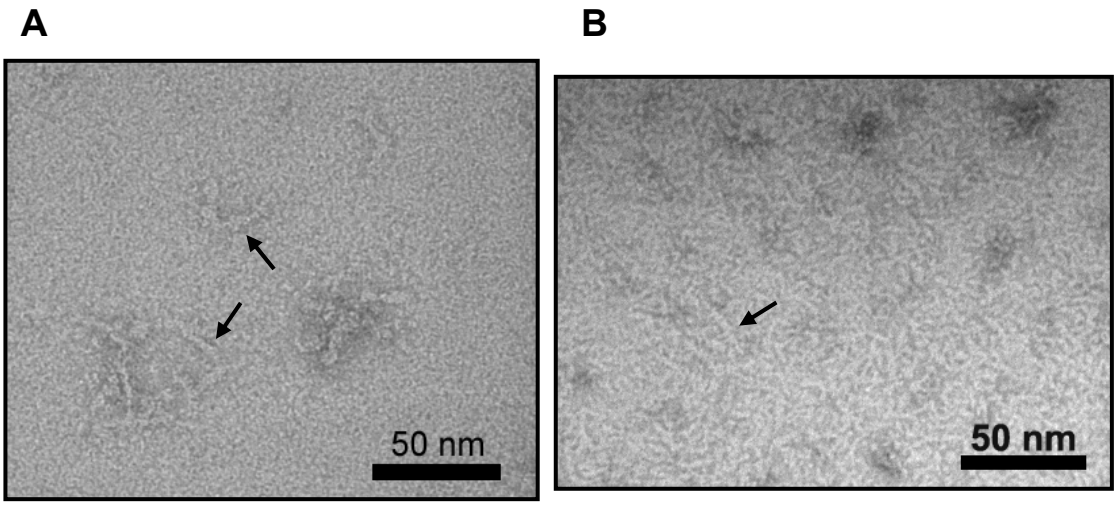

Figure 26. EM pictures of refolded np1ev2 protein. **A**, preparation 3 refolded np1ev2 protein in 8 M urea. **B**, preparation 4 refolded np1ev2 sample in 2 M urea and 2 mM DTT. In both **A** and **B**, the observed short filament-like structures are indicated in black arrow.

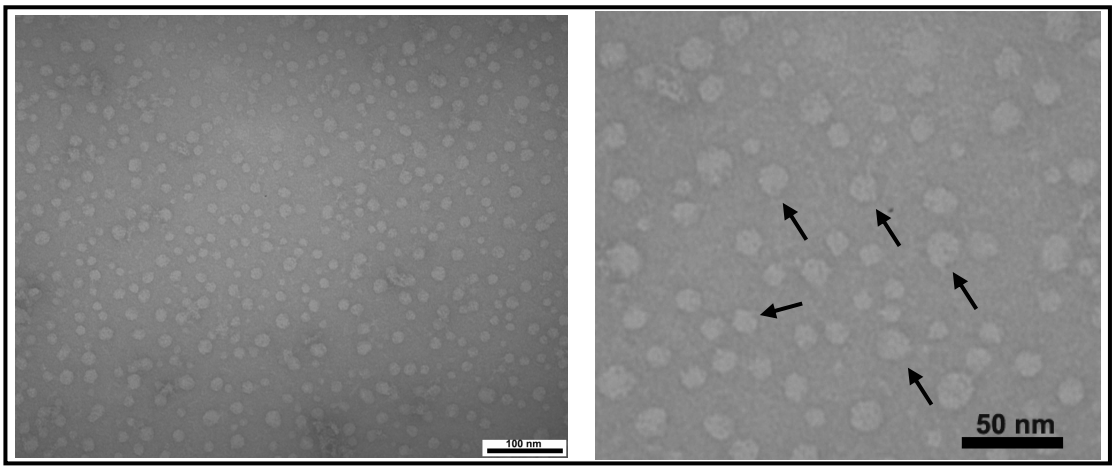

Figure 27. Preparation 4 refolded np2ev2 protein in 0 M urea and 2 mM DTT. The overall view of the sample is presented on the left and the enlarged version on the right. Observed flat, spherical shaped nanoparticles are indicated in black arrows.

Immunization results

Immunization studies are done in order to understand the immune response generated against the nanoparticles carrying the *Pseudomonas* pilin epitope. The immunization studies are done in Dr.Hodge's lab, using rabbit as the animal model.

Preliminary immunization studies

The nanoparticles of **np1, np1e and np2ev1** proteins are used for the immunization studies. The np1 nanoparticles, which do not carry the epitope, are used as the negative control. For preliminary immunization studies, the nanoparticles are prepared in Freund's complete/incomplete adjuvant (for immunization details refer to Materials and Methods section). The rabbits are immunized with four injections with a gap of four weeks between each injection. After the 4^{th} injection, the rabbits are slaughtered and the obtained serum is diluted to different dilutions. The different dilutions of the serum are titrated against the pilin peptide conjugated BSA protein to estimate the antibody response generated against the pilin epitope. The antibody titers are estimated using Enzyme-Linked Immunosorbent Assay (ELISA).

The ELISA results are summarized in Figure 28. From the ELISA results, it is observed that **none of the preimmune sera recognized the pilin peptide.** As expected, the final serum from rabbit immunized with np1 nanoparticles (np1 final serum)**,** does not show any binding against the pilin peptide. The final serum from rabbit immunized with np1e nanoparticles (np1e final serum), showed 50 % binding at 1: 29600 dilution. This observation indicates the high titers of antibody generated against the pilin epitope attached to np1e nanoparticles. The final serum from rabbit immunized with np2ev1 nanoparticles (np2ev1 final serum), showed 50 % binding at 1:4000 dilution and at 1:29600 dilution it showed less than 10 % binding. This observation indicates the low titers of antibody titers generated against the pilin epitope attached to np2ev1 nanoparticles.

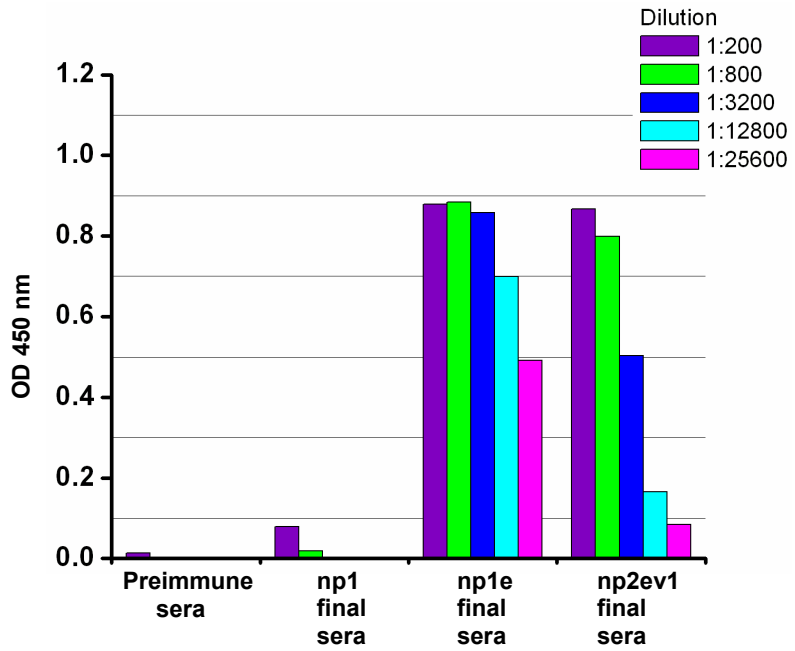

Figure 28. Each of three rabbits was immunized with either np1 or np1e or np2ev1 nanoparticles. np1e, np2ev1 nanoparticles carry the *Pseudomonas* (strain PAO) pilin epitope. Intramuscular route was used for immunization with 15 μg of nanoparticles formulated in Freund's adjuvant (Complete/Incomplete). Rabbits were immunized four times, with a gap of four weeks between each immunization. Pilin epitope specific antibodies in the sera were measured after the 4th immunization. Results are shown as optical density (OD; at 450 nm) for individual serum dilutions.

Comparison of profiles of immune response generated against np1e nanoparticles in the presence and absence of adjuvant

Based on the observation of strong immune response generated against pilin epitope attached to np1e nanoparticles as compared to np2ev1 nanoparticles, it was decided to compare the profiles of immune response generated against np1e nanoparticles in the presence and absence of Freund's adjuvant. To accomplish the above purpose, six rabbits are used, out of which three are immunized with np1e nanoparticles in 50% (v/v) Freund's adjuvant and three with np1e nanoparticles in 50% (v/v) phosphate buffered saline (PBS). The same immunization is followed as in the preliminary immunization studies. After the final immunization, the sera are collected from the rabbits and tested for their titer values against three different antigens: np1e nanoparticles, pilin peptide conjugated to BSA and native pilin protein.

The titer values are represented in dilution values at which 50% binding of the serum is observed. The obtained antibody titer values of the serum against each antigen are presented in Figure 29 (the average of the values obtained from all three rabbits). The average titer values against each antigen are summarized in Table 6.

The final sera from rabbits immunized with **np1e nanoparticles + adjuvant** showed a strong titer value (550, 000) against np1e nanoparticles. The same serum against pilin peptide conjugated to BSA and to native pilin protein showed titer values of 23293 and 44091, respectively. From the obtained titer values, it is observed that the titer values against pilin peptide conjugated to BSA and native pilin protein are ~ 20 times less when compared to the titer values obtained against np1e nanoparticles. This observation proves that a majority of the produced antibodies are not directed against pilin antigen, but rather are directed against np1e nanoparticle backbone.

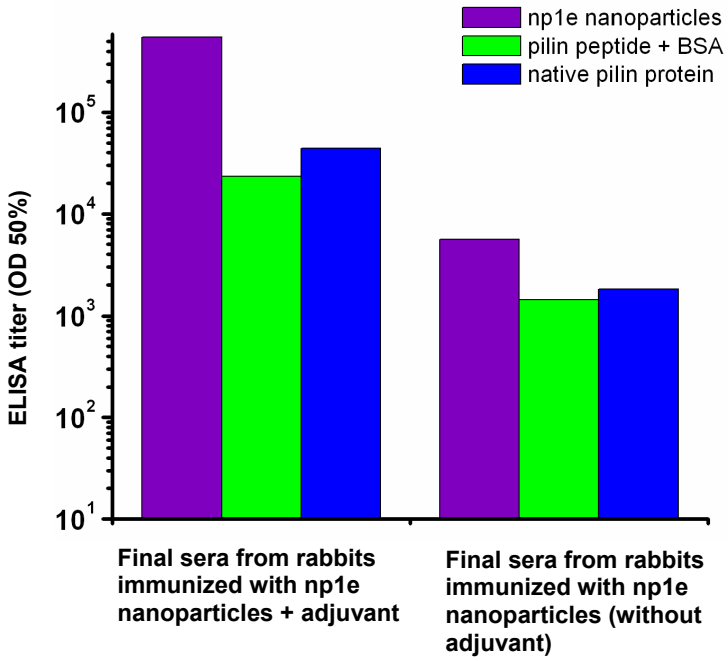

Figure 29. Two groups, each group containing three rabbits were immunized with np1e nanoparticles in 50% (v/v) Freund's adjuvant (Complete/Incomplete) system and np1e nanoparticles in 50% (v/v) phosphate buffered saline, respectively. In each group, four immunizations (intramuscular) were done with a gap of four weeks between each immunization. The sera obtained from each group after the 4th immunization was titrated against three different antigens coated to the ELISA wells: np1e nanoparticles itself (violet); pilin peptide conjugated to BSA (green); native pilin protein (blue). Results are shown in the dilution factor at which 50% binding was observed. The titer value shown for each antigen is the average of the values obtained from three rabbits. OD = Optical density.

The sera from rabbits immunized with **np1e nanoparticles without adjuvant** showed a weak titer value of 5591 against np1e nanoparticles. Against pilin peptide conjugated to BSA and to native pilin protein it showed titer values of 1446 and 1822, respectively. From the obtained titer values, it is clear that the immune response generated against the pilin epitope is very low in the absence of adjuvant. But, the important point to note is that in absence of adjuvant the antibody fraction directed towards the pilin epitope is much higher 25% compared to 4.2% with adjuvant (see Table 6). Therefore, the adjuvant seems to make the core particle more accessible to the immune system, probably by partial unfolding of the nanoparticles.

Table 6. Antibody titer values obtained against np1e nanoparticles in the presence and absence of Freund's adjuvant.

ELISA plate coated antigens	Antibody titer values[#]	
	with adjuvant[$]	without adjuvant[£]
np1e nanoparticles	550,000	5591
pilin peptide conjugated to BSA	23293	1446
Native pilin protein	44091	1822

 # - represents the dilution values at which 50% binding was observed; average of values obtained from three rabbits.

$ - final sera from rabbits immunized with np1e nanoparticles in Freund's adjuvant.

£ - final sera from rabbits immunized with np1e nanoparticles alone (no adjuvant).

Discussion

Chapter 2A: Recombinant production of peptide based nanoparticles and their Biophysical characterization

Purification results of proteins np1 and np2

We have expressed and purified np1 and np2 proteins to near homogeneity. The purified proteins were obtained in a single step using Ni^{2+}-affinity chromatography (Figure 3, A and B). By single step purification, we showed that the np1 and np2 proteins which will be the building blocks of nanoparticles can be produced in an efficient and economic way.

The less stable nature of trimeric coiled-coil domain of np2 protein in SDS-PAGE when compared to the np1 protein (Figure 3, A and B) can be explained on the basis of **interhelical ionic interactions** within the trimeric coiled-coil domain. We did not take into account hydrophobic interactions because we have the same hydrophobic residues at **a** and **d** positions of the trimeric coiled-coil domain of np1 and np2 proteins (Figure 1, A). Burkhard et al. showed that the interhelical ionic interactions improve the coiled-coil stability by designing the 'minimal coiled-coil domain'. In particular, the interhelical ionic interaction of **g-e'** type with an Arg (R) residue in **g** position and Glu (E) in **e'** position (**g-e' RE**) [21]. In addition, Burkhard et al. showed that the opposite arrangement of **g-e' RE** interhelical ionic interactions that is **g-e' ER** reduces the coiled-coil stability [22]. This could be the reason for the less stable trimeric coiled-coil domain of np2 protein, as we identified the **g-e' ER** interhelical ionic interactions whereas in np1 protein this region has favorable **g-e' RE** interhelical ionic interactions (Figure 30).

Self-assembly results of protein np1

In preparation 3 and preparation 4 refolding, refolding starts from 8 M urea concentration, using low protein concentration (100 µg/ml).

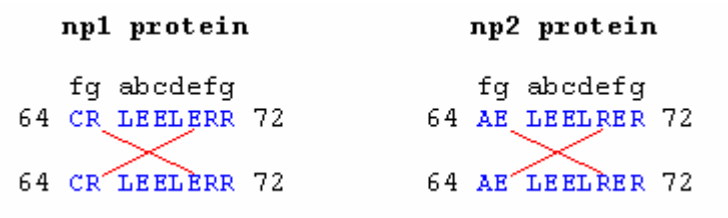

Figure 30. The trimeric coiled-coil region of np1 protein indicated with **g-e' RE** interhelical ionic interactions (red) whereas in np2 protein this region has **g-e' ER** interhelical ionic interactions (red). The heptad positions are indicated above the sequence. We followed the same residue numbering as in Figure 1, Chapter 2A.

We used low protein concentration in order to reduce intermolecular contacts, thus trying to avoid the intermolecular disulfide bridges between the cysteine residues of different np1 chains especially under oxidizing conditions of preparation 3 refolding. However, we cannot rule out the possibility of intermolecular disulfide bridges in oxidizing conditions of preparation 3 at 8 M urea where the monomeric chains of np1 protein will be mostly in its unfolded state. If this happens, it will lead to network of np1 unfolded monomeric chains linked through intermolecular disulfide bridges, and in subsequent refolding steps the oligomerization of the coiled-coil domains will further cross link the chains. This can lead to irregular aggregates. Such a behavior was observed in preparation 3 refolded np1 samples: EM picture revealed irregular aggregates along with the expected size (~ 17 nm) nanoparticles (Figure 5, A). The observed nanoparticles in preparation 3, tell us about the properly formed intramolecular disulfide bridges between the helices of coiled-coil domains within the folded np1 chains.

In preparation 4 refolding, there is no chance of intermolecular disulfide bridge formation because of its reducing condition refolding from 8 M to 0 M urea. At 0 M urea and in reducing condition, the cysteine residues of the refolded np1 protein are already shielded from the solvent. Therefore, upon oxidizing condition, which is the final step of preparation 4 will allow only the formation of intramolecular disulfide bridges. From our preparation 4 refolding EM picture, we observed the expected size (~ 17 nm in diameter) nanoparticles already in 0 M urea and in reducing condition (Figure 5, B).

The observed nanoparticles of expected size (~ 17 nm in diameter) under preparation 4 refolding showed our success in recombinant production of peptide based nanoparticles (see Figure 5, B and C). In addition, the molecular mass results of AUC confirmed the presence nanoparticles with icosahedral symmetry (4 even units) along with high molecular weight aggregates and even units (15-mers) (see Table 1, B). The observed high molecular weight aggregates in AUC could possibly correspond to the clumped nanoparticles, as we observe few clumped nanoparticles in EM picture (see Figure 5, C). By using CD spectroscopy, especially, thermal melting scan of nanoparticles, we showed that the observed nanoparticles are quite stable in solution (see Figure 12, B). The inaccessibility of thrombin cleavage site in thrombin cleavage reaction of nanoparticles (see Figure 13) shows about the compactly packed np1 subunits within the nanoparticle environment.

The preparation 4 refolding results of np1 protein was in contrary to the synthetic peptide (sp) results in chapter 2 where we showed the importance of intramolecular disulfide bridge in obtaining nanoparticles with icosahedral symmetry. But, the important point to note is that in synthetic peptide (sp) preparation 4 refolding results, we did not observe the refolded samples in 0 M urea and in reducing condition. We only observed the samples in 0 M urea and in oxidizing condition (Figure 3, D; chapter 1). Therefore, we cannot rule out the possibility of formed nanoparticles with icosahedral symmetry already in 0 M urea and in reducing condition. In addition, in our laboratory the np1 protein with the mutated cysteine (C) residues to alanine (A) residues was refolded under preparation 3 refolding and from EM picture the refolded protein was observed to form nanoparticles with icosahedral symmetry (~ 17 nm in diameter) (data not included in the thesis). Thus, it seems that the helices of two different oligomerization domain of single np1 chains come close enough in the absence of intramolecular disulfide bridge during refolding to favor the formation of nanoparticles with icosahedral symmetry.

Parameters studied to understand its influence on nanoparticle assembly property of np1 protein under preparation 4 refolding condition

Ionic strength

Ionic strength of the refolding buffer found to be an important parameter influencing the nanoparticle formation. The refolded np1 protein in physiological salt concentration (150 mM NaCl) is observed to form nanoparticles with icosahedral symmetry (~ 17 nm in diameter) (see EM picture Figure 5, C; AUC result Table 1, B). In contrary, the refolded np1 protein in 0 M NaCl is observed to form trimers and roughly 15-mers (even units) (see AUC result Table 2) and EM picture also confirmed the absence of nanoparticles with icosahedral symmetry (Figure 7, A). These findings support the possible role of ionic strength in stabilizing the ionic interactions during the assembly process of coiled-coil domains to form nanoparticles with icosahedral symmetry.

The observed icosahedral nanoparticles which were of mostly clumped in nature in high salt concentration (500 mM NaCl) (see EM picture Figure 7, B) can be explained as follows: N-terminus of np1 protein which is a non coiled-coil sequence is populated with more of hydrophobic amino acids (18 out of 22 amino acids), as shown in Table 7.

Table 7. Data representing the nature of the amino acids at N-terminus of np1 protein

N-terminus amino acid sequence of np1 protein		
MGHHHHHHGDWKWDGGLVPRGS (22 amino acids)		
very hydrophobic amino acids	MWWLV	Total amino acids (very hydrophobic + less hydrophobic) : 18
less hydrophobic amino acids	GHHHHHHG GGPGS	
very hydrophilic amino acids	DKDR	4 amino acids

We considered the 6-histidine residues at the N-terminus as less hydrophobic amino acids, because, the refolding was done at pH 7.5 which is around the pKa of histidine residue. In the nanoparticles, the N-terminus will be on the outer periphery, extending out from each chain of pentameric coiled-coil domain. In conditions like high salt concentration (500 mM NaCl), hydrophobic interactions are more favorable than ionic interactions because of the masking effect of ions on charged residues. Therefore, in 500 mM NaCl there are more chances of forming interparticle hydrophobic interactions between the N-terminus of neighboring nanoparticle, which will lead to clumping of nanoparticles.

pH of the refolding buffer

In addition to ionic strength, pH of the refolding buffer found to be another important parameter influencing the nanoparticle formation. pH mediated effect can be correlated to its influence on the electrostatic interactions between the charged residues. Therefore, we analyzed np1 sequence for stretch of negatively and positively charged residues that can be influenced during np1 refolding at different pH. From np1 sequence, we found that the C-terminus of trimeric coiled-coil domain of np1 protein, especially from residues 74 to 86 is populated with more of negatively charged amino acids (6 glutamic acid (E) residues compared to 3 arginine (R) residues) (for sequence details see Figure 1, A). In addition, the 6 consecutive histidine (H) residues at the N-terminus will either form positively charged patch at acidic pH or uncharged patch at neutral or basic pH. Based on these regions, in the following paragraphs we have discussed our observed refolding results of np1 protein at different pH (see Table 3).

In our refolding studies of np1 protein at pH 5.6, especially in 8 M urea, the np1 protein will be mostly in its unfolded state exposing the positively charged histidine residues at the N-terminus and negatively charged C-terminus. This can cause electrostatic interactions between N- and C-terminus of different np1 monomeric chains forming network of np1 chains linked to each other. Based on the observation of trimeric band in denaturing conditions of SDS-PAGE of np1 purified samples (see Figure 3, A), it seems that the trimeric coiled-coil domain of np1 protein folds already at urea concentrations that are moderately high (6 M urea). Therefore, the folding of trimeric coiled-coil domain at 6 M urea can further cross link the network of np1 chains, as this can lead to protein precipitation. Such a behavior was observed for np1 refolded samples at pH 5.6, as they precipitated in 6 M urea.

In pH 6.5 and 7.5 refolding, the N-terminal histidine residues will carry a neutral charge as the pKa of histidine residue is pH 6.0. Therefore, at pH 6.5 and 7.5 the uncharged histidine residues will not favor the electrostatic interactions with the negatively charged C-terminus of unfolded np1 monomeric chains in 8 M urea. In the subsequent urea concentration, the folding of the trimeric coiled-coil domain and the pentameric COMP domain will favor the formation of icosahedral nanoparticles.

Such a behavior was observed for np1 refolded samples at pH 7.5, as they formed nanoparticles with icosahedral symmetry (~ 17 nm in diameter) (see EM picture Figure 8, A). But, for np1 refolded samples at pH 6.5 we observed precipitation in 2 M urea. Also, the uncharged nature of histidine residues at pH 8.5 will not favor the electrostatic interaction with negatively charged C-terminus. This was supported by the observed nanoparticles with icosahedral symmetry in pH 8.5 refolded np1 samples, but they were found to be more of aggregated (see EM picture Figure 8, B).

Reducing agent (DTT)

The refolded np1 protein in 2 mM DTT concentration is observed to form nanoparticles with icosahedral symmetry already in 0 M urea and in 2 mM DTT (reducing condition) (see EM picture Figure 9). This observation was similar to the refolded np1 protein in 1 mM DTT, as here also we observed nanoparticles with icosahedral symmetry already in 0 M urea and in 1 mM DTT (reducing condition) (see EM picture Figure 5, B). Therefore, refolding at higher DTT concentration 2 mM DTT when compared to 1 mM DTT does not seem to influence the nanoparticle formation with icosahedral symmetry under preparation 4 refolding.

Glycerol

The observed nanoparticles with icosahedral symmetry in 10% glycerol (see EM picture Figure 5, C) were found to be more of clumped as we dialyzed out 10% glycerol (see EM picture Figure 10). In the nanoparticle, the N-terminus of np1 protein which is more of hydrophobic in nature (see Table 7), will be on the outer surface as it extends from each chain of pentameric coiled-coil domain of COMP. Thus, the outer surface of nanoparticles can be considered as more of hydrophobic in nature and the possible reason for nanoparticle clumping can be attributed to the interparticle hydrophobic interactions. Therefore, the observed nanoparticle clumping in the absence of 10% glycerol support the role of glycerol as a stabilizing agent by interacting with the hydrophobic outer surface of nanoparticles.

Self-assembly results of protein np2

In np2 protein we introduced charged residues at the interface between the two oligomerization domains (see Figure 2). The idea is to understand whether the ionic interactions between the charged residues can bring the helices of two different oligomerization domains in a close proximity that will favor the formation of nanoparticles with icosahedral symmetry.

From EM picture of oxidizing condition refolding results (preparation 3), we observed mostly flat, spherical shaped nanoparticles (Figure 11). Preliminary AUC analysis support that these nanoparticles might well correspond to even units (15 monomeric chains) (see Table 4, A). But, after initial runs of AUC, the high molecular weight species roughly corresponding to even units and possibly the aggregates of even units disappeared and we could detect only pentamers and trimers (refer to Table 4, A). It seems that the above observation could be due to precipitation of high molecular weight species. Also, in solution we observed precipitation of the refolded sample. This shows about the instable nature of the observed nanoparticles.

According to our design principles, if the two oligomerization domains of the monomeric chain properly folds they will first assemble into 'even units'. The even units are nanoparticles but they are not of icosahedral shaped nanoparticles. To form icosahedron four such even units has to assemble together (60 monomeric chains) (see Table 1 of Chapter 1). Further assembly of even units to form icosahedral nanoparticles is determined by the angle between the two different oligomerization domains. One of the factors which influence the angle is the interactions at the interface between the two different oligomerization domains. In np2 protein, we used ionic interactions at the interface to optimize the angle between the two domains. But from the EM picture, it seems that the angle formed between the two oligomerization domains is not optimal to form the icosahedral nanoparticles, as we observe presumably the even units. In addition, these loosely packed even units can enclose more even units to form different sized nanoparticles lacking the icosahedral symmetry. This could be the probable explanation for the observed nanoparticles within the big aggregates (see EM picture Figure 11; indicated in red arrows).

Chapter 2B: Peptide based nanoparticles as an antigen display carrier in vaccination

Purification results

All the purified protein samples for repetitive antigen display carry two different oligomerization domains in their protein sequence: a pentameric coiled-coil domain (COMP) and a *de novo* designed trimeric coiled-coil domain (Figure 16). The coiled-coil domains of COMP and the de novo-designed trimer are known to form very stable oligomers [22, 23]. Therefore, under denaturing conditions of SDS-PAGE the purified samples can form trimers and pentamers in addition to monomers. Such a behavior was observed for np1ev1 and np1ev2 purified samples, as we observed a strong trimeric band in addition to monomeric band under SDS-PAGE (Figure 19, A and 20, A). Similar behavior was observed for np1 purified samples under SDS-PAGE (Figure 3, A of chapter 2A). These results show the very stable nature of trimeric coiled-coil domain in these samples, as it already folds under denaturing conditions of SDS-PAGE.

In addition, cysteine residues present in np1 and np2 based protein samples (See Table 8) can influence the formation of different oligomeric states of these samples under SDS-PAGE, by forming intermolecular disulfide bridges between different monomeric chains.

Table 8. Data representing the cysteine (C) residues in np1 and np2 based proteins for repetitive antigen display.

Constructs	Domain	Residue number
np1 based proteins: np1e, np1ev1 and np1ev2	pentameric coiled-coil domain (COMP)[$]	Cys 55
	trimeric coiled-coil domain[$]	Cys 64
	pilin epitope[£]	Cys 134 and 147
np2 based proteins: np2e, np2ev1 and np2ev2	pilin epitope[£]	Cys 134 and 147

$ - residue numbering of np1 protein is followed as denoted in Figure 16, A.

£ - residue numbering of full length pilin protein is followed as denoted in Figure 15, B.

Especially, under denaturing conditions of SDS-PAGE, the protein chains will be usually in its unfolded monomeric form and the presence of cysteine residues at this stage mostly favor intermolecular disulfide bridges between different chains. Therefore, the observed dimeric and tetrameric band for np1e and np2e protein samples under SDS-PAGE (Figure 18, A and B), can possibly correspond to the intermolecular disulfide linked monomers (dimers) and dimers (tetramers). Similarly, the observed dimeric band for samples np2ev1 and np2ev2 in SDS-PAGE can be of intermolecular disulfide linked monomers (Figure 19, B and 20, B). The less intense or even absence of trimer band in these samples show the formation of trimeric coiled-coil domain is less favored that is less stable under denaturing conditions of SDS-PAGE.

Self-assembly results

np1 based proteins

np1 protein with pilin epitope (np1e)

The preparation 4 refolded np1e protein is observed to form nanoparticles of expected size (~ 17 to 18 nm in diameter) in refolding buffer containing 2 mM DTT (reducing condition) (see Figure 21, A). This observation shows that the **nanoparticle forming ability of np1 protein is not affected by the fusion of pilin epitope**. But upon oxidizing condition (removal of 2 mM DTT), we observed clumping of particles forming bigger aggregates (see Figure 21, B) and sometimes in solution we observed precipitation problem. This effect could possibly due to the interlinking of formed nanoparticles through interparticle disulfide bridges by the cysteine residues of pilin epitope. Because, in the observed nanoparticles which is in reducing condition (2 mM DTT), the surface exposed cysteine residues of pilin epitope will be in the reduced state and upon oxidizing condition there are chances of forming intramolecular, intermolecular and interparticle disulfide bridges. The formation of intramolecular and intermolecular disulfide bridges will not affect the individual nature of nanoparticles. Because, the intramolecular disulfide bridges will lead to disulfide bonded loop structures of pilin epitope (native state; see Figure 15, A) on the surface of nanoparticle and the intermolecular disulfide bridges will result in cross linking of pilin epitopes within nanoparticle.

But the formation of interparticle disulfide bridges will cross link the epitopes of adjacent nanoparticles as this will lead to aggregates. Such a behavior was observed for np1e nanoparticles in 0 M urea and no DTT (preparation 4).

np1e protein with extended trimeric coiled-coil by three heptad repeats (np1ev1) and six heptad repeats (np1ev2)

The presence of cysteine residues in np1ev1 and np1ev2 proteins (see Table 8) can lead to different possibilities of disulfide bridges during preparation 3 and preparation 4 refolding conditions (see Table 9). During refolding, especially at 8 M urea the protein chains of np1ev1 and np1ev2 will be mostly in its unfolded state. The unfolded nature at 8 M urea and the oxidizing condition (preparation 3) at this stage will increase the possibility of intermolecular disulfide bridge formation between cysteine residues of different monomeric chains. This will lead to network of disulfide linked monomeric chains. In addition, it seems that the trimeric coiled-coil domain of np1ev1 and np1ev2 proteins folds at relatively high urea concentration based on the observation of trimeric band at denaturing conditions of SDS-PAGE of np1ev1 and np1ev2 purified samples (Figure 19, A and 20, A). Therefore, the folding of the trimeric coiled-coil domain of these proteins at relatively high urea concentration can further cross-link the network of intermolecular disulfide linked monomeric chains. This will probably result in precipitation of the protein. Such a behavior was observed for np1ev1 and np1ev2 proteins refolded under preparation 3 refolding condition (Figure 23, A and 26, A).

Also, for the refolded np1ev1 (Figure 23, B and C) and np1ev2 (Figure 26, B) proteins in reducing condition (preparation 4), we observed aggregation and precipitation problem. This shows about the influence of the attached epitope sequences on the assembly of the nanoparticles and here it seems that the aggregation and precipitation problem is due to the cysteine residues of pilin epitope (Table 8). This statement was supported by the preparation 4 refolding results of np1ev1 protein fused with Salmonella D2 epitope (no cysteine residues) where we observed properly formed nanoparticles (D. Tropel, oral communication).

Table 9. Data depicting the cysteine (C) amino acid residue numbers and their possible type of disulfide bridges that can form during step-wise dialysis from 8 M to 0 M urea (preparation 3 and preparation 4). Data is shown for np1 and np2 based proteins.

Type of disulfide bridge	Constructs	Residue number*
Intramolecular£	np1 based proteins (np1e, np1ev1 and np1ev2)	55-64; 55-134; 55-147; 64-134; 64-147; 134-147
	np2 based proteins (np2e, np2ev1 and np2ev2)	134-147
Intermolecular€	np1 based proteins (np1e, np1ev1 and np1ev2)	55-64; 55-134; 55-147 64-134; 64-147; 55-55; 64-64 134-147; 134-134; 147-147
	np2 based proteins (np2e, np2ev1 and np2ev2)	134-147; 134-134; 147-147
Interparticle$	for both np1 and np2 based proteins	134-147; 134-134; 147-147

* - for domain localization of respective residue number refer to Table 8.

£ - within a peptide or protein chain

€ - between the peptide or protein chain

$ - between the nanoparticles

np2 based proteins

The np2 protein which forms the building block of np2e, np2ev1 and np2ev2 is observed to form mostly flat, spherical shaped nanoparticles (see Figure 11 of Chapter 2A). Preliminary AUC analysis of these nanoparticles showed us that it might well correspond to 'even units' (15 monomeric chains) (Table 4, A of Chapter 2A). Therefore, based on the AUC results, the observed flat, spherical shaped nanoparticles of np2ev1 (see Figure 24) and np2ev2 (see Figure 27) might well also correspond to even units.

Even units are of similar in size when compared to the icosahedral nanoparticles. This was supported by the calculated size of np2ev1 by FCS which is ~ 20 nm in diameter, well comparable to the size of computer modeled icosahedron of np2ev1 (23 nm in diameter) (Figure 17, B). But, the even units are not of icosahedral nanoparticles and according to our nanoparticle design principles, four such even units has to come together to form icosahedral shaped nanoparticles (60 monomeric chains) (see Table 1 of Chapter 1).

The association of even units to form icosahedral nanoparticles is determined by the angle between the two oligomerization domains within an even unit. One of the factor that determines the angle is the interactions at the interface between the two oligomerization domains. In np2 and np2 based proteins it is governed by the ionic interactions. Therefore, if the angle is not small enough to form icosahedron the even units can enclose less or more than four even units to form nanoparticles which are not of icosahedral in shape. Such type of nanoparticles is observed in np2ev1 protein (see Figure 24; highlighted in pink arrow). Based on the above results, it seems that the designed ionic interactions are not optimal enough to bring the helices of the two different oligomerization domains in close proximity to form icosahedral nanoparticles.

Immunization results

Preliminary immunization results

The objective of the preliminary immunization studies is to know the optimal nanoparticle size that can elicit very good immune response against the fused pilin antigen from *Pseudomonas*. We classified the nanoparticles fused with pilin antigen according to their computer designed model size (see Figure 17, B) which is as follows:

- Small size nanoparticles (~ 18 nm) - np1e, np2e
- Medium size nanoparticles (~ 23 nm) - np1ev1, np2ev1
- Large size nanoparticles (~ 29 nm) - np1ev2, np2ev2

From the refolding results, among the np1 based proteins (np1e, np1ev1 and np1ev2), np1e protein (small size nanoparticle) assembled into icosahedral nanoparticles of expected size (~ 18 nm in diameter) (see EM picture Figure 21, A and B).

For np1ev1 (medium size nanoparticle) and np1ev2 (large size nanoparticle) proteins, we faced aggregation and precipitation problem during or after refolding. From the refolding results of np2 based proteins, we observed mostly flat nanoparticles possibly the ‘even units’ (15-mers) and not the nanoparticles with icosahedral symmetry. But with refolded np2ev1 protein, in addition to flat nanoparticles we observed nanoparticles which were not of flat in shape (see EM picture Figure 24).

Therefore, based on the refolding results we decided to use np1e (small size nanoparticle), np2ev1 (medium size nanoparticle) and np1 as a negative control (small size nanoparticle without pilin antigen) for immunization studies.

From the preliminary immunization results, we observed much weaker antibody titers (1:4000) against np2ev1 nanoparticles fused with pilin antigen (see Figure 28). The possible reason could be due to instable nature of the nanoparticles in solution as we observed precipitation in the stored protein samples after 1 month at 4°C (after 1st immunization). It seems that the precipitation problem has drastically reduced the nanoparticle concentration in solution during the booster immunizations (second, third and fourth). In turn, this will affect the generated antibody response, as we see in np2ev1 nanoparticle immunization results.

Immunization results with np1e nanoparticles we observed good antibody titer values (1:29600) compared to np2ev1 nanoparticles (Figure 28). With stored np1e nanoparticles also we observed precipitation problem after 1 month at 4°C (after 1st immunization). But from the obtained antibody titer values, it seems that the precipitation rate was less in np1e nanoparticles when compared to np2ev1 nanoparticles.

In both np1e and np2ev1 nanoparticles, during dialysis from 0 M urea + 2 mM DTT to buffer containing no DTT (preparation 4 refolding), the formed nanoparticles can get interlinked with each other through interparticle disulfide bridge formation between cysteine residues of pilin antigen displayed on the surface of the nanoparticles (see Table 9). This could be the most likely reason for the aggregation of nanoparticles and slow precipitation over time.

Immunization results of np1e nanoparticles - In the presence and absence of Freund's Complete/Incomplete adjuvant

Virus like particles (VLPs) is a well recognized antigen carrier system in vaccination because of its potent stimulation of the immune response in the absence of adjuvant against the attached antigens (either coupled or fused) on its surface [9, 10].

VLPs themselves act as particulate adjuvant to boost the immune response against the attached antigens on its surface [24]. Our nanoparticle system resembles VLPs in properties like self-assembling, non-replicating, non-pathogenic and most importantly repetitive display of the attached antigens. Therefore, we wanted to understand our nanoparticle system efficiency as a particulate adjuvant by comparing the immunization results done with the nanoparticles formulated in Freund's complete/Incomplete adjuvant and in PBS buffer (no adjuvant). As we did not get good immune response with medium size nanoparticle of np2ev1 we did these studies with small size nanoparticle of np1e.

After the immunization the obtained final sera was titrated against three antigens: np1e nanoparticles, pilin peptide conjugated to BSA and to native pilin protein. From the immunization results of np1e nanoparticles formulated in Freund's complete/incomplete adjuvant, we observed 20-fold higher antibody titer values against the np1e nanoparticles (1:550,000) compared to the pilin peptide conjugated to BSA (1:23293) and to native pilin protein (1:44091) (see Figure 29). This observation clearly shows that the majority of the antibodies are directed against the nanoparticle backbone and not against the pilin antigen. The above observation is due to the:

- **Effect of Freund's complete/incomplete adjuvant on nanoparticles**

Freund's adjuvant is essentially paraffin oil and when mixed with the aqueous solutions of antigens it forms a viscous water-in-oil emulsion [25, 26]. Our nanoparticles are formed by the self-assembly of coiled-coils and hydrophobic interactions form the primary driving force for coiled-coil assembly. Therefore, when nanoparticles mixed with hydrophobic Freund's adjuvant, it can partially unfold the nanoparticles by interacting with the hydrophobic residues of coiled-coils and thus affecting the hydrophobic interactions within coiled-coils. This can expose the nanoparticles to the immune system and the results can be a strong immune response against the nanoparticles. It seems that such a result was observed in immunization results of np1e nanoparticles formulated in Freund's complete/incomplete adjuvant.

From the immunization results of np1e nanoparticles formulated in PBS buffer (no adjuvant) we observed that the antibody fraction directed towards the attached pilin antigen is 25% higher when compared to the nanoparticles formulated in Freund's adjuvant where it is 4.2%. This again supports the denaturing effect of Freund's adjuvant on nanoparticles. From the titration results of sera obtained from rabbits immunized against np1e nanoparticles (no adjuvant), we observed very low antibody titer values against pilin peptide conjugated to BSA (1:1446) and to native pilin protein (1:1822) (see Table 6). This suggest about the very poor antibody response against the pilin antigen attached to np1e nanoparticles in the absence of adjuvant. The possible reasons for this observation could be:

- **Accessibility of fused or coupled antigens to B-cell bound receptors**

Viruses are known for its property of inducing strong antibody mediated immune response in its host (T-cell independent). This property is conferred by the optimally exposed antigens on their surface in a repetitive and orderly fashion which efficiently cross link B-cell bound receptors and sends activation signal for subsequent proliferation of B-cells and antibody production [5, 6]. Also, for antigen carriers such as VLPs, optimal presentation of antigens is considered as an important factor in inducing strong antibody mediated immune response. From EM picture of np1e nanoparticles, we see aggregation property of nanoparticles upon removal of DTT (Figure 21, B). Therefore, the aggregation of np1e nanoparticles can possibly interfere with optimal presentation of pilin antigen and hence the antibody response.

- **Size of nanoparticle**

In particulate carrier based vaccine formulations, **particle size** is considered as one of the important parameter because of its influence on immune response [27]. For example, VLPs which are in the size range of viruses (22-150 nm) are used as a potential immunogen and also as a particulate carrier system in vaccine formulations [28].

Considering the size of np1e nanoparticle (~ 18 nm), it seems that it would be rather small to be recognized by the immune system. This statement was supported by the immunization results from our laboratory with medium size np1ev1 nanoparticles (~ 23 nm in diameter) displaying *Salmonella* epitope (D2), we obtained antibody titer values of 1:30000 without adjuvant (in collaboration with Cytos Biotechnology AG). This brings our nanoparticle system well in the range of VLPs.

The important observation from the immunization results is that **our nanoparticle system is able to represent the fused antigens in their native form**, as we see the generated antibodies recognize the native pilin protein (see Figure 29). In addition, it is observed that the nature of the attached epitope to the nanoparticle constructs has a significant influence on the formation of icosahedral nanoparticles.

Materials and Methods - Chapter 2A and 2B

Reagents and Enzymes

All enzymes were purchased from BioConcept – New England Biolabs (Allschwil, Switzerland) and chemicals from Sigma, Applichem and Bio-Rad unless stated otherwise. They were used according to the manufacturer's instructions. All oligonucleotides (Table 10) were synthesized by Microsynth AG (Balgach, Switzerland). Oligonucleotides had 5' phosphate and were quality assured by PAGE purification.

Bacterial strains and plasmids

Escherichia coli DH5 α cells (Invitrogen, USA) and BL21 (DE3) pLysS cells (Novagen, USA) were used as the cloning and expression host cells, respectively. For our expression studies, we have used modified form of the prokaryotic expression vector pPEP-T [29, 30] and throughout this chapter it will be described as mpPEP-T vector.

Molecular biology of designed constructs

The designed constructs are depicted in Figure 16 of Chapter 2B. The cloning strategy of the designed constructs will be described under two main headings: (i) molecular biology of np1 and np2 constructs; (ii) molecular biology of np1 and np2 based constructs.

Molecular biology of np1 and np2 constructs

Construction of np1 and np2 DNA sequences

***np1 DNA*:** Three pairs of oligonucleotides were synthesized to construct the np1 DNA (Table 10). In Figure 31, A, they were represented as fragment 1 to 3. Fragments 1 to 3 correspond to initial part, middle part and last part of np1 DNA, respectively. Each fragment was designed to have a 5' overhang which gives the specificity during assembly of the fragments. That is, the C-terminal 5' overhang of fragment 1 has specificity to N-terminal 5' overhang of fragment 2 and C-terminal 5' overhang of fragment 2 has specificity to N-terminal 5' overhang of fragment 3.

In addition, the fragment 1 was designed to have a precut BamHI restriction site at its N-terminus and fragment 3 to have a precut EcoRI restriction site at its C-terminus (Figure 31, A). The precut BamHI and EcoRI restriction sites were created for cloning purposes.

***np2 DNA*:** We have synthesized two oligonucleotides for the construction of np2 DNA (referred as fragment 1 and 2 in Table 10) (Figure 31, B). The first oligonucleotide (fragment 1; forward strand) encodes the N-terminal half of the np2 DNA and contains the appropriate restriction site (BamHI) at the 5' end for cloning in to the vector. The second oligonucleotide (fragment 2; reverse strand) encodes the C-terminal half of the np2 DNA and contains the EcoRI restriction site. The N- and C-terminal oligonucleotides were synthesized in such a way that they overlap by 20 nucleotides (highlighted in grey color; Figure 31, B). This was done in order to anneal the two oligonucleotides and then to use it for subsequent filling reaction of 5' overhangs to get the entire DNA fragment.

Oligonucleotide fragment assembly

All the oligonucleotides (both forward and reverse strand) (Table 10) of np1 and np2 constructs were dissolved in MilliQ water to a concentration of 100 μM.

The forward and reverse strand of each oligonucleotide were combined in 1 μM concentration and 5 μl of 20X SSC buffer (30 mM sodium citrate dihydrate pH 7.0 and 300 mM NaCl for 100 ml) and water were added to give 50 μl. Annealing reaction was done in a thermocycler by first incubating at 90°C for 1 min followed by 70°C for 1 min and then cooling at 1°/15 sec to 20°C (T*personal*, Biometra, UK) to give the annealed product. The annealed products were desalted using Micro Bio-Spin P-30 columns as per the manufacturers protocol (Bio-Rad, USA) and then checked in 4% NuSieve GTG-Agarose (Cambrex Bio Science, USA) to confirm the annealing reaction. Annealed products were stored at -20°C until required.

Preparation of mpPEP-T vector for cloning

For the cloning of np1 and np2 DNA in to mpPEP-T vector, the vector DNA was prepared as follows: 1µg mpPEP-T vector, 1µl of 10X NEBuffer EcoRI (10 mM Tris-HCl, 10 mM $MgCl_2$, 50 mM NaCl and 1 mM DTT pH 7.9), 1 µl of 10X BSA, 1 units of EcoRI and BamHI enzyme and water up to 10 µl were combined and incubated at 37°C for 3 hrs. Double digested vector was recovered using QIAquick Gel Extraction Kit (Qiagen, Switzerland) from a 1% agarose gel. After gel extraction, the digested vector ends were dephosphorylated by adding both 1 unit of shrimp alkaline phosphatase (Promega, USA) and 1 µl of 10X SAP reaction buffer (50 mM Tris-HCl and 10 mM $Mgcl_2$ pH 9.0) to a final volume of 10 µl, followed by incubation at 37°C for 15 min, then heat inactivation (15 min, 65°C).

Preparation of mpPEP-T-np1 and mpPEP-T-np2 constructs

The annealed oligonucleotides of np1 DNA were depicted in the Figure 31, A. In np2 annealed oligonucleotides (Figure 31, B), the 5' overhang was filled in with Klenow polymerase (Roche, Switzerland) and dNTPs. After the filling reaction, the np2 DNA was double digested with BamHI and EcoRI enzymes.

Dephosphorylated mpPEP-T vector was ligated to fragments 1 to 3 of np1 DNA and in other reaction to np2 insert. The ligation reaction was done as follows: Equimolar concentration of insert (vector: insert ratio 1:3), 100 ng of dephosphorylated plasmid DNA and water were added and incubated at 45°C for 5 min. Then the reaction mixture was cooled in ice and then 1 µl of 10X T4 DNA ligase buffer (50 mM Tris-HCl pH 7.5, 10 mM $MgCl_2$, 10 mM DTT, 1 mM ATP, 25 µg/ml BSA) along with 1 unit of T4 DNA ligase and incubated at 16°C overnight.

Transformation

Five µl of ligated mixture was added to 100 µl of DH5α competent cells and was incubated on ice for 30 min. Followed by heat shock treatment for 90 sec at 42°C, and incubated on ice for further 2 min. Then, 0.9 ml LB medium was added and incubated at 37°C for 1h with shaking at 225 rpm.

Followed by centrifugation of cells at 7000 rpm, 5 min, and the obtained pellet was kept in 100 µl of LB and the remaining LB was thrown out. The pelleted cells were mixed with the LB by gentle tapping and the mixture was plated on LB-agar plates (ampicillin 100 µg/ml) and incubated overnight at 37°C. Putative positive colonies were picked from plates and placed in a 3 ml LB-ampicillin (100 µg/ml) broth and grown overnight at 37°C with shaking at 180 rpm.

Plasmid mini prep was done from the grown cultures using QIAprep spin mini prep kit (Qiagen, Switzerland) and the obtained plasmid DNA was subjected to enzymatic digestion with BamHI and EcoRI enzyme to verify the presence of the insert in the transformed bacterial colonies. Products were analyzed by 2% gel electrophoresis. DNA sequencing (Microsynth AG, Balgach, Switzerland) was done to verify the putative positive clones using T7 promoter and terminator primer sequences.

Molecular biology of np1 and np2 based constructs

Construction of DNA cassettes involved in generation of np1 and np2 based constructs

***Pseudomonas pilin epitope DNA cassette*:** A pair of oligonucleotides (forward and reverse strand) encoding the pilin DNA was synthesized (Table 10; Figure 32, A). The oligonucleotides have a precut XhoI and EcoRI restriction sites at their N- and C-terminus, respectively (Figure 32, A).

***Extension I trimeric coiled-coil DNA cassette*:** A pair of oligonucleotides (forward and reverse strand) encoding the extension I trimeric coiled-coil DNA was synthesized (Table 10; Figure 32, B). The oligonucleotides have a precut XhoI and XmaI restriction sites at their N- and C-terminus, respectively (Figure 32, B).

***Extension II trimeric coiled-coil DNA cassette*:** A pair of oligonucleotides (forward and reverse strand) encoding the extension II trimeric coiled-coil DNA was synthesized (Table 10; Figure 32, C). The oligonucleotides have a precut XhoI and SalI restriction sites at their N- and C-terminus, respectively (Figure 32, C).

Preparation of np1 and np2 based constructs

The synthesized oligonucleotides (Figure 32) were annealed and purified according to the protocol described under section 'Oligonuclotide fragment assembly'.

mpPEP-T-np1e and mpPEP-T-np2e constructs: Insertion of pilin epitope DNA sequence (Figure 32, A) into mpPEP-T-np1 and mpPEP-T-np2 plasmids resulted in mpPEP-T-np1e and mpPEP-T-np2e plasmids, respectively. The XhoI and EcoRI restriction enzyme sites in mpPEP-T-np1 and mpPEP-T-np2 plasmids was used for inserting pilin epitope DNA sequence.

mpPEP-T-np1ev1 and mpPEP-T-np2ev1 constructs: Insertion of extension I trimeric coiled-coil DNA sequence (Figure 32, B) into mpPEP-T-np1e and mpPEP-T-np2e plasmids resulted in mpPEP-T-np1ev1 and mpPEP-T-np2ev1 plasmids, respectively. The XhoI and XmaI restriction enzyme sites in mpPEP-T-np1e and mpPEP-T-np2e plasmids was used for inserting extension I trimeric coiled-coil DNA sequence.

mpPEP-T-np1ev2 and mpPEP-T-np2ev2 constructs: Insertion of extension II trimeric coiled-coil DNA sequence (Figure 32, C) into mpPEP-T-np1ev1 and mpPEP-T-np2ev1 plasmids resulted in mpPEP-T-np1ev2 and mpPEP-T-np2ev2 plasmids, respectively. The XhoI and SalI restriction enzyme sites in mpPEP-T-np1ev1 and mpPEP-T-np2ev1 plasmids was used for inserting extension II trimeric coiled-coil DNA sequence.

Table 10: Oligonucleotides

Constructs	Oligonucleotide sequence
np1	fragment 1 (forward & reverse strand) (P) 5' GATCCGATGAAATGTTGCGTGAATTACAGGAAACCAACGCTGCTCTGCAAGACGTTCGTGAACTGCTGCGTCAAC 3' (P) 5' AACCTGTTGACGCAGCAGTTCACGAACGTCTTGCAGAGCAGCGTTGGTTTCCTGTAATTCACGCAACATTTCATCG 3' fragment 2 (forward & reverse strand) (P) 5' AGGTTAAACAGATCACCTTTCTGAAATGTCTGCTGATGGGTGGTCGTCTGCTGTGTCGTCTGGAAGAACTGGAACGT 3' (P) 5' AGACGACGTTCCAGTTCTTCCAGACGACACAGCAGACGACCACCCATCAGCAGACATTTCAGAAAGGTGATCTGTTT 3' fragment 3 (forward & reverse strand) (P) 5' CGTCTGGAAGAACTGGAACGTCGTCTGGAAGAACTCGAGCGTGCCTGATAAG 3' (P) 5' AATTCTTATCAGGCACGCTCGAGTTCTTCCAGACGACGTTCCAGTTCTTCC 3'
np2	fragment 1 (forward strand) (P) 5' GGATCCGACGAAATGCTGCGTGAACTGCAGGAAACCAACGCTGCTCTGCAGGACGTTCGTGAACTGCTGCGTCAG CAGGTTAAACAGATCCGTCGTCTGAAACGTCTGCTGCGTG 3' fragment 2 (reverse strand) (P) 5' GAATTCTTATCAGGCACGTTCCAGTTCTTCCAGACGACGTTCCAGTTCTTCCAGACGTTCACGCAGTTCTTCCAGTTC AGCCAGCAGACGACCACCACGCAGCAGACGTTTCAGA 3'
Pseudomonas pilin epitope	fragment 1 (forward & reverse strand) (P) 5' TCGAGCGTGCCCGGGGGCTGAACCGTACCGCTGACGGTGTTTGGGCTTGCAAATCCACCCAGGACCCGATGTTCA CCCCGAAAGGTTGCGACAACTGATAAG 3' (P) 5' AATTCTTATCAGTTGTCGCAACCTTTCGGGGTGAACATCGGGTCCTGGGTGGATTTGCAAGCCCAAACACCGTCA GCGGTACGGTTCAGCCCCCGGGCACGC 3'
Extension I trimeric Coiled-coil	fragment 1 (forward & reverse strand) (P) 5' TCGAGCGTGCTATCAACACCGTCGACCTGGAACTGGCTGCTCTGCGTCGTCGTCTGGAAGAACTGGC 3' (P) 5' CCGGGCCAGTTCTTCCAGACGACGACGCAGAGCAGCCAGTTCCAGGTCGACGGTGTTGATAGCACGC 3'
Extension II trimeric Coiled-coil	fragment 1 (forward & reverse strand) (P) 5' TCGAGCGTGCTATCTCCGCTATCAAAGCTGACCTGTCCGCTCTGAAAGCTAACCTGGCTTCCCTGCAGGCTGACATCA ACACCG 3' (P) 5' TCGACGGTGTTGATGTCAGCCTGCAGGGAAGCCAGGTTAGCTTTCAGAGCGGACAGGTCAGCTTTGATAGCGGAG ATAGCACGC 3'

(P) - 5' phosphorylation; All the oligonucleotide pairs (forward and reverse strand) were underlined for their complementary regions.

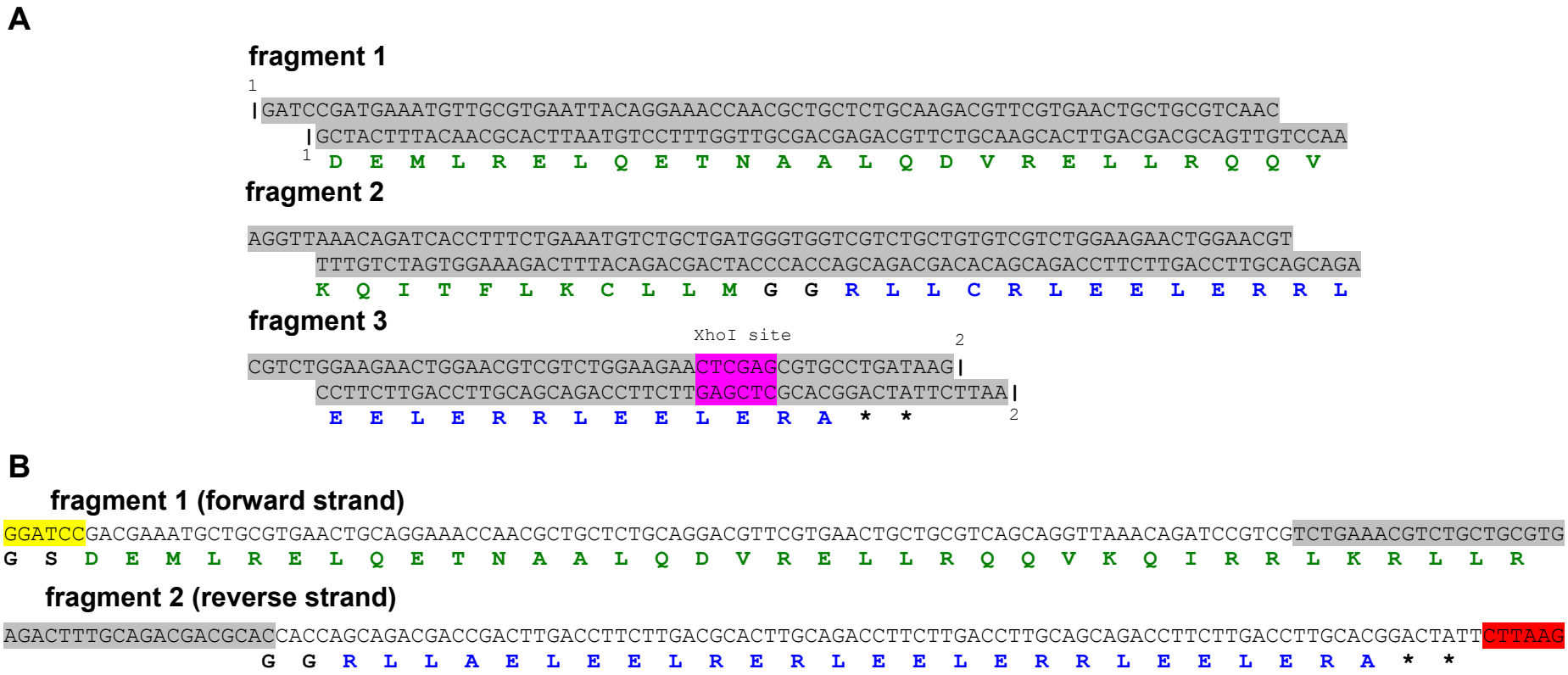

Figure 31. **A**, the initial part (fragment 1), middle part (fragment 2) and last part (fragment 3) of np1 DNA. 1 - precut BamHI restriction enzyme site; 2 - precut EcoRI restriction enzyme site. The introduced XhoI restriction enzyme site for cloning purposes in fragment 3 of np1 DNA was highlighted in pink. **B**, N-terminal half (fragment 1) and C-terminal half (fragment 2) of np2 DNA. Highlighted grey colored letters represent the 20 bp overlapping region between fragment 1 and 2. Highlighted yellow and red colored letters represent the BamHI and EcoRI restriction enzyme sites, respectively. In both **A** and **B**, each fragment was represented along with their amino acid sequences (bold colored letters). Green colored bold letters represent the pentameric coiled coil domain of COMP and the blue colored bold letters represent the *de novo* designed trimeric coiled coil. * represent the stop codons.

Figure 32. **A**, *Pseudomonas* pilin epitope DNA sequence. Amino acid sequence of pilin epiotpe was represented below the DNA sequence (bold red colored). The introduced XmaI restriction enzyme site for cloning purposes was highlighted in pink. **B**, Extension I trimeric coiled coil DNA sequence. Amino acid sequence of extension I trimeric coiled coil was represented below the DNA sequence (bold turquoise colored). The introduced SalI restriction enzyme site for cloning purposes was highlighted in pink. **C**, Extension II trimeric coiled coil DNA sequence. Amino acid sequence of extension II trimeric coiled coil was represented below the DNA sequence (bold turquoise colored). 1- precut XhoI restriction enzyme site; 2 - precut EcoRI restriction enzyme site; 3 - precut XmaI restriction enzyme site; 4 - precut SalI restriction enzyme site.

Protein biology of designed constructs

Construction of mpPEP-T expression plasmid

We have constructed mpPEP-T expression plasmid (Figure 33, B) for the expression of DNA constructs that assembles into nanoparticles upon refolding. The rational behind the construction of mpPEP-T plasmid was initially we expressed our nanoparticle constructs in pPEP-T expression plasmid but upon refolding we faced the precipitation problem. We thought the problem might be with the laminin oligomerization domain in pPEP-T expression plasmid (Figure 33, A). Therefore, to construct pPEP-T expression without laminin oligomerization domain, we synthesized an oligonucleotide sequence (codes for 22 aa) devoid of laminin domain and had precut ends of Nco I and BamH I restriction sites (Figure 33, C). This oligonucleotide sequence was inserted into the pPEP-T plasmid which also had precut ends of Nco I and BamH I restriction sites to yield mpPEP-T expression plasmid. The inserted oligonucleotide sequence codes for the following residues: 6X-Histidine tag (pink), residues for UV detection (two tryptophan (W) residues; red), residue for coupling reactions (lysine (K); yellow) and thrombin recognition sequence (LVPRGS) (grey) (Figure 33, C). The nanoparticle constructs were cloned in between BamHI and EcoRI restriction enzyme sites.

Protein expression

All the nanoparticle constructs in mpPEP-T vector were transformed into *E.coli* strain BL21 (DE3) pLysS (Novagen, Merck Biosciences) as described in section 'Transformation'. The transformed cells were plated on fresh ampicillin (100 μg/ml) and chloramphenicol (30 μg/ml) LB agar plates and incubated at 37°C overnight. A single colony from the transformed plate was inoculated in 50 ml LB broth with ampicillin (200 μg/ml) and chloramphenicol (30 μg/ml) and grown overnight at 28°C with shaking at 180 rpm. 1% of the overnight grown culture was inoculated into 3 liters of the same medium as above and incubated at 37°C with shaking at 200 rpm.

Protein expression was induced when OD_{600nm} reached 0.5 by adding IPTG to a final concentration of 1 mM. After induction at 37°C for 3 hrs, the cell pellet was collected by centrifugation at 6000g for 20 min at 4°C (Sorvall, GSA rotor) and frozen at -80°C until later use.

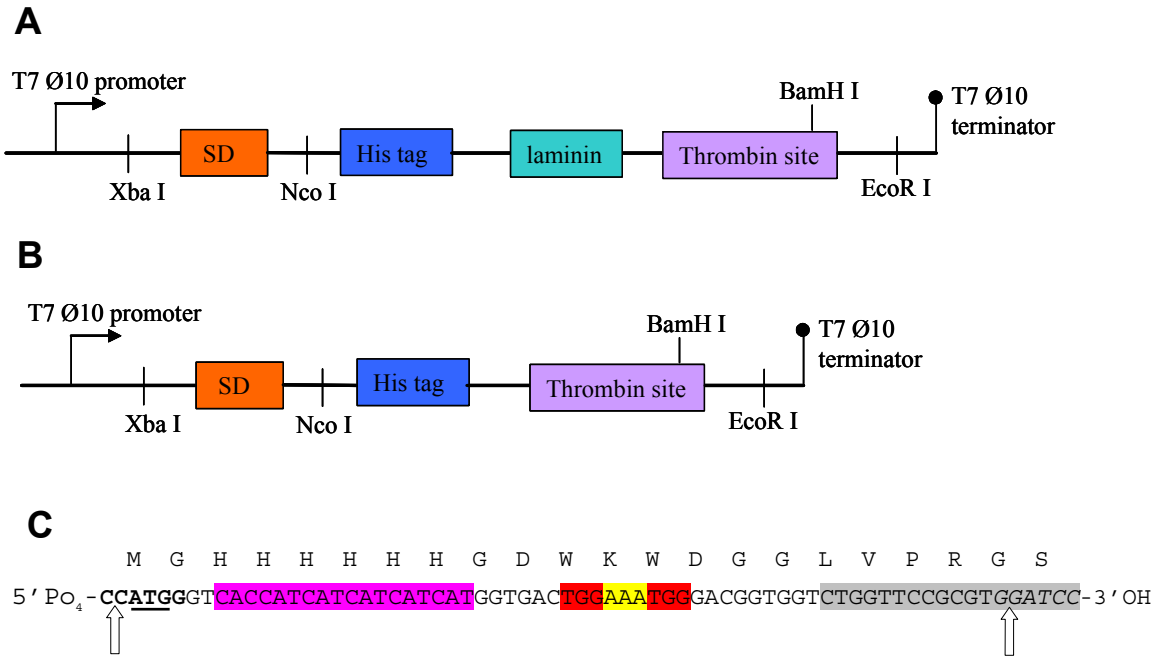

Figure 33. Overview of the mpPEP-T expression plasmid design. **A**, schematic representation of pPEP-T expression vector, highlighting transcriptional start (promoter) and stop (terminator) signals and 6X histidine tag followed by 34aa residue oligomerization domain of laminin as the N-terminal fusion along with the thrombin cleavage site. The gene to be expressed was cloned in between the BamHI and EcoRI sites. **B**, construction of mpPEP-T vector was done by digesting the pPEP-T vector with NcoI and BamHI and inserting the oligonucleotide sequence that removed the laminin oligomerization domain. **C**, oligonucleotide sequence used to create the mpPEP-T vector. Highlighting the Nco I site (bold) and BamH I restriction enzyme sites (italic), initial codon (underlined) and also the sequence that codes for 6X Histidine sequence (pink), for UV detection (red), for coupling reactions (yellow) and the thrombin recognition sequence (gray). Cleavage sites of Nco I and BamH I were highlighted by an arrow. Amino acid residues coded by oligonucleotide sequence was highlighted above the oligonucleotide sequence (22 amino acids).

Protein purification under denaturing conditions using nickel column affinity chromatography

Following expression, bacterial pellets (from 3 liter culture) were thawed in ice and to each gram of pellet (wet weight) 3 ml of lysis buffer (8 M Urea, 10 mM Tris pH 8.0 and 100 mM NaH_2Po_4) was added along with 10 mM β-mercaptoethanol.

Pellets were thoroughly resuspended in lysis buffer and sonicated on ice for 5 min (4 sec of sonication and 6 sec of gap). The supernatant was recovered after centrifuging the lysate at 12,000g at 4°C for 30 min.

The resulted cleared lysate was mixed with 4 ml of the Ni^{2+}-NTA slurry (Qiagen, Switzerland) and gently shaked for 1 hr in room temperature (batch method). After the incubation, the lysate and the Ni^{2+}-NTA slurry were loaded on to the econo-column (Bio-Rad, USA) and the resultant flow through was collected for analysis. Then the column matrix was subjected to three separate wash steps with lysis buffer of different pH (pH 6.3, 5.9 and 5.0) and in all these buffers 10 mM β-mercaptoethanol was added. The pH 5.0 washing step was included to remove the contaminant FKBP-type peptidyl-prolyl cis-trans isomerase (20 kDa protein) which was co-eluting with the purified samples initially. It was also reported to be a major contaminant of *E. coli* in denaturing IMAC-based procedures [31]. After wash step, the bound protein samples were eluted with lysis buffer pH 8.0, containing different concentrations of imidazole. 10 mM β-mercaptoethanol was included in elution buffers. The eluted samples were analyzed using SDS-PAGE and western blotting as described in Materials and Methods section of Chapter 3.

Prior to refolding step, the purified samples were dialyzed against the buffer (8 M Urea, 20 mM Tris-HCl pH 7.5, 150 mM NaCl, 2 mM DTT) to remove the imidazole. In addition, in the above buffer 10 mM EDTA was added to chelate the Ni^{2+} metal ions that might have leached along with the samples. The idea behind this step was to avoid the metal mediated cross linking of polyhistidine tag to form aggregates [32].

Estimation of protein concentration

For all the samples, protein concentrations were calculated using the absorbance value at 280 nm with extinction coefficient (M^{-1} cm^{-1}) and molecular weight (Daltons) of the protein (Table 11).

Extinction coefficient and the molecular weight of the proteins was calculated using ProtParam tool (http://www.expasy.ch/tools/protparam.html) [33]. For protein concentration measurements, we have also used the dye binding method [34] using Bio-Rad Bradford assay reagent with BSA as the standard.

Table 11. Physico-chemical properties of np1 and np2 based proteins#

Constructs		Molecular weight (Daltons)	Number of amino acids	Isoelectric point (pI)	Extinction coefficient (M^{-1} cm^{-1})
np1 and np1 based proteins	np1	10289.7	86	6.05	11125
	np1e	13341.2	114	6.30	16750
	np2ev1	15518.7	133	6.08	16750
	np2ev2	17614.1	154	6.08	16750
np2 and np2 based proteins	np2	10372.7	86	6.59	11000
	np2e	13424.2	114	7.03	16625
	np2ev1	15601.7	133	6.60	16625
	np2ev2	17697.1	154	6.60	16625

- All the properties were calculated using the online tool PROTPARAM from the expasy server (http://www.expasy.org/tools/protparam.html) [33].

Refolding conditions

The protein refolding procedure was carried out using two different refolding regimes.

Preparation 3 (denaturation, renaturation under oxidizing conditions)

The purified protein in denaturing conditions was refolded by step wise dialysis procedure. Initially, the denatured protein was dialyzed against the **refolding buffer 20 mM Tris pH 7.5, 150 mM NaCl and 10% glycerol** containing 8 M urea followed by 6 M urea, 4 M urea, 2 M urea and no urea in the same buffer as above. Finally, the protein was concentrated to the required concentration for further characterization in the buffer 20 mM Tris pH 7.5, 150 mM NaCl and 10% glycerol.

Preparation 4 (denaturation, renaturation under reducing conditions)

In this condition also the step wise dialysis procedure was followed. Initially, the protein was dialyzed against the **refolding buffer 20 mM Tris pH 7.5, 150 mM NaCl, 10% glycerol** containing 8 M urea and reducing agent (1 mM or 2 mM DTT) followed by 6 M urea + DTT, 4 M urea + DTT, 2 M urea + DTT and 0 M urea + DTT in the same refolding buffer as above. Finally, the refolded protein samples were dialyzed against either 20 mM Tris or Hepes buffer pH 7.5, containing 150 mM NaCl and 10% glycerol to remove DTT and concentrated to required concentration for further characterization in the same buffer. During refolding in both the conditions, the protein concentration was kept at 0.1 mg/ml.

Thrombin cleavage reaction

The refolded np1 and np2 nanoparticles were subjected to thrombin cleavage to remove the N-terminal amino acids that were of expression plasmid origin. Theoretically, 1 U of thrombin can able to cleave 1 mg of protein. In our cleavage conditions, we tried with different higher concentrations of thrombin (2x, 5x, 10x, 20x and 50x) to protein concentration to understand the optimal concentration of thrombin for cleavage.

We used human plasma thrombin (Sigma, USA) and the cleavage reactions were carried out at room temperature for 16 to 18 hrs with gentle shaking or sometimes for 24 hrs.

Biophysical methods

Circular Dichroism (CD) measurements

The CD measurements were acquired on an Aviv 62A DS spectropolarimeter. The far-ultraviolet spectra (200-250 nm) were measured in a 1 mm path-length quartz cell at 4°C. The spectra were normalized for concentration and path length to obtain the mean molar residue ellipticity (θ, theta) after subtraction of the buffer contribution. The melting and annealing curves were measured at 222 nm and in case of melting curve it was from 4° to 90°C (1 degree per minute) and for annealing curve 90° to 4°C.

The following formula was used to calculate the concentration independent theta (θ) values (deg cm^2 $dmol^{-1}$): **θ (observed) * MRW / [10 * path length (cm) * concentration (mg/ml)]**, where MRW - mean residue weight (molecular mass of the peptide or protein divided by number of amino acids). Data analysis and the wavelength scan plots were performed with the pro Fit software package (QuantumSoft, Switzerland).

Electron microscopy (EM) analysis

Electron microscopy analysis was performed by Dr. Gia Machaidze in Professor Ueli Aebi group, M.E. Muller Institute, University of Basel and also by Vesna Olivieri in Microscopy center, Pharmazentrum, University of Basel.

To prepare samples for electron microscopy, 5 µl protein samples were applied to a freshly glow discharged 200 mesh copper grids coated with parlodium/carbon film for 45 sec, washed 3 times with water and finally the samples were stained in 2% uranyl acetate for 15-20 sec. Excess of stain on the grids was removed using blotting paper and subsequently air-dried. The particles were examined using either Hitachi 7000 or Philips Morgagni 268D model transmission electron microscope with an acceleration voltage 80 or 100 kV.

Analytical ultracentrifugation (AUC)

AUC experiments were performed by Ariel Lustig, Biophysics Department, Biozentrum, University of Basel (http://www2.biozentrum.unibas.ch/auc/)

Sedimentation velocity (SV) and Sedimentation equilibrium data were recorded using Optima XLA analytical ultracentrifuge (Beckman Instruments, Palo Alto, California).

All runs were performed at 20°C using An-60 Ti rotor in 12 and 4 mm thickness double-sector cells. np1 and np2 nanoparticles were analyzed in the buffer 20 mM Tris or Hepes pH 7.5 containing 150 mM NaCl or no NaCl, 10% glycerol.

For all runs we used a partial specific volume $(\overline{\nu})$ of 0.73 mL/g and a buffer density (ρ) of 1.029 g/mL and in case of SV a buffer viscosity of 1.26 centipoise (cP) was used. The molecular masses (M) were calculated from SE data using the SEGAL computer program [35]. The formula that the SEGAL program uses to calculate the molecular mass (M) of the sample was given below:

$$M = 2RT/ (1- \overline{(\nu)}\rho) \omega 2 * d (\ln c)/d (r^2) \qquad \textbf{Equation 1}$$

Where R is Gas constant and T is the absolute temperature. ω is angular velocity, c is concentration (g/L) and r is radial distance from the axis of rotation.

Fluorescence correlation spectroscopy (FCS)

FCS measurements were performed by Dr. Per Rigler, Chemistry Department, University of Basel.

Instrumentation: A commercial confocal fluorescence laser scanning microscope (Zeiss LSM 510 META/Confocor2) equipped with the following laser lines: 405, 458, 477, 488, 514, 543 and 633 nm, was used to excite the sample either to obtain laser scanning micrographs or FCS data.

In LSM mode the appropriate wavelength with corresponding filter set was chosen. In order to get high signal to noise micrographs, the laser beam was typically focused on the sample with a 40x water immersion objective (Zeiss C-Apochromat, 40x, NA 1.2) and the sensitivity of the detectors (photon multiplier tubes) was adjusted accordingly. For FCS measurements dye molecules or labeled nanoparticles were excited with the appropriate wave length and filters in order to obtain maximal signal to noise ratio. A droplet of 5 µl was applied to the glass surface of a 8-well chamber (NUNC, USA) which had previously been positioned inside the xy-stage above the immersion objective through which the laser beam passes. Fluorescence emission was collected through the same objective and finally detected by highly sensitive avalanche photo diodes. The intensity fluctuations were analyzed in terms of an autocorrelation function.

Evaluation of FCS data: The analysis of the autocorrelation curve of a single species was carried out by a nonlinear least squares' fitting program by either using a commercial software package (LSM 510/Confocor2 software package, Zeiss AG) or a home-made procedure (Igor Pro, Wavemetrics Inc.) using the autocorrelation function:

$$G(\tau) = 1 + \frac{1}{N} \cdot \frac{1}{\left(1 + \frac{\tau}{\tau_D}\right)} \cdot \frac{1}{\sqrt{1 + R^2 \frac{\tau}{\tau_D}}} \cdot \left(1 - T + T \cdot e^{-\tau/\tau_T}\right) \quad \textbf{Equation 1}$$

where N and τ_D denote the mean number and the diffusion time of the fluorescent particles, respectively. τ is the channel time and R is the ratio between ω_z and ω_{xy} corresponding to the extensions of the Gaussian volume element of the laser beam in the axial and radial direction, respectively. The fraction and the lifetime of triplet states are denoted by T and τ_T, respectively.

The diffusion time (τ_D) is related to the laser beam dimensions and the translational diffusion coefficient *D* by:

$$\tau_D = \frac{\omega_{xy}^{\ 2}}{4D} \qquad \textbf{Equation 2}$$

With the assumption that the studied species are spherical, the hydro-dynamic radii, R_h, can be obtained from the Stoke-Einstein equation:

$$D = kT/(6\pi\eta R_h) \qquad \textbf{Equation 3}$$

where η is the viscosity, k is Boltzmann's constant and T is the absolute temperature.

By combining Equation 2 and Equation 1 we can now write the general autocorrelation function for multiple fluorescent species:

$$G(\tau) = 1 + \frac{1}{N} \cdot \sum_{i=1}^{M} \frac{f_i}{\left(1 + \frac{4D_i\tau}{\omega_{xy}}\right)} \cdot \frac{1}{\sqrt{1 + \frac{4D_i\tau}{\omega_z}}} \cdot \left(1 - T + T \cdot e^{-\tau/\tau_T}\right) \qquad \textbf{Equation 4}$$

Immunization protocol

Immunization experiments were done by Daniel Kao in Dr. Robert S. Hodges lab, University of Colorado Health Sciences Center, Denver, USA.

For our immunization studies we have used rabbit as the animal model. 4 injections were performed with a gap of 4 weeks between each immunization. During each immunization, rabbits were immunized with 15 μg of nanoparticles and administered through intramuscular route in the hind leg.

For preliminary immunization studies, nanoparticles (np1, np1e and np2ev1) were formulated with 50% (v/v) Freund's incomplete/complete adjuvant (Freund's complete adjuvant for the initial injection and Freund's incomplete adjuvant for the subsequent injections). For detail immunization studies with np1e nanoparticles, nanopartilcles were formulated with two different formulations: one with 50% (v/v) Freund's incomplete/complete adjuvant and the second one with 50% (v/v) phosphate buffered saline (PBS) (no adjuvant). The idea is to assess the immune response generated against np1e nanoparticles in the presence and absence of adjuvant.

After the final immunization (4th injection), rabbits were exsanguinated. The obtained serum was analyzed for antibody response using Enzyme-Linked Immunosorbent Assay (ELISA). A standard sandwich ELISA was used to measure anti pilin antibodies. Briefly the ELISA plates were coated with different antigens such as nanoparticles itself, pilin peptide conjugated to bovine serum albumin (BSA) and native pilin protein (200 µl of 0.1 µM of each antigen per well) . These plates were then incubated with different dilutions of rabbit sera and then incubated with an anti-rabbit IgG secondary antibody conjugated to horseradish peroxidase (HRP). Then the substrate was added and product formation was measured by monitoring the absorbance at 450 nm.

References - Chapter 2A and 2B

1. Sorensen, H.P., and Mortensen, K.K. (2005). Advanced genetic strategies for recombinant protein expression in Escherichia coli. J Biotechnol *115*, 113-128.
2. Lupas, A. (1996). Coiled coils: new structures and new functions. Trends Biochem Sci *21*, 375-382.
3. Burkhard, P., Stetefeld, J., and Strelkov, S.V. (2001). Coiled coils: a highly versatile protein folding motif. Trends Cell Biol *11*, 82-88.
4. Sreerama, N., and Woody, R.W. (2000). Estimation of protein secondary structure from circular dichroism spectra: comparison of CONTIN, SELCON, and CDSSTR methods with an expanded reference set. Anal Biochem *287*, 252-260.
5. Bachmann, M.F., Rohrer, U.H., Kundig, T.M., Burki, K., Hengartner, H., and Zinkernagel, R.M. (1993). The influence of antigen organization on B cell responsiveness. Science *262*, 1448-1451.
6. Bachmann, M.F., Hengartner, H., and Zinkernagel, R.M. (1995). T helper cell-independent neutralizing B cell response against vesicular stomatitis virus: role of antigen patterns in B cell induction? Eur J Immunol *25*, 3445-3451.
7. Bachmann, M.F., and Zinkernagel, R.M. (1996). The influence of virus structure on antibody responses and virus serotype formation. Immunol Today *17*, 553-558.
8. Baschong, W., Hasler, L., Haner, M., Kistler, J., and Aebi, U. (2003). Repetitive versus monomeric antigen presentation: direct visualization of antibody affinity and specificity. J Struct Biol *143*, 258-262.
9. Jegerlehner, A., Tissot, A., Lechner, F., Sebbel, P., Erdmann, I., Kundig, T., Bachi, T., Storni, T., Jennings, G., Pumpens, P., Renner, W.A., and Bachmann, M.F. (2002). A molecular assembly system that renders antigens of choice highly repetitive for induction of protective B cell responses. Vaccine *20*, 3104-3112.
10. Lechner, F., Jegerlehner, A., Tissot, A.C., Maurer, P., Sebbel, P., Renner, W.A., Jennings, G.T., and Bachmann, M.F. (2002). Virus-like particles as a modular system for novel vaccines. Intervirology *45*, 212-217.

11. Pumpens, P., Borisova, G.P., Crowther, R.A., and Grens, E. (1995). Hepatitis B virus core particles as epitope carriers. Intervirology *38*, 63-74.
12. Pumpens, P., and Grens, E. (1999). Hepatitis B core particles as a universal display model: a structure-function basis for development. FEBS Lett *442*, 1-6.
13. Cachia, P.J., and Hodges, R.S. (2003). Synthetic peptide vaccine and antibody therapeutic development: prevention and treatment of Pseudomonas aeruginosa. Biopolymers *71*, 141-168.
14. Doig, P., Todd, T., Sastry, P.A., Lee, K.K., Hodges, R.S., Paranchych, W., and Irvin, R.T. (1988). Role of pili in adhesion of Pseudomonas aeruginosa to human respiratory epithelial cells. Infect Immun *56*, 1641-1646.
15. Ramphal, R., Sadoff, J.C., Pyle, M., and Silipigni, J.D. (1984). Role of pili in the adherence of Pseudomonas aeruginosa to injured tracheal epithelium. Infect Immun *44*, 38-40.
16. Woods, D.E., Bass, J.A., Johanson, W.G., Jr., and Straus, D.C. (1980). Role of adherence in the pathogenesis of Pseudomonas aeruginosa lung infection in cystic fibrosis patients. Infect Immun *30*, 694-699.
17. Ramphal, R., Guay, C., and Pier, G.B. (1987). Pseudomonas aeruginosa adhesins for tracheobronchial mucin. Infect Immun *55*, 600-603.
18. Irvin, R.T., Doig, P., Lee, K.K., Sastry, P.A., Paranchych, W., Todd, T., and Hodges, R.S. (1989). Characterization of the Pseudomonas aeruginosa pilus adhesin: confirmation that the pilin structural protein subunit contains a human epithelial cell-binding domain. Infect Immun *57*, 3720-3726.
19. Lee, K.K., Doig, P., Irvin, R.T., Paranchych, W., and Hodges, R.S. (1989). Mapping the surface regions of Pseudomonas aeruginosa PAK pilin: the importance of the C-terminal region for adherence to human buccal epithelial cells. Mol Microbiol *3*, 1493-1499.
20. Campbell, A.P., McInnes, C., Hodges, R.S., and Sykes, B.D. (1995). Comparison of NMR solution structures of the receptor binding domains of Pseudomonas aeruginosa pili strains PAO, KB7, and PAK: implications for receptor binding and synthetic vaccine design. Biochemistry *34*, 16255-16268.
21. Burkhard, P., Meier, M., and Lustig, A. (2000). Design of a minimal protein oligomerization domain by a structural approach. Protein Sci *9*, 2294-2301.

22. Burkhard, P., Ivaninskii, S., and Lustig, A. (2002). Improving coiled-coil stability by optimizing ionic interactions. J Mol Biol *318*, 901-910.
23. Guo, Y., Kammerer, R.A., and Engel, J. (2000). The unusually stable coiled-coil domain of COMP exhibits cold and heat denaturation in 4-6 M guanidinium chloride. Biophys Chem *85*, 179-186.
24. Grgacic, E.V., and Anderson, D.A. (2006). Virus-like particles: passport to immune recognition. Methods *40*, 60-65.
25. Freund, J. (1956). The mode of action of immunologic adjuvants. Bibl Tuberc, 130-148.
26. Billiau, A., and Matthys, P. (2001). Modes of action of Freund's adjuvants in experimental models of autoimmune diseases. J Leukoc Biol *70*, 849-860.
27. Xiang, S.D., Scholzen, A., Minigo, G., David, C., Apostolopoulos, V., Mottram, P.L., and Plebanski, M. (2006). Pathogen recognition and development of particulate vaccines: does size matter? Methods *40*, 1-9.
28. Noad, R., and Roy, P. (2003). Virus-like particles as immunogens. Trends Microbiol *11*, 438-444.
29. Kammerer, R.A., Antonsson, P., Schulthess, T., Fauser, C., and Engel, J. (1995). Selective chain recognition in the C-terminal alpha-helical coiled-coil region of laminin. J Mol Biol *250*, 64-73.
30. Brandenberger, R., Kammerer, R.A., Engel, J., and Chiquet, M. (1996). Native chick laminin-4 containing the beta 2 chain (s-laminin) promotes motor axon growth. J Cell Biol *135*, 1583-1592.
31. Mukherjee, S., Shukla, A., and Guptasarma, P. (2003). Single-step purification of a protein-folding catalyst, the SlyD peptidyl prolyl isomerase (PPI), from cytoplasmic extracts of Escherichia coli. Biotechnol Appl Biochem *37*, 183-186.
32. Sprules, T., Green, N., Featherstone, M., and Gehring, K. (1998). Nickel-induced oligomerization of proteins containing 10-histidine tags. Biotechniques *25*, 20-22.

33. Gasteiger, E., Hoogland, C., Gattiker, A., Duvaud, S., Wilkins, M.R., Appel, R.D., and Bairoch, A. (2005). Protein Identification and Analysis Tools on the ExPASy Server. (In) John M. Walker (ed): The Proteomics Protocols Handbook, Humana Press, 571-607.

34. Bradford, M.M. (1976). A rapid and sensitive method for the quantitation of microgram quantities of protein utilizing the principle of protein-dye binding. Anal Biochem *72*, 248-254.

35. Machaidze, G., and Lustig, A. (2006). SEGAL, a semi-automatic program for fitting sedimentation equilibrium patterns from analytical ultracentrifugation. Journal of Biological Physics and Chemistry *6*, 91-102.

Chapter 3

Design and analysis for using non coiled-coil oligomerization domains in peptide based nanoparticle design principles

Design Principles

In chapter 1 and 2, we showed that the viral symmetry based designed peptides can be self-assembled into regular icosahedral nanoparticles. In these studies, the basic building blocks of nanoparticles are the coiled-coil oligomerization motifs, which represent the most frequently encountered oligomerization motifs of proteins [1-3]. Also, we wanted to study whether oligomerization motif other than coiled-coils can be used in our design principles along with coiled-coil oligomerization motif to form regular icosahedral nanoparticles? Therefore, the aim of this chapter is to use non coiled-coil oligomerization motif along with coiled-coil oligomerization motif and to study their self-assembly properties.

Based on the aim of the project, we made the following *de novo* design. The monomeic chain of small, globular, three-fold related β-propeller structure of the foldon domain [4] which is a trimerization domain of T4 phage fibritin protein, and has been linked to the monomeric chain of coiled-coil pentamerization domain of COMP [5] to reproduce correctly the relative three dimensional (3D) configuration of the three-fold and five-fold symmetry elements of an icosahedral virus capsid (Figure 1) [6]. The two-fold symmetry element was then generated by interaction between these two domains.

In order to characterize the *de novo* design, we engineered four different constructs (UC1 to UC4). The schematic representation and the amino acid sequences of these constructs are shown in Figure 2, A and B. **Construct UC1** depicts the *de novo* model comprising the foldon domain (residues 55-82; highlighted in blue), COMP domain (residues 85-126; highlighted in green) and two glycine (GG) residues (highlighted in brown) which act as a linker region, linking the foldon domain to the COMP domain. The cysteine residues (Cys^{122} and Cys^{125}) at the C-terminal end of COMP domain can possibly form intermolecular disulfide bridges within the pentameric coiled coil of COMP, as in the crystal structure of COMP domain [5]. The glycine residues are used to provide flexibility between two domains relative to each other.

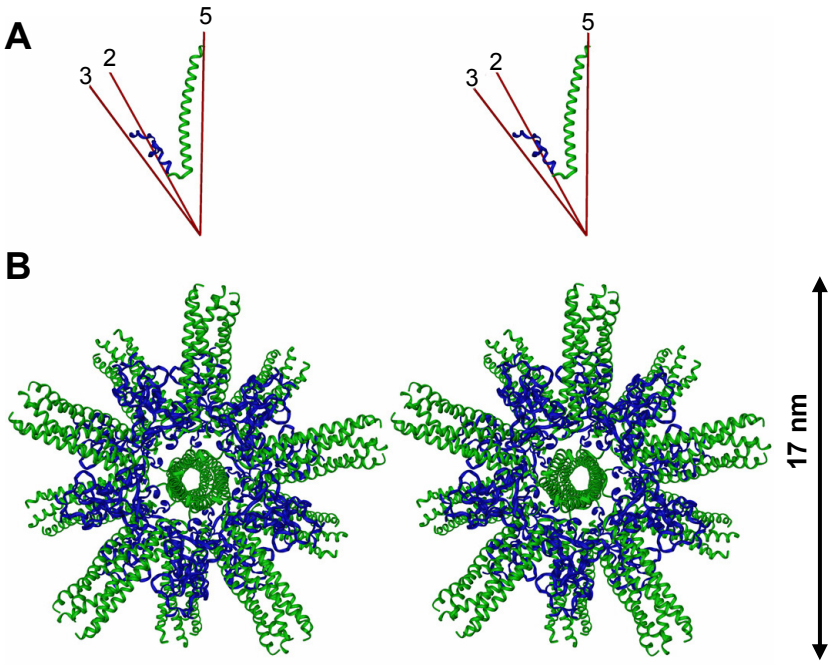

Figure 1. Design of icosahedral nanoparticles (stereo). **A**, The picture depicts the monomeric chain of foldon domain (blue) joined to the monomeric chain of COMP domain (green) as a single subunit. The COMP domain in the subunit was placed along the 5-fold axis of the icosahedron and the foldon domain along the 3-fold axis of the icosahedron. The rotational symmetry axis of the icosahedron (5, 3 and 2) was shown as red lines and was viewed along the centre of the icosahedron. **B**, computer designed model obtained by applying the symmetry elements along the 3-fold and 5-fold axes of the icosahedron. The view was along the 5-fold symmetry axis of the icosahedron. The pictures were adopted from [6].

In **construct UC2**, a single point mutation is introduced in the foldon domain (aspartic acid (D)^{64} to cysteine (C)^{64}; bold and underlined residue), otherwise it is the same as that of construct UC1. The principle behind the mutation of amino acid (D) to (C) is to favor the formation of a disulfide bridge with the same residue of another monomeric building block, to which it is symmetrically related by the two-fold rotation axis of the icosahedron, with the intention to connect two neighboring foldon trimers in the icosahedron related by this two-fold symmetry (Figure 3). By doing so, the objective is to stabilize the nanoparticles. In the foldon domain structure [4], the above mutated aspartic acid (D) residue is located in the loop region which connects the β hairpin motif to the end of the last α helical segment and is not involved in any kind of interaction expected to stabilize the trimeric form of the foldon domain. So, the mutation of residue (D) to (C) should not abolish the oligomeric state of the foldon domain.

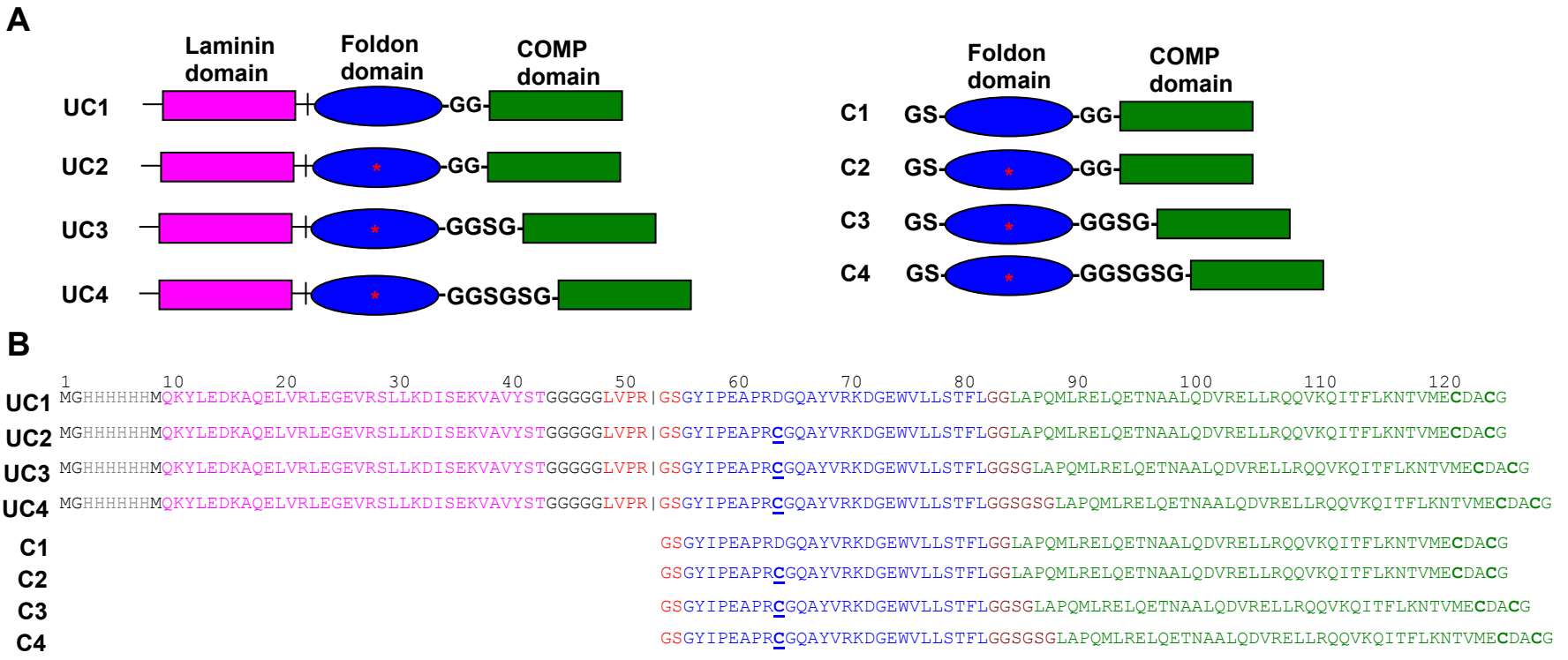

Figure 2. **A**, schematic representation of constructs involved in this study. UC1 to UC4 represent the expressed constructs along with the N-terminal vector coded laminin domain (pink rectangle). Blue oval shape - foldon domain; green rectangle - COMP domain. The brown colored amino acids in between the foldon and COMP domain represent the linker residues. * represents the mutated amino acid aspartic acid (D) to cysteine (C) in the foldon domain. Vertical line (|) represents thrombin cleavage site. C1 to C4 represent the thrombin cleaved constructs UC1 to UC4. In C1 to C4 constructs, the two extra amino acids at the N-terminus which are result of thrombin cleavage, are highlighted red. **B**, amino acid sequence of UC1 to UC4 and C1 to C4 constructs. In UC1 to UC4 constructs, the N-terminal 54 amino acids are vector sequences coding for His-tag (grey), laminin domain (pink) and thrombin recognition sequence (red). The green and blue colored amino acids represent the foldon and COMP domain, respectively. The mutated aspartic acid (D) to cysteine (C) amino acid in the foldon domain is indicated in bold and underlined. The C-terminal cysteine residues of the COMP domain are indicated in bold.

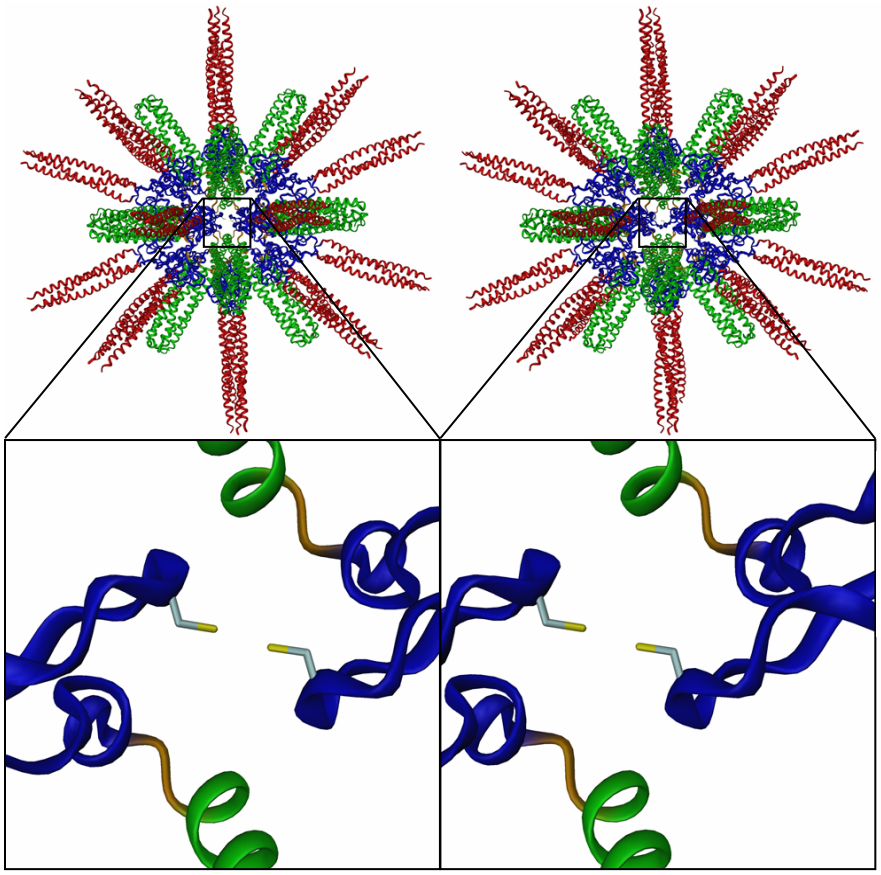

Figure 3. Computer model of UC2 nanoparticle (stereo), showing the laminin domain (red), foldon domain (blue) and the COMP domain (green). Within the nanoparticle, two monomeric building blocks are highlighted with a special emphasis on the engineered intermolecular disulfide bridge between the foldon domains (blue), which are related by the two-fold symmetry axis of the icosahedron.

According to our nanoparticle design principles (chapter 1), if the two different oligomeric domains of the monomeric building blocks folds properly, the monomeric building blocks will first assemble into 'even units'. The monomer content of even unit will depend on the least common multiple (LCM) of the oligomeric state of the domains involved. Therefore, in our design 15 monomers will form an even unit (Figure 4). One of the factors that determine the further assembly of these even units into nanoparticles would probably be the length of the linker region that links the two oligomerization domains together. To test this principle, we extended the linker region of UC2 construct by four (GGSG) and six residues (GGSGSG) resulting in **UC3 and UC4 constructs**, respectively.

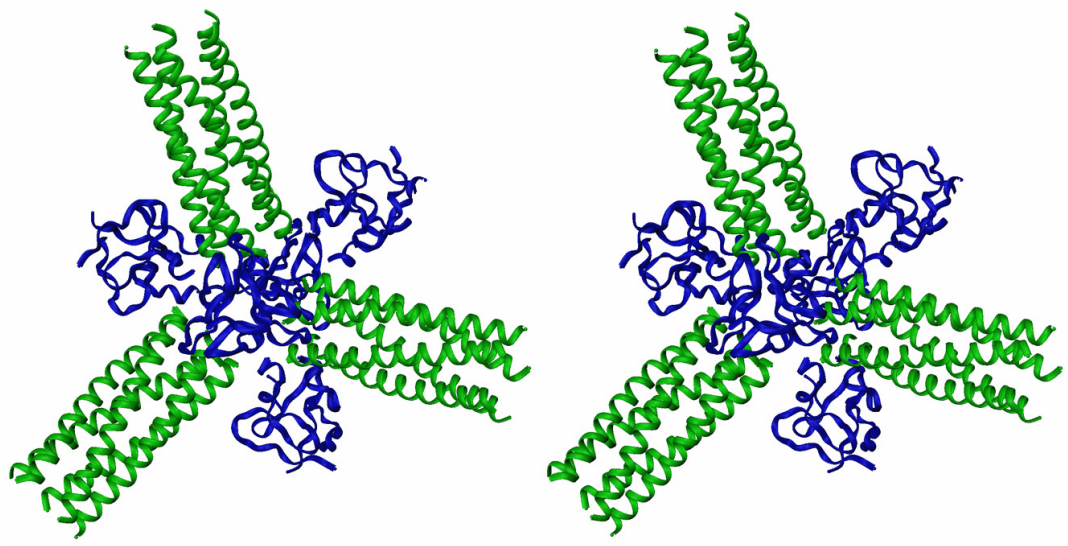

Figure 4. Computer model of an 'even unit' comprising 15 monomeric building blocks (stereo). The pentameric coiled-coil domain of COMP and the foldon domain are highlighted in green and blue, respectively. The view is down the three-fold symmetry axis.

All the four constructs (UC1 to UC4) has an additional 54 amino acids at the N-terminus which is a result of cloning in pPEP-T expression vector. This region includes the vector coded His-tag (residues 3-8; grey), laminin fusion protein (residues 10-43; pink) and thrombin recognition sequence (residues 49-54; red). After thrombin cleavage, all the four constructs will have two extra residues (glycine (G) and serine (S)) at their N-terminus. The thrombin cleaved constructs are depicted in Figure 2, A as C1 to C4.

Results

Purification results of uncleaved proteins UC1 to UC4

The 6xHis-tagged proteins are purified by means of Ni^{2+}-affinity column chromatography under denaturing conditions. The purification results for all four constructs are summarized in Figure 5.

From the purification results, it is observed that in all the purified proteins the monomeric protein (black arrow) started to elute during the wash step pH 8.0 (lane 2) and pH 6.3 (lanes 3 and 4) (UC1-14182.1 daltons; UC2-14170.2 daltons; UC3-14314.3 daltons; UC4-14458.4 daltons).

The reason for this could be the over saturation of the Ni^{2+} binding sites in the column by the His-tagged proteins, which would be an indication of very good protein expression.

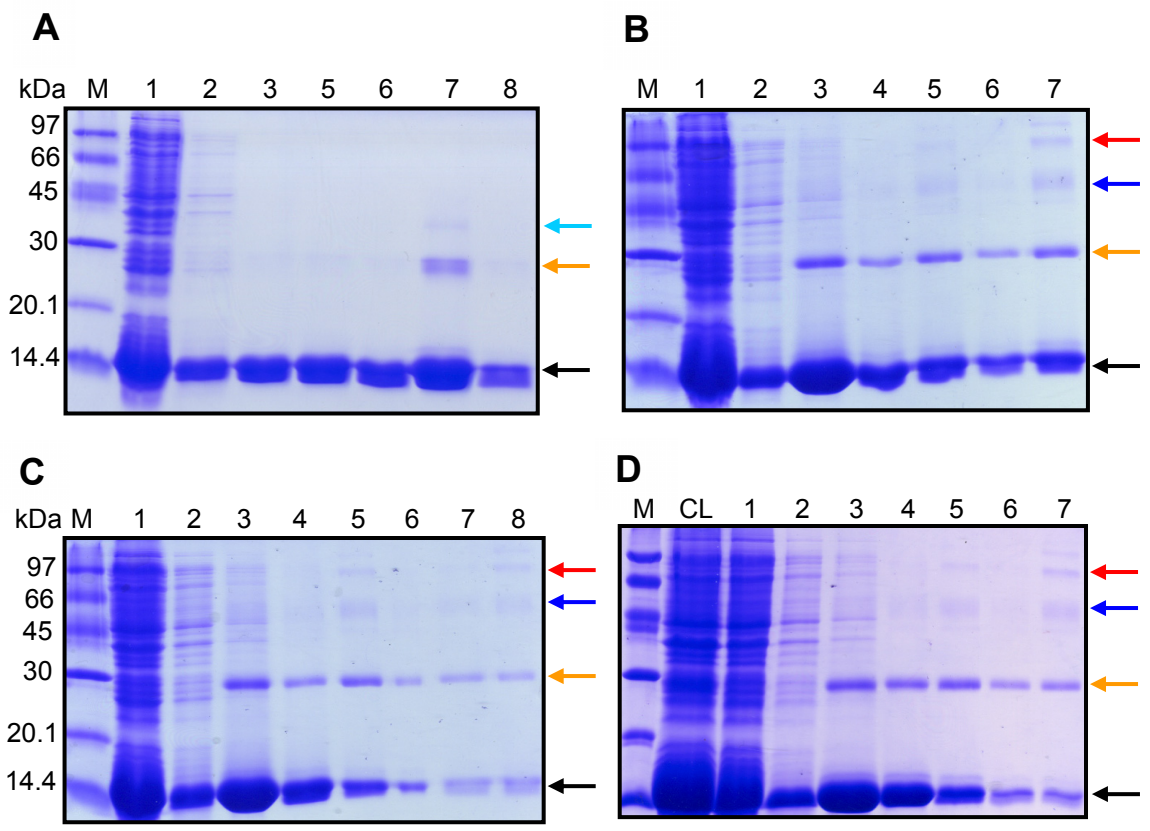

Figure 5. 15% SDS-PAGE analysis of purified samples of uncleaved proteins UC1 to UC4. **A**, UC1 purified fractions; **B**, UC2 purified fractions; **C**, UC3 purified fractions; **D**, UC4 purified fractions. The figure lane labels are explained as follows and it applies to all the four constructs: M - molecular weight marker in kilo Daltons (kDa); CL - cleared lyaste; lane 1 - Flow through; lane 2 - pH 8.0 wash fraction; lanes 3 and 4 - pH 6.3 wash fractions; lanes 5 and 6 - pH 5.9 elution fractions; lanes 7 and 8 - pH 4.5 elution fractions. The black, orange, sky blue, blue and red arrows represent the monomer, dimer, trimer, tetramer and pentamer forms of the above proteins, respectively.

For proteins UC2, UC3 and UC4 (Figure 5, B, C and D) a strong band is observed above the monomeric protein in both wash (lanes 2, 3 and 4) and elution fractions (lanes 5, 6, 7 and 8) which correspond to a theoretically calculated dimer (orange arrow) (UC2-28340.4 daltons; UC3-28628.6 daltons; UC4-28916.8 daltons). The observation of dimer could be due to the formation of a disulfide bridge between the monomers.

In the purified fractions of UC1 protein (Figure 5, A), the dimeric band (28364.2 daltons) is observed only in pH 4.5 elution fraction 1 (lane 7) along with a faint band corresponding to a theoretically calculated trimer (sky blue arrow) (42546.3 daltons). However, for UC2, UC3 and UC4 purified samples, in addition to dimeric band the possible higher order oligomers are also observed in the pH 5.9 and 4.5 elution fractions (lanes 5, 7 and 8). The observed oligomers correspond to a theoretically calculated tetramer (blue arrow) (UC2-56680.8 daltons; UC3-57257.2 daltons; UC4-57833 daltons) and pentameric (red arrow) (UC2-70851 daltons; UC3-71571.5 daltons; UC4-72292 daltons) forms of the protein.

The eluted fractions (pH 5.9 and 4.5) of proteins UC1 to UC4 are analyzed by western blotting using anti His-tag monoclonal antibody. The western blotting results supported the presence of monomeric and dimeric forms observed on the SDS-PAGE of all the purified proteins (Figure 6).

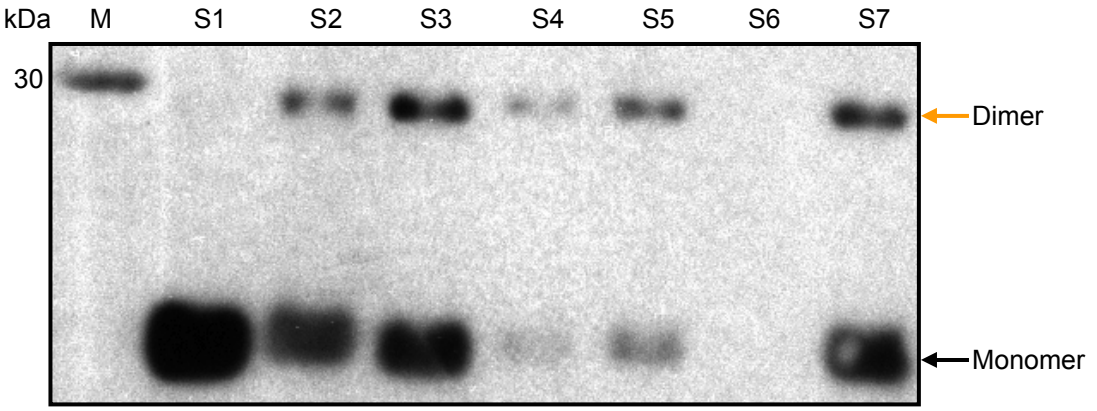

Figure 6. Western blot analysis of purified samples of uncleaved proteins UC1 to UC4. Purified fractions of pH 5.9 and 4.5 eluted samples of UC1 (S1, S2), UC2 (S3, S4), UC3 (S5, S6) and a purified fraction of pH 5.9 eluted sample of UC4 (S7). Anti His-tag monoclonal antibody is used. The monomer and dimer band is indicated by the black and the orange arrow, respectively. M - Molecular weight marker in kiloDaltons (kDa).

Thrombin cleavage and Purification results of cleaved proteins C1 to C4

The purified uncleaved UC1 to UC4 samples are dialyzed against thrombin cleavage buffer cleaved by thrombin and purified, as described in the Materials and Methods section. The SDS-PAGE results of the cleaved, purified samples of C1 to C4 are summarized in Figure 7.

The cleaved monomeric band of C1 protein (8368.5 daltons) is observed in the flow-through samples as expected (Figure 7, A; lanes FT1 to FT3) (green arrow). This result confirmed successful cleavage of the His-tag along with the upstream fusion domain laminin. The cleavage is further supported by the elution of uncleaved full length protein (black arrow) along with the cleaved His-tagged N-terminal fusion domain (5831.6 daltons) (orange arrow) in the pH 6.3 wash fractions (lanes W1 to W3) and in the pH 5.9 elution fraction (lane E1) (Figure 7, A).

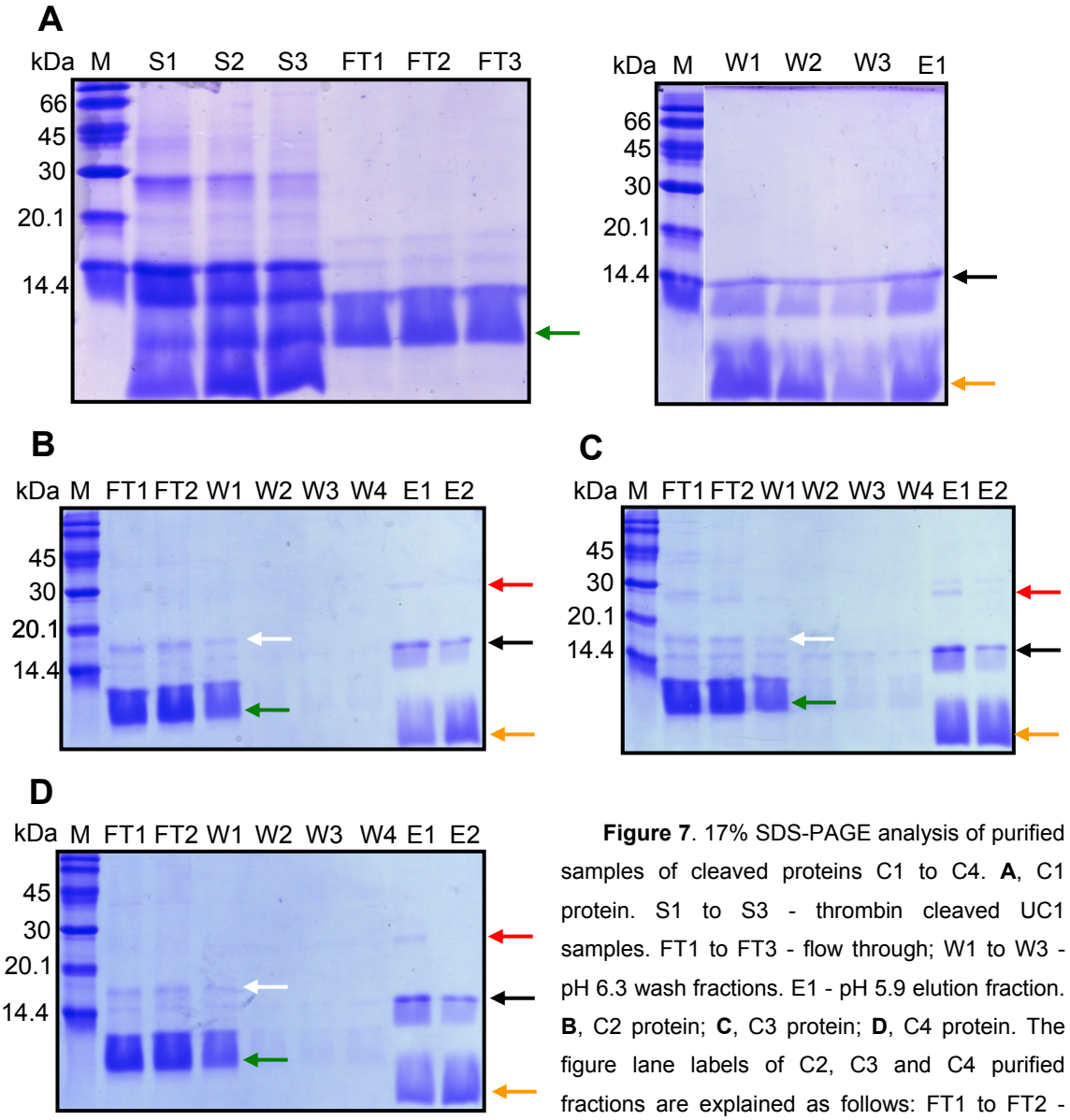

Figure 7. 17% SDS-PAGE analysis of purified samples of cleaved proteins C1 to C4. **A**, C1 protein. S1 to S3 - thrombin cleaved UC1 samples. FT1 to FT3 - flow through; W1 to W3 - pH 6.3 wash fractions. E1 - pH 5.9 elution fraction. **B**, C2 protein; **C**, C3 protein; **D**, C4 protein. The figure lane labels of C2, C3 and C4 purified fractions are explained as follows: FT1 to FT2 - flow through; W1 to W4 - pH 8.0 wash fractions; E1 - pH 6.3 wash fraction; E2 - pH 5.9 elution fraction. M - Molecular weight marker in kiloDaltons (kDa). The monomeric and dimeric forms of the cleaved proteins C1 to C4 are indicated by green and white arrows, respectively. The monomeric and dimeric forms of the uncleaved proteins UC1 to UC4 are indicated by black and red arrows, respectively. The cleaved His-tagged laminin fusion domain is indicated by an orange arrow.

For cleaved proteins C2, C3 and C4 (Figure 7, B, C and D), the expected monomeric band (C2-8356.6 daltons; C3-8500.7 daltons; C4-8644.8 daltons) is observed in the flow-through samples (lanes FT1, FT2) and in the pH 8.0 wash fraction (lane W1) (green arrow). This again confirmed the successful cleavage of the His-tagged N-terminal fusion domain laminin. In the above samples, in addition to the monomeric band we observed a band which correspond to a theoretically calculated cleaved dimeric band (C2-16713.2 daltons; C3-17001.4 daltons; C4-17289.6 daltons) (white arrow).

As observed for C1 protein, the uncleaved full length protein (black arrow) and the cleaved His-tagged laminin fusion domain (orange arrow) of proteins C2 to C4 is eluted at pH 6.3 wash fraction (lane E1) and at pH 5.9 elution fraction (lane E2). In case of the pH 6.3 wash fraction, we also observed the uncleaved dimeric band (red arrow).

The cleaved and purified samples of the C1 to C4 are subjected to western blotting using anti His-tag monoclonal antibody. The objective is to confirm the cleavage of the His-tag by comparing with the uncleaved fractions of pH 6.3 step. From the western blot results, it is clear that the purified fractions of C1 to C4 are devoid of His-tag, since none of them shows recognition by anti His-tag monoclonal antibody (Figure 8; lanes S2, S4, S6 and S8).

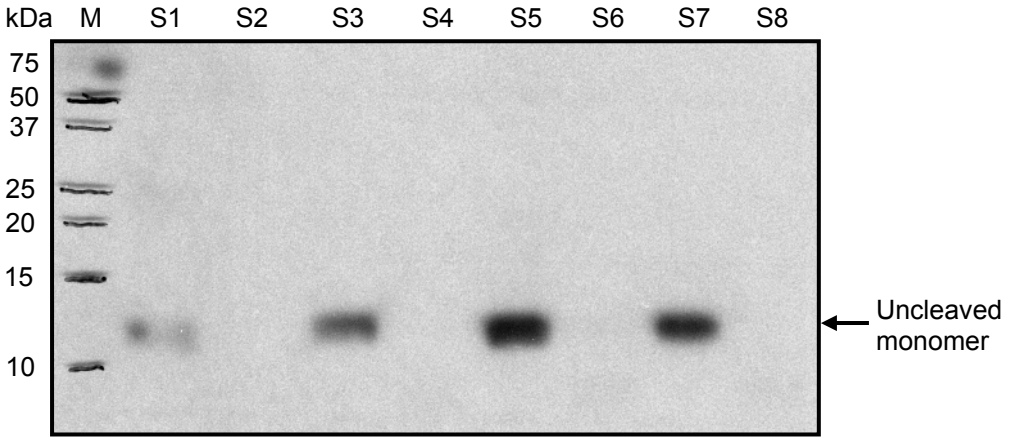

Figure 8. Western blot analysis of purified samples of cleaved proteins C1 to C4. The thrombin cleaved sample of UC1 protein (S1) is compared with the purified fraction of cleaved C1 protein (S2). In the same way, the purified uncleaved pH 6.3 eluted fractions of UC2 (S3), UC3 (S5) and UC4 (S7) are compared with the purified fractions of cleaved C2 (S4), C3 (S6) and C4 (S8), respectively. Anti His-tag monoclonal antibody is used. M - Molecular weight marker in kiloDaltons (kDa).

Self-assembly properties of cleaved proteins C1 to C4

The cleaved proteins C1 to C4 (Figure 2, A) are studied for their self-assembling properties. Because of the presence of cysteine amino acids in these proteins as they can form different combinations of intra- and intermolecular disulfide bridges during refolding, we tried with two different refolding conditions. In the first refolding condition, the purified protein samples in 8 M urea are refolded by means of step-wise dialysis of the urea completely under oxidizing condition (preparation 1). In the second refolding condition, the protein samples are refolded by step-wise dialysis of the urea under reducing condition (2 mM DTT) up to 0 M urea, followed by the oxidizing condition by dialyzing out the reducing agent (2 mM DTT) (preparation 2).

The self-assembly behavior of the cleaved proteins under these two different refolding conditions are analyzed by Blue Native (BN)-PAGE and AUC to determine the molecular weight of the oligomers formed. Furthermore, the morphology of the oligomers is investigated by EM.

Self-assembly properties of protein C1

BN-PAGE results: For protein C1, refolded under preparation 1 condition we observed a band corresponding to pentamers (41.9 kDa) (Figure 9; lane 3). However, for the preparation 4 refolded samples we observed an additional band which corresponds to decamers (10-mers) (83.8 kDa) (Figure 9; lane 4).

AUC results: The refolded samples under both conditions (preparation 1 and 2) gave a molecular mass which corresponds to pentamers (Table 1).

EM results: In both preparation 1 (Figure 10, A) and preparation 2 (Figure 10, B) refolded samples of C1 protein, we observed short fragment like structures. Based on the results of BN-PAGE and AUC, the observed short fragment like structures might well correspond to pentamers and decamers.

Table 1: AUC results for refolded protein C1. Monomer molecular weight 8.37 kDa

Refolding condition	Concentration (mg/ml)	Rotor speed (rpm)	Sedimentation Equilibrium MW (kDa)	
			Observed MW	No. of monomers
preparation 1	0.05	18000	44	5.3
	0.1	20000	40	4.8
preparation 2	0.1	18000	44	5.3
	0.2	20000	43	5.1

Self-assembly properties of protein C2

BN-PAGE results: For protein C2, refolded under preparation 1 condition we observed bands corresponding to trimers (25.1 kDa), pentamers (41.9 kDa) and 15-mers (even units) (125.6 kDa) (Figure 9; lane 6). However, for preparation 2 refolded samples we observed bands which correspond to pentamers and even units and we did not observe the trimeric band (Figure 9; lane 7).

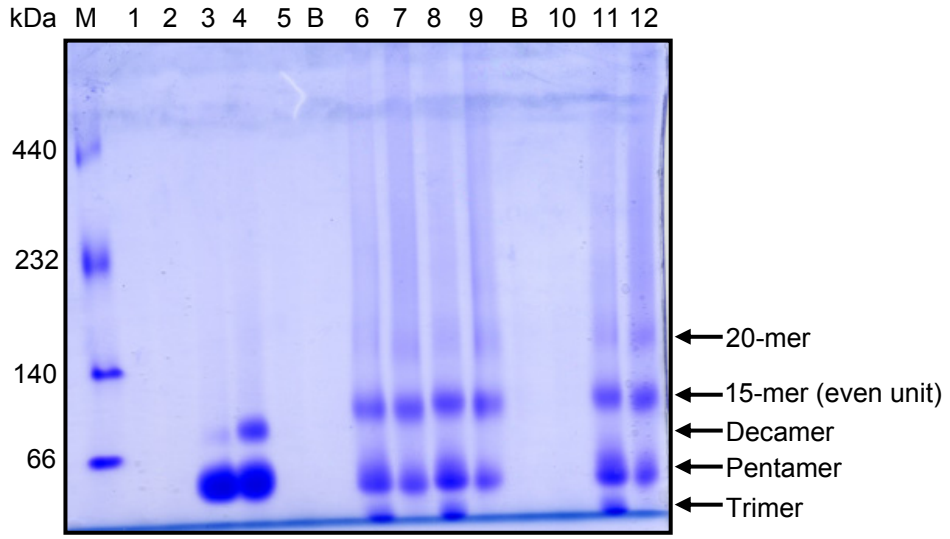

Figure 9. 5 - 12% gradient Blue Native (BN) PAGE of refolded uncleaved (UC1 to UC4) and cleaved (C1 to C4) proteins. The figure lanes are explained as follows: M - High molecular weight native gel marker; lane 1 corresponds to UC1 sample (preparation 2 refolded). Analyzed in the buffer 20 mM Tris pH 8.5, 150 mM NaCl and 2 mM DTT; lanes 2, 5, 10 correspond to UC1, UC2 and UC4 samples, respectively (preparation 2 refolded). Analyzed in the buffer 20 mM Tris pH 8.0, 150 mM NaCl and 2 mM DTT; lanes 3, 6, 8 and 11 correspond to preparation 1 refolded samples of C1, C2, C3 and C4, respectively; lanes 4, 7, 9 and 12 correspond to preparation 2 refolded samples of C1, C2, C3 and C4, respectively; both preparation 1 and preparation 2 refolded samples are analyzed in the buffer 20 mM Tris pH 7.5, 150 mM NaCl; B- blank lanes. In each lane, ~ 15 µg of protein was loaded.

AUC results: The refolded samples under both conditions (preparation 1 and 2) gave molecular mass values which correspond to pentamers and 20-mers (Table 2). Based on the results of BN-PAGE, the observed 20-mers might well correspond to the mixture of even units and possibly the even units linked to pentamers through disulfide bridges.

EM results: In both preparation 1 (Figure 10, C) and preparation 2 (Figure 10, D) refolded samples, we observed nanoparticles but not of regular in shape. In addition, we observed a lot of background material. Based on the results of BN-PAGE and AUC, the observed nanoparticles which are not of regular in shape might well correspond to even units and 20-mers, and background material to trimers and pentamers.

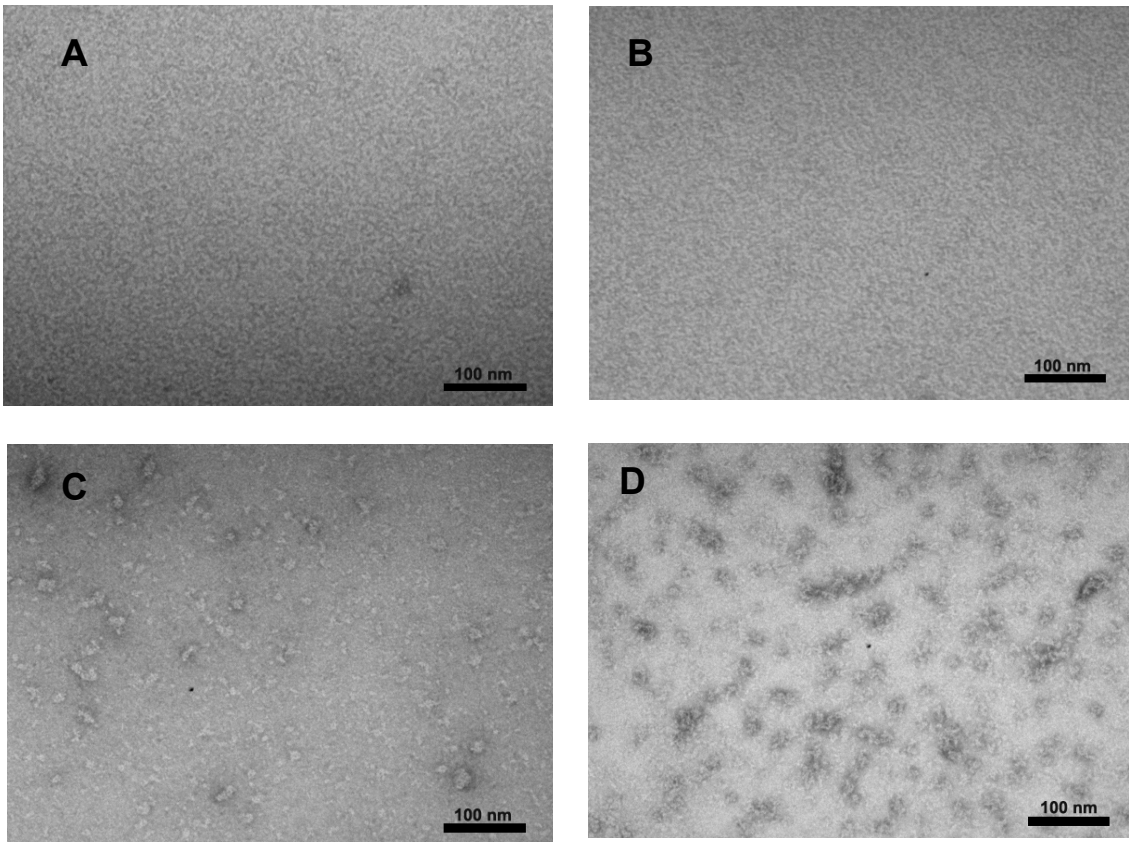

Figure 10. Electron micrographs of C1 and C2 refolded proteins. **A** and **C** correspond to preparation 1 refolded C1 and C2 proteins, respectively. **B** and **D** correspond to preparation 2 refolded C1 and C2 proteins, respectively. The pictures were prepared by negative staining with 2% uranyl acetate; the concentration of the protein was 50 µg/ml.

Table 2. AUC results for refolded protein C2. Monomer molecular weight 8.37 kDa

Refolding condition	Concentration (mg/ml)	Rotor speed (rpm)	Sedimentation Equilibrium MW (kDa)	
			Observed MW	No. of monomers
preparation 1	0.2	18000	44 + 166	5.3 + 19.8
	0.4	12000	46 + 164	5.5 + 19.6
preparation 2	0.4	12000	51 + 179	6 + 21.4

Self-assembly properties of protein C3

BN-PAGE results: For protein C3, refolded under preparation 1 condition we observed bands corresponding to trimers (25.5 kDa), pentamers (42.5 kDa) and even units (127.5 kDa) (Figure 9; lane 8). However, for preparation 2 refolded samples we observed bands which correspond to pentamers and even units but not to trimers (Figure 9; lane 9).

AUC results: The preparation 1 refolded sample gave molecular mass values which correspond to pentamers and 20-mers (Table 5). On the other hand, preparation 2 refolded samples gave molecular mass values which correspond to pentamers and 30-mers (Table 3). The observation of 30-mers possibly suggests the two self-assembled even units. Again, the observation of 20-mers might well correspond to mixture of even units and possibly the even units linked to pentamers through disulfide bridges.

Table 3. AUC results for refolded protein C3. Monomer molecular weight 8.5 kDa

Refolding condition	Concentration (mg/ml)	Rotor speed (rpm)	Sedimentation Equilibrium MW (kDa)	
			Observed MW	No. of monomers
preparation 1	0.13	14000	49 + 183	5.8 + 21.5
	0.4	12000	56 + 176	6.6 + 20.7
preparation 2	0.16	12000	45 + 245	5.3 + 28.8
	0.2	12000	52 + 253	6.1 + 29.8

Self-assembly properties of C4 protein

BN-PAGE results: For C4 protein, refolded under preparation 1 condition we observed bands corresponding to trimers (25.9 kDa), pentamers (43.2 kDa) and even units (129.7 kDa) (Figure 9; lane 11). However, for preparation 2 refolded sample we observed bands which correspond to pentamers (43.2 kDa) and even units (129.7 kDa) and in addition we observed an additional faint band which corresponds to 20-mers (Figure 9; lane 12).

AUC results: The refolded samples under both conditions (preparation 1 and 2) gave a molecular mass values which correspond to pentamers and high molecular weight species. The high molecular weight species seems to be the mixed population of 20-mers and 30-mers (Table 4).

Table 4. AUC results for refolded C4 protein. Monomer molecular weight 8.6 kDa

Refolding condition	Concentration (mg/ml)	Rotor speed (rpm)	Sedimentation Equilibrium MW (kDa)	
			Observed MW	No. of monomers
preparation 1	0.13	12000	48 + 314	5.6 + 36.5
	0.2		52 + 294	6 + 34.2
	0.4		175 + 248	20.3 + 28.8
preparation 2	0.14		48 + 234	5.6 + 27.2
	0.2		44 + 231	5.1 + 26.9
	0.45		200	23.3

EM results for refolded proteins C3 and C4: In both, preparation 1 refolded samples of C3 and C4 (Figure 11, A and C) and in preparation 2 refolded samples of C3 and C4 (Figure 11, B and D), we observed nanoparticles but not with regular shape.

Based on the BN-PAGE and AUC results of C3 and C4 proteins, the observed nanoparticles which are not of regular in shape might well correspond to even units and multiples thereof.

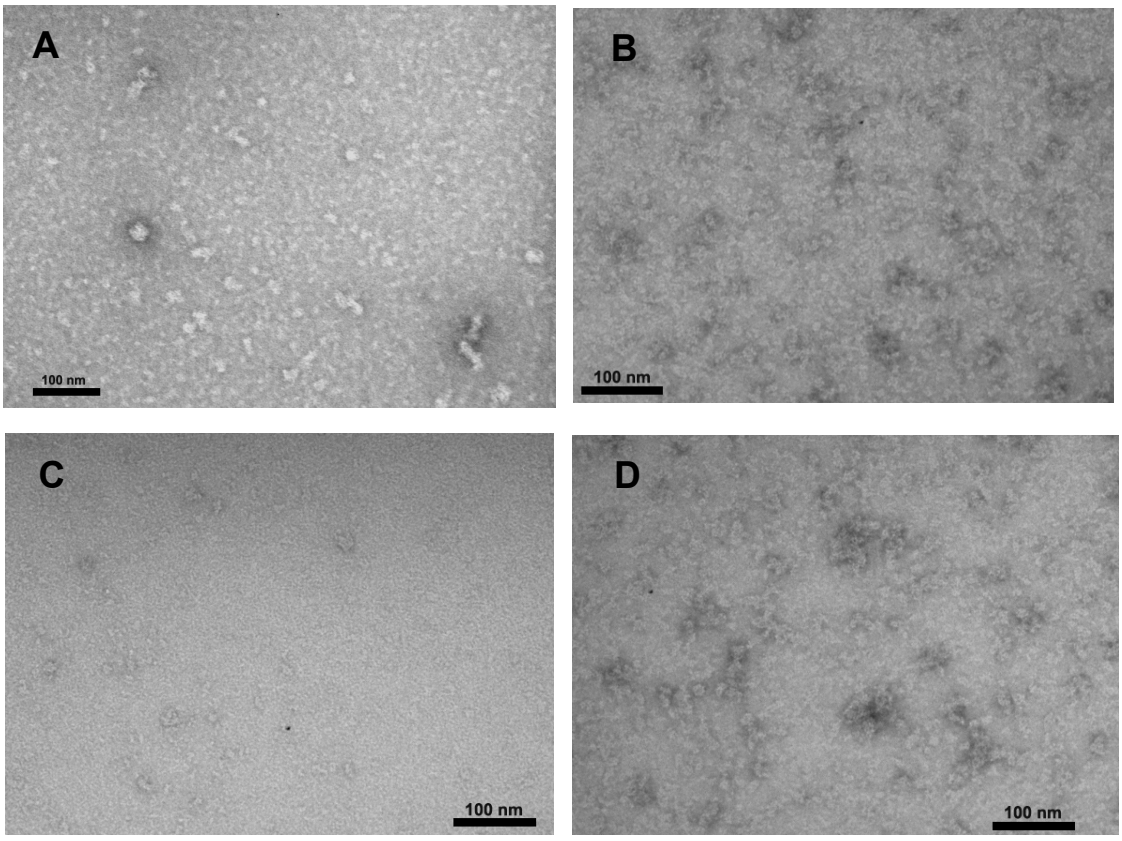

Figure 11. Electron micrographs of C3 and C4 refolded proteins. **A** and **C** correspond to preparation 1 refolded C3 and C4 proteins, respectively. **B** and **D** correspond to preparation 2 refolded C3 and C4 samples, respectively. The pictures were prepared by negative staining with 2% uranyl acetate; the concentration of the protein was 50 µg/ml.

Self-assembly properties of uncleaved proteins UC1 to UC4

From the self-assembly studies of cleaved proteins C1 to C4, we understood that the cleaved proteins do not form icosahedral nanoparticles composed of 60 monomers. This observation prompted us to study the self-assembly properties of uncleaved proteins UC1 to UC4 (for construct details refer to Figure 2).

For self assembly studies, the purified samples of uncleaved proteins UC1 to UC4 in 8 M urea are subjected to step wise dialysis of the urea under reducing condition and at low protein concentration (preparation 2). The reason for reducing condition (2 mM DTT) refolding is that the initial refolding experiment of UC2 protein under oxidizing condition (preparation 1), showed precipitating behavior of the protein at 4 M urea concentration. Therefore, we decided to refold the proteins under reducing condition refolding (preparation 2).

Initial refolding results of UC1 protein

Initially for UC1 protein, the reducing condition refolding (preparation 2) is done at pH 7.5. However, the refolded protein started to precipitate in refolding buffer containing 0 M urea and 2 mM DTT (reducing condition). Subsequent change to the refolding buffer containing 0 M urea and no DTT (oxidizing condition), the refolded protein precipitated heavily. From the EM analysis of sample in 0 M urea and no DTT, large aggregated structures with few individual icosahedral nanoparticles are observed (Figure 12, A). The possible reason for precipitation in the refolding buffer containing 0 M urea and 2 mM DTT could be due to pI of the protein which is calculated to be 6.29. In addition, the observed heavy precipitation upon oxidizing condition could be due to linking of aggregates through intermolecular disulfide bridges. Therefore, the UC1 samples are refolded at pH 8.0 and 8.5 and analyzed in the refolding buffer containing 0 M urea and 2 mM DTT (reducing condition). The refolded samples are found to be stable in 0 M urea containing 2 mM DTT. From EM pictures, the refolded samples at pH 8.0 and 8.5 are observed to form icosahedral nanoparticles (Figure 12, B and C).

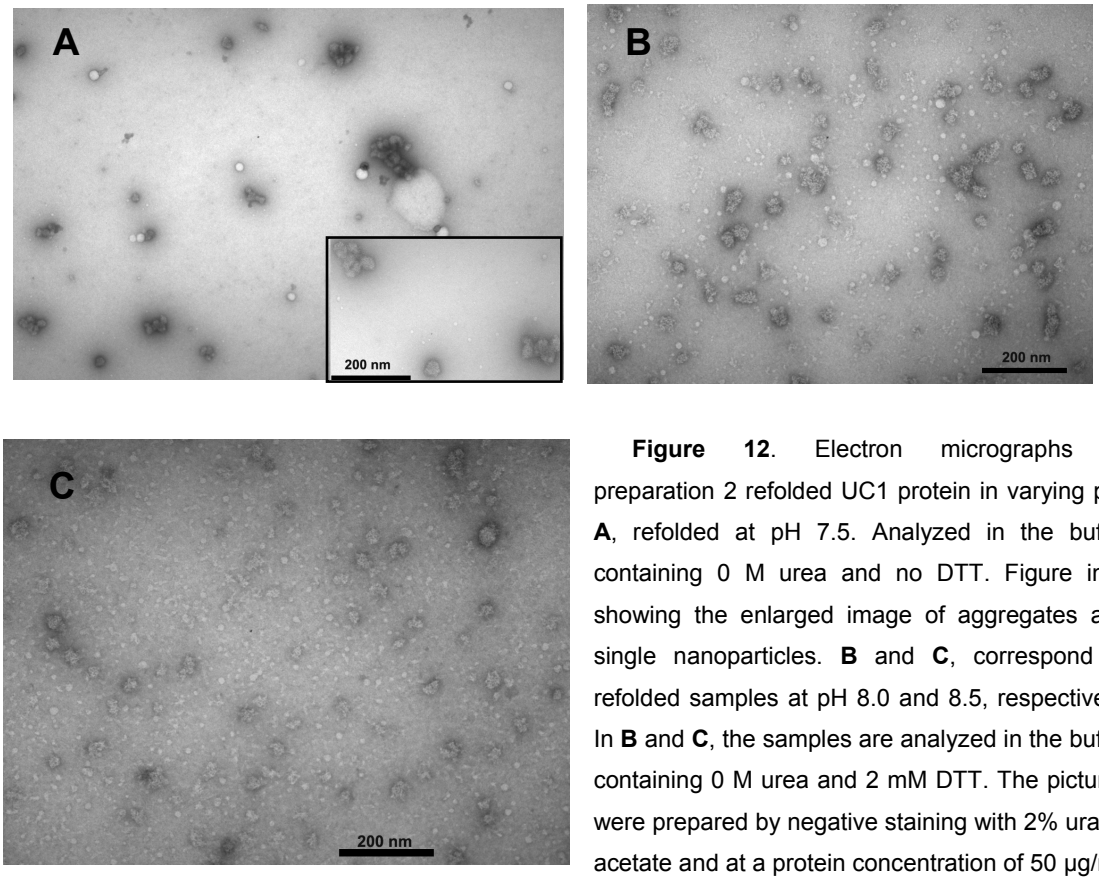

Figure 12. Electron micrographs of preparation 2 refolded UC1 protein in varying pH. **A**, refolded at pH 7.5. Analyzed in the buffer containing 0 M urea and no DTT. Figure inlet showing the enlarged image of aggregates and single nanoparticles. **B** and **C**, correspond to refolded samples at pH 8.0 and 8.5, respectively. In **B** and **C**, the samples are analyzed in the buffer containing 0 M urea and 2 mM DTT. The pictures were prepared by negative staining with 2% uranyl acetate and at a protein concentration of 50 µg/ml.

Self-assembly properties of proteins UC1, UC2, UC3 and UC4

To compare their self-assembly properties, all four proteins are refolded under reducing condition (preparation 2) and the pH of the refolding buffer is kept at 8.0. The protein samples are refolded up to 0 M urea containing 2 mM DTT and analyzed in the same buffer for EM and AUC studies.

EM results: From the EM pictures, all four proteins are observed to form icosahedral nanoparticles (Figure 13, A to D).

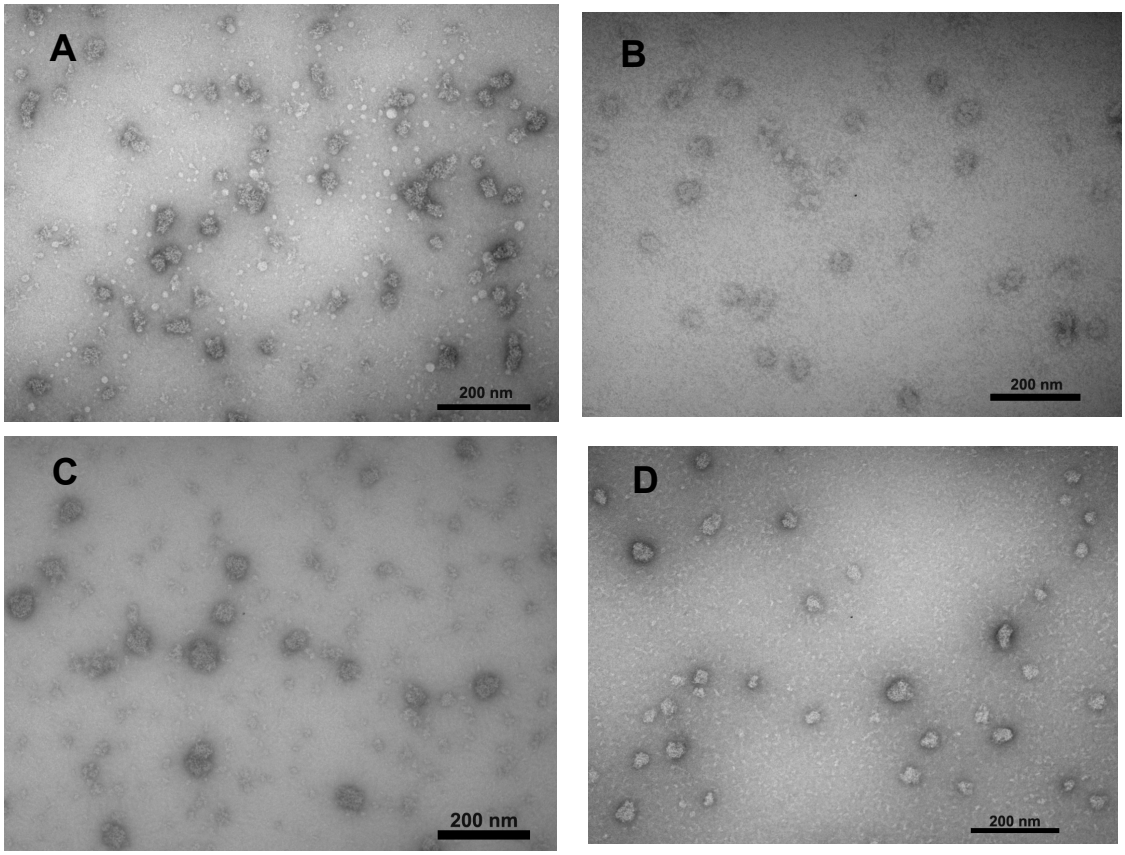

Figure 13. Electron micrographs of refolded UC1 to UC4 proteins. **A**, UC1; **B**, UC2; **C**, UC3; **D**, UC4. All the four proteins were refolded under reducing condition after denaturation (preparation 2) and finally studied in the buffer 20 mM Tris pH 8.0, 150 mM NaCl and 2 mM DTT. The pictures were prepared by negative staining with 2% uranyl acetate; the concentration of the protein was 50 µg/ml.

AUC results: The AUC results for uncleaved proteins are summarized in Table 5. The sedimentation equilibrium (SE) results for the UC1 to UC4 proteins refolded at pH 8.0, showed high molecular weight aggregates ranging from 17.3 MDa to 1.7 MDa.

For the UC1 protein refolded at pH 8.5, the SE results at lower speed (2800 rpm) showed molecular weight values ranging from 7.2 MDa to 611 kDa. The smallest molecular weight species 611 kDa corresponds to a molecular weight of 3 even units. At higher speed (4800 rpm), the smallest molecular weight species showed mixed population of molecular weight values 632 kDa (3 even units) and 756 kDa (3.6 even units). Therefore, the observed low molecular weight species can corresponds to icosahedral nanoparticles composed of 4 even units. This is supported by the EM picture of UC1 protein refolded at pH 8.5, where we observed icosahedral nanoparticles (Figure 12, C). The observed high molecular weight aggregates in all refolded proteins (UC1 to UC4) suggest the aggregating nature of the icosahedral nanoparticles.

BN-PAGE results: The BN-PAGE results for UC1, UC2 and UC4 proteins, showed no bands in the separating gel (5 - 12 % gradient gel) (Figure 9; lanes 1, 2, 5, 10). This shows that the loaded proteins got stuck in the stacking gel (4.5%). The reason could be aggregation of the icosahedral nanoparticles to high molecular weight aggregates. The aggregation behavior is also evident from AUC results (Table 5).

Table 5: AUC results for uncleaved proteins UC1 to UC4

Construct[#]	Concentration (mg/ml)	Rotor speed (rpm)	Sedimentation velocity ($S_{20,w}$)	Sedimentation Equilibrium MW (kDa)		
				Observed	No. of particles (60-mers)	Expected MW for an even unit (15-mers) & for a nanoparticle (60-mers)
UC1 refolded in pH 8.0 buffer	0.5	22000	74 S + 59 S + 52 S + 46 S	8199 + 5049 + 4078 + 2767 + 1791[$] (2800 rpm)	9.6 + 5.9 + 4.8 + 3.3 + 2.1	even unit - 212.7 nanoparticle - 850.9
UC1 refolded in pH 8.5 buffer	0.48	28000	56 S + 34 S + 28 S	7244 + 2682 + 2756 + 611 (3200 rpm)	8.5 + 3.2 + 3.2 + 3 even units	
		50000	7.8 S	632 + 756 (4800 rpm)	3 even units + 3.6 even units	
UC2 refolded in pH 8.0 buffer	0.19	16000	211 S + 138 S + 109 S + 57 S	13434 + 11263 + 4128 (2400 rpm)	15.8 + 13.2 + 4.9	even unit - 212.6 nanoparticle - 850.2
		48000	low S 1-2			
UC3 refolded in pH 8.0 buffer	0.27	16000	241 S + 157 S	17314 + 9379 + 7361 + 4240 (2400 rpm)	20.2 + 10.9 + 8.6 + 4.9	even unit - 214.7 nanoparticle - 858.9
		48000	no sedimentation			
UC4 refolded in pH 8.0 buffer	0.28	16000	194 S + 164 S + 194 S	16151 + 7509 + 4019 + 2331 (2400 rpm)	18.6 + 8.7 + 4.6 + 2.7	even unit - 216.9 nanoparticle - 867.5

All the constructs are refolded in reducing condition (preparation2) after denaturation up to 0 M urea and 2 mM DTT and analyzed in the buffer 20 mM Tris pH 8.0 or 8.5, 150 mM NaCl and 2 mM DTT.

$ Only small concentration which is not detected as a boundary in sedimentation velocity.

CD spectroscopy results for refolded proteins UC1 to UC4 and C1 to C4

We performed CD experiments in order to understand the secondary structural contents of the refolded samples, because the laminin and COMP domain in the refolded samples are well characterized α-helical coiled-coil proteins [5, 7, 8]. Also, the foldon domain is a well studied β-hairpin motif structure [4].

CD spectroscopy results for proteins UC1 to UC4

The uncleaved UC1 to UC4 samples showed a typical and similar α-helical spectrum (Figure 14, A to D; open circles). For uncleaved proteins UC1 to UC4, if both the laminin and COMP domain folds into an α-helical structure, the theoretical α-helical content will be: UC1, UC2 proteins - 61.4 %; UC3 protein- 60.5 %; UC4 protein - 59.5 %. The theoretical α-helical content is calculated using the formula: (number of amino acids from COMP domain (44)) + (number of amino acids from laminin domain (34) / (total number of amino acids). The calculated α-helical content values from CD spectra using CD Pro software (Table 6; indicated in red boxes) [Sreerama, N et al., 2000] are similar to the theoretically calculated values. Also, the theoretically calculated β-sheet content values (UC1 and UC2 - 7.9%; UC3 - 7.8% and UC4 - 7.6%) are similar to the calculated β-sheet content values from CD spectra (Table 6; indicated in pink boxes). The theoretical β sheet content is calculated using the formula: (number of amino acids contributing to β sheet structure in foldon domain (10))/ (total number of amino acids). The above results support the formed α-helical structures in both the laminin and COMP domain and the β-sheet structures in the foldon domain.

CD spectroscopy results for proteins C1 to C4

The CD spectrum of both preparation 1 (p1; closed circles) and preparation 2 (p2; open squares) refolded C1 to C4 proteins also showed a typical and similar α-helical spectrum (Figure 14, A to D). The cleaved proteins C1 to C4 showed a higher α-helical spectrum compared to the α-helical spectrum of UC1 to UC4 samples.

The α-helical content values calculated from CD spectra using CD Pro software (Table 6; cleaved samples C1 to C4) showed 8 to 10% higher α-helical content values compared to the theoretically calculated α-helical content values (C1, C2 constructs - 58.7 %; C3 construct - 57.1%; C4 construct - 55.7%). The theoretical α-helical content of C1 to C4 constructs is calculated using the formula: (number of amino acids from COMP domain (44)) / (total number of amino acids). The calculated β-sheet content values from the CD spectra of C1 to C4 samples (Table 6) showed ~ 6% less when compared to the theoretically calculated β-sheet content values (C1, C2 - 13.3%; C3 - 13%; C4 - 12.7%).

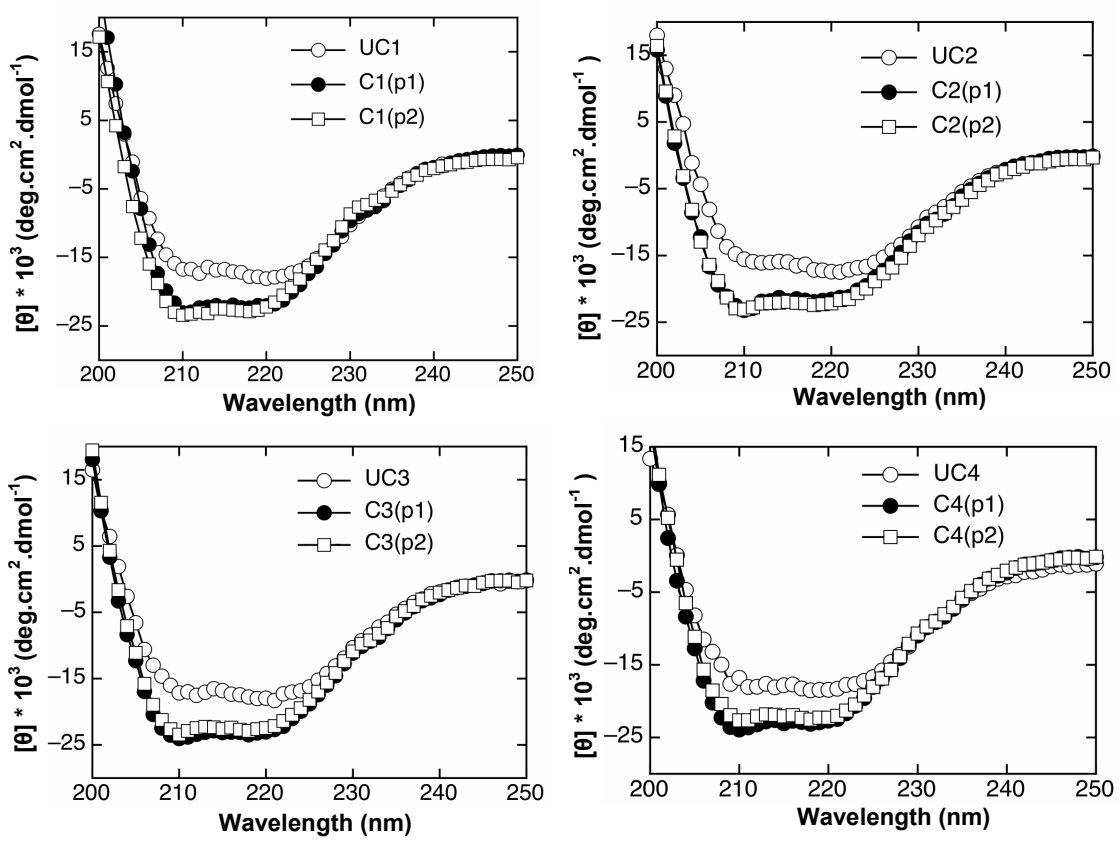

Figure 14. Far-UV Circular Dichroism (CD) analysis of uncleaved (UC1 to UC4) and cleaved (C1 to C4) samples. In **A**, **B**, **C** and **D**, open circles (○) represent the preparation 2 refolded CD spectrums of UC1, UC2, UC3 and UC4 samples, respectively; closed circles (●) represent the preparation 1 (p1) refolded CD spectrums of C1, C2, C3 and C4 samples, respectively; open squares (□) represent the preparation 2 (p2) refolded CD spectrums of C1, C2, C3 and C4 samples, respectively. UC1 to UC4 samples were studied in the buffer 20 mM Tris pH 8.0, 150 mM NaCl and 2 mM DTT. C1 to C4 samples were studied in the buffer 20 mM Tris pH 7.5, 150 mM NaCl. The protein concentration was always 0.1 mg/ml.

Table 6: Estimation of secondary structural contents from CD spectra using CD Pro software [9]. (http://lamar.colostate.edu/~sreeram/CDPro)

Secondary structures	CDPro analysis programs	Calculated secondary structures (%) from the CD spectra											
		uncleaved UC1#	cleaved C1&	cleaved C1$	uncleaved UC2#	cleaved C2&	cleaved C2$	uncleaved UC3#	cleaved C3&	cleaved C3$	uncleaved UC4#	cleaved C4&	cleaved C4$
α - helix	CDSSTR	55.7	68.3	63.1	55.4	74.1	70.9	55.4	74.6	68.5	56.4	74.1	67.1
	SELCON3	55.3	65.9	64.4	52.8	66	67.3	52.4	69.3	68.1	57.3	67.9	65.9
	CONTINLL	54.1	63.3	54.4	52.8	61.2	62.3	53	61.9	61.6	51.5	61.3	60.4
β - sheet	CDSSTR	12.5	9.8	14.3	10.7	6.7	9.2	10.5	10.1	10	15.4	8.5	10.5
	SELCON3	11	4.7	4.6	13.2	4.3	3.9	9.6	2.8	3.8	8.2	2.9	4.3
	CONTINLL	9.2	5.4	9.7	11.1	4.9	5.1	9.4	4.5	4.9	10.6	4.3	5.3
Turns (T)	CDSSTR	11.2	9.5	10.6	13.2	6.7	7.2	10.9	6.6	10.3	10.4	8.8	10.4
	SELCON3	15.3	11.2	11.7	16.1	11.7	11.4	14.2	10.5	11.1	12.6	10.4	12.1
	CONTINLL	13.6	10	14.5	14.4	12.1	11.9	14.7	12	12.6	14.5	12.6	13.3
Unordered (U)	CDSSTR	20.9	11.3	12	21.6	11.6	12.7	22.9	8.4	10.2	17.7	9.1	11.2
	SELCON3	21.3	20.5	20.6	16.9	20.9	19.7	24.2	18.8	19	24.4	18.8	20.4
	CONTINLL	23.1	21.3	21.4	21.8	21.8	20.8	23	21.6	20.9	23.4	21.8	21

- uncleaved proteins UC1 to UC4, refolded in reducing condition after denaturation up to 0 M urea buffer containing 2 mM DTT and analyzed in the buffer 20 mM Tris pH 8.0, 150 mM NaCl and 2 mM DTT.

& - cleaved proteins C1 to C4, refolded completely in oxidizing condition after denaturation (preparation 1).

$ - cleaved proteins C1 to C4, refolded in reducing condition up to 0 M urea and then to oxidizing condition (preparation 2).

Discussion

For the sake of simplicity, the cysteine in the foldon domain will be called 1 and the two cysteines at the C-terminus of COMP domain will be called 2 and 3, in order to explain the different combinations of intra- and intermolecular disulfide bridges that could form during preparation 1 and preparation 2 refolding conditions.

Cleaved proteins C1 to C4

The cleaved proteins C1 to C4 (Figure 2, A) was rationally designed so as to form nanoparticles of regular icosahedral symmetry, consisting of 60 monomeric building blocks. Computer modeling predicted that such particles would each have a diameter of about 17 nm (Figure 1, B). The observed oligomeric forms of these proteins after refolding under preparation 1 and preparation 2 conditions are discussed in the following sections.

Self-assembly result of protein C1

The pentameric coiled-coil domain of COMP is known to form very stable oligomers [10]. During refolding out of 8 M urea, the coiled-coil domain of COMP will already form in urea concentrations that are moderately high. Formation of helices within the COMP domain will bring the two cysteines of the COMP domain (2 and 3) in close contact. Under oxidizing conditions with low protein concentration (preparation 1) intramolecular disulfide bridge formation will then immediately and predominantly occur. Therefore, the pentamers observed in the preparation 1 refolded sample of C1 (Figure 9; lane 3) (Table 1) suggest the folded COMP domain with the intramolecular disulfide bridges (2-3). During preparation 2 refolding, there is no possibility of forming either intra- or intermolecular disulfide bridges because of its reducing condition refolding up to 0 M urea. As a result, the cysteine residues will be in reduced state up to 0 M urea, however, upon proceeding to oxidizing condition (0 M urea and no DTT), they will form disulfide bridges. Therefore, the pentamers and decamers observed in preparation 2 refolded samples (0 M urea and no DTT) (Figure 9; lane 4) can be the intramolecular disulfide linked pentamers (2-3) and two pentamers linked through intermolecular disulfide bridges (either 2-2, 2-3 or 3-3) (Table 7), respectively.

The observed pentamers and decamers for C1 protein suggest that the trimeric foldon domain is not folded in these structures. Because, if the trimeric foldon domain folds along with the pentameric COMP domain they will assemble into 'even units' (15-mers) (Figure 4). In addition, it seems that the folding rate of pentamer domain is faster than the trimer domain, as this will inhibit the folding of trimer domain. Schematic models of a pentamer and a decamer are shown in Figure 15, B and C, respectively.

Table 7. Data depicting the cysteine (C) amino acid residue numbers and their possible type of disulfide bridges that can form during step-wise dialysis from 8 M to 0 M urea (preparation 1 and preparation 2).

Type of disulfide bridge	Constructs	Residue number*
Intramolecular£	Uncleaved protein UC1 Cleaved protein C1	2-3
	Uncleaved proteins UC2, UC3 and UC4 Cleaved proteins C2, C3 and C4	1-2; 1-3; 2-3
Intermolecular€ and Interparticle$	Uncleaved protein UC1 Cleaved protein C1	2-2; 2-3; 3-3
	Uncleaved proteins UC2, UC3 and UC4 Cleaved proteins C2, C3 and C4	1-1; 1-2; 1-3 2-2; 2-3; 3-3

* - cysteine amino acid in the foldon domain is denoted as 1 and the two cysteine amino acids at the C-terminus of COMP domain is denoted as 2 and 3.

£ - within a peptide or protein chain

€ - between the peptide or protein chain

$ - between the nanoparticles.

Self-assembly result of proteins C2, C3 and C4

For proteins C2, C3 and C4, the even units observed in both preparation 1 and preparation 2 refolding conditions (Figure 9; lanes 6, 7, 8, 9, 11 and 12), are evidence of the properly folded COMP and the foldon domain. In addition, the observed even units support properly formed intermolecular disulfide bridges between the monomeric chains of foldon domain (1-1) and between the monomeric chains of COMP domain (2-3). A schematic model of an even unit is shown in Figure 15, D.

C2, C3 and C4 proteins have an additional cysteine residue in the foldon domain (1) in addition to the two cysteines in the COMP domain (2 and 3) (for sequence details see Figure 2, B). During refolding out of 8 M urea under oxidizing conditions (preparation 1) if the unfolded monomeric chains form either 1-2 or 1-3 intramolecular disulfide bridges, it will lead to formation of pentamers or trimers. Therefore, the trimers observed in preparation 1 refolded samples of C2, C3 and C4 (Figure 9; lane 6, 8 and 11) support the folded foldon domain with 1-2 or 1-3 intramolecular disulfide bridges. During reducing condition refolding up to 0 M urea (preparation 2), the formation of 1-2 or 1-3 intramolecular disulfide bridges is not possible, as this is supported by the absence of trimers in preparation 2 refolded samples of C2, C3 and C4 proteins (Figure 9; lane 7, 9 and 12). A schematic model of a trimer is shown in Figure 15, A. The observation of trimers and even units in the refolded samples of C2, C3 and C4 proteins and not in the refolded samples of C1 protein, support the folded trimeric foldon domain. Therefore, for proteins C2, C3 and C4 the mutation of Asp (D) to Cys (C) (for sequence details see Figure 2, B) in the foldon domain seems to stabilize the foldon domain in terms of its folding property.

Also, BN-PAGE result (Figure 9) for proteins C2, C3 and C4 refolded under both preparation 1 (lanes 6, 8 and 11) and preparation 2 conditions (lanes 7, 9 and 12) showed 20-mers. AUC result for proteins C2, C3 and C4 suggest the higher order oligomers (more than 15-mers) could be a mixture of 20-mers and 30-mers (see Table 2, 3 and 4). The observation of 20-mers suggests the linked even units and pentamers through intermolecular disulfide bridges. A schematic model of 20-mers is shown in Figure 15, E. Furthermore, the observed pentamers in both the refolding conditions for proteins C1 to C4 suggests it as a common ‘intermediate form’ during the refolding process.

For proteins with extended linkers C3 (four residues) and C4 (six residues) there is no significant observation regarding assembly when compared to the proteins with two residues of linker region C1 and C2 (see Figure 9). This suggests that for proteins C3 and C4, the increased linker size does not help the observed even units to assemble further into icosahedral nanoparticles.

The even units observed in proteins C2, C3 and C4 support our design principles (Figure 4). Even units are nanoparticles but not with icosahedral symmetry. But, the observed even units failed to associate further into icosahedral nanoparticles (see EM pictures of Figure 10, C and D and Figure 11).

Uncleaved proteins UC1 to UC4

The preparation 2 refolded proteins UC1 to UC4 were observed to form icosahedral nanoparticles (see EM pictures of Figure 13). The observation of icosahedral nanoparticles in uncleaved proteins UC1 to UC4 can be explained on the basis of domain architecture. The domain architecture of uncleaved proteins comprises a 34 amino acid N-terminal laminin domain followed by the foldon and the COMP domain (refer to Figure 2, A). The laminin domain was derived from the C-terminal region of laminin β-chain of mouse (1750-1784 amino acids) and from the literature this region was known to be α-helical region with a heptad repeat pattern characteristic of coiled-coils [8, 11]. In our study, the formation of α-helical structures in the laminin domain of the uncleaved proteins was supported by the α-helical content values calculated from the CD spectra of these proteins (refer to results section of CD spectroscopy).

Kammerer, R et al. [12] showed using AUC technique that the laminin β-chain of residues 1700-1786, tends to associate into trimers. This study includes the laminin domain residues of uncleaved proteins. Therefore, the laminin domain in the uncleaved proteins, based on its α-helical structure with the heptad repeat pattern and the likely trimeric form suggest it as a trimeric coiled-coil structure. In addition, the trimerization potential of foldon domain [13, 14] will also influence the formation of trimeric coiled-coil structure in the laminin domain. Hence, the monomeric chain comprising the laminin domain together with the foldon domain as a trimeric oligomerization domain connected to the pentameric oligomerization domain of COMP (Figure 16), mimics the design principles of our structure based designed peptide which was shown to form regular icosahedral nanoparticles (chapter 1).

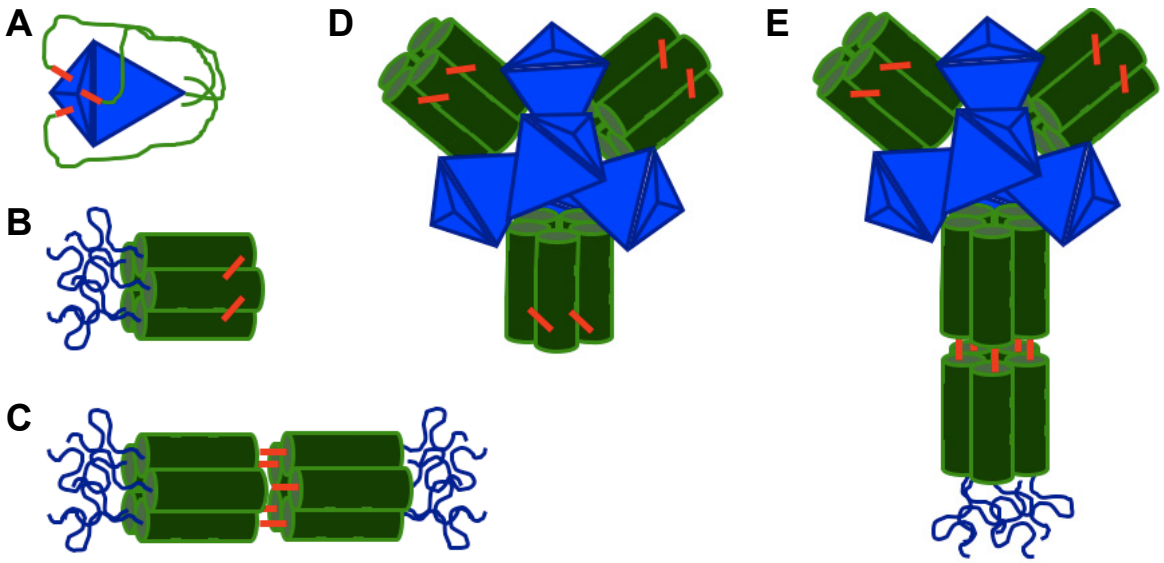

Figure 15. Proposed schematic models for observed oligomers of proteins C1 to C4. **A**, trimer with intramolecular disulfide bridge (either 1-2 or 1-3). **B**, pentamer with intramolecular disulfide bridge (2-3). **C**, two pentamers of **B** linked through intermolecular disulfide bridge. **D**, even unit with properly formed intermolecular disulfide bridge between the monomeric chains of foldon domain (1-1) and between the monomeric chains of COMP domain (2-3). **E**, Even unit of **D** linked to pentamer of **B** through intermolecular disulfide bridge. In all the models, the blue and green represent the foldon domain and the COMP domain, respectively. Red line represents the disulfide bridge.

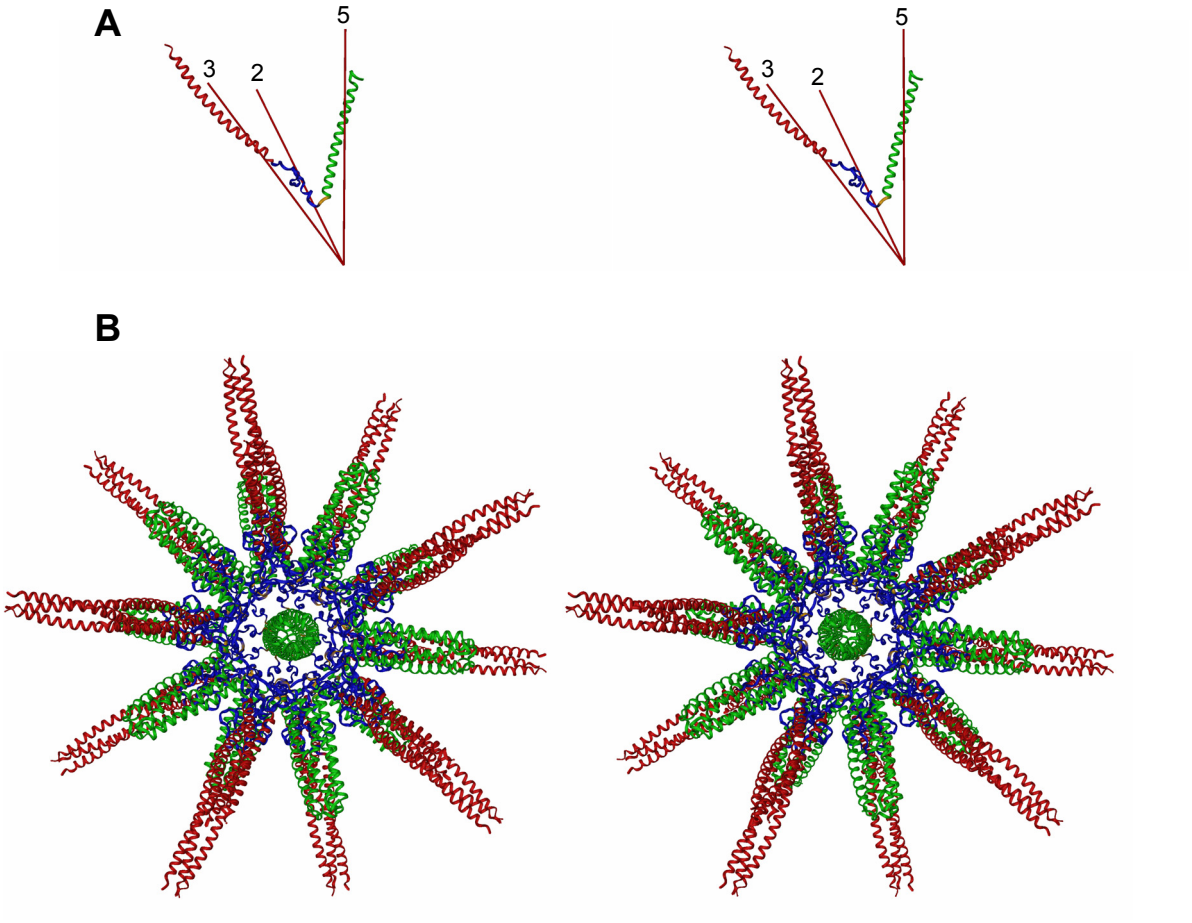

Figure 16. **A**, the laminin domain (red) along with the foldon domain (blue) forms the trimeric oligomerization domain and it is connected to the pentameric oligomerization domain of COMP (green) as a single chain. The two different oligomerization domains are shown along their respective symmetry axis of the icosahedron. The three symmetry axes (5, 3 and 2) extending from the center of the icosahedron are shown as red lines. **B**, applying the symmetry elements to the monomeric chain of section **A** generates an artificial nanoparticle with icosahedral symmetry. The view is down the five-fold symmetry axis.

Materials and Methods

Reagents and Enzymes

All enzymes were purchased from BioConcept – New England Biolabs (Allschwil, Switzerland) and chemicals from Sigma, Applichem and Bio-Rad unless stated otherwise. They were used according to the manufacturer's instructions. All oligonucleotides (Table 8) were synthesized by Microsynth AG (Balgach, Switzerland). Oligonucleotides had 5' phosphate and were quality assured by PAGE purification.

Bacterial strains and plasmids

Escherichia coli DH5 α cells (Invitrogen, USA) and BL21 (DE3) pLysS cells (Novagen, USA) were used as the cloning and expression host cells, respectively. For our expression studies, we have used prokaryotic expression vector pPEP-T [15, 16].

Molecular biology of designed constructs

The constructs used in this study are depicted in Figure 2, A. The cloning strategy of these constructs was done as follows:

Oligonucleotide fragment assembly

All the oligonucleotides (both forward and reverse strand) (Table 8) of UC1 to UC4 constructs were dissolved in MilliQ water to a concentration of 100 μM. The forward and reverse strand of each oligonucleotide were combined in 1 μM concentration and 5 μl of 20X SSC buffer (30 mM sodium citrate dihydrate pH 7.0 and 300 mM NaCl for 100 ml) and water were added to give 50 μl. Annealing reaction was done in a thermocycler by first incubating at 90°C for 1 min followed by 70°C for 1 min and then cooling at 1°/15 sec to 20°C (T*personal*, Biometra, UK) to give the annealed product. The annealed products were desalted using Micro Bio-Spin P-30 columns as per the manufacturers protocol (Bio-Rad, USA) and then checked in 4% NuSieve GTG-Agarose (Cambrex Bio Science, USA) to confirm the annealing reaction. Annealed products were stored at -20°C until required.

Table 8: Oligonucleotides of UC1 to UC4 constructs

Constructs	Oligonucleotide sequences
UC1	fragment 1 (forward & reverse strand) (P) 5' GATCCGGTTACATCCCGGAAGCTCCGCGTGACGGTCAGGCATACGTTCGTAAAGACG 3' (P) 5' TTCACCGTCTTTACGAACGTATGCCTGACCGTCACGCGGAGCTTCCGGGATGTAACCG 3' fragment 2 (forward & reverse strand) (P) 5' GTGAATGGGTTCTGCTGTCCACCTTCCTGGGTGGTCTGGCTCCGCAGATGCTGCGTGAAC 3' (P) 5' CTGCAGTTCACGCAGCATCTGCGGAGCCAGACCACCCAGGAAGGTGGACAGCAGAACCCA 3' fragment 3 (forward & reverse strand) (P) 5' TGCAGGAAACCAACGCTGCTCTGCAGGACGTTCGTGAACTGCTGCGTCAGCAGGTTAAAC 3' (P) 5' GATCTGTTTAACCTGCTGACGCAGCAGTTCACGAACGTCCTGCAGAGCAGCGTTGGTTTC 3' fragment 4 (forward & reverse strand) (P) 5' AGATCACCTTCCTGAAAAACACCGTTATGGAATGCGACGCTTGCGGTTGATAAG 3' (P) 5' AATTCTTATCAACCGCAAGCGTCGCATTCCATAACGGTGTTTTTCAGGAAGGT 3'
UC2	fragment 1_1 (forward & reverse strand) (P) 5' GATCCGGTTACATCCCGGAAGCTCCGCGTTGCGGTCAGGCATACGTTCGTAAAGACG 3' (P) 5' TTCACCGTCTTTACGAACGTATGCCTGACCGCAACGCGGAGCTTCCGGGATGTAACCG 3'
UC3	fragment 2_1 (forward & reverse strand) (P) 5' GTGAATGGGTTCTGCTGTCCACCTTCCTGGGTGGTTCGGGTCTGGCTCCGCAGATGCTGCGTGAAC 3' (P) 5' CTGCAGTTCACGCAGCATCTGCGGAGCCAGACCCGAACCACCCAGGAAGGTGGACAGCAGAACCCA 3'
UC4	fragment 2_2 (forward & reverse strand) (P) 5' GTGAATGGGTTCTGCTGTCCACCTTCCTGGGTGGTTCGGGTTCGGGTCTGGCTCCGCAGATGCTGCGTGAAC 3' (P) 5' CTGCAGTTCACGCAGCATCTGCGGAGCCAGACCCGAACCCGAACCACCCAGGAAGGTGGACAGCAGAACCCA 3'

(P) - 5' phosphorylation; all the oligonucleotide pairs (forward and reverse strand) were underlined for their complementary regions.

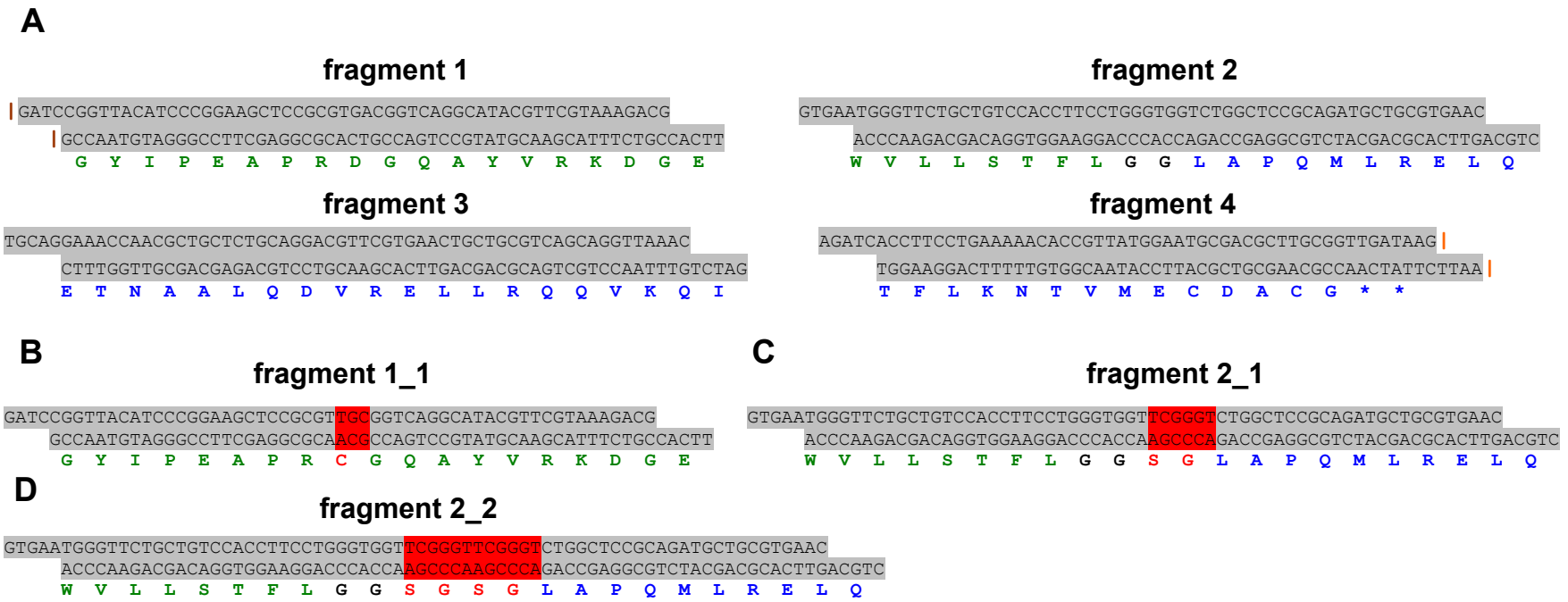

Figure 17. **A**, fragments 1 to 4 (sequential order) which have the overlapping bases at their ends constitute the UC1 construct. Fragment 1 has pre cut BamHI restriction site (marked in brown colored solid line) and fragment 4 has pre cut EcoRI restriction site (marked in orange colored solid line). Below each fragment their corresponding amino acid sequences were highlighted (bold colored letters). Green colored bold letters, correspond to the foldon domain of the T4 phage fibritin protein followed by two glycine residues (bold black color) as the linker which were then linked to the blue colored bold letters correspond to COMP (Cartilage Oligomeric Matrix Protein) domain. ***** denotes stop codons. **B**, fragment 1_1 which has the aspartic acid (D) to cysteine (C) mutation (highlighted in red color) along with the fragment 2, 3 and 4 constitutes the UC2 construct. **C**, Fragment 2_1 which has two extra glycine residues (highlighted in red color) as linker was inserted in between fragment 1_1 and fragment 3 which was then followed by fragment 4 constitutes the UC3 construct. **D**, fragment 2_2 which has two more extra glycine residues (highlighted in red color) as linker was inserted in between fragment 1_1 and fragment 3 which was then followed by fragment 4 constitutes the UC4 construct.

Preparation of pPEP-T-UC1, UC2, UC3 and UC4 constructs

The annealed oligonuclotides and their involvement in the construct deign of UC1 to UC4 constructs were depicted in the Figure 17. For the cloning of UC1 to UC4 DNA fragments in to pPEP-T vector, the vector DNA was prepared as follows: 1 µg of pPEP-T vector, 1 µl of 10X NEBuffer EcoRI (10 mM Tris pH 7.9, 10 mM $MgCl_2$, 50 mM NaCl and 1 mM DTT), 1 µl of 10X BSA, 1 units of EcoRI and BamHI enzyme and water up to 10 µl were combined and incubated at 37°C for 3 hrs. Double digested vector was recovered using QIAquick Gel Extraction Kit (Qiagen, Switzerland) from a 1% agarose gel. After gel extraction, the digested vector ends were dephosphorylated by adding 1 unit of shrimp alkaline phosphatase (Promega, USA) and 1 µl of 10X SAP reaction buffer (50 mM Tris pH 9.0, 10mM $Mgcl_2$) to a final volume of 10 µl, followed by incubation at 37°C for 15 min, then heat inactivation (15 min, 65°C). Dephosphorylated plasmid DNA was ligated to the fragments that corresponds to the respective constructs UC1 to UC4 as follows: Equimolar concentration of assembled oligonuclotide fragments (vector to insert ratio 1:3), 100 ng of dephosphorylated plasmid DNA and water were added and incubated at 45°C for 5 min. Finally, the reaction mixture was cooled in ice and 1 µl of 10X T4 DNA ligase buffer (50 mM Tris pH 7.5, 10 mM $MgCl_2$, 10 mM DTT, 1 mM ATP, 25 µg/ml BSA) along with 1 unit of T4 DNA ligase was added and incubated at 16°C overnight.

Transformation

Five µl of ligated mixture was added to 100 µl of DH5α competent cells and was incubated on ice for 30 min, heat shocked for 90 sec at 42°C, and incubated on ice for further 2 min. Then, 0.9 ml of LB medium was added and incubated at 37°C for 1h with shaking at 225 rpm. Followed by centrifugation of cells at 7000 rpm, 5 min and the pelleted cells were kept in 100µl of LB and the remaining LB was thrown out. The cells were mixed with the LB by gentle tapping and the mixture was plated on LB-agar plates (ampicillin 100 µg/ml) and incubated overnight at 37°C.

Putative positive colonies were picked from plates and placed in a 3 ml LB-ampicillin (100 µg/ml) broth and grown overnight at 37°C with shaking at 180 rpm.

Plasmid mini prep was done from the cultures using QIAprep spin mini prep kit (Qiagen, Switzerland) and the obtained plasmid DNA was subjected to enzymatic digestion with BamHI and EcoRI enzyme to verify the presence of the insert in the transformed bacterial colonies. Products were analyzed by 2% gel electrophoresis. DNA sequencing (Microsynth AG, Balgach, Switzerland) was done to verify the putative positive clones using primers of T7 promoter and terminator sequence.

Protein expression & Purification

Protein expression

For UC1 to UC4 constructs (Figure 2, A), we followed the same protocol for protein expression. The sequence verified positive clones were transformed into *E.coli* strain BL21 (DE3) pLysS cells as described in section 3.3.3. The transformed cells were plated on ampicillin (100 μg/ml) and chloramphenicol (30 μg/ml) LB agar plates and incubated at 37°C overnight. A single colony from the plate was inoculated in 50 ml LB broth with ampicillin (200 μg/ml) and chloramphenicol (30 μg/ml) and grown overnight at 28°C with shaking at 180 rpm. 1% of the overnight grown culture was inoculated into 3 liters of LB with ampicillin (200 μg/ml) and chloramphenicol (30 μg/ml) and incubated at 37°C with shaking at 180 rpm. Protein expression was induced when the cell density at OD_{600nm} reached 0.5 by adding IPTG to a final concentration of 1 mM. After induction at 37°C for 3 hr, the cell pellet was collected by centrifugation at 6000 g for 20 min at 4°C (Sorvall, GSA rotor) and frozen at -80°C until further use. The physicochemical properties of the expressed proteins UC1 to UC4 were outlined in Table 9 along with the thrombin cleaved counterparts of UC1 to UC4 proteins (C1 to C4).

Protein purification under denaturing conditions using nickel-column affinity chromatography

Purification principle: The purification procedure was carried out by exploiting the pKa of histidine residues in the 6xHis tag. The histidine residues in the 6xHis tag will have a pKa of approximately at pH 6.0 and at high pH (8.0), it will be uncharged and the imidazole ring of histidine residues binds to the Ni^{2+}-NTA resin.

But at acidic pH (pH 5.9 and 4.5), the imidazole ring of histidine residues will get protonated and under these conditions the 6xHis-tagged proteins can no longer bind to the nickel ions and will dissociate from the Ni^{2+}-NTA resin. During the elution process, monomers generally elute at approximately pH 5.9, whereas aggregates and proteins that contain more than one 6xHis tag elute at approximately pH 4.5.

Methodology: Following expression, bacterial pellets (from 3 liter culture) were thawed on ice and to each gram of pellet (wet weight) 3 ml of lysis buffer pH 8.0 (8 M Urea, 10 mM Tris, 100 mM NaH_2PO_4) was added along with 10 mM β-mercaptoethanol. Pellets were thoroughly resuspended in lysis buffer and sonicated on ice for 5 min (4 sec of sonication and 6 sec of gap) followed by centrifugation at 16000 rpm at 4°C for 45 min to recover the supernatant from the cell debris. The resultant supernatant was mixed with Ni^{2+}-NTA slurry (Qiagen, Switzerland) and the amount of nickel resin was determined by the level of protein expression (usually 1 ml of resin can bind up to 10 to 15 mg of protein) and it has to be optimized. The mixture was then gently mixed for 1 hr at room temperature (batch method).

Table 9: Physico-chemical properties of UC1 to UC4 (uncleaved) and C1 to C4 (cleaved) proteins#

Constructs	Molecular weight (Daltons)	Number of amino acids	Isoelectric point (pI)	Extinction coefficient (M^{-1} cm^{-1})
UC1	14182.1	127	6.29	11585 (1 g/l=0.817)
C1	8368.5	75	4.93	8605 (1 g/l=1.028)
UC2	14170.2	127	6.58	11585 (1 g/l=0.818)
C2	8356.6	75	5.26	8605 (1 g/l=1.030)
UC3	14314.3	129	6.58	11585 (1 g/l=0.809)
C3	8500.7	77	5.26	8605 (1 g/l=1.012)
UC4	14458.4	131	6.58	11585 (1 g/l=0.801)
C4	8644.8	79	5.26	8605 (1 g/l=0.995)

All the properties were calculated using the online tool PROTPARAM from the expasy server (http://www.expasy.org/tools/protparam.html) [17].

After the incubation, the lysate and the Ni-NTA slurry were loaded on the econo column (Bio-Rad, USA) and the resultant flow through was collected for analysis.

Then the column matrix was subjected to two separate wash steps: one with lysis buffer pH 8.0 and second one with wash buffer 1 pH 6.3 (8 M Urea, 10 mM Tris, 100 mM NaH_2PO_4) along with 10 mM β-mercaptoethanol. Finally, the protein elution was performed using elution buffer 1 pH 5.9 (8 M Urea, 10 mM Tris, 100 mM NaH_2PO_4) and elution buffer 2 pH 4.5 (8 M Urea, 10 mM Tris, 100 mM NaH_2PO_4) along with 10 mM β-mercaptoethanol.

Thrombin cleavage and purification of cleaved products

The eluted constructs were dialyzed against the thrombin cleavage buffer 20 mM Tris pH 8.4, 150 mM NaCl and 2.5 mM $CaCl_2$. The dialysis was performed in a step-wise manner from 8 M Urea to 6 M followed by 4 M and 2 M and finally to 0 M urea. For cleavage reactions, 1 U of human plasma thrombin (Sigma, USA) was used per mg of protein and the reactions were carried out at room temperature for 16 to 18 hrs with gentle shaking or sometimes for 24 hrs.

The resultant digested samples were purified as follows: Initially the digested samples were mixed with Ni^{2+}-NTA slurry and the amount of nickel slurry that was used depending on the amount of protein used for cleavage (1 ml of nickel slurry can bind up to 10 to 15 mg of protein). The mixture was then incubated at room temperature with gentle shaking for 1hr (batch method). Followed by packing of mixture on the econo columns and the resultant flow through fractions were collected to analyze for the presence of cleaved constructs C1 to C4 (Figure 3, A). The bound uncleaved samples were eluted using the same elution buffer 1 and 2 as mentioned in the section ‘Protein purification’.

Analysis of purified samples

SDS-PAGE

Standard SDS-PAGE was performed [18] using Bio-Rad mini gel apparatus (Bio-Rad, USA). 15% and 17% SDS-PAGE were run to analyze the purified samples of UC1 to UC4 and C1 to C4 proteins, respectively. The protein samples were mixed with 1X sample buffer (45 mM Tris pH 6.8, 10% glycerol, 1% SDS, 0.01% bromophenol blue and 50 mM DTT) before loading on SDS-PAGE. After the run, protein bands were visualized using Coomassie Brilliant blue R-250 (Bio-Rad, USA).

Western blot

Electrophoretic transfer of proteins from polyacrylamide gels to nitrocellulose membrane was done as described in the literature [19, 20].

We used 0.2 μm size nitrocellulose membrane (Sigma, USA) and Bio-Rad Mini-PROTEAN 2 Electrophoresis / Mini Trans-Blot Module for the transfer process. The transfer was carried out in the presence of blotting buffer (20 mM Tris buffer pH 8.3, 150 mM glycine and 20% methanol) at 100V, 4°C for 1 hour. Immunological detection of proteins was carried out as follows: The electroblotted nitrocellulose membrane was transferred to TTBS buffer (20 mM Tris pH 7.4, 150 mM NaCl, 0.1 (v/v) Tween 20) containing 5% (W/V) dry skim milk powder to prevent non-specific binding of primary antibody and incubated for 1 hour at room with gentle shaking. Subsequently, the nitrocellulose membrane was transferred to a fresh solution of TTBS buffer containing 5% (W/V) milk powder and the monoclonal antibody (1: 3000 dilutions) raised in mouse against the polyhistidine tag (Sigma) and incubated for 1 hour at room temperature with gentle shaking. The nitrocellulose membrane was then transferred to a fresh TTBS solution without milk powder and incubated for 10 minutes with gentle shaking. This procedure was repeated four times (wash step). After the wash step, the nitrocellulose membrane was transferred to a fresh solution of TTBS buffer containing 5% (W/V) milk powder and the anti-mouse IgG (Fc specific) antibody (1:5000 dilutions) raised in goat and conjugated to horseradish-peroxidase enzyme (Sigma) and incubated for 1 hour at room temperature with gentle shaking. Again, the membrane was washed extensively in TTBS buffer as described before (second wash step).

The second time washed nitrocellulose membrane was incubated in ECL western blotting detection reagents according to the manufacturers protocol (Amersham Biosciences). The nitrocellulose membrane was subsequently exposed to Kodak X-OMAT XAR-5 radiography film (Sigma) for 15 seconds to 30 minutes, until the positive bands were visualized by enhanced chemiluminescence.

Estimation of protein concentration

For all the samples, protein concentrations were calculated using the absorbance value at 280 nm with extinction coefficient (M^{-1} cm^{-1}) and molecular weight (Daltons) of the protein.

Extinction coefficient and the molecular weight of the proteins was calculated using ProtParam tool (http://www.expasy.ch/tools/protparam.html) [17]. For protein concentration measurements, we have also used the dye binding method [21] using Bio-Rad Bradford assay reagent with BSA as the standard.

Refolding conditions

The protein refolding procedure was carried out using two different refolding regimes.

Preparation 1 (denaturation, renaturation under oxidizing conditions)

The purified protein in denaturing conditions was refolded by step wise dialysis procedure. Initially, the denatured protein was dialyzed against the buffer 20 mM Tris pH 7.5, 150 mM NaCl containing 8 M urea followed by 6 M urea, 4 M urea, 2 M urea and no urea in the same buffer as above. Finally, the protein was concentrated to the required concentration for further characterization in the buffer 20 mM Tris pH 7.5, 150 mM NaCl.

Preparation 2 (denaturation, renaturation under reducing conditions)

In this condition also the step wise dialysis procedure was followed. Initially, the protein was dialyzed against the buffer 20 mM Tris pH 7.5, 150 mM NaCl and 2 mM DTT containing 8 M urea followed by 6 M urea, 4 M urea, 2 M urea and no urea in the same buffer as above. Finally, the protein was dialyzed against the buffer 20 mM Tris base pH 7.5, 150 mM NaCl at pH 7.5 to remove DTT and concentrated to required concentration for further characterization in the same buffer.

During refolding in both the conditions, the protein concentration was kept at a concentration of 0.1 mg/ml.

Analytical Ultracentrifugation

Analytical ultracentrifugation (AUC) was carried out on an Optima XL-A analytical ultracentrifuge (Beckman Instruments, Palo Alto, CA) equipped with a 12-mm Epon double-sector cell in an An-60 Ti rotor.

Sedimentation equilibrium runs were performed at 20°C at rotor speeds of 12,000 to 18,000 rpm and protein concentrations of 0.1 to 0.5 mg/ml. Average molecular masses were evaluated by using a floating base-line computer program SEGAL that adjusts the baseline absorbance to obtain the best linear fit of ln (absorbance) versus the square of the radial distance [22]. A partial specific volume ($\bar{\nu}$) of 0.73 mL/g and a buffer density (ρ) of 1.005 g/mL was used. The formula that the SEGAL program uses to calculate the molecular mass (M) of the sample was given below:

$$M = 2RT/ (1-\bar{\nu}\rho)\ \omega 2 * d (\ln c)/d (r^2)$$ **Equation 1**

Where R is Gas constant and T is the absolute temperature. ω is angular velocity, c is concentration (g/L) and r is radial distance from the axis of rotation. All the AUC measurements were performed at the AUC facility in the Biozentrum by Ariel Lustig (http://www2.biozentrum.unibas.ch/auc/).

Electron Microscopy

Protein samples were prepared for electron microscopy (EM) by negative staining with 2 % uranyl acetate and at a protein concentration of 50 or 100 µg/ml. They were analyzed and photographed on a Philips Morgagni 268D model transmission electron microscope with an acceleration voltage of 80 kV. Electron microscopy analysis was performed by Vesna Olivieri in Microscopy center, Pharmazentrum, University of Basel and also by Dr. Gia Machaidze in Professor Ueli Aebi group, M.E. Muller Institute, University of Basel.

Circular Dichroism (CD) measurements

The CD measurements were acquired on an Aviv 62A DS spectropolarimeter. The far-ultraviolet spectra (200-250 nm) were measured in a 1 mm path-length quartz cell at 4°C. The spectra were normalized for concentration and path length to obtain the mean molar residue ellipticity (θ, theta) after subtraction of the buffer contribution.

The following formula was used to calculate the concentration independent theta (θ) values (deg cm^2 $dmol^{-1}$): **θ (observed) * MRW / [10 * path length (cm) * concentration (mg/ml)]**, where MRW - mean residue weight (molecular mass of the peptide or protein divided by number of amino acids).

Data analysis and the wavelength scan plots were performed with the pro Fit software package (QuantumSoft, Switzerland).

Blue-Native PAGE (BN-PAGE) electrophoresis

For all the samples, 15 µg of protein per gel lane was resuspended in the buffer composed of 50 mM Bistris-HCl pH 7.0, 500 mM 6-aminocaproic acid and 50% glycerol. Samples were resolved on 5-12% gradient acrylamide gel overnight at 100 V; anode buffer composition 50 mM Bistris-HCl pH 7.0; cathode buffer contained 50 mM Tricine, 15 mM Bistris-HCl pH 7.0 with 0.005% Coomassie G250 (Bio-Rad, USA) [23]. High molecular weight standards for native gel electrophoresis (Amersham Biosciences, USA) were stained with Coomassie R250 (Bio-Rad, USA).

References

1. Burkhard, P., Stetefeld, J., and Strelkov, S.V. (2001). Coiled coils: a highly versatile protein folding motif. Trends Cell Biol *11*, 82-88.
2. Delahay, R.M., and Frankel, G. (2002). Coiled-coil proteins associated with type III secretion systems: a versatile domain revisited. Mol Microbiol *45*, 905-916.
3. McAlinden, A., Smith, T.A., Sandell, L.J., Ficheux, D., Parry, D.A., and Hulmes, D.J. (2003). Alpha-helical coiled-coil oligomerization domains are almost ubiquitous in the collagen superfamily. J Biol Chem *278*, 42200-42207.
4. Tao, Y., Strelkov, S.V., Mesyanzhinov, V.V., and Rossmann, M.G. (1997). Structure of bacteriophage T4 fibritin: a segmented coiled coil and the role of the C-terminal domain. Structure *5*, 789-798.
5. Malashkevich, V.N., Kammerer, R.A., Efimov, V.P., Schulthess, T., and Engel, J. (1996). The crystal structure of a five-stranded coiled coil in COMP: a prototype ion channel? Science *274*, 761-765.
6. Sanner, M.F., Stolz, M., Burkhard, P., Kong, X.P., Min, G., Sun, T.T., Driamov, S., Aebi, U., and Stoffler, D. (2005). Visualizing Nature at Work from the Nano to the Macro Scale. NanoBiotechnology *1*, 7-21.
7. Barlow, D.P., Green, N.M., Kurkinen, M., and Hogan, B.L. (1984). Sequencing of laminin B chain cDNAs reveals C-terminal regions of coiled-coil alpha-helix. Embo J *3*, 2355-2362.
8. Sasaki, M., Kato, S., Kohno, K., Martin, G.R., and Yamada, Y. (1987). Sequence of the cDNA encoding the laminin B1 chain reveals a multidomain protein containing cysteine-rich repeats. Proc Natl Acad Sci U S A *84*, 935-939.
9. Sreerama, N., and Woody, R.W. (2000). Estimation of protein secondary structure from circular dichroism spectra: comparison of CONTIN, SELCON, and CDSSTR methods with an expanded reference set. Anal Biochem *287*, 252-260.
10. Guo, Y., Kammerer, R.A., and Engel, J. (2000). The unusually stable coiled-coil domain of COMP exhibits cold and heat denaturation in 4-6 M guanidinium chloride. Biophys Chem *85*, 179-186.

11. Paulsson, M., Deutzmann, R., Timpl, R., Dalzoppo, D., Odermatt, E., and Engel, J. (1985). Evidence for coiled-coil alpha-helical regions in the long arm of laminin. Embo J *4*, 309-316.
12. Kammerer, R.A., Antonsson, P., Schulthess, T., Fauser, C., and Engel, J. (1995). Selective chain recognition in the C-terminal alpha-helical coiled-coil region of laminin. J Mol Biol *250*, 64-73.
13. Stetefeld, J., Frank, S., Jenny, M., Schulthess, T., Kammerer, R.A., Boudko, S., Landwehr, R., Okuyama, K., and Engel, J. (2003). Collagen stabilization at atomic level: crystal structure of designed (GlyProPro)10foldon. Structure *11*, 339-346.
14. Papanikolopoulou, K., Teixeira, S., Belrhali, H., Forsyth, V.T., Mitraki, A., and van Raaij, M.J. (2004). Adenovirus fibre shaft sequences fold into the native triple beta-spiral fold when N-terminally fused to the bacteriophage T4 fibritin foldon trimerisation motif. J Mol Biol *342*, 219-227.
15. Kammerer, R.A., Antonsson, P., Schulthess, T., Fauser, C., and Engel, J. (1995). Selective chain recognition in the C-terminal alpha-helical coiled-coil region of laminin. J Mol Biol *250*, 64-73.
16. Brandenberger, R., Kammerer, R.A., Engel, J., and Chiquet, M. (1996). Native chick laminin-4 containing the beta 2 chain (s-laminin) promotes motor axon growth. J Cell Biol *135*, 1583-1592.
17. Gasteiger, E., Hoogland, C., Gattiker, A., Duvaud, S., Wilkins, M.R., Appel, R.D., and Bairoch, A. (2005). Protein Identification and Analysis Tools on the ExPASy Server. (In) John M. Walker (ed): The Proteomics Protocols Handbook, Humana Press, 571-607.
18. Laemmli, U.K. (1970). Cleavage of structural proteins during the assembly of the head of bacteriophage T4. Nature *227*, 680-685.
19. Towbin, H., Staehelin, T., and Gordon, J. (1979). Electrophoretic transfer of proteins from polyacrylamide gels to nitrocellulose sheets: procedure and some applications. Proc Natl Acad Sci U S A *76*, 4350-4354.
20. Burnette, W.N. (1981). "Western blotting": electrophoretic transfer of proteins from sodium dodecyl sulfate--polyacrylamide gels to unmodified nitrocellulose and radiographic detection with antibody and radioiodinated protein A. Anal Biochem *112*, 195-203.

21. Bradford, M.M. (1976). A rapid and sensitive method for the quantitation of microgram quantities of protein utilizing the principle of protein-dye binding. Anal Biochem *72*, 248-254.
22. Machaidze, G., and Lustig, A. (2006). SEGAL, a semi-automatic program for fitting sedimentation equilibrium patterns from analytical ultracentrifugation. Journal of Biological Physics and Chemistry *6*, 91-102.
23. Schagger, H. (2001). Blue-native gels to isolate protein complexes from mitochondria. Methods Cell Biol *65*, 231-244.

APPENDIX

CURRICULUM VITAE

Dr. Senthilkumar Raman

Work address	M.E. Muller Institute for Structural Biology, Biozentrum, University of Basel, Klingelbergstrasse 50/70, CH-4056 Basel, Switzerland.
Private address	Spalenring 6, CH-4055. Basel, Switzerland.
Phone	+41 763695214 (private)
E-mail	senthil.kumar@unibas.ch
Date of birth	16/07/1978 (Tamil Nadu, India)
Nationality	Indian
Marital status	Single

EDUCATION

2007	**PhD in Biophysics**, *Biozentrum, University of Basel, Switzerland.*
2001	**Post Graduate Diploma in Bioinformatics**, *Madurai Kamaraj University, Tamil Nadu, India. (http://biotechmku.org/adbic.html)*
2000	**Master of Life Sciences (specialization in Microbiology)**, *Bharathidasan University, Tamil Nadu, India. (www.nfmc.res.in/nfmc/index.html)*

SCIENTIFIC EXPERIENCES

2007 – 2008 **Post-doctoral position**, *laboratory of the Professor. Ueli Aebi, M.E. Muller Institute for Structural Biology, Biozentrum, University of Basel, Switzerland. Supervisor: Associate Professor. Peter Burkhard*

Characterization of peptide based nanoparticles as a vaccine carrier

- Expressed and purified different vaccine constructs
- Characterized the vaccine constructs using Electron Microscopy (EM) and Dynamic Light Scattering (DLS).

2002 – 2007 **PhD Thesis,** *M.E. Muller Institute for Structural Biology, Biozentrum, University of Basel, Switzerland. Supervisor: Associate Professor. Peter Burkhard.*

Design and analysis of peptide based nanoparticles.

- Standardized expression and purification protocol for peptide based nanoparticles
- Optimized refolding conditions to get peptide based nanoparticles
- Biophysical characterization of peptide based nanoparticles using Electron Microscopy (EM) and Analytical Ultra Centrifugation (AUC)
- Studies on peptide based nanoparticles as a vaccine tool (immunization studies was done in collaboration with Dr. Robert S. Hodges lab, University of Colorado Health Sciences Center, Denver, USA)

2001 – 2002 **Research Fellow**, *Center for DNA Fingerprinting and Diagnostics (CDFD), Hyderabad, India. Supervisor: Dr. Akash Ranjan*

Homology modeling of Polyphosphate glucokinase from *Mycobacterium tuberculosis*

- Learnt Homology modeling (Modeller software) and model verification tools (Ramachandran plot, Verify3D and WHAT IF)

2000-2001 **Post Graduate Diploma in Bioinformatics work**, *Madurai Kamaraj University, Tamil Nadu, India.*

SeGENE a web based approach to search and extract genes from Genomes (developed for in-house purpose)

- Coded using C-language and web enabling was done using CGI-Perl script
- Worked on Unix operating system

1995-2000 **Master of Life Sciences. Master Thesis work** (December 1999 - April 2000)**,** *Indian Institute of Science (IISC), Bangalore, India. Supervisor: Professor. S. Vijaya*

Study of replication mechanism of Japanese Encephalitis virus (JEV) & purification of NS3 polypeptides foe use as exogenous antigens in T-cell proliferation assays

- Learnt cloning and PCR technique; Inclusion body preparation technique and SDS-PAGE.

SKILLS

Wet Lab skills

Molecular biology	Cloning, PCR, Site directed mutagenesis
Biochemistry	Protein over-expression and purification, Chromatography (Affinity and Gel filtration). Protein characterization techniques: Native-PAGE, SDS-PAGE, and Western-blot.
Microscopy	Transmission Electron Microscopy (TEM). Both sample preparation and analysis.
Biophysical	Dynamic Light Scattering (DLS), Analytical Ultra Centrifugation (AUC) and Circular Dichroism (CD) spectroscopy.

Computer skills

Operating systems	Unix and Windows
Languages	C-language and Perl scripting

PUBLICATIONS LIST

1. Raman, S.K., Kao, D.J., Tropel, D., Graff, A., Machaidze, G., Hodges, R.S., and Burkhard, P. (2005). *Peptide Based Nanoparticles as a Platform for Vaccine Design.* **Nanotech 2005** Vol. 1, 47-50.
2. Raman, S., Machaidze, G., Lustig, A., Aebi, U., and Burkhard, P. (2006). *Structure-based design of peptides that self-assemble into regular polyhedral nanoparticles*. **Nanomedicine** 2, 95-102.
3. Raman, S., Machaidze, G., Lustig, A., Olivieri, V., Aebi, U., and Burkhard, P. (2007). *Design and analysis for using non coiled-coil oligomerization domains in peptide based nanoparticle design principles*. (**manuscript in preparation**)
4. Kaba, S., Brando, C., Mittelholzer, C., Raman, S., Burkhard, P., Lanar, DE. (2007). *A non-adjuvanted nanoparticle vaccine confers long-lasting protection against rodent malaria by a T-cell independent type 2 mechanism.* (**manuscript in preparation**)

POSTER PRESENTATIONS

1. Graff.A, Raman.S, Tropel.D, Machaidze.G, Aebi.U, Burkhard.P. *Peptide nanoparticles for Biomedical applications*. **International Conference on Nanoscience and Technology (ICN+T) 2006**, Basel, Switzerland.
2. Raman.S, Meli.A, Burkhard.P. *Design of Peptidic nanoparticles*. **Biozentrum Conference 2003**, Basel, Switzerland.

COURSES AND WORKSHOPS

- Attended **7 day Graduate course on 'Key Issues in Drug Discovery and Development',** 2004**.** Conducted by ETH Zurich and University of Basel in collaboration with Novartis and Hoffmann-La Roche.
- Attended workshop on '**Basic course on Microscopy**', from 09.08.2004 to 20.08.2004. Conducted by Zentrum for Microscopy, University of Basel, Switzerland.

LANGUAGES KNOWN

- English (Reading/ Writing/ Conversation)
- Tamil (Mother tongue)

REFEREES

Associate Professor. Dr. Peter Burkhard
The Institute of Materials Science
University of Connecticut
Storrs, CT 06269-3136
USA.
E-mail: pburkhard@ims.uconn.edu
Phone +1 860 486 3830

Professor. Dr. Ueli Aebi
M.E.Muller Institute for Structural Biology
Biozentrum, University of Basel
CH -4056
Switzerland.
E-mail: ueli.aebi@unibas.ch
Phone +41 61 267 2261